

Dissertation
submitted to the
Combined Faculties for the Natural Sciences and for Mathematics
of the Ruperto-Carola University of Heidelberg, Germany
for the degree of
Doctor of Natural Sciences

Put forward by
Pierre-Alain Loizeau
born in Cholet, France

Oral examination: 5th June, 2014

Development and test of
a free-streaming readout chain
for the CBM Time of Flight Wall

Referees: Prof. Dr. Norbert Herrmann
 Prof. Dr. Ulrich Uwer

Zusammenfassung

Gegenstand dieser Dissertation sind Entwicklung und Test eines frei laufenden Ausleseverfahrens für die Flugzeitwand (TOF) des CBM-Experiments (Compressed Baryonic Matter). Mit dem Ziel, das Phasendiagramm stark wechselwirkender Materie zu erforschen, strebt CBM die Messung seltener Reaktionsprodukte in Schwerionenkollisionen an, deren Produktionswirkungsquerschnitt und Phasenraumverteilungen sehr stark von der Beschaffenheit ihrer baryonischen Entstehungsumgebung abhängen. Die Messung dieser seltenen Teilchen, in der vorliegenden Arbeit am Beispiel der Antiprotonen illustriert, setzt die Fähigkeit des Detektors zu exzellenter Teilchenidentifikation (PID) voraus sowie einen neuen, frei laufenden Ausleseansatz. In CBM wird die Identifikation geladener Teilchen durch die Flugzeitwand geleistet, die auf MRPC-Detektoren (Multi-gap Resistive Plate Chamber) basiert. Ein Schwerpunkt dieser Arbeit liegt auf der Überprüfung des frei laufenden, als integrierte Schaltung (ASIC) realisierten Zeit-Digital-Wandlers (TDC) GET4, dessen Entwicklung dabei vom Prototypen hin zu einem nahezu finalen Design vorangetrieben wurde. Für die neueste untersuchte Version konnte gezeigt werden, dass sie den Anforderungen von CBM bzgl. Zeitauflösung, Effizienz, Ratenfähigkeit und Stabilität gerecht wird. Darüber hinaus wurde eine Neustrukturierung der TOF-spezifischen Software-Komponenten innerhalb der Software-Rahmenstruktur CBMROOT vorgenommen, um die Methoden zur Verarbeitung und Analyse von simulierten und experimentellen Daten zusammenzuführen. Diese Software wurde schließlich dazu verwendet, eine Abschätzung der zu erwartenden Datenraten und der Anzahl der benötigten Komponenten in der frei laufenden Ausleseelektronik der Flugzeitwand vorzunehmen.

Abstract

This thesis presents the development and test of a free-streaming readout chain for the Time of Flight (TOF) Wall of the Compressed Baryonic Matter (CBM) experiment. In order to contribute to the exploration of the phase diagram of strongly interacting matter, CBM aims at the measurement of rare probes, whose yields and phase space distributions are significantly influenced by their environment. Many of the possible signals, of which the antiprotons was investigated within this thesis, require an excellent Particle Identification (PID) and a new readout paradigm called free-streaming. In CBM, the PID for charged particles is provided by a TOF wall based on Multi-gap Resistive Plate Chambers (MRPC). Within the thesis, a central component of the TOF readout chain, the free-streaming ASIC-TDC, was evaluated and pushed from the prototype level to a close to final design, for which it could be demonstrated that it fulfill all the CBM requirements: resolution, rate capability and stability. Additionally, the CBM TOF software in the CBMROOT software framework was reorganized to merge the processing and analysis of real and simulated data. A data unpacker and a realistic digitizer were implemented with a common output data format. The digitizer was used to estimate the data rates and number of components in a free-streaming readout chain for the full wall.

Contents

1	Introduction	1
1.1	Heavy Ions collisions physics	1
1.2	Self-triggered and data-driven readout	9
1.3	Time of Flight as Particle Identification tool	11
1.4	Thesis objective	15
2	The Compressed Baryonic Matter experiment	17
2.1	The Facility for Antiproton and Ion Research	17
2.2	Physics goals	19
2.2.1	Running scenarios and rate requirement	21
2.3	The Compressed Baryonic Matter experiment	22
2.3.1	Dipole magnet	25
2.3.2	Micro-Vertex Detector (MVD)	25
2.3.3	Silicon Tracking System (STS)	26
2.3.4	Ring-Imaging Cherenkov Detector (RICH)	26
2.3.5	Muon Chamber System (MUCH)	26
2.3.6	Transition Radiation Detector (TRD)	27
2.3.7	Time-of-Flight System (TOF)	27
2.3.8	Electromagnetic Calorimeter (ECAL)	27
2.3.9	Projectile Spectator Detector (PSD)	27
2.3.10	Online event selection and data acquisition	27
2.4	Free-Streaming readout	28
2.4.1	Free-Streaming Readout concept	28
2.4.2	Use-case study for CBM-TOF free-streaming data: anti-proton selection	31
3	The CBM Time Of Flight Wall	37

CONTENTS

3.1	Charged Hadron identification in CBM	37
3.2	Requirements for the CBM TOF Wall	39
3.3	Multi-gap Resistive Plate Chambers	41
3.4	Timing MRPC Signal Acquisition	47
3.4.1	Electronics	47
3.4.2	Requirements for the readout chain	50
3.4.3	TDC calibration: Non-linearities	50
3.4.4	Data calibration for discriminator effects: Walk	52
3.5	CBM TOF Wall design	57
4	The TOF wall Readout chain	61
4.1	Chain Concept	61
4.2	Readout chain components	63
4.2.1	The PADI pre-amplifier and discriminator	63
4.2.2	The GSI Event-Driven TDC with 4 channels	68
4.2.3	Clock system	74
4.2.4	Readout Controller	76
4.2.5	Reference triggered system	78
4.2.6	Software	79
4.2.7	Summary: Readout Chain Prototype	79
4.3	GET4 Proto Evaluation	80
4.3.1	Software Processing	80
4.3.2	First beamtime at COSY with GET4 Proto	83
4.3.3	Second beamtime at COSY with GET4 Proto	85
4.4	GET4 v1.0 Evaluation	90
4.4.1	The GET4 v1.0 chip	91
4.4.2	Software Processing	97
4.4.3	Beamtime at GSI with GET4 v1.0	101
4.4.4	Pulser test of GET4 v1.0	106
4.4.5	Cosmic tests with GET4 v1.0	106
5	Data flow and simulation	117
5.1	Goals	117
5.1.1	Unified analysis software	117
5.1.2	Common data format for unpacked TDC data	118

5.1.3	Readout chain dimensioning	119
5.2	The CBMROOT framework	120
5.2.1	FAIRROOT	120
5.2.2	CBM specifics	120
5.3	A CBM-TOF data unpacker in CBMROOT	121
5.3.1	Classes organization	121
5.3.2	Results: Comparison with the GO4 unpacker	128
5.4	Wall geometry implementation	129
5.5	A CBM-TOF digitizer in CBMROOT	130
5.5.1	Classes organization	130
5.5.2	Digitization	132
5.5.3	Clusterization (Hit building)	137
5.5.4	Results	139
5.6	Components dimensioning results	141
5.7	Towards a time based analysis	144
6	Conclusion and Outlook	147
A	CBM MMRPC prototypes	153
A.1	RPC-P1	153
A.2	RPC-P2	153
A.3	RPC-P3	156
B	Triggered components	157
B.1	VME, RIO and MBS	157
B.2	VULOM based boards	157
B.2.1	TRIGLOG	158
B.2.2	SCALORMU	159
B.3	CAEN V1290	159
B.4	VFTX	160
C	Keywords and Acronyms	163
C.1	LVDS	163
C.2	SPI	163
C.3	NIM standard	164
C.4	SYNC signal and SYNC messages	164

CONTENTS

C.5 D type flip-flop	165
Bibliography	167

List of Figures

1.1	Sketch of the phase diagram for strongly-interacting matter with some of the phases predicted by theory	2
1.2	Abundances of mesons and strange baryons measured in central nucleus-nucleus collisions as a function of the invariant energy \sqrt{s}	3
1.3	The energy dependence of freeze-out temperature and baryo chemical potential	4
1.4	The hadronic freeze-out line in the plane temperature versus net-baryon density as obtained in the statistical model with the values of μ_B and T that have been extracted from the experimental data in Ref. [13]	5
1.5	Multiplicities of various types of strange clusters in central Pb+Pb reactions at $E_{\text{lab}} = 5A$ GeV from the hybrid approach and energy dependence of multistrange Λ hypernuclei yields relative to the yields of Λ at midrapidity for central nucleus-nucleus collisions, calculated with the statistical model	6
1.6	Particle multiplicities times branching ratio for central Au+Au collisions at 25A GeV	8
1.7	General concept of a free-streaming readout chain.	9
1.8	Flux of particles per cm^2 and s as obtained for a wall position at 10 m from the target for an interaction rate of 10 MHz in an URMQ simulation of Au+Au collisions at 25 A GeV	14
1.9	Maximum momentum for which a $n_{\sigma_{\text{TOF}}} \geq 3$ is ensured as function of TOF system resolution and as function of TOF measurement length (right) . . .	15
2.1	Layout of the Facility for Antiproton and Ion Research (FAIR)	18
2.2	Three stages of a U+U collision at a laboratory beam energy of 23A GeV as calculated with the UrQMD model	20
2.3	The CBM experimental setup in the electron configuration: with RICH and TRD	23
2.4	The CBM experimental setup in the muon configuration: with MUCH and a reduced TRD, no ECAL	24

LIST OF FIGURES

2.5	Comparison of the digitization and readout in triggered and free-streaming systems	29
2.6	CBM FEE/DAQ tree concept	30
2.7	Antiproton production probability in central events and yield per day at an interaction rate of 10 MHz for Au + Au collisions as function of incident beam energy and available energy in the CMS	32
2.8	Acquisition days needed to achieve a statistics of 10^5 \bar{p} events as function of beam energy	33
2.9	Acquisition days needed to achieve a specified significance for the anti-proton signal, for different interaction rates at a beam energy of 4 A GeV	34
3.1	M^2 versus momentum distribution for reconstructed tracks in a CBM simulation with an example of PID cuts	39
3.2	Squared mass as a function of momentum and mass spectra for momentum bins at $p = 1, 3$ and 5 GeV/c	40
3.3	Calculated particle flux in the CBM TOF wall placed 10 m (red) and 6 m (blue) behind target using as event generator URQMD for 10 MHz minimum bias Au+Au reactions at 10 A GeV and 25 A GeV	42
3.4	Hit density (hits/cm ² /event) of primary and secondary charged particles in central Au+Au collisions at an incident energy of 25 A GeV with the TOF wall at a distance of 10 m from the target in comparison to the situation at 10 AGeV, 6 m	43
3.5	Example of the structure of a typical MRPC with n gaps	44
3.6	Working principle of an RPC	45
3.7	Readout types of MRPCs	46
3.8	Measured rate capability (maximum operating flux) as function of $1/\rho d$	47
3.9	Example of signals from a differential strip MRPC	48
3.10	Example of processed signals from a differential strip MRPC	49
3.11	Bin size (left) and bin position (right) for a selected channel on a GET4 v1.0 board during cosmics tests	51
3.12	DNL (left) and INL (right) for a selected channel on a GET4 v1.0 board during cosmics tests	52
3.13	Sketch of the origin of the time-walk effect in a leading edge discriminator	53
3.14	Sketch of the procedure used to obtain the correction values for the walk effect in our setups	55
3.15	Difference between the mean time of Plastic scintillator 0 and the mean time of Plastic scintillator 1 as function of the Plastic scintillator 0 left side TOT before (left) and after (right) the walk correction	56

3.16	Reference system time difference before (left) and after (right) the walk correction	57
3.17	Modular design of the TOF Detector	58
3.18	Proposed design for the CBM TOF wall outer area	59
3.19	Proposed design for the CBM TOF wall inner area	59
4.1	General concept of a free-streaming readout chain	62
4.2	Concept of a free-streaming readout chain for TOF	63
4.3	Simplified block schematics for the PADI chip family	64
4.4	The PADI2 time resolution dependence to input signal amplitude for different threshold voltages	65
4.5	Block diagram of PADI-6	66
4.6	Measured PADI-7 time resolution versus input signal amplitude for the given threshold values VTHR	67
4.7	FEET-PADI PCB equipped with two PADI-3 chips	68
4.8	FEET-PADI6 system, with a baseboard fully equipped with 4 PADI daughter PCBs, each hosting two PADI-6 or 7 chips	69
4.9	Simplified block diagram of the GET4 Proto TDC ASIC	70
4.10	Definition of time stamp and fine time in GET4	70
4.11	Timing diagram of the external synchronization of the time-stamp counter in GET4	71
4.12	Simplified state diagrams of the token ring in the GET4 readout part for the GET4 Proto	73
4.13	FEET-GET4 PCB equipped with two GET4 Proto chips	74
4.14	CBM TOF wall clock system diagram	76
4.15	CLOSY2 board naked and in its protective case	76
4.16	SYSCORE v2 board, used for the GET4-ROC	77
4.17	A schematic overview of the Frontend Module for the GET4 read-out	78
4.18	The free-streaming readout chain prototype based on the GET4 TDC	80
4.19	Cleaning and hit building procedure	81
4.20	Software organization for the first COSY beamtime (in 2010), with the three steps, their software and input/output formats	82
4.21	Software organization for the second beamtime at COSY (in 2011), with the three steps, their software and input/output formats	83
4.22	Example of the effect of a stuck buffer during COSY2010 beamtime	84

LIST OF FIGURES

4.23	Data rate on the GET4 channel corresponding to the PMT on the front scintillator left side, as a function of time during the COSY 2010 beamtime first run with free-streaming readout	86
4.24	Setup used for the beamtime in COSY in November 2011	86
4.25	The synchronization in the hybrid system in COSY 2011 beamtime	87
4.26	Fine Time distribution of the Leading edges for the first and eventual second hits per event	89
4.27	Difference between the time of PMT6 measured in the triggered system and the same recorded in the free-streaming system corrected using the trigger signal	90
4.28	Detailed path of the PMT6 and the trigger signals in the COSY 2011 setup	91
4.29	Simplified state diagrams of the token ring in the GET4 readout part for the GET4 v1.0	93
4.30	Baseboard for the GET4 v1.x chips, fully equipped with four daughter boards and a SYSCORE v2 ROC adapter board	95
4.31	Backside of a GET4 v1.x daughter board, with four bonded GET4 v1.0 chips	95
4.32	Simulation of the data rate capability of the GET4 v1.0 ASIC in 24-bit readout mode	96
4.33	Simulation of the data rate capability of the GET4 v1.0 ASIC in 32-bit readout mode	96
4.34	Software organization for the unpacking of VFTX (triggered FPGA TDC) data	98
4.35	Software organization for the “pseudo-triggered” unpacking of GET4 data .	100
4.36	Software organization for the free-streaming unpacking of GET4 data . . .	101
4.37	Photograph of the GET4 v1.0 setup with part of the triggered setup during the beamtime at GSI in November 2012	102
4.38	Connection scheme of parallel operation of the GET4 v1.0 setup and triggered setup during the beamtime at GSI in November 2012	103
4.39	DLL flag per TDC hit message for each GET4 channel in the first GET4 v1.0 run in beamtime at GSI in November 2012	104
4.40	Evolution of the data and error messages rate as well as Scintillators data trigger rate in the first GET4 v1.0 run in beamtime at GSI in November 2012	105
4.41	Error pattern from error messages for each GET4 channel in the first GET4 v1.0 run in beamtime at GSI in November 2012	105
4.42	Setup for pulser tests of GET4 v1.0 in the laboratory	106
4.43	Rate capability test of GET4 v1.0 operated in 24 bit mode with a pulser .	107
4.44	Setup scheme and trigger geometry of the Setup used for the cosmic rays test of GET4 v1.0	107

4.45	Connection scheme of the setup used for the cosmic rays test of GET4 v1.0	108
4.46	Example of the velocity correction on the data acquired during the 2013 cosmics test	109
4.47	Example of the track angle correction on the data acquired during the 2013 cosmics test	110
4.48	Performance of the VFTX system in terms of efficiency and resolution as function of high voltage	113
4.49	Comparison of the system performance of the GET4 v1.0 and VFTX sys- tem in terms of efficiency and resolution as function of high voltage	113
4.50	Comparison of the system resolution obtained in the GET4 v1.0 TDC at 11.5kV HV for the events with multiple data on at least one TDC channel and events where all TDC channels had at most one full hit	114
4.51	Left and right TOT in the VFTX systems for hits where the corresponding data was not found in the GET4 system, RPC OR triggering, first common strip	114
5.1	Status of the TOF wall analysis software prior to the integration of the unpackers in CBMROOT	118
5.2	TOF wall software organization with all analysis and simulation steps in CBMROOT	119
5.3	CBMROOT Unpacker organization in logical steps with main output formats	121
5.4	Detailed unpack step in CBMROOT with the supported MBS sub-events, the corresponding unpacking classes and output data formats	124
5.5	Details of the unpacker monitoring with the corresponding unpacking classes and input data formats	124
5.6	Details of calibration with the corresponding processing classes and input data/output formats	126
5.7	Details of the mapping step in the CBMROOT unpacker with the corre- sponding processing class and input/output data formats	127
5.8	Details of the conversion step in the CBMROOT unpacker with the corre- sponding processing class and input/output data formats	128
5.9	3D view of the standard wall geometry in CBMROOT	130
5.10	Comparison of the digitization chains for TOF in CBMROOT	132
5.11	Illustration of the method used to generate total TOT values for the clusters following the experimental distribution	134
5.12	Simulated hit rate per electronic channel in 10 MHz Au+Au collisions at SIS100 (10A GeV) and SIS300 (25A GeV)	143
5.13	Same data as in Fig. 5.12, after resorting the channels in rate bins	143

LIST OF FIGURES

5.14	Currently available TOF wall analysis softwares organization using CBM-ROOT and pure ROOT macros	146
A.1	A pictorial view of the cross section of this fully symmetric differential RPC-P1	154
A.2	Photograph of the prototype RPC-P1 embedded in a gas tight aluminum box	154
A.3	Photograph of the RPC-P2 embedded in its gas tight aluminum box, float glass version	155
A.4	Photograph of the RPC-P2 prototype embedded in the gas tight aluminum box, low-resistive glass version	155
A.5	Photograph of the RPC-P3 prototype for the low rate region	156
B.1	Photograph of a VULOM 3 board	158
B.2	Photograph of a CAEN V1290A board	160
B.3	INL compensation table readout from the FLASH memory for a channel on a V1290A board	160
B.4	Photograph of a VFTX 1 board	162
B.5	Bin width plot for both signal edges on a selected channel of a VFTX 1 board	162
C.1	Example of a single slave SPI connection	164
C.2	Symbol of a D flip flop elements with its usual input/output names	166

List of Tables

1.1	Comparison of the energy ranges and reaction rates of current (STAR, PHENIX, NA61) and future experiments (MPD, HADES@FAIR, CBM) on dense baryonic matter	7
2.1	Ion species and their kinetic energy per nucleon for a beam rigidity of 100 Tm at the SIS100 and 300 Tm at the SIS300	19
2.2	CBM Main Observables and running conditions	22
2.3	CBM Observables and required detectors	25
3.1	Characteristics of the the TOF Wall regions	58
4.1	Main technical parameters of PADI-3 and PADI-6/7	67
4.2	Content of the internal event word in the GET4 Proto case	72
4.3	RMS values of timing jitter for the output signal at CLOSY2 and after 2 times cascading over 20 m distance	75
4.4	Time resolution measured on the early prototype of the readout chain with PADI-3 equipped on FEET-PADI, GET4 Proto equipped on FEET-GET4 and ROC loaded on SYSCORE v2	80
4.5	Content of the internal event word in the GET4 v1.0 case	93
4.6	Simulated maximum event rates for GET4 v1.0	97
4.7	Summary of the system performance for the different digitizer systems in the 2013 cosmic test at 11.5kV high voltage	112
4.8	Summary of the GET4 v1.0 to VFTX comparison in the 2013 cosmic test .	116
5.1	Fields definitions of the Unique Identifier for the detector channels	127
5.2	Comparison of the system performance obtained with the GO4 unpacker and the CBMROOT unpacker for both digitizer systems in the 2013 cosmic test at a high voltage of 11.5 kV	129
5.3	Characteristics of the RPC and SM types used for the wall geometry in the simulations	131

LIST OF TABLES

5.4	Example of efficiencies and purity obtained for the five main hadrons identified by TOF	140
5.5	Example of efficiencies and purity losses as well as Relative efficiency losses obtained for the five main hadrons identified by TOF	141
5.6	Range of values when considering all the centrality-energy-generator cases for each of the comparison criteria	142
5.7	Number of channels, needed FEE chips and ROCs for the full SIS300 TOF wall for both GET4 and the FPGA TDC option	142
5.8	Numbers of Electronic channels, FEE chips (Discriminators), TDCs, ROCs (SYSCORE v3) and optical links needed for the full TOF wall (SIS300 configuration) for the option with GET4 as TDC	145
5.9	Numbers of Electronic channels, FEE chips (Discriminators), TDCs, ROCs (TRB3 of HADES) and optical links needed for the full TOF wall (SIS300 configuration) for the option with FPGA TDCs	145
C.1	Truth table of a D type flip-flop	165

Chapter 1

Introduction

1.1 Heavy Ions collisions physics

The characterization of the phases of strongly-interacting matter is a challenging research field in nuclear physics which is pursued at many heavy-ion accelerator facilities. Theory predicts various phases depending on the temperature and baryon density (or baryon chemical potential) [1]. This is depicted in Fig. 1.1, where the location of some of these predicted phases is shown.

The hadronic phase, at moderate T and moderate μ_B , is a gas-like phase where baryons, anti-baryons and mesons are dominant. At high temperatures, the so-called Quark-Gluon-Plasma (QGP) is expected. This is a phase where the quarks and gluons are de-confined: they are not anymore bound into hadrons. Lattice QCD calculations at these temperatures and vanishing μ_B predict a cross-over transition from the hadronic phase to the QGP [2]. At higher μ_B values, a critical point is expected also from Lattice QCD calculations, followed by a first order phase transition at decreasing T and increasing μ_B values [3]. How far this first order transition extends towards the cold and dense matter depends on the model used. Some of the models predict an additional phase between the hadrons gas and the QGP for non zero baryo-chemical potential, where matter would not yet be de-confined but chiral symmetry would be restored, forming the so-called quarkyonic matter [4]. In this three phases case, a triple point could be present [5]. Further phases are also predicted at low temperature and extreme baryon chemical potential. On the experimental side, getting a better grip on the properties of those phases and the positions of the transitions between them is a major objective of recent heavy ion programs [6]. For example, measurements show evidence for the cross-over from QGP to hadron gas in the high temperature/low density corner reached at the top Relativistic Heavy Ion Collider (RHIC) [7] [8] and Large Hadron Collider (LHC) [9] energies. These evidence are found in observables such as the quenching of high p_T particle jets relative to proton-proton collisions or the scaling of elliptic flow with the number of constituent quarks.

The phase diagram of nuclear matter is also interesting due to its links to the evolution of the early universe and to the properties of dense stellar objects. In the early universe, it is

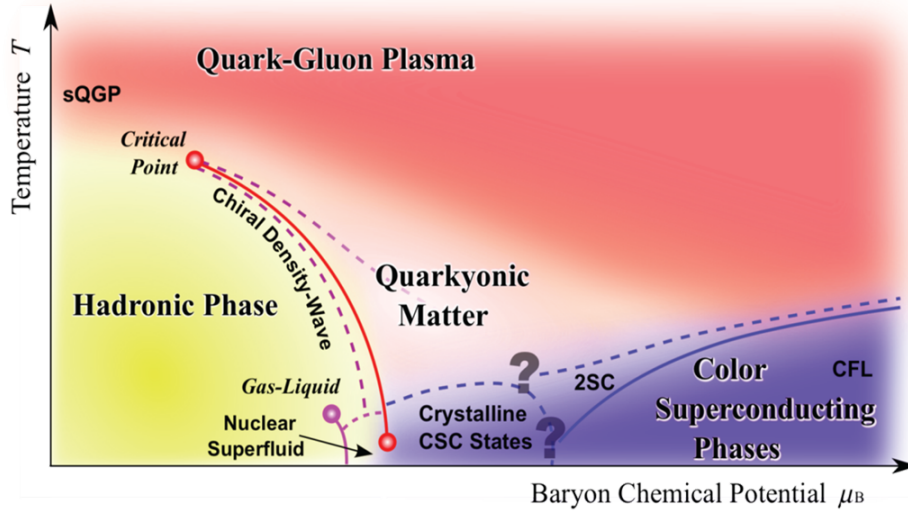


Figure 1.1: Sketch of the phase diagram for strongly-interacting matter with some of the phases predicted by theory. Figure taken from [1].

assumed that matter went through a phase transition similar to what is probed nowadays in high energy heavy-ion collisions, going from a QGP to nucleons. Cold and dense stars, such as neutron stars, correspond to the other side of the phase diagram. It is not yet sure in which state matter is in the core of these objects. This could be the phases predicted for low temperature and extreme baryon chemical potential. Theoretical models, however, provide through the equation of state (EOS) a link between the maximal mass and size of the neutron star, the state reached in the core and the state at the interface with the star crust. Knowing which phases are available and the parameters of the EOS would allow to constrain more tightly the models used to describe such objects.

The main method to explore the phase diagram around the predicted first order phase transition is to use heavy ion collisions at intermediate beam energies, e.g. center of mass energies $\sqrt{s_{NN}}$ from 2 to 200 GeV. In heavy ion collisions, a fireball is formed when the nuclei collide, accompanied in case of peripheral collisions by spectator remnants of the nuclei. The properties of the fireball depend on the collision parameters, as for example the beam energy, the beam and target material or the centrality of the collision. Different locations in the phase diagram can be probed by varying the collision parameters. Measuring the production yields and spectra of the particles created in the collision allows to characterize the properties of the fireball and eventually to extract those of the probed phase(s).

Fig. 1.2 presents the excitation functions of the measured hadron multiplicities for central heavy ion (Au+Au, Pb+Pb) collisions at the Alternating Gradient Synchrotron (AGS) at BNL, Super Proton Synchrotron (SPS) at CERN and RHIC. Most of the easily accessible (bulk) measurements in this energy range were already done or are under preparation in the past and existing AGS, SPS and RHIC programs. However, due to the low statistics,

the rare particles, e.g. the ϕ meson, $\bar{\Lambda}$ or $\Omega/\bar{\Omega}$, are not yet measured at the lowest energies.

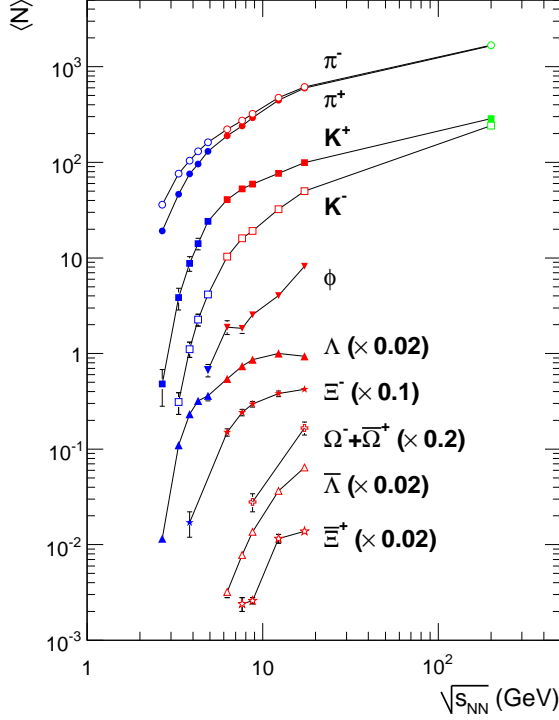


Figure 1.2: Abundances of mesons and strange baryons measured in central nucleus-nucleus collisions as a function of the invariant energy \sqrt{s} . Figure taken from [10].

The thermal (a.k.a statistical) model allows to extract from the experimentally measured particle yields the values of the fireball temperature (T) and baryo chemical potential (μ_B) at a specific stage of the fireball evolution: the chemical (hadronic) freeze-out [11]. This stage is the moment where inelastic collisions stop. In the model, the yield of each particle species is expressed as a function of the fireball volume V , the temperature T , the chemical potentials of the conserved quantities μ_B , μ_S and μ_Q and of the species properties m_0 , B (baryon number), S (strangeness) and Q (charge). Of the five general parameters (V , T , μ_B , μ_S , μ_Q), only three are in fact independent. The charge chemical potential μ_Q is fixed to ensure the conservation of the isospin asymmetry of the collision system. The strangeness chemical potential μ_S is removed by the conservation of the initial strangeness neutrality. By using ratios of particle yields, an additional parameter can be dropped: the fireball volume V . A set of available ratios of measured particle yields is then fitted to find the (T, μ_B) pair describing best the data. Results of such a fit on available heavy-ion measurements are shown in Fig. 1.3. It uses data from the SchwerIonen Synchrotron (SIS) at GSI, from the AGS at BNL, from the SPS at CERN and from RHIC at BNL [11]. On the top left side are presented the values of T from the fit as function of beam energy, where one can observe a saturation around $\sqrt{s_{NN}} = 10$ GeV at $T \sim 165$ MeV. The bottom left side shows the corresponding μ_B values, which are all decreasing with increasing energy. The limitation in chemical freeze-out temperature is not explained trivially. Fig. 1.3 right side place in a phase diagram the (μ_B, T) freeze-out pairs obtained from the fits. On top of the fits data are added phase limits and the

position of the corresponding critical point from a lattice QCD calculation [3], as well as lines corresponding to thermal model freeze-out curves with fixed parameters. The dashed red curve correspond to a fixed total baryon density and the dotted one to a fixed energy density. One can observe that with the exception of the temperature saturation, the position of the freeze-out points do not match any of the models. It must be remarked that the chemical freeze-out corresponds to an already expanded (dilute) system. Whether this particular point in the system evolution really relate to the dense phase is dependent on the model used for the analysis. One point around $\mu_B = 550$ MeV seems to break the regular trend of the other data points, at a beam energy of $\sqrt{s_{NN}} \sim 5$ GeV. As data are sparse no conclusion can be drawn for now on whether this structure is real.

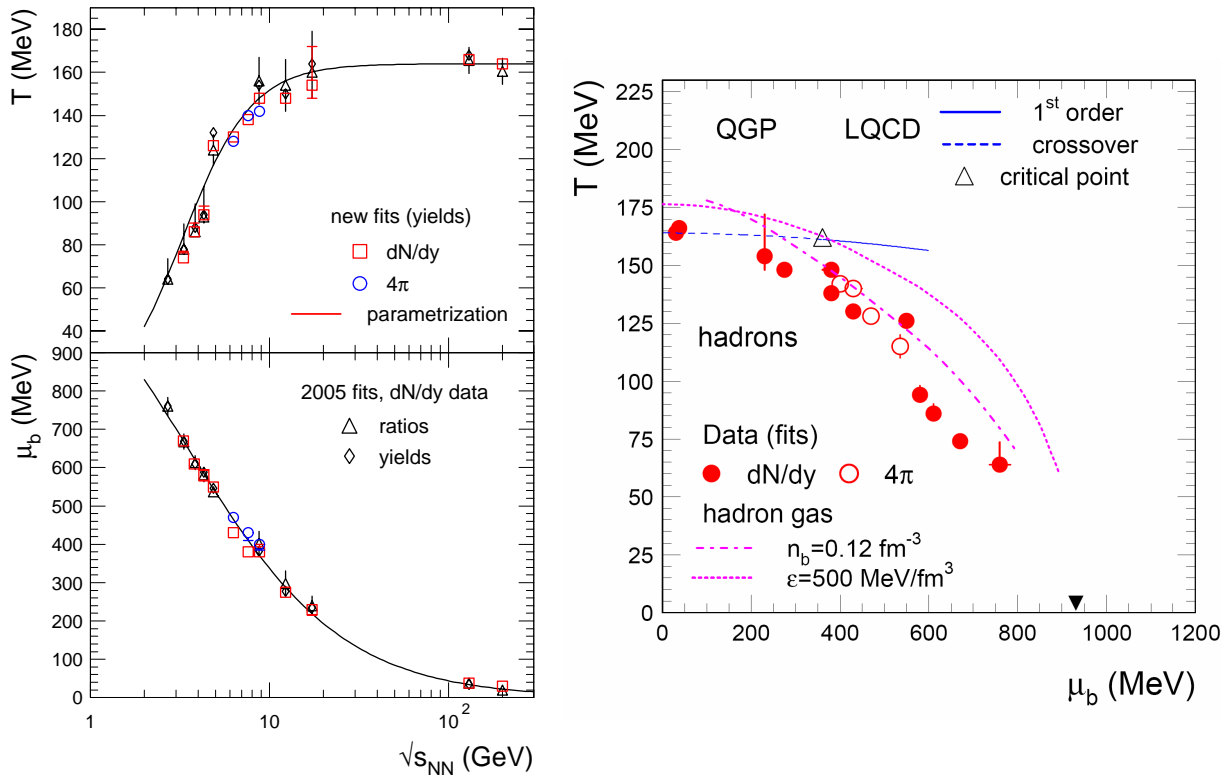


Figure 1.3: The energy dependence of freeze-out temperature and baryo chemical potential. Left panel: the results of fits using dN/dy data, both with ratios and yields. The lines are parametrizations for T and μ_b . Right panel: the phase diagram of hadronic and quark-gluon matter in the T - μ_b plane. The experimental values for the chemical freeze-out are obtained from the combined points of the left panel. They are shown together with results of lattice QCD calculations, the predicted critical point is marked by the open triangle [3]. Also included are calculations of freeze-out curves for a hadron gas at constant energy density ($\epsilon=500 \text{ MeV/fm}^3$) and at constant total baryon density ($n_b=0.12 \text{ fm}^{-3}$). The full triangle indicates the location of ground state nuclear matter (atomic nuclei). Figure taken from [11].

An alternative representation of the freeze-out points is to use the net baryon density ρ_B and energy density ϵ , which can be calculated from the μ_B and T fit values [12]. One can also use the (ρ_B, T) combination to highlight the density at freeze-out. Using

the experimental values, μ_B can be parametrized as function of beam energy and T approximated as a function of μ_B . It is then possible to display the expected freeze-out position as in Fig. 1.4. From this parametrization, the highest density at freeze-out is expected to be reached between 20 and 40 A GeV for fixed target experiments (beam kinetic energy) or between 6 and 10 A GeV for collider experiments (total beam energy). In the figure, the red points show as example the steps of an energy scan at RHIC (collider experiments) and the blue points represent the energies available for heavy ions at the new Facility for Antiproton and Ion Research (FAIR) (fixed target experiments).

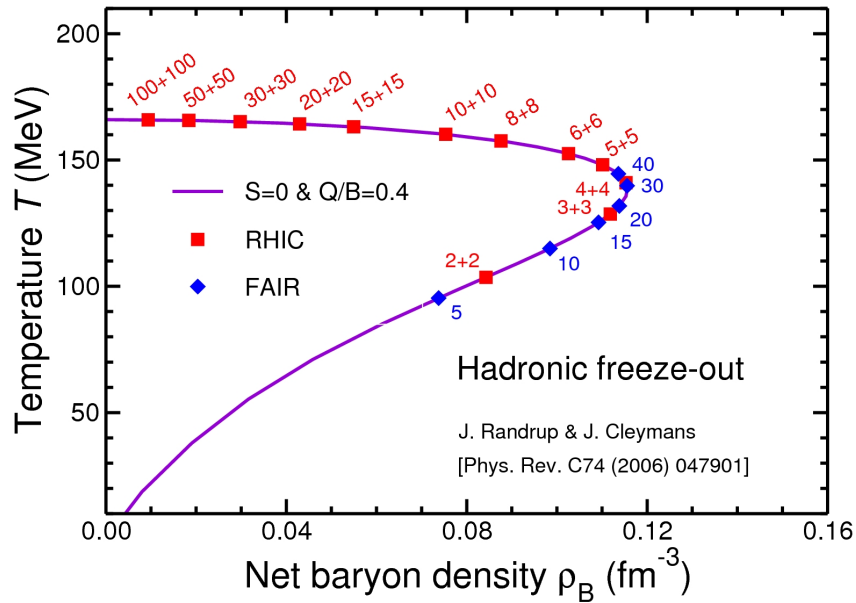


Figure 1.4: The hadronic freeze-out line in the plane temperature versus net-baryon density as obtained in the statistical model with the values of μ_B and T that have been extracted from the experimental data in Ref. [13]. The curve corresponds to Au+Au collisions. The symbols represent beam energies (in A GeV) at either RHIC (total energy in each beam), or FAIR (kinetic energy of the beam for a stationary target). The Figure is taken from [12].

FAIR also provide the opportunity to perform many other interesting studies aside from the phase diagram exploration. One of them is the measurement of the yields and decay chains of hypernuclei in the same energy range. Recently, ${}^3_{\Lambda}\text{H}$ and ${}^4_{\Lambda}\text{H}$ signals were found in Ni+Ni Collisions at 1.91 A GeV measured with the FOPI detector at GSI, Darmstadt [14]. Theoretical calculations predict that not only single hypernuclei, but also double hypernuclei and even clusters of strange baryons and nucleons (Metastable Exotic Multi-hypernuclear Objects or MEMOS) should be produced for beam kinetic energies of 2 to 35 A GeV, the range where FAIR will operate [6]. If they exist, these strange clusters could also be present in neutron stars. Fig. 1.5 (left) shows the multiplicities obtained in simulation for some of these clusters by adding a combination of microcanonical description and MEMO production by coalescence to the URQMD v2.3 model [15]. The modeled system is central Pb+Pb collisions at $E_{\text{lab}} = 5$ A GeV. Predicted multiplicities cover many

order of magnitudes, the most accessible ones starting at 10^{-3} to 10^{-5} per central event. The yield of some multi-strange hypernuclei relative to the yield of Λ as predicted by the statistical model is shown on the right side of Fig. 1.5. Here one can observe that the maximum yield happens around $\sqrt{s_{NN}} = 5$ -6 GeV (beam energy of 11-18 A GeV).

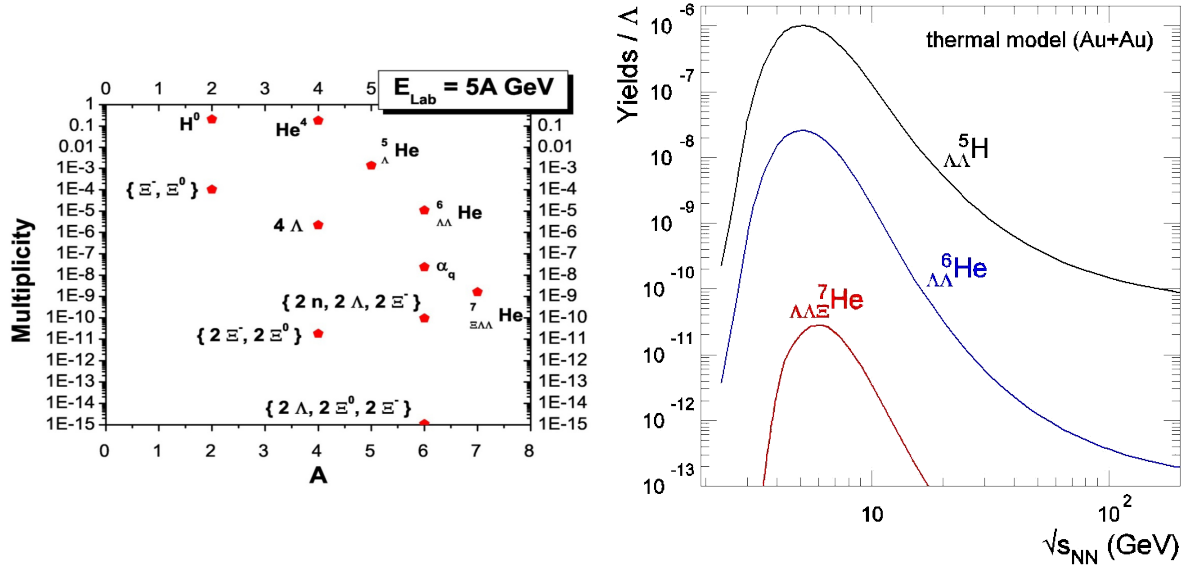


Figure 1.5: (left): Multiplicities of various types of strange clusters in central Pb+Pb reactions at $E_{\text{lab}} = 5A$ GeV from the hybrid approach. Figure taken from [15]. (right): The energy dependence of multistrange Λ hypernuclei yields relative to the yields of Λ at midrapidity for central nucleus-nucleus collisions, calculated with the statistical model. Figure taken from [6].

The Compressed Baryonic Matter experiment

The Compressed Baryonic Matter (CBM) is an experimental setup which will be installed at the Facility for Antiprotons and Ions Research (FAIR) in Darmstadt, Germany. FAIR will comprise in its final configuration two synchrotrons, SIS100 and SIS300. These synchrotrons will deliver beams of protons and heavy ions to CBM. In the first FAIR phase, only SIS100 will be available, providing proton beams up to 29 GeV and gold beams up to 11 A GeV. With SIS300, the second phase of FAIR will make available proton beams up to 89 GeV and gold beams up to 35 A GeV. FAIR, its accelerator complex and the expected time-lines will be described in more details in Section 2.1. CBM is a modular setup, which can be adapted to the observables looked after, e.g. with a configuration to measure vector mesons decays to di-leptons in the electron channel and another to measure them in the muon channel. It will be able to operate up to an interaction rate of 10 MHz. The CBM setup will be described in Section 2.3.

From its first day of operation, CBM will allow to (re)measure the yields and spectra of both bulk particles and rare particles, as e.g. the ϕ meson or the hyperons and their anti-

particles. In the energy range accessible with SIS100 ($\sqrt{s_{NN}}$ from 2.35 to 4.75 GeV), data are either scarce or inexistent for these strange particles (see Fig. 1.2). A beam energy scan, as for example 2, 4, 6, 8 and 10 A GeV, will provide the needed data to complete the excitation functions of the rare species and to compare the excitation function of bulk ones to existing data from AGS. Once available, SIS300 will allow to bridge the gap to the SPS data. By combining this energy scan with a collision system scan, e.g. with C, Ca, Ni, Xe and Au as beam and target material, the chemical freeze-out line can be explored with small steps in the (μ_B, T) plane. This will allow to determine whether an irregularity is really present around $\mu_B \sim 550$ MeV and $T \sim 120$ MeV.

In the future, this energy range will also be explored in a complementary way by beam energy scans at existing and new heavy ion facilities, as can be seen in Table 1.1. This includes approaching the expected maximum in density from both higher and lower energies, as was shown in Fig. 1.4. The Multi-Purpose Detector (MPD) is an experimental setup planned to be installed on a newly built Nuclotron based Ion Collider Facility (NICA) at the Joint Institute for Nuclear Research (JINR) in Dubna [16]. All experiments in Table 1.1 can access bulk observables. However, only CBM is designed to acquire data at high event rates, aiming at typical running scenarios of 100 kHz interaction rate for most observables and of up to 10 MHz interaction rate for the most demanding probes. This allows access to rare probes with yields as low as 10^{-5} to 10^{-7} per central event. The charmed particles and the strange clusters are good examples of these rare particles.

Table 1.1: Comparison of the energy ranges and reaction rates of current (STAR, PHENIX, NA61) and future experiments (MPD, HADES@FAIR, CBM) on dense baryonic matter. Table from [17].

Experiment	Energy range (Au/Pb beams)	Reaction rates (Hz)	Limiting factor
PHENIX & STAR @RHIC, BNL	$\sqrt{s_{NN}} = 7 - 200$ GeV	1 - 800	limitation by luminosity
NA61 @SPS, CERN	$E_{kin} = 20 - 160$ A GeV $\sqrt{s_{NN}} = 6.4 - 17.4$ GeV	80	limitation by detector
MPD @NICA, Dubna	$\sqrt{s_{NN}} = 4 - 11$ GeV	1000	design lumin. of $10^{27} \text{ cm}^{-2} \text{ s}^{-1}$ for Heavy Ions
CBM & HADES @FAIR, Darmstadt	$E_{kin} = 2 - 35$ A GeV $\sqrt{s_{NN}} = 2.7 - 8.3$ GeV	$10^5 - 10^7$	limitation by detector

Fig. 1.6 shows the prediction by the HSD model for particle abundances in the decay channels measured by CBM for central Au+Au collisions at 25 A GeV. In this calculation, the yields of the charmed particles are predicted to be two orders of magnitude lower than the anti-hyperons, which are themselves five orders of magnitude under the yields of the bulk particles. The MEMOs production at FAIR energies is also in the same order of magnitude. The maximum double hypernuclei yield happens around $\sqrt{s_{NN}} = 5-6$ GeV (11-18 A GeV), which is corresponding to the FAIR SIS300 energy range.

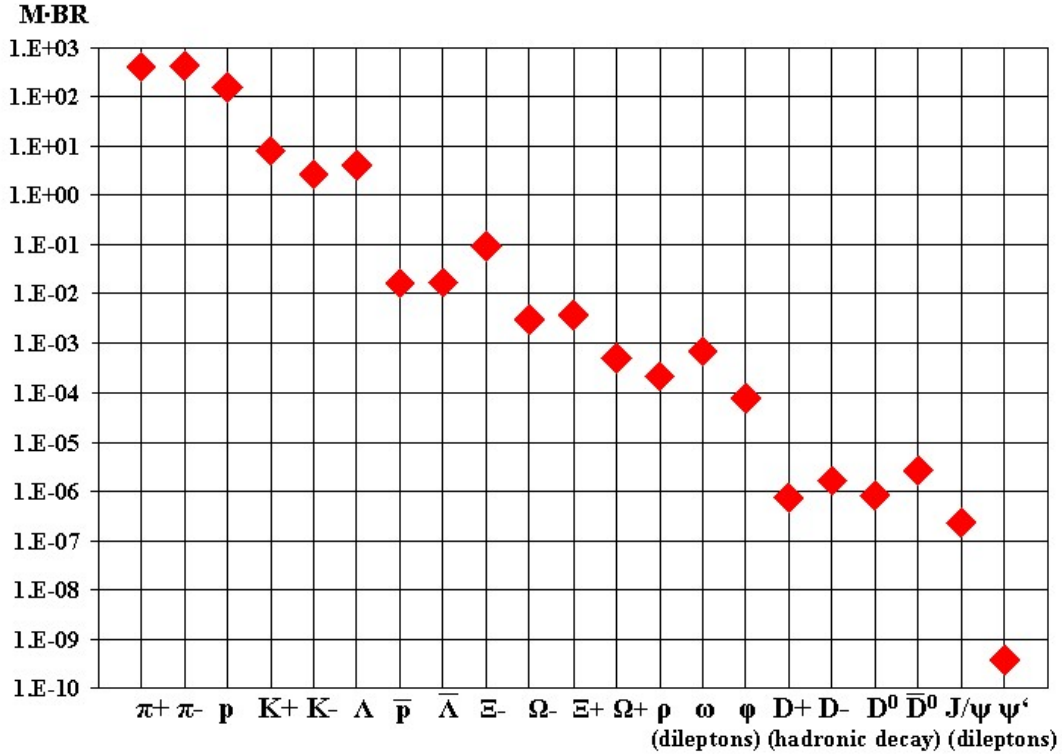


Figure 1.6: Particle multiplicities times branching ratio for central Au+Au collisions at 25A GeV as calculated with the HSD transport code [18] and the statistical model [19]. For the vector mesons (ρ , ω , ϕ , J/ψ , ψ') the decay into lepton pairs was assumed, for D mesons the hadronic decay into kaons and pions. Figure taken from [20].

The maximal archiving rate of the CBM experiment is planned to be 100 kHz. For the 10 MHz interaction rate to bring a statistics improvement, an event selection of a factor 100 has to be performed with high efficiency and purity. Many of the rare probes looked after in CBM don't have clear signatures detectable in hardware, as for example a high momentum particle or simple combinations of detector signals. To select events without these signatures, one needs primarily a reconstruction of the secondary vertices, while a Particle Identification (PID) helps to reduce the background. As an example the multi-strange hyperons are identified through the topology of their weak decays to pions, protons and kaons: $\Xi^- \rightarrow \Lambda \pi^-$ and $\Omega^- \rightarrow \Lambda K^-$, with $\Lambda \rightarrow p \pi^-$. The decay momentum of a few hundreds of MeV/c leads to kaons with momentum of a few GeV/c, which are compatible with Time of Flight (TOF) PID methods. The tracking calculations needed to obtain the vertices require lots of computing power and induce a wide range of latency depending of the number of tracks in the event, therefore making it difficult to implement a fast hardware decision. To still allow a selection on e.g. vertices topology, CBM will use a so called free-streaming system that combines self triggered electronics, high speed data transport and online event selection [21] [22].

1.2 Self-triggered and data-driven readout

To cope with the high computational effort and high event reduction needed to operate at maximum interaction rate, CBM event selection will be based on the free-streaming system mentioned earlier. While some other heavy-ion/high-energy experiments already used partial online event selection, like LHCb with its hardware Level 0 trigger and software High Level Trigger [23], CBM will be the first one where all event selection decisions will be done online by software. A schematic view of a free-streaming system is depicted in Fig. 1.7. Free-streaming is a generic term used to qualify a system combining self-triggered (triggerless) front-end electronics, a free-streaming data transport network and an online time based event building and event selection. A free-streaming chain has usually at least three layers of readout elements: first the readout of the front-end electronics, then the transport network and finally the input of the event builder. Depending on the needs, the transport can be itself sub-divided in a few readout layers organized in a tree-like fashion, with tasks like aggregating input data links to fewer output links or pre-processing the data.

In usual triggered system only a few fast detectors are equipped with self-triggered front-end electronics. The data from these are used to feed a fast hardware trigger system which itself controls the readout and/or clearing of the slower detectors. In a free-streaming system, all front-end electronics channels are self-triggered. This means that they digitize and time stamp any signal passing the thresholds.

As all valid physical data are acquired and need to be transported, a high bandwidth network is necessary. In CBM this network is called free-streaming because the data are transmitted asynchronously: each readout layer constantly pushes its available data to the next level. In addition, the transmission of control information backward to previous readout layers is reduced to a minimum. In such a system the task of throwing out data if needed and warning the control system about it is shifted to the input buffer of each readout level. One or more layer of pre-processing (pre-calibration, data formatting, data reduction through detector geometry correlation, ...) will probably be part of the transport system for most detector sub-systems in CBM.

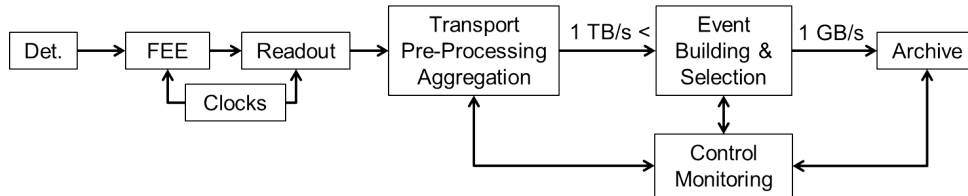


Figure 1.7: General concept of a free-streaming readout chain. FEE stands for Front-End Electronics.

The data are organized in time-based containers either in the last stage of the transport network or in the input stage of the First Level Event Selector (FLES), the computer farm where event building and selection is performed. The time-based containers are called micro-time-slices and group all data from a single detector transport link for a duration in the order of $1 \mu\text{s}$. The micro-time-slices are then grouped into the so-called

time-slices which will contain all data from the full experiment for a duration in the order of 100 micro-time-slices duration. This scheme allows for an easy overlap of a few micro-time-slices duration between adjacent time-slices.

The event building is done online in a big computer farm inside FLES. In each time slice all tracks are first reconstructed using fast algorithms and vertices are detected. This reconstruction is done in 4 dimensions (time and space) as there is no event limit at this point. Primary vertices can then be recognized, allowing to define “events”. The data corresponding to each primary vertex are extracted from the micro-time slices by using a selection window in time and space. The extracted data are stored then in an event container. In case of minimum bias trigger the event container can directly be sent to the event writing stage. In case of triggers linked to the topology of the primary and secondary vertices, the already available information from the tracking stage can be directly used to select which events should be sent to the event writing. In case of more involved triggers or if background is high, the PID information from dedicated detectors is extracted and calibrated. In CBM those detectors will be the Ring Imaging Cerenkov detector (RICH) and the Transition Radiation detector (TRD) for electron identification, the MUon Chamber for muon identification and the Time-of-Flight system (TOF) for the charged hadrons identification.

The scheme pursued by CBM introduces new challenges compared to traditional triggered systems. On the front-end electronics and free-streaming transport side, the main challenges are the time synchronization and the data volume. If one wants to be able to use a time based tracking and later a time based event selection, it is necessary that all data in the experiment can be placed in a common time frame. This is ensured by time stamping them against a common clock. Additional mechanisms are also needed to ensure that the internal counters of all time-stamping elements stay in synchronization. The data volume is a challenge through two aspects: the sensitivity to the noise and the experimental data integrity. The fact that all front-end electronic components are self-triggered means that a big increase of noise on a single channel could overload all parts of the readout chain (digitization and transport) connected to it, if no safety features are implemented. Data bursts from unstable beam conditions could have the same effect. The free-streaming principle of the data transport added to the time-based treatment of data also makes it more difficult to ensure that full events are available for selection. In a worst case scenario two parts of the experiment readout chain (links or detectors) could become fully saturated and start losing data in an alternating way, leading to all events collected in the event builder being incomplete. The main method to avoid such scenario is to perform proper simulation to estimate with a safety margin the minimal number of transport elements needed to push through all data generated in nominal operating conditions.

On the online reconstruction side, the main challenges are the time based reconstruction, the event reduction factor needed to operate at the highest CBM interaction rate and the need for some online calibration. The time based reconstruction requires really good synchronization between the different parts of the experiments, which can be realized at the readout stage. It also requires an efficient time-slice building mechanism, in order to ensure that data digitized in the same time interval are grouped from all detectors

before being sent to the processing nodes. The next challenge is the data reduction requirement. It is currently assumed that CBM will have an archiving rate in the order of 1 GByte/s [24]. If one assumes an event size of at least 10 kByte for the full experiment and minimum bias Au+Au collisions at the maximum available beam energy, this leads to a maximum event writing rate of 100 kHz. The event size in fact depends on which CBM sub-detectors are in use. Therefore an event rate reduction factor of 100 or more will be needed to run at the highest interaction rate of 10 MHz. The last challenge is the need for online calibration. This is especially true for the event selections involving TOF as PID method. As will be shown in next section, TOF relies on the precise timing at the ps level. It is known that some of the digitization technologies that could be used in the CBM TOF system present non-linearities which require calibration to convert the digital information into a meaningful timing. To use the TOF PID result in the event selection in a reliable way, an online calibration almost at the same quality level as usual offline methods will be needed.

The principle of a free-streaming system, the system used in CBM and a use-case example of what can be gained from a free-streaming event selection with TOF will be presented in Section 2.4.

1.3 Time of Flight as Particle Identification tool

TOF principle

Charged hadrons can be identified unambiguously by measuring both their electric charge and their mass. The charge and momentum of the particle can be obtained from the curvature of its trajectory in a magnetic field, obtained from tracking as is done in the Silicon Tracking System (STS) for CBM. But the mass cannot be measured directly. From the expression of the particle velocity relative to speed of light, one can express the mass of the particle as function of its momentum and time of flight, as shown in the following equations:

$$\beta = \frac{v}{c} = \frac{L}{Tc} \quad (1.1)$$

$$\beta = \frac{p}{\sqrt{(mc)^2 + p^2}} \quad (1.2)$$

$$m = \frac{p}{c} \sqrt{\frac{c^2 T^2}{L^2} - 1} \quad (1.3)$$

where T is the time of flight, L the track length over which this time is measured and c the speed of light.

Two particles A and B having different masses m_A and m_B but the same momentum can then be separated through their different time of flight. Eq. 1.3 can be reordered to

extract the time of flight instead of the mass. The difference of the times is then [25]:

$$\Delta T = T_A - T_B = \frac{L}{c} \left(\sqrt{1 + \left(\frac{m_A c}{p} \right)^2} - \sqrt{1 + \left(\frac{m_B c}{p} \right)^2} \right) \quad (1.4)$$

Assuming $p \gg mc$ for both particles (relativistic particles), one can make the approximation $\sqrt{1 + (mc/p)^2} \approx 1 + (mc)^2/2p^2$. The separation power, i.e. the TOF difference expressed in units of the TOF system time resolution σ_{TOF} , can then be expressed as [25]:

$$n_{\sigma_{TOF}} = \frac{|\Delta T|}{\sigma_{TOF}} \simeq \frac{Lc}{2p^2 \sigma_{TOF}} |m_A^2 - m_B^2| \quad (1.5)$$

One can use Eq. 1.3 to obtain the different contributions to the resolution of the m^2 values, assuming the errors of all parameters are Gaussian:

$$\frac{\sigma_{m^2}}{m^2} = 2 \sqrt{\left(\frac{\sigma_p}{p} \right)^2 + \left(\frac{pT}{mL} \right)^4 \left(\frac{\sigma_T}{T} \right)^2 + \left(\frac{pT}{mL} \right)^4 \left(\frac{\sigma_L}{L} \right)^2} \quad (1.6)$$

Typical values in heavy ion experiments are in the order of $\sigma_p/p \approx 1\%$ for the momentum resolution and $\sigma_L/L \approx 0.1\%$ for the track length resolution. As a consequence, with $\sigma_T/T \approx 10\%$ for time differences in order of ns, the time measurement dominates the mass resolution, especially for high momentum due to the p^2 factor. This justifies the fact that the separation power of TOF is expressed as function of the system time resolution only.

Usually a separation power of $n_{\sigma_{TOF}} \geq 3$ is required to assign the proper identification to individual particles. As the system resolution is fixed, there is always a momentum limit above which misidentification happens between species with adjacent masses (π/K , K/p). To increase this limit, one can either improve the system time resolution or increase the path length over which the time-of-flight is measured. The system resolution depends on the electronics performance, the time reference performance and the TOF detector performance. The path length is constrained by the available space in the experimental area (other detectors, cave size) and by the fact that one of the three main species identified by the TOF method, the kaons, have a limited life time. The decay length of kaons is $c\tau = 3.712$ m, so a shorter measurement length leads to more detected kaons. On the other hand relativistic time dilation increases the decay length for higher momentum particles, for which a longer path length would provide a better separation power relative to pions and protons.

Resistive Plate Chambers as TOF detectors

The two detector types used to build most TOF systems are plastic scintillators readout with PhotoMultipliers (PMT) and Resistive Plate Chambers (RPC). While Plastics with PMTs fulfill the requirement for TOF systems in terms of resolution and efficiency, their

high cost per channel, mostly due to the PMT, restrict them to small systems. Therefore, the technology based on RPCs is the only affordable one nowadays to build large systems with in the order of 100k channels.

RPC are related to Parallel Plate Chambers (PPC) [26], which are detectors based on a gap filled with gas between two metallic plates used as High Voltage (HV) electrodes. Sparks are generated when particles cross the PPC, which discharge the whole plate. This leads to large signals but limited rate capability due to the recharge time. The Pestov counter in 1971 [27] and later the first RPC in 1981 [28] tackle this problem by replacing at least one of the metallic electrodes by resistive material. The resistivity of the electrode then limits the discharge spread to the area around the impact point of the charged particle. This allows the rest of the electrode to stay efficient, increasing the rate capability. In 1996 RPCs were further modified by adding one or more resistive material plates between the electrodes, forming the so-called Multigap RPC or MRPC [29]. These additional plates are left electrically floating and are separated by few mm. Compared to RPCs with a single wide gap in the order of a cm, this allows to improve the time resolution without losing efficiency. Finally MRPCs were adapted to timing measurements with resolutions in the 100 ps range by using smaller gaps (order of 200-300 μm) and glass plates as resistive material.

Timing MRPCs are the detector chosen to build the CBM TOF system. The working principle of these detectors will be described in more details in Section 3.3.

CBM case

The TOF detector in CBM will be a wall covering the polar angles between 2.5° to 35° in X and 2.5° to 25° in Y. This corresponds to about 13.5 m width and 9 m height at a 10 m distance from the target. The particle flux obtained in simulation for the typical CBM conditions, 10 MHz interaction rate and Au+Au collision at 25 A GeV, is shown in Fig. 1.8. Values are ranging from under $1 \text{ kHz}\cdot\text{cm}^{-2}$ on the outer area to up to $50 \text{ kHz}\cdot\text{cm}^{-2}$ at small polar angles. To cope with such a gradient, different RPC types and different readout electrode layouts will be used, leading to an estimated channel count of about 100k with channel surfaces from few dm^2 to few cm^2 .

The nominal position of the CBM TOF wall will be at 10 m from the target for the typical SIS300 beam kinetic energy of 25 A GeV for Au+Au. However, in the first FAIR phase, only SIS100 will be available, with beam energies up to 11 A GeV for Au+Au. Therefore, to compensate for lower particles momenta and to detect more kaons before they decay, it is planned to move the wall closer to the target. The nominal position for SIS100 will be at around 6 m from the target. A system of rails parallel to the beamline allows to move the wall back and forth between those positions. Fig. 1.9 present the dependence of the highest momentum for which $n_{\sigma_{\text{TOF}}} \geq 3$ can be ensured as function of the system resolution (left) and measuring distance (right) for the main particle pairs discriminated with TOF. In CBM, electrons can be identified using other detectors, so the most critical pair to discriminate is pions and kaons. The main requirement for the CBM TOF wall performance is to allow for a 3σ separation of pions and kaons up to 4 GeV/c momentum

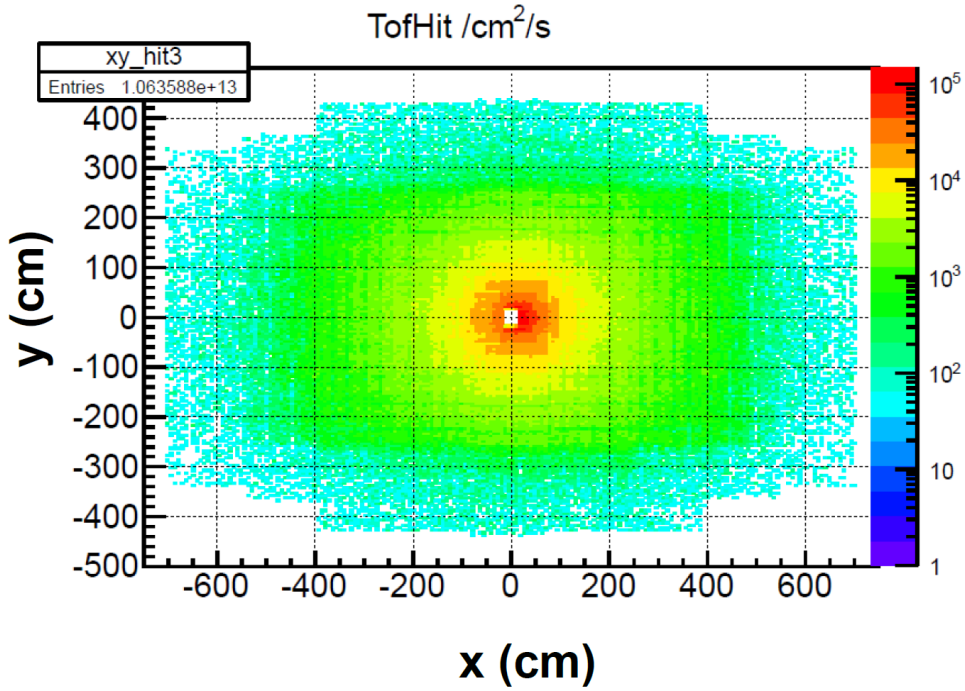


Figure 1.8: Flux of particles per cm^2 and s as obtained for a wall position at 10 m from the target for an interaction rate of 10 MHz in an URMQ simulation of Au+Au collisions at 25 A GeV. Figure taken from [30].

at the nominal position of 10 m from target. The left plot shows that this leads to a required system time resolution of 80 ps (green dashed line). This resolution in turn allows to separate these two species up to 3 GeV/c momentum when the wall is moved to 6 m, as indicated by the green dashed line in the right plot.

The wall will be presented in more details in Chapter 3. Its global requirements are:

- Based on MRPC counters
- System time resolution of 80 ps or below (include time reference, electronics, clock system and RPCs)
- Efficiency above 95%
- Readout channel granularity from a few cm^2 to 1 dm^2
- Rate capability of 1-50 kHz/cm^2
- Free-streaming readout
- Total number of channels ~ 100000
- Total area 120-140 m^2

The global requirement translate into the following readout chain requirements (for more details see Subsection 3.4.2):

- Time over Threshold measurement
- Hit rate up to 400 kHz/ch
- Electronics time resolution $< 40\text{ps}$ (TDC $< 25\text{ps}$)
- Double hit resolution $< 5\text{ns}$

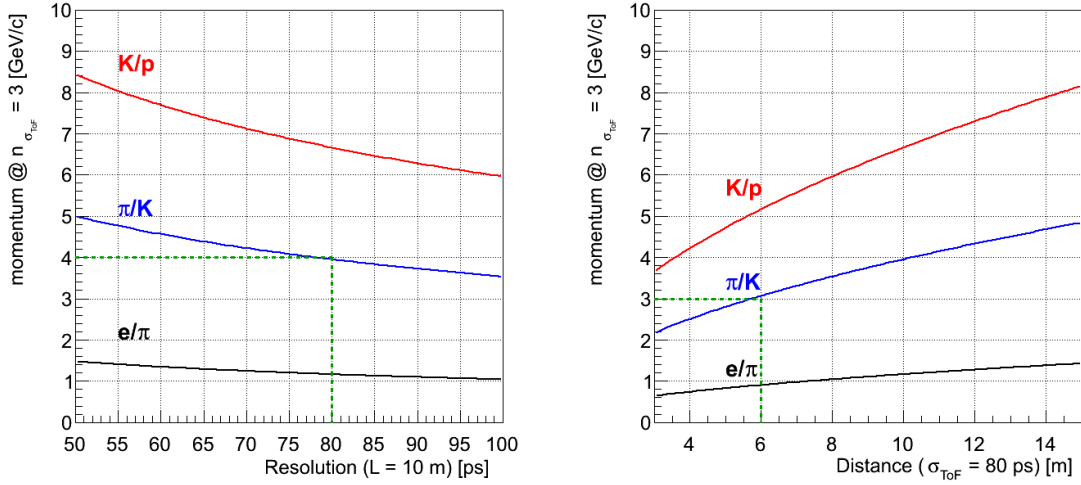


Figure 1.9: Maximum momentum for which a $n_{\sigma_{TOF}} \geq 3$ is ensured as function of TOF system resolution (left), assuming the nominal CBM TOF wall position at 10 m from the target, and as function of TOF measurement length (right), assuming the nominal CBM TOF resolution of 80 ps. The value is plotted for the three main charged particle pairs which can be separated with TOF: e/π (black), π/K (blue) and K/p (red).

- Low power consumption
- Synchronization mechanism between TDC and Readout Controller
- Optical communication between Readout Controller and DAQ

Building a free-streaming readout chain for such a detector presents challenges. The first one concerns time synchronization: the timing at below 100 ps resolution require specific high quality clocks with few ps jitter for the Time to Digital Converters (TDC). These clocks have to be synchronized to the experiment main clock used for time-stamping data in other detectors. The second challenge is the gradient in rate per readout channel. Even with adapted channel layout, the rate per channel covers a range from 1 kHz to more than 200 kHz. Due to this an optimization of the readout tree (channels, TDC, readout controllers, data pre-processors) has to be done to minimize the number of necessary components while still keeping a proper safety margin against data bursts.

1.4 Thesis objective

This thesis is organized in six chapters presenting the development and test of a free-streaming readout chain for the CBM Time of Flight Wall, in both its hardware and software aspects. Chapter 2 describes the CBM experiment and its physics goals. The last section of this chapter explains in details the principle of a free-streaming readout and how it is implemented in the CBM case. A study of the improvement gained in a specific physics use case by using the possibilities opened by the free-streaming readout

was done for this thesis and is also part of this chapter. Chapter 3 presents the CBM TOF wall, the MRPC detectors working principles and how signals from such counters are acquired. Chapter 4 focuses on the testing and improvement of the hardware side of the TOF readout chain. This chapter presents the components of the chain and the methods used to process the free-streaming data and the reference triggered data. The results obtained with the readout chain and the changes they induced in the chain design are also presented in this chapter. It is concluded by results from a two weeks long cosmic rays test with the improved chain. This test is the first time a free-streaming CBM TOF readout chain was successfully operated. Chapter 5 focuses on the software and simulation side of the chain characterization. An unpacker and a digitizer were written within this thesis as a first step towards a common TOF analysis framework that is compatible with CBMROOT. Their organization and results are shown in this chapter. The digitizer is used to obtain from URQMD simulations an estimation of the minimal number of readout chain components needed to operate the CBM TOF wall. The thesis is concluded by a summary and an outlook in Chapter 6.

Chapter 2

The Compressed Baryonic Matter experiment

The Compressed Baryonic Matter experiment is one of the four scientific pillars of the new Facility for Antiproton and Ion Research (FAIR), which is under construction in Darmstadt, Germany [31]. It will be dedicated to the study of the physics of hadrons and quarks in compressed nuclear matter. This includes the search for phase transitions in the phase diagram of strongly interacting matter as well as the study of strange and charmed particles production at FAIR energies. The setup is designed to allow for the measurement of both bulk observables and rare probes at interaction rates up to 10 MHz.

The first part of this chapter, Section 2.1, presents the Facility for Antiproton and Ion Research and its accelerator complex. It is followed by a description of CBM physics goals in Section 2.2. A brief discussion of CBM running scenarios and of the motivations for an online event selection is done in Section 2.2.1. Section 2.3 then presents the CBM setup and its detector systems. This chapter is concluded by a description of the *free-streaming readout* concept in CBM in Section 2.4.1 and an example of how the Time-of-Flight Particle Identification could be used with such a readout system in Section 2.4.2.

2.1 The Facility for Antiproton and Ion Research

The Facility for Antiproton and Ion Research (FAIR) is an international project currently under construction aside the existing GSI facility in Darmstadt, Germany. Its two synchrotrons will allow unique research programs in nuclear, hadron, atomic and plasma physics [32]. Using the existing SIS18 synchrotron as injector, it will be composed of two new synchrotrons, SIS100 and SIS300, the Superconducting Fragment Separator (Super-FRS), the storage ring for antiprotons (High-energy Storage Ring HESR), the Collector Ring (CR), and the New Experimental Storage Ring (NESR). Fig. 2.1 shows a model of the accelerator and experimental complex.

The experiments at FAIR are grouped in four experimental pillars:

- CBM

- the anti-Proton ANnihilation at DArmstadt (PANDA)
- Nuclear STructure, Astrophysics and Reactions (NuSTAR)
- Atomic, Plasma Physics and Applications (APPA)

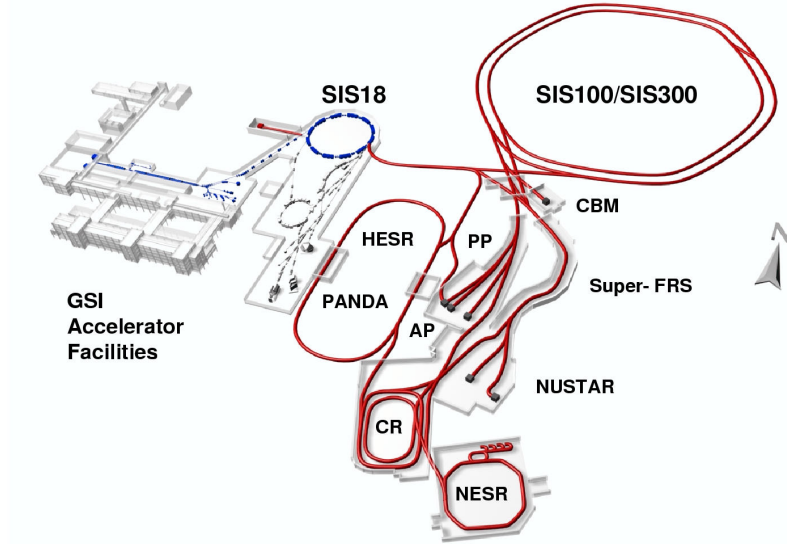


Figure 2.1: Layout of the Facility for Antiproton and Ion Research (FAIR) [32].

The two synchrotrons will be used to deliver the proton and heavy-ion beams to the CBM cave. The name of each one refers to its magnetic rigidity, on the model of the existing SIS18 and its 18 Tm. The beam kinetic energies per nucleon available can be obtained from the the rigidity at which the dipole magnets are set:

$$E/A = \sqrt{(0.3 \cdot B \cdot r \cdot Z/A)^2 + m^2} - m \quad (2.1)$$

where Z and A are the charge and atomic number of the beam particle, $B \cdot r$ the rigidity of the magnets and m the mass of a nucleon. From the maximum rigidities of each synchrotron, 100 Tm for SIS100 and 300 Tm for SIS300, one can obtain the maximum beam energies for typical beams, as listed in Table 2.1. The first phase of FAIR will provide in 2018 the SIS100 beams of proton up to 29 GeV and of Au-ions up to 11 A GeV. A few years later SIS300 will provide beams of proton up to 90 GeV and of Au-ions up to 35 A GeV (the so-called FAIR Phase II [31]). The beam energies available for other nuclei depend on their Z/A ratio. Both machines, SIS100 and SIS300, will be able to extract beam to the CBM cave at an intensity of up to 10^9 ions per second, which translates into a 10 MHz interaction rate for a 1% interaction target. It will in addition be possible with SIS300 to deliver beam to more than one experiment in parallel.

Table 2.1: Ion species and their kinetic energy per nucleon for a beam rigidity of 100 Tm at the SIS100 and 300 Tm at the SIS300. Table taken from [6].

Available in			2018	ca. 2025-2030
beam	Z	A	E/A GeV SIS100	E/A GeV SIS300
p	1	1	29	89
d	1	2	14	44
Ca	20	40	14	44
Ni	28	58	13.6	42
In	49	115	11.9	37
Au	79	197	11	35
U	92	238	10.7	34

2.2 Physics goals

The Compressed Baryonic Matter (CBM) experiment is designed to study the early and dense phase of the fireball generated in heavy-ion collisions. The main physics goal of CBM is the characterization of the phase transitions and properties of hadrons in nuclear matter at high density. The study of the fireball properties will be done through the systematic measurement of various observables by a scan on both beam energies and collision systems. CBM also provides a perfect tool to perform other measurements at the FAIR energies, e.g. searching for the existence of theoretically predicted multi-strange bound objects.

Three stages of the fireball evolution in an Uranium on Uranium collision at 23 A GeV are presented on Fig. 2.2. These snapshots were obtained in a simulation with the URQMD transport model [33]. They illustrate the emission stage of various particle species which could be used to probe the fireball properties and evolution. Charmed particles such as D mesons and J/ψ mesons could be used to probe the initial stage of the reaction, as this is where charm quarks are expected to be produced. For the intermediate stage of the collision, where the high densities are expected to be reached, both low mass vector mesons (ω , ρ , ϕ) and multi-strange hyperons (Ξ , Ω) are interesting probes. The vector mesons are produced throughout the full collision in $\pi\pi$ annihilation and are later decaying into mesons or into lepton pairs (10^{-4} suppressed channel). The di-lepton channel, even if it is highly suppressed, is still interesting as leptons are not effected by final state interactions, thus allowing to look into the fireball. The multi-strange hadrons and ϕ meson have small hadronic cross sections and thanks to this keep information about the dense phase of the interaction, particularly in their collective flow. The third snapshot illustrate the chemical freeze-out of the fireball, at which point the bulk of the particles are emitted. No more primary particles are produced after this point. Up to date mostly these bulk particles (p, K, π , Λ) were measured in heavy-ion collisions at FAIR energies. CBM is optimized to measure the probes from the high density intermediate stages, which are not accessible to other experiments in the same energy/system size range.

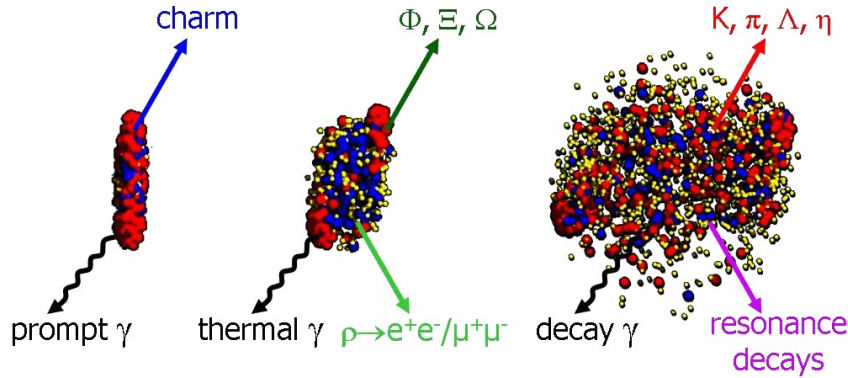


Figure 2.2: Three stages of a U+U collision at a laboratory beam energy of 23A GeV as calculated with the UrQMD model [33]: The initial stage where the two Lorentz-contracted nuclei overlap (left), the high density phase (middle), and the final stage (freeze-out) when all hadrons have been formed (right). Different particles are created in different stages of the collisions or escape from the interaction region at different times (see text). Almost 1000 charged particles are created in such a collision, most of them being pions. Figure taken from [6].

The part of the CBM program related to the search for a phase transition in compressed baryonic matter will make use of the energy range of both, SIS100 and SIS300. This includes for example the following observables:

- The study of low mass vector mesons: their mass spectra are expected to be modified in case of chiral symmetry restoration in the dense phase. The ρ meson is especially interesting as it decays for a large part inside the medium. Measuring these spectra in the dilepton channel at FAIR energies will allow to bridge the gap in data between HADES measurements at SIS18 [34] and CERES ones [35].
- The measurement of the excitation functions of yields, spectra and collective flow for bulk particles: the collective flow of hadrons is an interesting observable for CBM because it originates from the pressure inside the early fireball. Measuring its dependence on beam energy and collision system size is supposed to give access to the equation of state of baryonic matter, which is of importance to understand dense stellar object as for example neutron stars. It is also expected that the flow pattern will present some changes as for example an onset of the scaling with quark number at the beam energies for which a new phase becomes available.
- Event-by-event fluctuations of the hadrons yields and spectra: they are expected to appear in case the critical point or the coexistence phase of a first order phase transition are approached.
- The charmed particles production. At SIS100, this will allow to characterize the production mechanism of charm-anticharm pairs around threshold energies. These measurements provide a reference for charm production in nucleus-nucleus interactions both at SIS100 and SIS300. Using medium size ions, the nucleon-nucleon threshold for charmonium (J/ψ) production of 11.16 GeV in fixed target collisions

can be surpassed already at SIS100. With SIS300, the thresholds for production of both charmonia and D mesons are surpassed and a detailed study of the excitation function of their yields and spectra in nucleus-nucleus collisions is possible. A change in the ratio of the the production yields for charmonia and for open charm for a specific energy and collision system would provide a hint that a deconfined phase was present.

- Existence and production yields of hypernuclei, strange dibaryons and massive strange clusters: single and double hypernuclei are known to exist (e.g. ${}^3_{\Lambda}\text{H}$, ${}^4_{\Lambda}\text{H}$, ${}^4_{\Lambda\Lambda}\text{H}$, ...) but their production mechanism in heavy ion reactions is not yet fully determined.

Massive strange objects (e.g. $\{\Xi^-, \Xi^0\}$, $\{2\Lambda, 2\Sigma^-\}$, $\{2\Xi^-, 2\Xi^0\}$, ...) are predicted by theory calculations but not yet observed. As their yields in heavy ion collision is expected to have a maximum at SIS300, high rate measurements in CBM are particularly suited to find them through their weak decays to charged hadrons.

- Sub-threshold production of strange and anti-strange baryons: this is of special interest for the physics in the first phase of FAIR at the SIS100 machine. The multi-strange hyperons yields at sub-threshold energies provide hints toward the equation of state as these particles are then produced in multi-step processes that are sensitive to the fireball density. Up to now a single multi-strange particle data point is available for the SIS100 energy range: Ξ^- @ 6 A GeV. CBM will complete this by measuring the excitation function of Ξ^- , $\bar{\Xi}^+$, Ω^- and $\bar{\Omega}^+$ in the incident energy range from 4 to 10 A GeV.

2.2.1 Running scenarios and rate requirement

The maximal event archiving rate of CBM will be between 10 kHz and 100 kHz depending on the setup used (see Section 2.4). Therefore, CBM typical running conditions for bulk observables, where no event selection is needed, will be around 25 kHz interaction rate. The interaction rate could eventually be even lower for dedicated calibration runs. However, in order to acquire sufficient statistics for the most extreme cases, such as the J/ψ in the dilepton channel, the highest interaction rate is needed: 10 MHz. An event selection factor of 100 to 1000 is then necessary, which is feasible by a proper pion/electron separation for the di-electron channel or by requesting a minimal number of muons for the di-muon channel. For the D mesons, the event selection is based on the identification of the secondary vertex, which allows to reject 99% of the reactions. The interaction rate in this specific case is however limited to 100 kHz by the readout of the detector dedicated to this precise vertex detection (see Subsection 2.3.2). Even at this slightly reduced interaction rate, the resources needed to perform the track reconstruction in heavy ion collisions vary a lot depending on the tracks multiplicity. As a consequence, an online event selection is here fitting better than a trigger realized with hardware components, where a fixed latency for decision is required.

Table 2.2 presents the running conditions planned for CBMs main observables and whether they need an online trigger or not. One can remark that only the vector mesons in the di-muon channel and the charmed particles require higher rates and the online selection.

Other observables can in principle be studied by recording minimum bias events at the highest possible archiving rate.

Table 2.2: Main Observables and required running conditions: minimal interaction rate, necessity of an online event selection. When only Au+Au is indicated as collision system, lighter ions are still possible. The R column indicates the minimal interaction rate planned. Data taken from [6] and [36].

Observables	Collisions Systems		R (MHz)	Online Trigger
	SIS100	SIS300		
π , K, p	Au+Au up to 11 A GeV	Au+Au up to 35 A GeV	0.025	no
Hyperons			0.025	no
Hypernuclei			0.025	no
Vector mesons to e^+e^-	Au+Au up to 11 A GeV	Au+Au up to 35 A GeV	0.025	no
Vector mesons to $\mu^+\mu^-$	Au+Au up to 11 A GeV	Au+Au up to 35 A GeV	0.5	yes
Open charm	p+A up to 30 GeV Ca+Ca up to 14 A GeV	p+A up to 89 GeV Au+Au up to 35 A GeV	0.1	yes
Charmonium	p+A up to 30 GeV Ca+Ca up to 14 A GeV Au+Au up to 11 A GeV	p+A up to 89 GeV Au+Au up to 35 A GeV	10	yes

However, as the online selection will anyhow be available for all running conditions, it can be used to enhance the proportion of interesting events for lower rate observables, especially the rare ones. As an example, requesting for identified anti-proton in the event should then lead to an enhanced probability of reconstructing multi-strange anti-hyperons, which are normally identified through their decay vertex topology. A similar argument is possible with the reconstruction of hypernuclei and heavy strange clusters, which are usually studied with the invariant mass method. In heavy-ion collisions strangeness is conserved and the initial strangeness content is zero. As a consequence, asking for the presence of N particles containing an \bar{s} quark selects events where the corresponding amount of s quarks is available in the event sample for the formation of the aforementioned objects.

These event selection methods are made possible by using self triggered electronics combined to a fully online event selection. This is the so-called *free-streaming readout* concept which will be described in Section 2.4 .

2.3 The Compressed Baryonic Matter experiment

The Compressed Baryonic Matter (CBM) is a multi-purpose experimental setup aiming at a systematic measurement of most particles produced in nuclear collisions, including the most rare ones, with high precision and high statistics. The measurement will be

performed over the full SIS100/SIS300 energy range in nucleus-nucleus, proton-nucleus and proton-proton collisions. To achieve the high statistics requirement for the most rare probes, such as charmed particles, CBM is designed to operate at the highest possible beam intensity. This requires the development of fast high granularity detectors, triggerless electronics and fast online event reconstruction and selection methods.

CBM is designed as a modular “toolkit” setup. Its different configurations allow to measure all relevant observables presented in the previous section, albeit in different acquisition runs. The two main configurations are the so-called *electron setup* and *muon setup*, which will be presented later. If the need arises, other configurations will be possible, as most CBM sub-systems can be either removed from the beamline or shifted along it using a rail system. All sub-systems are designed for the most extreme running scenarios at SIS300, even if most of the data acquisition will happen in more relaxed conditions, as described in Section 2.2.1

The core of the experimental setup is a silicon tracking and vertices detection system installed in a superconducting magnet. This system consists of a Micro-Vertex Detector (MVD) based on pixels modules and a Silicon Tracking System (STS) based on micro-strips modules. The magnet and STS are the two parts of CBM which are present and placed at the same position in all configurations.

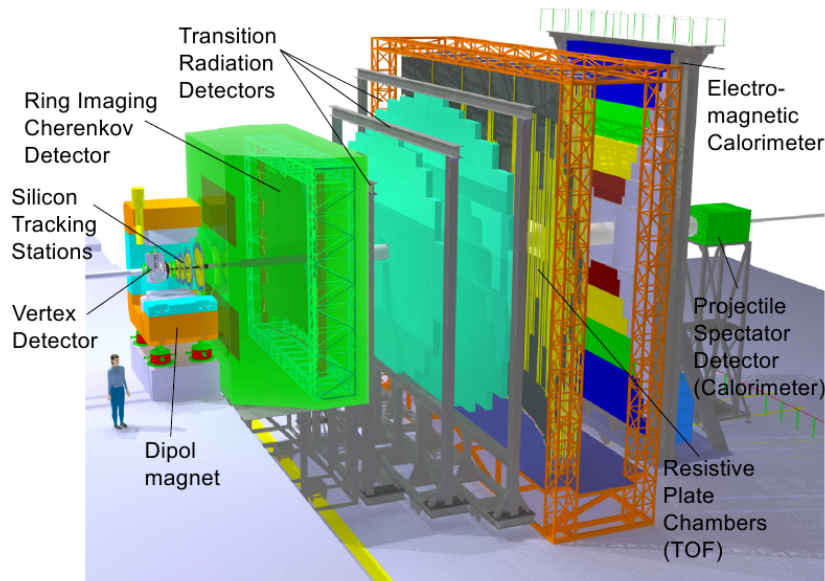


Figure 2.3: The CBM experimental setup in the electron configuration: with RICH and TRD. Figure taken from [20].

The electron identification is performed using a Ring Imaging CHerenkov detector (RICH) and a multi-station Transition Radiation Detector (TRD). As an alternative to the RICH, a MUon CHamber system (MUCH) can be used to measure muons. In this case MUCH is replacing the RICH and the number of TRD stations is reduced.

The charged hadron identification is provided by a Time of Flight wall (TOF) based on

the Resistive Plate Chambers (RPC) technology, placed nominally 10 m behind the target position.

When running with the electron version of the setup, an Electromagnetic Calorimeter (ECAL) is used to obtain information on photons and neutral particles in selected phase space area. Finally a Projectile Spectator Detector (PSD) is needed to determine the collision centrality as well as for getting enough information to compute the orientation of the reaction plane for collective flow measurement.

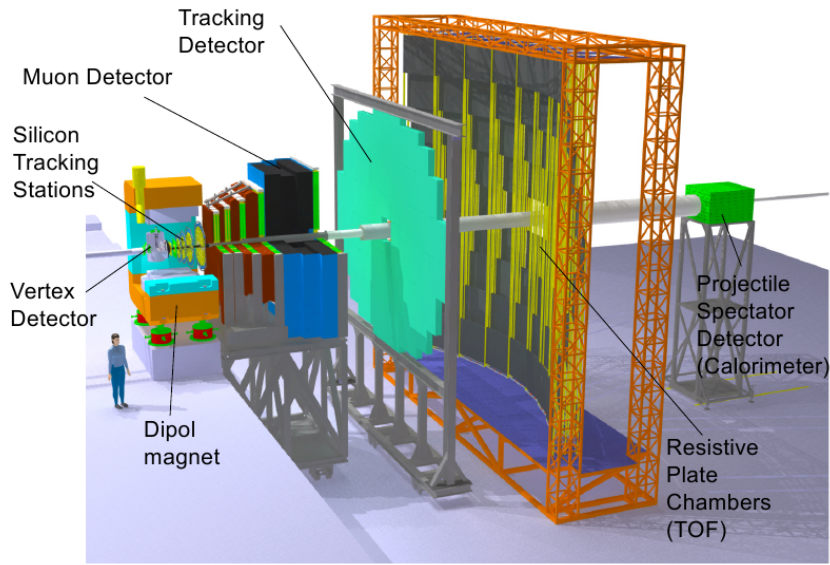


Figure 2.4: The CBM experimental setup in the muon configuration: with MUCH and a reduced TRD, no ECAL. Figure taken from [20].

The last component of the CBM setup is its unique data acquisition and online event selection system. It is based on self-triggered front-end electronics, a free-streaming and high bandwidth readout system and fast tracking and calibration algorithm running in a computer farm, the First Level Event Selector (FLES), based on many core parallel components.

Fig. 2.3 and 2.4 present the CBM experimental setup in the two main use cases, respectively when focusing on electron measurement (MVD, STS, RICH, TRD, TOF, ECAL, PSD) and when focusing on muons measurement (MVD, STS, MUCH, TRD, TOF, PSD). Table 2.3 presents the details of use cases for the various part of the CBM setup for the main physics observables. One can remark that TOF is used in almost all measurement. Following sections present the sub-detectors of CBM, from the closest to the target to the furthest downstream.

Table 2.3: Observables and required detectors: Micro-Vertex Detector MVD, Silicon Tracking Station STS, Ring Imaging Cherenkov detector RICH, Muon Chambers MuCh, Transition Radiation Detector TRD, Time Of Flight TOF, Electromagnetic Calorimeter ECAL, Projectile Spectator Detector PSD. Detectors marked as (x) can be used to suppress background. Table taken from [6].

Observables	MVD	STS	RICH	MuCh	TRD	TOF	ECAL	PSD
π , K, p		x	(x)		(x)	x		x
Hyperons		x			(x)	(x)		x
Open charm	x	x	(x)		(x)	(x)		x
Electrons	x	x	x		x	x		x
Muons		x		x		(x)		x
Photons							x	x
Photons via e^\pm conversion	x	x	x		x	x		x

2.3.1 Dipole magnet

A superconducting dipole magnet will be used in CBM, providing a magnetic field integral of 1 Tm while still keeping a large aperture of $\pm 25^\circ$ in vertical direction and $\pm 35^\circ$ in horizontal direction. The target and tracking detectors (Micro-Vertex Detector and Silicon Tracking System) are located inside the magnet [21].

2.3.2 Micro-Vertex Detector (MVD)

Open charm particles decay within a few hundred of μm from the primary vertex. To separate the decay vertices, a detector with an excellent position resolution but also a very low material budget is needed. Monolithic Active Pixel Sensors (MAPS) provide a good solution for this, reaching position resolution of 3 to 6 μm for pixel sizes ranging from $18 \times 18 \mu\text{m}$ to $20 \times 40 \mu\text{m}$. CBM MVD will be built from 3 layers of MAPS placed in the target vacuum at 5, 10 and 15 cm distance to the target, with a total thickness of around 300 to 500 μm of silicon equivalent (sensor + cooling + support) [21]. This geometry allows a secondary vertex position resolution on the order of 50 to 100 μm along the beam axis.

This detector will be readout at a constant frequency. The readout of all pixels in a MAPS is called a frame. The readout frequency for MVD will be 100k frames per second. The MVD will be installed mostly during open charm dedicated runs.

One of the main challenge in the development of MAPS for CBM is to achieve a sufficient radiation tolerance to survive 10^{12} minimum bias Au+Au collisions at 25 A GeV while keeping the low material budget and good resolution.

2.3.3 Silicon Tracking System (STS)

The STS will provide track and momentum information for charged particles. The design requirement is a momentum resolution in the order of $\Delta p/p = 1\%$. To achieve this, STS will be built out of 8 layers of silicon micro-strips detectors placed from 30 cm to 1 m behind the target, inside the dipole magnet field. The targeted resolution imposes severe constraints on the material budget. Due to this the sensors will be placed on light weight vertical ladders and the electronics will be positioned at the extremities of the ladders. So called micro-cables are then used to readout the sensors. The chosen micro-strips sensors are double-sided with a stereo angle of 7.5° , a strip pitch of $58 \mu\text{m}$ and strip lengths from 20 to 60 mm. Single sensors thickness will be $300 \mu\text{m}$.

With ~ 1.8 M readout channels STS is the component with the most channels in the CBM setup. More details about this detector can be found in the CBM-STs Technical Design Report [24].

2.3.4 Ring-Imaging Cherenkov Detector (RICH)

A Ring Imaging Cherenkov Detector is used in CBM to separate electrons from pions up to a momentum of $10 \text{ GeV}/c$ [21]. The detector is based on a 1.7 m long CO_2 gas radiator followed by two arrays of mirrors (above and below beam axis) focusing the Cherenkov rings on two photo-detector planes. The photo-detector planes are shielded from the magnetic field by the magnet yokes. It is currently planned to employ Multi Anode Photo Multiplier Tubes (MAPMTs), for a total of around 55000 channels. Simulations of CBM with these detectors predict a pion suppression in the order of 500-1000. This rejection reaches 10^4 when combined with the information of the Transition Radiation Detector.

2.3.5 Muon Chamber System (MUCH)

In CBM the Muon detector is complementary to the RICH detector: they occupy the same space along the beam line and are meant to be used alternatively [21]. This leads to the two CBM setups. The task of the MUon CHamber system is to identify muons in the high background caused by the high track multiplicity of heavy-ion collisions at FAIR energies. This is needed to identify low-mass vector mesons and charmonium in the di-muon channel. The current concept in CBM is to use 6 layers of iron with increasing thicknesses to absorb the hadrons, with tracking planes in-between. The thickness of the first three absorbers would be 20 cm, followed by layers of 30 cm, 35 cm and finally 100 cm thickness. Each tracking layer would be made of 3 tracking gas chambers, using either straw tubes or GEM technology. The main challenge both for the tracking chamber operation and for the track reconstruction is here the hit rate in the first tracking station, which reaches $3 \text{ MHz}/\text{cm}^2$ for a 10 MHz Au+Au interaction rate at the highest energy. GEM chambers were already tested successfully up to $1.4 \text{ MHz}/\text{cm}^2$ with pion beam. MUCH is planned to have around 500k channels.

As the multiplicity gets low after the muon absorber, track segments in the last tracking section are good candidates for the online event selection.

2.3.6 Transition Radiation Detector (TRD)

The Transition Radiation Detector will be composed of three stations with three detector layers each [21]. It will provide an identification for electrons and positrons with $p > 1.5 \text{ GeV}/c$ ($\gamma \geq 1000$) and tracking between STS and TOF for all charged particles. The pion suppression for the 9 TRD layers is expected to be well above 100 for an electron efficiency of 90%. The layers are equipped with rectangular pads and oriented so as to provide a position resolution in the order of $300\text{-}500 \mu\text{m}$. When the high rate close to the beam pipe in the first station ($\sim 100 \text{ kHz}/\text{cm}^2$ for 10 MHz minimum bias Au+Au at 25 A GeV) is also taken into account, this leads to a channel count in the order of 750k for an active area of 600 m^2 .

2.3.7 Time-of-Flight System (TOF)

The Time of Flight system purpose is to identify charged hadrons. It will be a wall composed of Multi-gap Resistive Plate Chambers (MRPC). As this thesis concern the readout chain of this sub-component, it will be described in more details in Chapter 3.

2.3.8 Electromagnetic Calorimeter (ECAL)

The Electromagnetic calorimeter is based on a proven technology, the “shashlik” type calorimeter [21], already in use in the HERA-B, PHENIX or LHCb experiments. It will measure direct photons and photons from neutral mesons decays. It will be composed of modules built from alternating lead and scintillator layers, each 1 mm thick. The modules will have areas ranging from $3 \times 3 \text{ cm}^2$ to $12 \times 12 \text{ cm}^2$. The modular construction allow to easily measure different regions of phase space depending on the needs.

2.3.9 Projectile Spectator Detector (PSD)

The Projectile Spectator Detector will be used to provide enough information for collision centrality determination and reaction plane determination [21]. It is done by a lead-scintillator hadron calorimeter measuring the energy of the projectile spectator fragments. The reaction plane is needed for the measurement of collective flow.

2.3.10 Online event selection and data acquisition

In order to obtain high statistics measurement of rare probes, CBM will have to operate at high interaction rate. The full setup including the online event selection and data acquisition systems will be designed for the maximum interaction rate of 10 MHz [21].

In such conditions, the expected mean event size of around 10 kByte for the full setup and minimum bias Au+Au collisions correspond to an input data rate in the order of 100 GByte/s. For an assumed archiving rate of 1 GByte/s, this means that the First Level Event Selector (FLES) will have to allow for a selection factor of 100 or more. This selection will be performed in a high performance computer farm located a few hundred meters away from the CBM cave on the GSI site.

As this thesis subject concern a part of the data acquisition system, it will be described in more details in Section 2.4 together with the online selection system. Chapter 4 describes the development done during this thesis for the TOF wall part of the data acquisition system, while Chapter 5 presents the efforts made to dimension the TOF readout system through simulation and to prepare the development of the online selection software.

2.4 Free-Streaming readout

2.4.1 Free-Streaming Readout concept

The very high interaction rates of up to 10 MHz needed to achieve the CBM physics goals lead to strong constraints on the detectors performance, but also of course on the Data Acquisition (DAQ) system capacities. In CBM the DAQ will be free-streaming (also called free-running), which means that no global hardware trigger (level 0 or level 1 in typical systems) will be available. Instead the system is a combination of self-triggered front-end electronics, fast free-streaming data transport, online event reconstruction and online event selection.

The difference between triggered FEE and self-triggered FEE operation is illustrated in Fig. 2.5.

In conventional triggered readout, most of the front-end electronics (FEE), especially those connected to slow detectors, store either digitized data in buffers or even the analog signal in passive components, e.g. capacitors. Signals from a few fast detectors, readout by dedicated FEE, are then used to reach a first selection decision within a pre-determined latency. The event decision is then propagated back in the form of a so-called *trigger signal* to all components which were not part of the dedicated trigger system. On reception of the trigger signal, the FEE will tag the data with an event number and propagate them to the readout network. The data are usually selected by their distance to the trigger arrival time, by means of a predefined time window (triggered readout, as in Fig. 2.5 middle part) or by an analog buffer with a fixed time constant (triggered digitization, as in Fig. 2.5 top part). By doing this, only relevant data are transferred to the computer farm, where more complex triggers (high level) can be built to further select interesting events. The remaining events are then prepared for storage and saved. Such a system has the advantage of providing “for free” a synchronization between the different parts of the experiment, as the trigger signal and event number are used to build the data containers. Event building is reduced to putting together all sub-events with the same event number. In a free-streaming system, without a global trigger being propagated backward to the

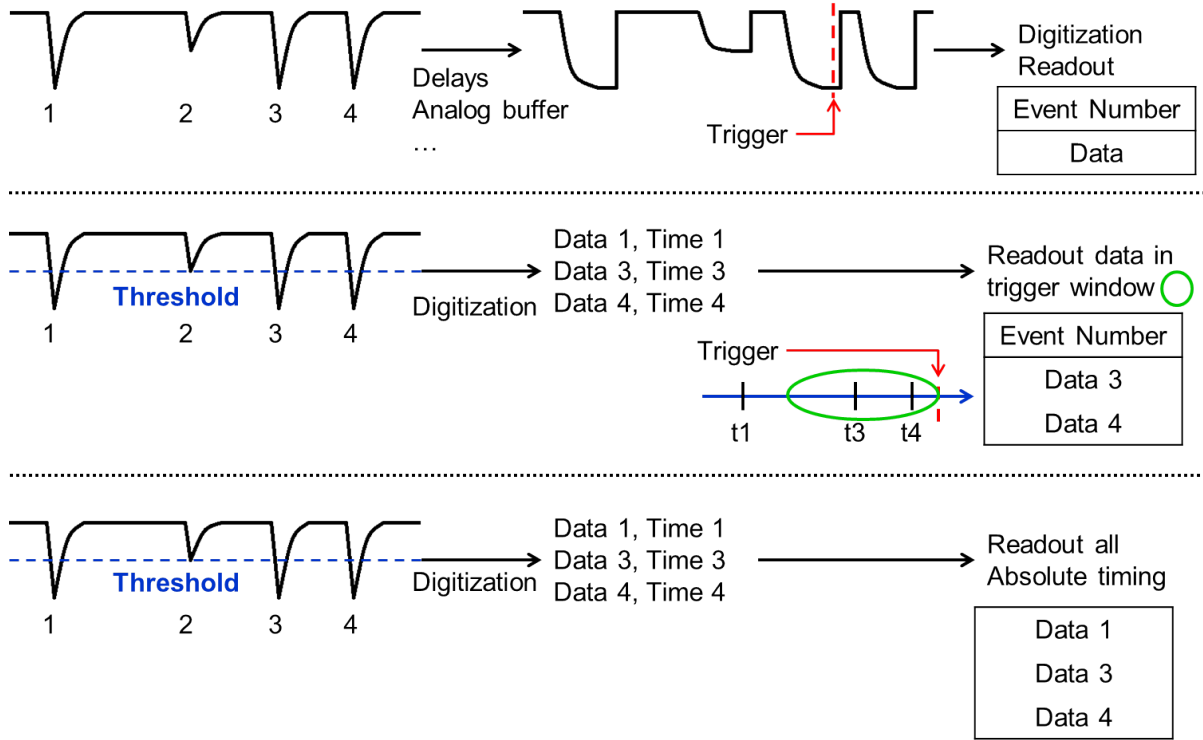


Figure 2.5: Comparison of the digitization and readout for a same set of input signals in two types of triggered systems and in a free-streaming system. Top is a sketch of triggered digitization, middle of triggered readout and bottom of free-streaming readout. The red arrow indicates the trigger.

FEE, each readout layer must decide by itself which data should be kept. For the FEE, this means a self-triggered operation mode, where any signal passing a previously set threshold is digitized, time-stamped against a common clock and stored in a first buffer.

For the readout components, it means that each layer of the transport network has to decide whether to keep the data and push them through the network or throw them out, depending on the status of its own buffer(s) and on its coarse information about the network status. As much as possible, the transmission of general commands such as throttling is avoided to keep a simple network organization. Data from the attached FEE boards are continuously readout by each unit of the first readout layer and stored in their buffers. These data are pushed toward the second level of readout as soon as available. There, in order to reduce the amount of data to transport, a first pre-processing is eventually performed on the raw data, using event independent features as for example detector geometry or FEE characteristics. For this reason the components in this layer are either called Data Combiner Board (DCB) if they just aggregate the data stream or Data Processing Board (DPB) if they perform some treatment/selection/formatting on the data. If needed this is done more than one time to pre-process data from bigger logical units (detector modules, sectors, ...) until the longer data links to the computer farm are optimally filled.

At the computer farm, called First Level Event Selector (FLES) in the CBM case [37], the data packets from the full experiment are first grouped together according to their absolute timestamps. This allows to build the so-called time-slice data containers, which contain all data from a defined time interval. These time-slices are then spread over many computing nodes where the reconstruction is done (Tracks, vertices, Multiplicity per time bin, ...). When an interesting feature is detected, an event time interval is used to select all related data. A second reconstruction/selection using event-wise information can then be performed (PID by TOF, ...). Finally, after the event selection is passed, either the raw data or the partially reconstructed data are formatted for storage and archived for more detailed offline analysis, as is also done in triggered systems.

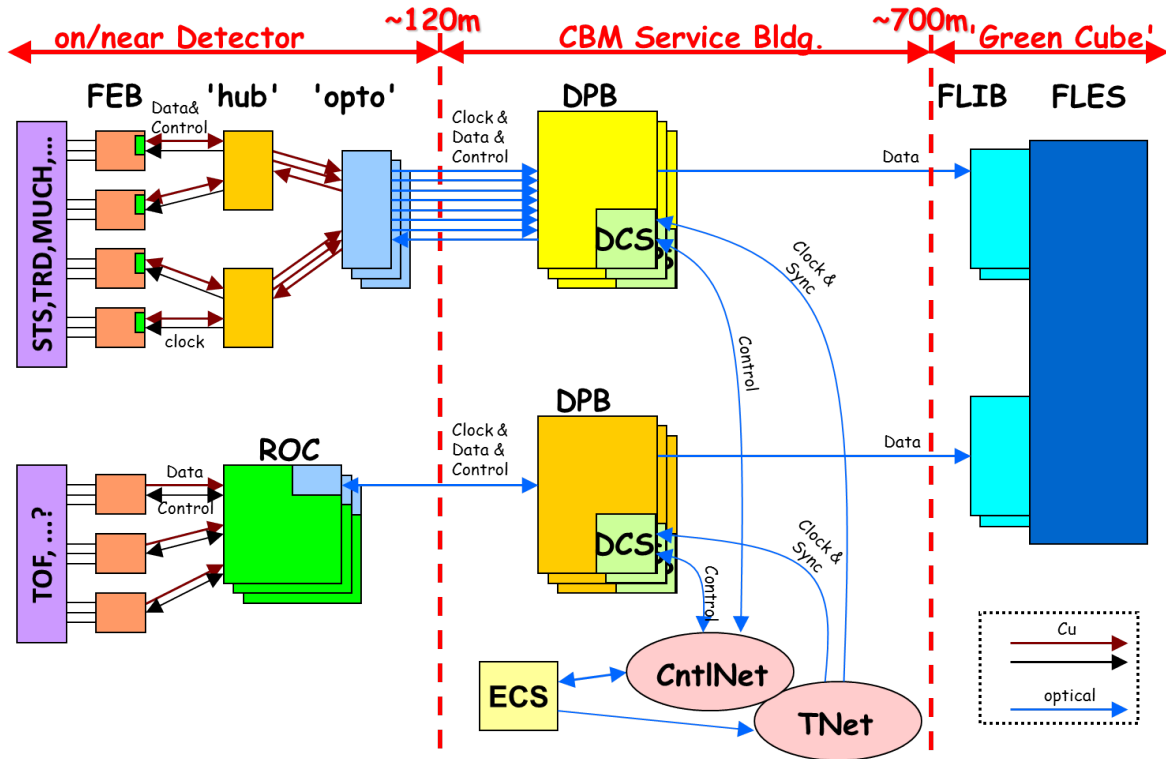


Figure 2.6: CBM FEE/DAQ tree concept. Data are pushed from the FEE on the left side through one or more layers of data combining/processing nodes toward the FLES. This last one is hosted in the GSI “Green Cube” computer farm and uses First Level event selector Interface Board (FLIB) to receive data from the experiment. The ‘hub’ and ‘opto’ are ASICs dedicated to the readout of Front-End Boards (FEB) while the ReadOut Controller (ROC) is based on FPGA boards. Figure taken from [38]

The main advantage of this new readout scheme is that almost any complex physics signal can be used to select events, allowing to easily add new selection criteria not planned in the initial design. The other advantage is that no “readout deadtime” exist in such a system, as long as the transport network and the buffer depth at each readout level are properly dimensioned. The only remaining “deadtime” is the intrinsic double-hit capability of the FEE. This concept allows to reach the high interaction rates in the order of MHz planned for CBM. Combining both of these advantages is what makes the high statistics

measurement of rare probes described in Sections 2.2 and 2.4.2 possible.

Of course, this new readout concept brings also new constraints. The first one is that all units performing the time stamping of the data have to be synchronized by a common clock, precise at the nanosecond level on the full experiment scale. This is required in order to merge the incoming continuous data streams at the event builder level. The event building also brings strong constraints on the input buffers and input network routing of the FLES. Contrary to a triggered system where the data packets come by bunch and are synchronized by event number, here the only way to re-align the data stream is to use the messages timestamps and gather all matching data in a common computing node. Another constraint is that some data rate monitoring has to be implemented at each readout level, together with an automatic procedure in case of buffer overflows. Otherwise, due to the self-triggered FEE, a single oscillating readout channel could saturate all layers of its readout chain. If this was to happen in different parts of the setup simultaneously, the situation may arise that these parts lose data in an alternating way and most events become incomplete. To prevent this, each readout layer must be able to mark a part of the data as incomplete and assign different priority to messages in case of saturation. Three types of messages are present in the CBM network: data messages, time synchronization messages and control messages (error, commands, ...). Losing a data message has less consequence than losing a synchronization marker or an error message. The first readout layer also needs to have the ability to switch off a FEE channel automatically, by increasing the FEE channel threshold, masking the channel at the FEE internal readout level or masking the full FEE chip at the first readout layer level. The last constraint is on the software used for the event selection. As it will use high level event reconstruction, it need to be as close as possible to the offline analysis software to ensure a good selection quality. In the same time it has to be optimized for speed and low resource consumption due to the huge amount of raw data to process.

Fig. 2.6 presents the CBM FEE/DAQ tree concept and the transfer link lengths involved in this specific case. For the longest one, total data rates of 100 GByte/s to 1 TByte/s are expected for the highest interaction rate/beam energy combinations, corresponding to a minimum bias event size between 10 and 100 kByte (setup and beam energy dependent). The writing capability is estimated to be 1 GByte/s. Thus the online selection has to provide event selection factors between 100 and 1000. In parallel to the unidirectional data network, a bidirectional network is used as Control Network (CntlNet) and a unidirectional one is used as Time Network (TNet) to provide the common clock to all readout components. These additional networks are monitored and controlled by the Experiment Control System (ECS).

2.4.2 Use-case study for CBM-TOF free-streaming data: anti-proton selection

To give an impression of the possibilities that such a high rate experiment offers even at the SIS100 machine, the case of anti-protons is discussed in the following.

Anti-protons are interesting both in themselves and as decay product of anti-hyperons.

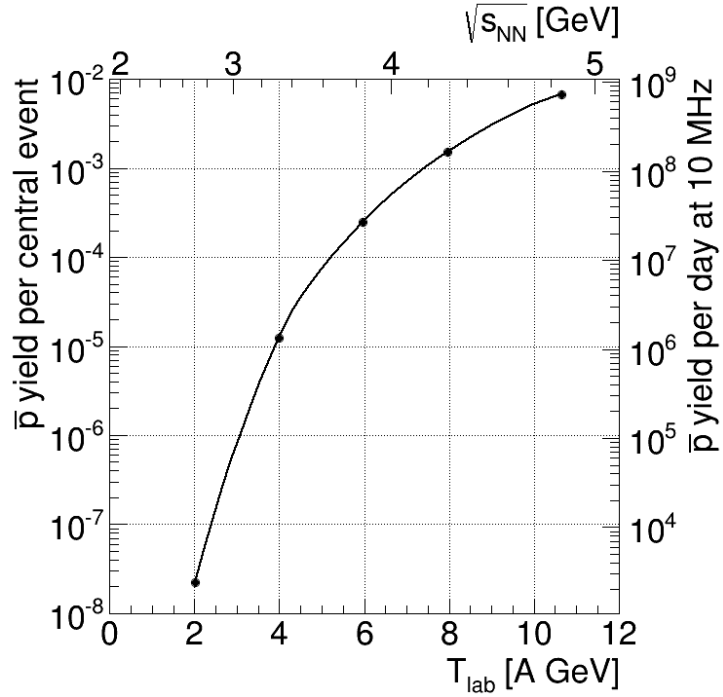


Figure 2.7: Antiproton production probability in central events (left axis) and yield per day(right axis) at an interaction rate of 10 MHz for Au + Au collisions as function of incident beam energy (bottom axis) and available energy in the CMS (top axis). Figure taken from [20], values from [11].

The production threshold for anti-protons in a free nucleon-nucleon interaction is as high as $\sqrt{s_{NN}} = 3.76$ GeV, corresponding to a beam kinetic energy of 5.65 A GeV. Thus the production of anti-proton at a beam energy of 4 A GeV is already sub-threshold and involves multi-step processes. Measuring the production cross-section could provide information about the medium in which the anti-protons were formed. The detailed measurement of the anti-proton collective flow for the SIS100 energy range is interesting, especially if sufficient statistics is obtained to study its dependences on rapidity and transverse momentum. A better knowledge of these dependences would allow to resolve ambiguities between the different contributions to the anti-proton yield, i.e. absorption, annihilation, scattering and potentials. The typical requirement for a significant differential flow measurement is a mean statistics of 10^4 counts per bin. This means that global statistics in the order of 10^5 identified anti-protons per energy and collision system are required.

A selection of events containing anti-proton would also select all events where other anti-baryons with decays containing anti-protons are present, thus enhancing the anti-hyperon content of the event sample.

Fig. 2.7 presents the yields per central event obtained from a thermal model calculation and the corresponding identified anti-proton statistics obtained for a day of operation at 10 MHz interaction rate assuming an anti-proton PID efficiency of $\epsilon = 0.5$. One can observe that the predicted yield drops quickly for sub-threshold energies, but that sufficient statistics can still be obtained within a few days in these conditions for a beam

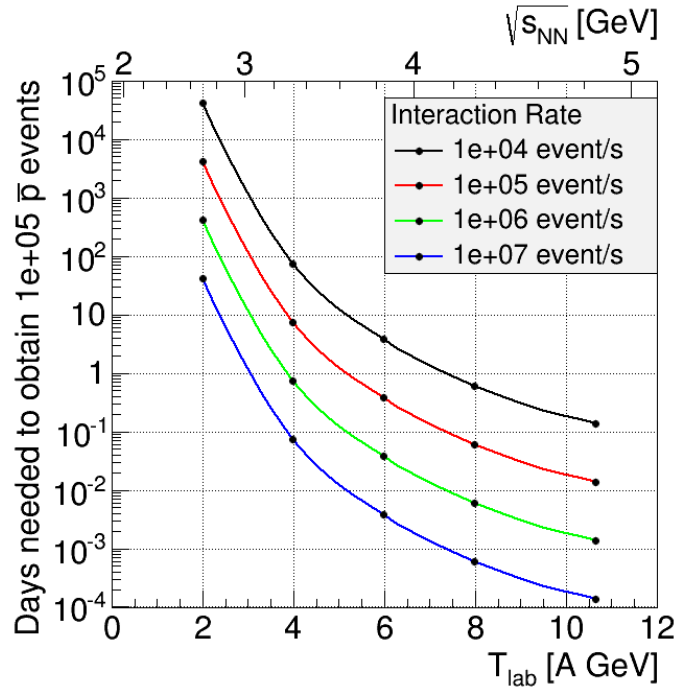


Figure 2.8: Acquisition days needed to achieve a statistics of 10^5 \bar{p} events as function of beam energy for Au+Au collisions. Yield values are from [11].

energy of e.g. 4 A GeV.

However, the online selection is a necessary condition to operate at 10 MHz interaction rate, as CBM data archiving capability will be limited at around 10^5 minimum bias events per second. For anti-proton the online selection is only possible by using the track fitting from STS and the PID obtained from TOF. Lower interaction rates can also be considered, where only the event building is needed.

Fig. 2.8 demonstrates the principle feasibility of the measurement of an anti-proton excitation function when using a free-streaming system. This plot shows the number of data taking days needed to obtain the required 10^5 anti-protons as function of beam energy and for different interaction rates. The anti-proton PID efficiency is the same as for Fig. 2.7. The SIS100 accelerator does not allow for parallel operation, so the available beamtime has to be shared between the four FAIR experimental pillars. If the periods without available beam for experiments (e.g. maintenance, ...) are also taken into account, the total CBM beamtime with this machine will be limited to approximately 60 days per year. Ten days is therefore a reasonable estimate for the maximum duration of data taking for a single (system, energy) point, most of the data points being acquired in a shorter time. From Fig. 2.8 it is clear that for energies above 4 A GeV, saving all minimum bias events without any event selection at an interaction rate of 100 kHz would be sufficient to obtain the desired statistics within a time limit of ten days. Lower energies can be accessed by using higher interaction rates: for example the 10 MHz maximum interaction rate permits to stay under ten days of acquisition at 2.5 A GeV. The high rate possible in CBM therefore allows in principle for the necessary systematic studies.

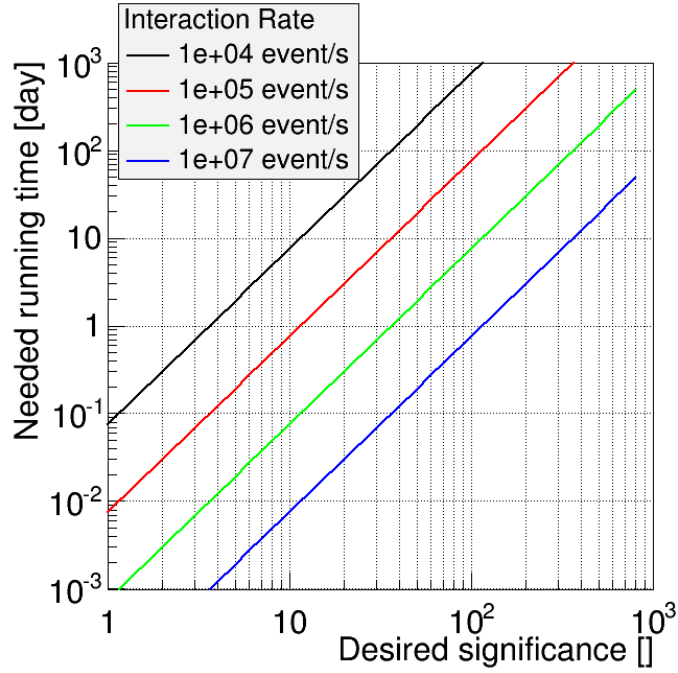


Figure 2.9: Acquisition days needed to achieve a specified significance for the anti-proton signal, for different interaction rates, Au+Au collisions and a beam energy of 4 A GeV. An anti-proton PID efficiency of 50% and a signal over background ratio of 0.01 are used. Anti-proton yield values are from [11].

However, the criteria for a successful measurement is the significance of the anti-proton signal. The significance Σ can be expressed as function of the signal over background ratio S/B as in Eq. 2.2.

$$\Sigma = \frac{S}{\sqrt{S+B}} = \sqrt{S} \frac{\sqrt{S/B}}{\sqrt{1+S/B}} = \Sigma_0(S) \frac{\sqrt{S/B}}{\sqrt{1+S/B}} \quad (2.2)$$

As reference for measurements one can take the significance in the case where there is no background, $\Sigma_0(S)$. Current full system simulations of CBM indicate that the S/B value can be as low as 0.01 for anti-protons. This currently seems to be the limit for the extraction of a valid signature, since otherwise the background cannot be controlled sufficiently well by event mixing. According to Eq. 2.2, with this S/B value and for an equal number of detected anti-protons, the significance of the signal is a tenth of $\Sigma_0(S)$. Therefore, a hundred times more statistics are required to obtain a significance equivalent to the reference case.

The necessary increase of statistics can be obtained in the same acquisition duration by increasing the interaction rate. As an example, Fig. 2.9 presents the acquisition duration needed to obtain a significance value at a beam energy of 4 A GeV for a S/B value of 0.01 and different interaction rates. The reference significance obtained for 10^5 signal counts without background is ~ 316 . In the figure, one can see that even for the low S/B value,

it is possible to obtain an equivalent significance value for the anti- proton signal while keeping the acquisition duration under ten days by using the maximal interaction rate of CBM of 10 MHz instead of the 100 kHz required when no background is present.

The high rate capability of CBM therefore enables the measurement of the excitation function of anti-protons into the sub-threshold region.

Chapter 3

The CBM Time Of Flight Wall

Charged hadron identification in CBM is realized using the Time Of Flight method. Section 3.1 will explain how particle identifications can be obtained with the TOF method. The general requirements on the performance and characteristics of the CBM TOF system are derived in Section 3.2 from the particle identification requirements and from the most extreme running conditions at SIS100 and SIS300.

Section 3.3 motivates the choice of timing Multi-gaps Resistive Plate Chambers (MRPC). This is done by describing their structure, working principle and typical performance. General considerations on the electronics used for the readout of timing MRPCs are given in Section 3.4, followed by the requirements for the electronic chain in CBM specific case and by descriptions of the two main calibration procedures needed to process the data from this electronic chain.

Finally, Section 3.5 briefly introduces the current conceptual wall design as defined in the CBM TOF Technical Design Report.

3.1 Charged Hadron identification in CBM

The charged hadron identification with the Time Of Flight (TOF) method requires the measurement of the particle momentum p , the sign of its electric charge and its velocity (cf. Eq. 3.1). The velocity is obtained by measuring the time T needed by the particle to travel a known distance L .

$$m^2 = \frac{p^2}{c^2} \left(\frac{c^2 T^2}{L^2} - 1 \right) \quad (3.1)$$

Using the magnetic field from the dipole magnet, the data points in the STS detector deliver the track parameters, which include the momentum and sign of the charge of the particle. The track is then extrapolated toward the TOF wall, where it is associated with the closest measured TOF hit, delivering the path length L . The TOF hit provides a time T_1 , from which the reference time T_0 has to be subtracted to obtain the time of flight. In case the TRD is present in the setup, its position information can be used to improve the track extrapolation.

The main contribution to the deviations between the assigned mass and the real particle mass is due to the time resolution of the system (see Section 1.3). If σ_T is the time resolution, the resolution on the squared mass can be expressed as:

$$\sigma_{m^2} = 2p^2 \frac{T}{L^2} \sigma_T \quad (3.2)$$

It can be remarked that as this expression does not contain the particle mass, the mass resolution will be in first order the same for all particles having the same momentum. Due to the quadratic dependence on the momentum, the mass separation between particles species with adjacent masses will be smaller than the combined widths of their m^2 distributions for high momenta, leading to misidentification.

With the TOF method, particles can be identified on two levels: either on a single track basis or on a statistical basis. To identify the species of single tracks, some boundaries are defined in the (p, m^2) plane. The efficiency and purity corresponding to these cuts are estimated by using simulated data, where the real particle species of a track is known from the Monte-Carlo generator. The efficiency is obtained by applying the cuts to all tracks originally belonging to a selected particle species. The purity is estimated by applying the same cuts on all tracks having the same charge sign as the investigated particle species. The purity value is then calculated as the fraction of tracks truly belonging to the chosen particle species among the tracks selected by the cut. An example of this kind of identification cuts is shown in Fig. 3.1 for positively charge particles in a simulation with 100k central Au+Au collisions at 25 A GeV. In order to obtain the cut values, a Gaussian distribution was first fitted to the m^2 distribution of single particle species in different momentum bins. The $\pm 3\sigma$ values of the Gaussian distribution are then used as lower and upper boundaries for this particle species in each momentum bin. The single particle species distribution can be produced in simulated data using information from the Monte-Carlo generator. The boundaries in the (p, m^2) plane obtained for pions, kaons and protons are plotted on top of the positive particles distribution for illustration.

For the identification on statistical basis, one assumes that the m^2 distribution of each species in a momentum bin can be described by a Gaussian centered around its nominal mass and having the squared mass resolution from Eq. 3.2 as width. A combination of the Gaussian distributions of all expected species can be fitted to the measured m^2 distribution for all tracks in a momentum bin. As all species share the same squared mass resolution for a given momentum, the only free parameters are the amplitudes of each species and the common width of the Gaussian distributions. Once all momentum bins are fitted, a probability to be of a specified particle species can be assigned to the tracks depending on their measured momentum and m^2 . An example of this kind of momentum bins fit is shown in Fig. 3.2. From the (p, m^2) distribution of reconstructed tracks in a simulation of 200k Au+Au collisions at 25 A GeV, the squared mass spectra in three momentum bins was extracted and fitted with three Gaussian corresponding to pions, kaons and protons. While the kaons are well separated from the pions and protons in the plots corresponding to momenta of 1 and 3 GeV/c, a statistical unfolding is needed to estimate their yields for higher momenta, as in the 5 GeV/c spectra displayed in the bottom right plot.

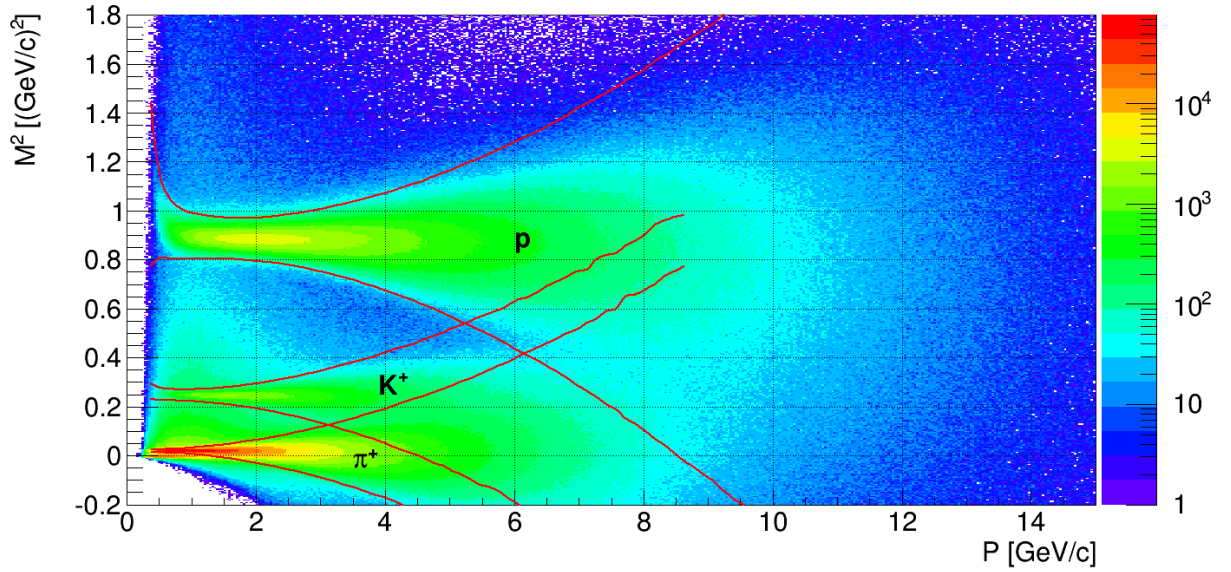


Figure 3.1: M^2 versus momentum for reconstructed tracks in a CBM simulation. The simulation contains 100k events in central Au+Au collisions at 25 A GeV. A 80 ps time resolution and a realistic TOF wall geometry (see Section 5.4) were used. The red lines represent hypothetic PID cuts obtained by the 3σ value of a Gaussian fit in several momentum bins of the single species distribution for pions, kaons and protons. Simulation data from [39]

3.2 Requirements for the CBM TOF Wall

In CBM, the nominal position of the TOF system is at 10 m from the target. It has to provide an angular coverage matching the STS acceptance: 2.5° to 35° along the X axis and 2.5° to 25° along Y axis. A wall of 9 m height and 13.5 m width is designed in order to fulfill this criteria. At the nominal distance from target, a full system time resolution of at most 80 ps is required to identify kaons of 5 GeV/c momentum with a reasonable purity of 50%. This time resolution value includes all possible contributions, e.g. the detector itself, electronics jitter, channels alignment and the T_0 time reference. Therefore, the detector time resolution for a single channel has to be below 60 ps. A detection efficiency of 95 % or better is also needed. If possible, the wall should also be movable along the beam axis to adapt to the different running conditions. For example at SIS100 energies, a TOF wall at a distance of 6 m from the target improves the particle identification efficiency for kaons, since some of them decay in-flight before reaching the wall.

Two of the constraints for the detector choice and the detector design are the particle flux and the hit density for central events in the CBM typical collision system (25 A GeV Au+Au). The strong flux constraint stems from the most extreme CBM interaction rate of 10 MHz needed to measure rare probes as for example J/Ψ and Ψ' with sufficient statistics, while the hit density constraint originates from the double hits in readout channels during central events at similar conditions.

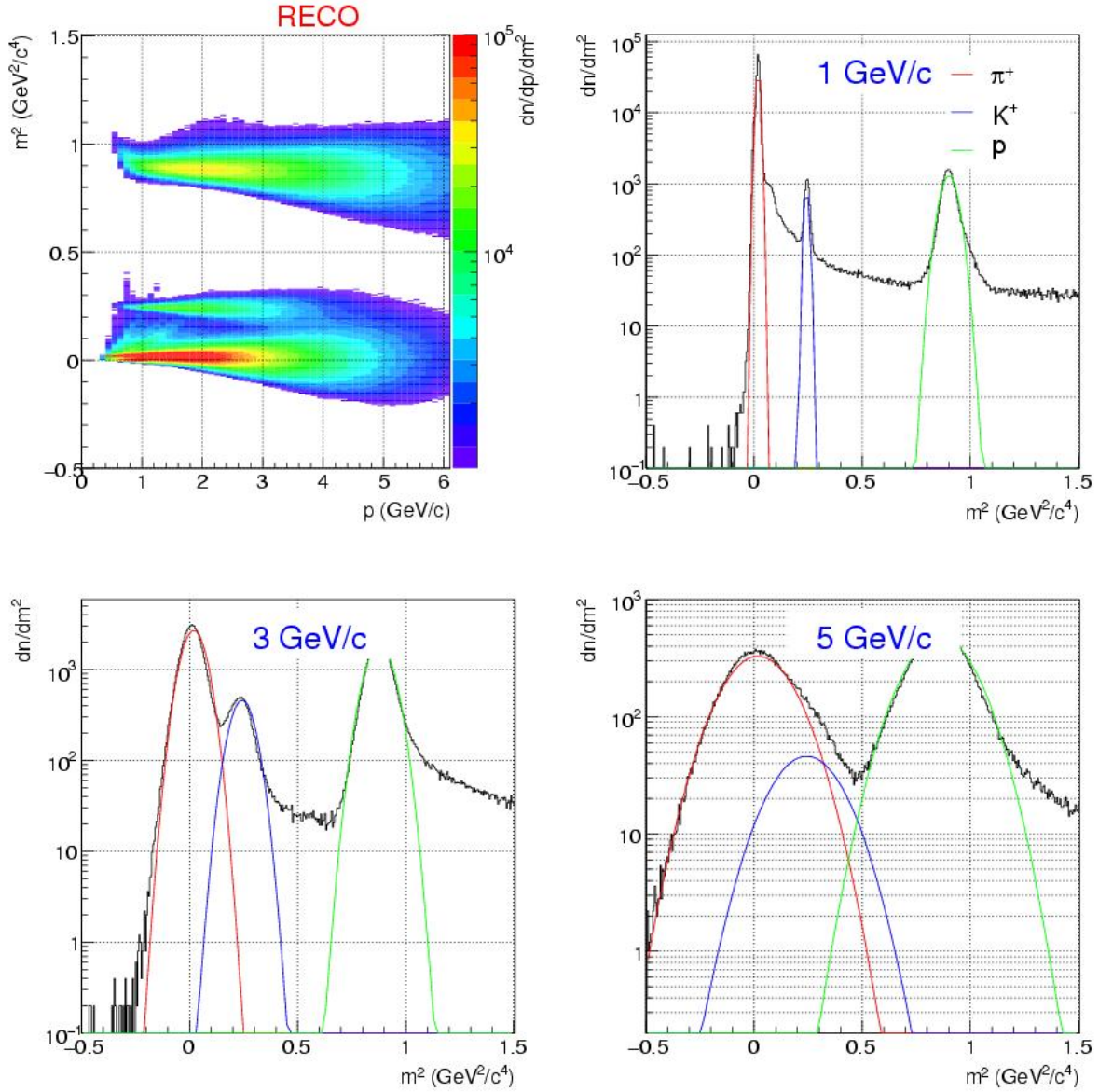


Figure 3.2: m^2 versus momentum plot for reconstructed tracks assuming 80 ps time resolution (200k events, central Au+Au collisions at 25 AGeV). In addition mass spectra for momentum bins at $p = 1, 3$, and 5 GeV/c are shown. Tails are due to mismatches and double hits in TOF. Figure taken from [6].

The particle flux in units of kHz/cm² along the X and Y axis for typical CBM running conditions at SIS100 and SIS300 is shown in Fig. 3.3. It was obtained by simulating minimum bias Au+Au collisions for a TOF wall placed at 6 m from target at a beam energy of 10 A GeV (SIS100 conditions, in blue) and for a TOF wall placed at 10 m from target at a beam energy of 25 A GeV (SIS300 conditions, in red). It can be seen that some of the detectors will have to withstand fluxes up to 50 kHz/cm² while most of the wall will stay under 10 kHz/cm². One can also remark that the flux requirements do not increase when going closer to the target for lower energies. Therefore, detectors

designed for SIS300 conditions are suited for a wall at a 6 m distance from the target in SIS100 conditions. Note that the high flux values above 100 kHz/cm^2 (between $X = 0$ and $X = 50 \text{ cm}$) are due to an artefact of the event generator which does not fragments properly the projectile and instead separates it into free protons and neutrons.

In order to limit the proportion of possibly distorted hits, a double hit probability per readout channel of less than 5% is required for the TOF wall. This leads to constraints in the granularity of the counters. The highest probability for multiples hits is found in central events. The hit multiplicity per central event and cm^2 along the X and Y axis for both SIS100 and SIS300 typical cases is presented in Fig. 3.4. From this multiplicity, it is possible to obtain the maximal area per readout channel. For example, a multiplicity value of 10^{-2} hits per event and cm^2 close to the beam pipe leads to a maximal channel area of 4 to 5 cm^2 in the innermost part of the wall (close to the beam pipe). An estimation of 100k readout channels was made when taking these constraints into consideration.

In order to fulfill the above mentioned requirements, it was decided to use Multi-gap Resistive Plate Chambers (MRPCs) to build the wall. MRPCs have the additional advantage that the cost per readout channel is about 100 €, which is far less than all alternatives (plastic scintillators, diamond, ...). The MRPCs and their typical signal acquisition systems will be presented in the following sections.

3.3 Multi-gap Resistive Plate Chambers

The Multi-gap Resistive Plate Chambers (MRPC) are a type of gas detectors that can be used for timing purposes. A cross-section of a typical MRPC design is shown in Fig. 3.5. As the name suggest, MRPC are based on a stack of gas-gaps. The gas gaps limits are defined by parallel plates made of a resistive material. The typical bulk resistivity of the materials used for timing MRPCs is between 10^9 and $10^{13} \Omega\text{cm}$. Float glass is a commonly used material for the resistive plates, with a bulk resistivity around $10^{13} \Omega\text{cm}$. Different kind of spacers are used between the resistive plates to maintain the size of the gas gap over the full detector area. Fishing lines are often used for this purpose. High voltage (HV) electrodes placed outside the stack of resistive plates are used to create a uniform electric field across the gas gaps. The output signal is obtained on readout electrodes placed behind the HV electrodes and separated from these by an insulator.

In many aspects MRPCs can be approximated as the simple superposition of single gas gaps. Therefore a single gap configuration will be used to explain the working principles of the detector before discussing the benefits of the multi-gap configuration.

Working principle of a single gap timing RPC

The working principle of a single gap RPC is sketched in Fig. 3.6 through four steps and two possible situations. In this sketch the green bands represent the resistive plates, the black bands the HV electrodes, the gray bands an insulator and the orange bands channels in a copper readout electrode. The typical size of the gap between the resistive

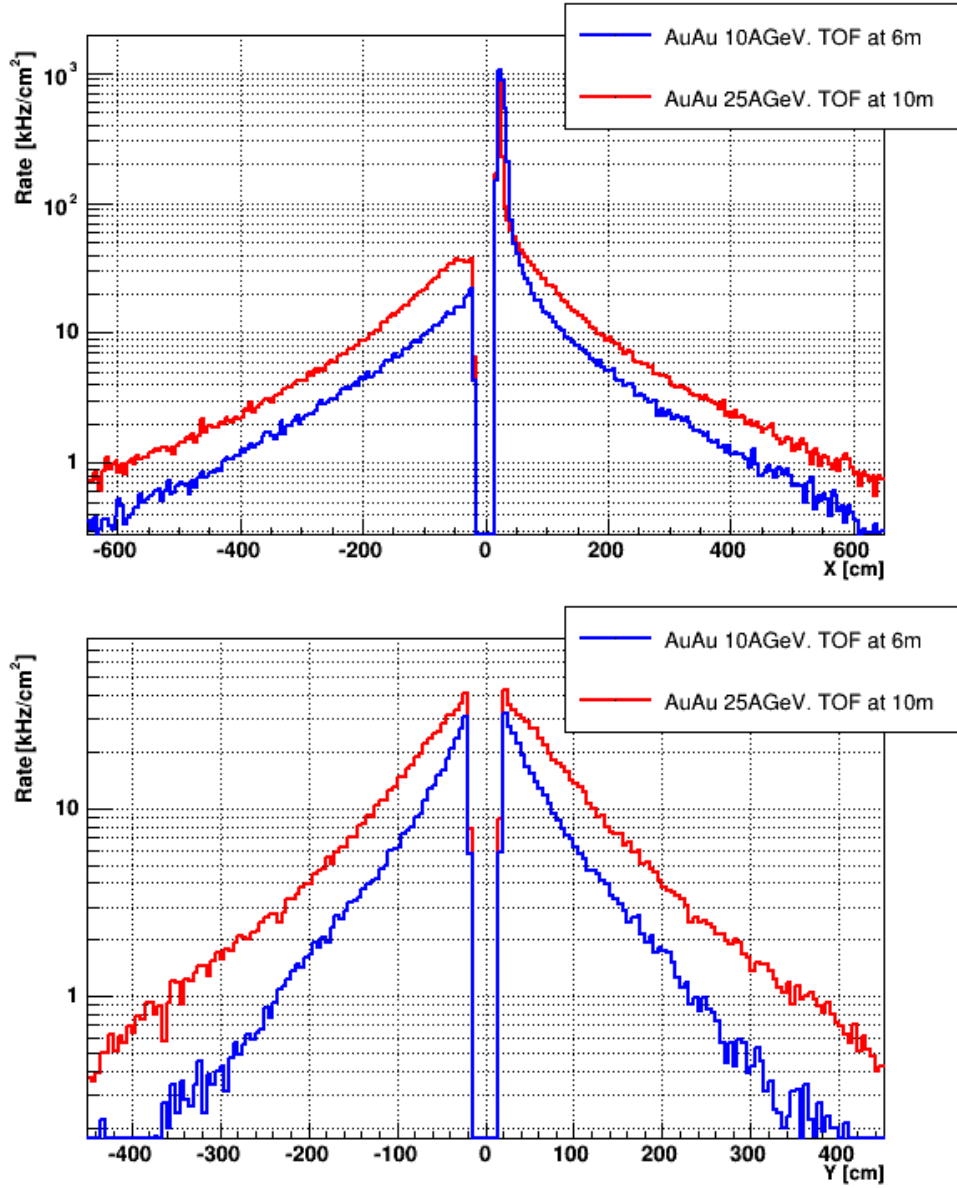


Figure 3.3: Calculated particle flux in the CBM TOF wall placed 10 m (red) and 6 m (blue) behind the primary interaction point using as event generator URQMD and a target interaction rate of 10 MHz minimum bias Au+Au reactions at two different incident energies, depicting the running conditions at SIS300 (red) and SIS100 (blue). The particle flux includes the contribution of secondary particles produced in the upstream material of CBM. Upper part: Flux as function of X at Y=0 (i.e. left/right of the beam axis), the X-axis also defines the deflection plane of the particles' trajectories in the magnetic field. Lower part: Flux as function of Y at X=0. Figure taken from [20].

plates is a few hundred μm . When a high voltage is applied between the anode and cathode electrodes, the resistive plates charge up, leading to the formation of the electric field E_0 . Typical field values are around 100 kV/cm. When a charged particle cross the

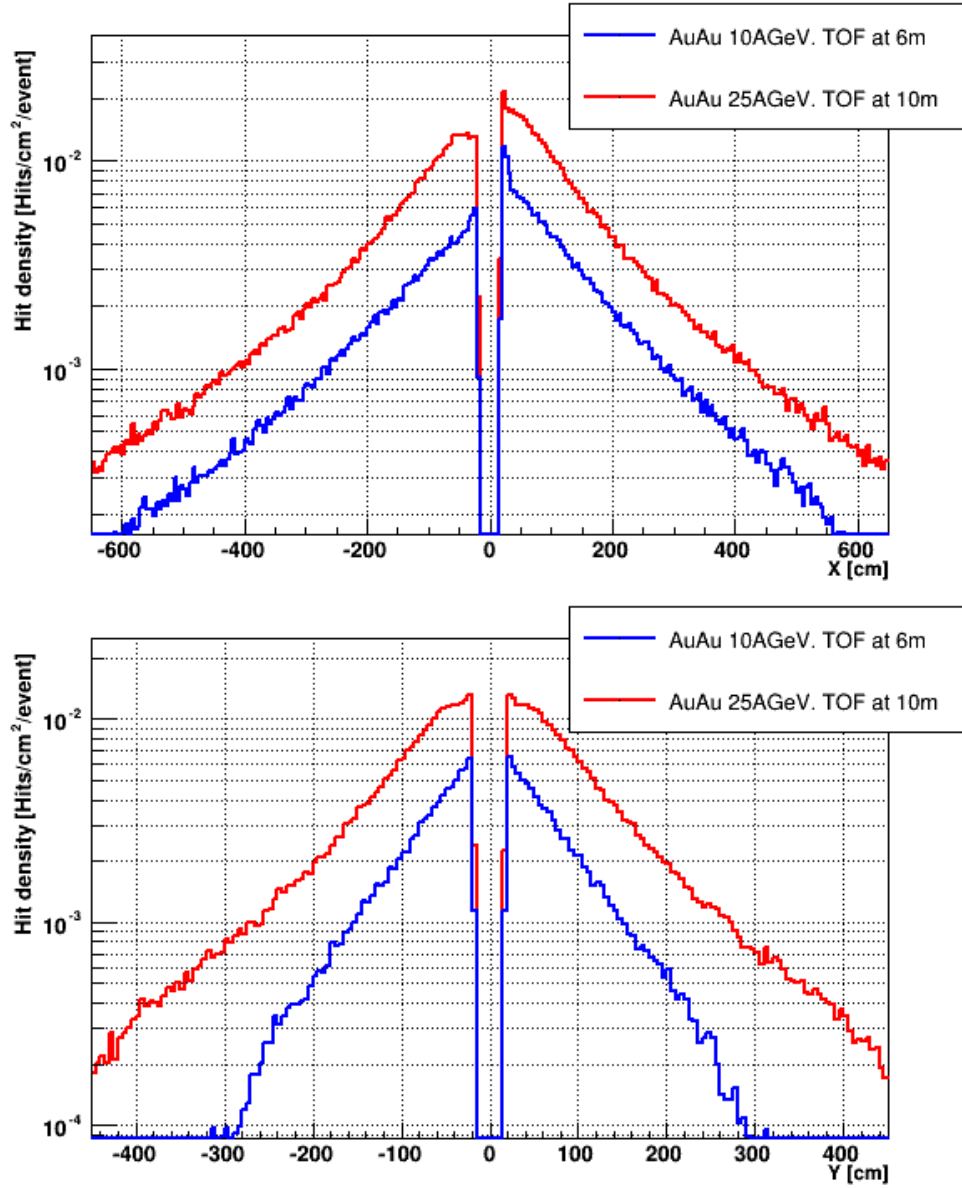
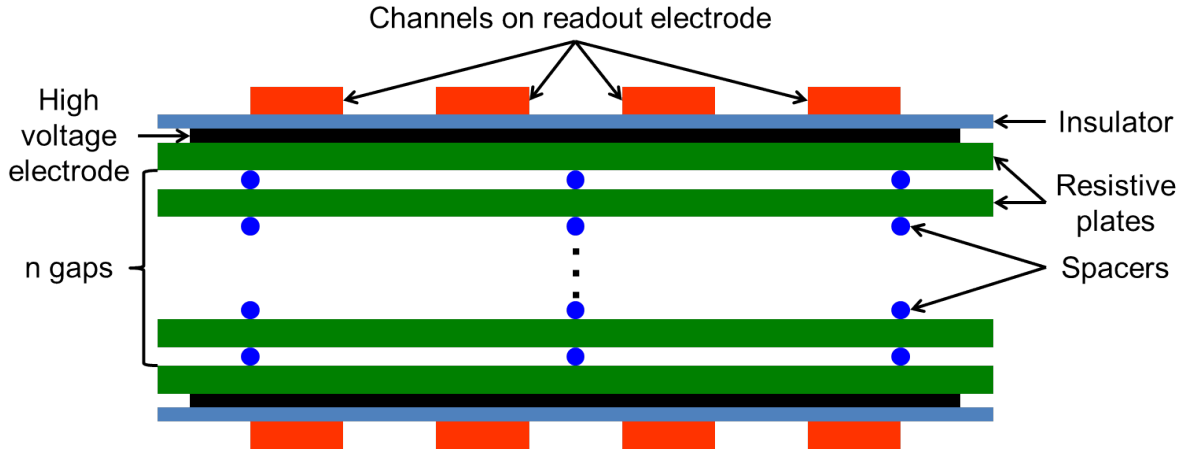


Figure 3.4: Hit density (hits/cm²/event) of primary and secondary charged particles in central Au+Au collisions at an incident energy of 25 A GeV with the TOF wall at a distance of 10 m from the target (red) in comparison to the situation at 10 AGeV, 6 m. (top panel: as function of X, bottom panel: as function of Y, cf. Fig. 3.3). Figure taken from [20].

gas gap, it can interact with the gas molecules and ionize them, as visualized in sub-figure (a). Each ionization create a pair of electron and ion. Due to the high electric field, the electrons drift with increasing velocities toward the anode. When they have gained sufficient kinetic energy, they can ionize other gas molecules. The newly generated electrons then go through the same process, leading to the formation of the so-called avalanche. Meanwhile, the ions drift also toward the cathode, but with a much smaller


 Figure 3.5: Example of the structure of a typical MRPC with n gaps.

velocity. Therefore they do not contribute significantly to the avalanche growth. The moving charges in the gap induce a signal on the readout electrodes, which is positive on the cathode side and negative on the anode side. The avalanche growth and signal induction are illustrated in sub-figure (b). The electrons then reach the resistive plate on the anode side while the ions are still inside the gas gap (cf. sub-figure (c1)). The ions also reach the surface of the opposite resistive plate. The charge accumulation leads to a reduction of the local electric field on this particular place, as pictured in sub-figure (d1). This reduces the gain in the gas gap and produces a temporary blind spot until all charges have drifted through the resistive plates. The time needed to eliminate the charges limits the rate capability of the counter and depends on the resistivity of the plates.

The right part of Fig. 3.6 describe a side effect of the avalanche that one tries to avoid. As part of the avalanche process, photons are emitted isotropically on the UltraViolet (UV) range. These photons can generate secondary ionizations, leading to further avalanches, until a conductive tunnel is created. This process is called streamer and is depicted in sub-figures (c2) and (d2). The streamers generate larger signals than the normal avalanches and have more readout channels firing. This leads to higher electronics channel multiplicities and a bigger dead area, thus limiting the rate capability. In the worst case streamers can even develop into a spark. To limit the streamers probability, a gas quenching UV photons (usually iso-butane) is added to the gas mixture. A gas mixture often used for timing MRPC is 85% Tetrafluoroethane, 10% SF_6 and 5% iso-butane. This is the mixture used by the CBM-TOF group for its tests.

Multi-gap RPC properties

In the multiple gap RPC configuration, the internal resistive plates are left electrically floating. These plates then get charged up electro-statically until an equal electric field is achieved in all gas gaps. In normal operation, there is no net charge gain due to the avalanches on any of these plates: the electrons from avalanches in the gap on the cathode side recombine with the ions from avalanches in the gap on the anode side. Therefore, all

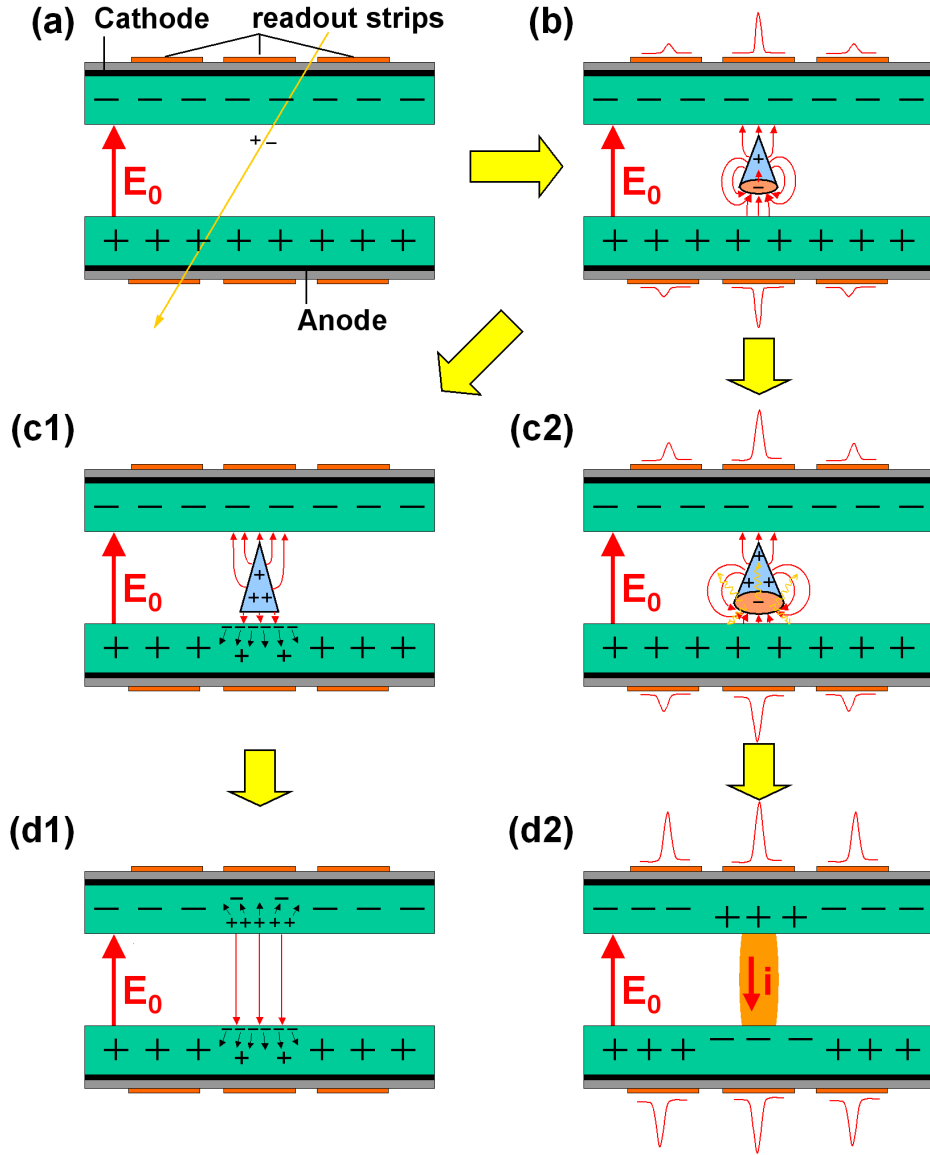


Figure 3.6: Working principle of an RPC. (a) A traversing particle (thin yellow arrow) ionizes the gas in the gap. (b) Electrons and ions drift towards the electrodes developing an avalanche and inducing a signal in the readout electrode. (c1) Since the drift velocity of the ions is much smaller than for the electrons their contribution to the signal is negligible. (d1) The charges are deposited on the surface of the resistive material building up an opposite electric field. This temporarily leads to a blind spot in the counter which is limiting the rate capability. (c2) At certain conditions and with a certain probability an avalanche can develop into a streamer (d2) leading to very large signals in the readout electrode. Figure taken from [40].

gaps can be considered as identical. The efficiency can be defined as the percentage of crossing particles which generate a signal above the electronics threshold. Naively, if ϵ is the efficiency of a single gap, the efficiency for an n - gap detector scales as $1 - (1 - \epsilon)^n$.

In fact the real efficiency obtained is higher because signals from different gaps can add up and produce an induced signal above the electronics threshold. Detector efficiencies in the order of 99% are obtained with 8 to 10 gaps counters. Typical time resolution values for timing MRPCs are in the order of 50-70 ps including electronics [41] [42] [43] [44]. The world record for the time resolution without the electronics contribution is at 20 ps for a 24 gaps MRPC [45].

The main parameters for the construction of the MRPC are the number of gaps, the gap size, the readout channel design, the material of the resistive plates and their thickness. The number of gaps influence the efficiency and resolution of the counters. The gap size is linked to the time resolution. The readout electrode can be designed either as a pad which is readout on only one side or as a strip which is readout on both ends. The strip readout allows to extract the position along the channel by using the time difference between the signals on each end. This is however at the cost of a doubling of the number of electronic channels and of a signal size reduced by half at the electronics input. For the readout of the MRPC, two concepts exist (see Fig. 3.7):

- One possibility is to readout signals on only one electrode. The signals are then acquired relative to the ground of the high-voltage system. This is called single-ended readout (Fig. 3.7a).
- The other possibility is to readout signals from both electrodes (Fig. 3.7b). These signals then have opposite polarity and the total amplitude is double compared to that of the single-ended readout. This is called differential readout. One constraint of this readout type is that the readout electronics need to be differential.

Finally the parameters of the resistive plates can be used to improve the rate capability.

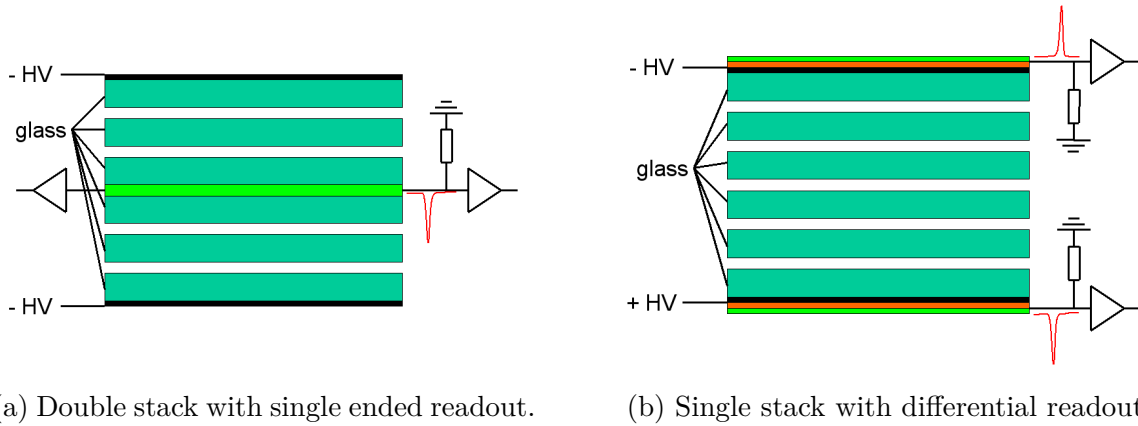


Figure 3.7: Readout types of MRPCs. Figures taken from [40].

Rate Capability

As mentioned earlier, the rate capability of MRPCs is linked to the time needed to remove the charge deposited on the resistive plates surface. A comparison between the CBM requirements and the results of different options to increase the rate capability was done in Ref. [46]. The summary figure of this comparison is shown in Fig. 3.8. Here, the

rate capability is defined as the particle flux for which either the time resolution becomes 20 ps worse or the efficiency gets 5% lower than the values obtained in the low (zero) flux case. The rate capabilities are plotted as function of the inverse of the resistivity: $1/\rho d$, with ρ the bulk resistivity of the plates and d the thickness of the plates. The values are normalized to those obtained for standard float glass: $\rho_0 d_0 = 300 \text{ G}\Omega\text{cm}^2$.

One can observe in this figure that existing designs already provide the rate capability to insure a coverage of the flux range expected for the CBM TOF wall. The best compromise between cost and particle flux capability for this application can be achieved by using in the same system MRPCs with different materials and readout channel geometries.

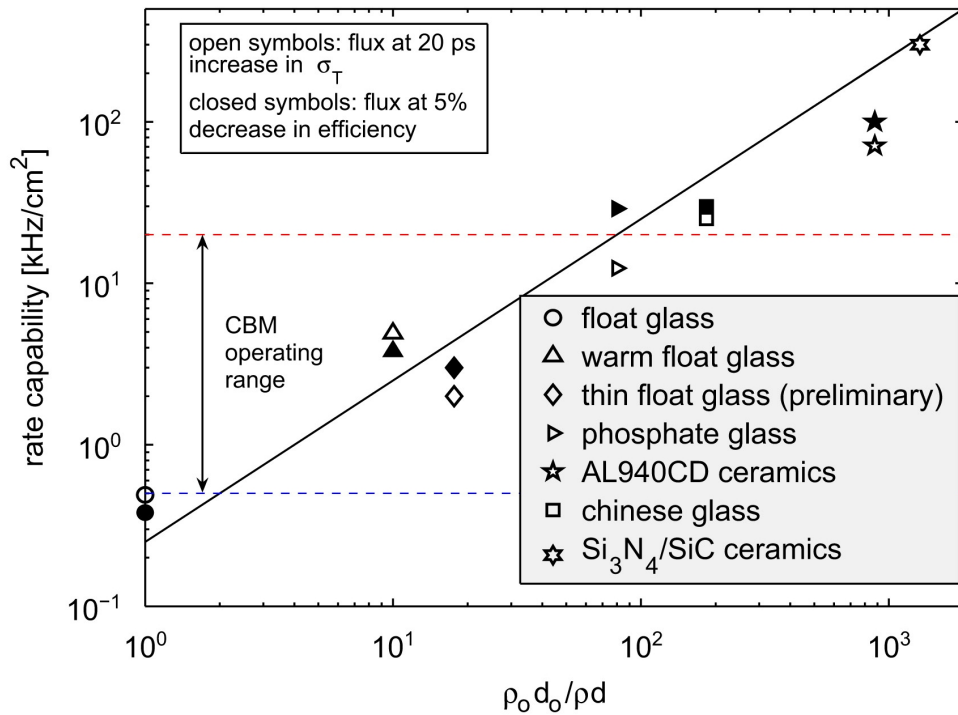


Figure 3.8: Measured rate capability (maximum operating flux) as function of $1/\rho d$ normalized to $\rho_0 d_0 = 300 \text{ G}\Omega\text{cm}^2$. Data taken from [47] (\circ), [48] (\triangle), [49] (\diamond), [50] (\triangleright), [51] (\star), [52] (\square) and [53] (\star). Figure is taken from [46].

3.4 Timing MRPC Signal Acquisition

3.4.1 Electronics

Timing MRPC signals have typically charges in the order of 10-300 fC and rise times in the order of 0.2-0.4 ns. Examples of MRPC signals measured through 100 Ω resistors are shown in Fig. 3.9. Signals from a strip MRPCs with a strip pitch in the order of 1 cm have amplitudes in the order of 20 mV. For thinner strips, the induced charge is spread over more than one readout strip, leading to signals in the order of 3-5 mV for a strip pitch in

the order of 2.54 mm. The Front-End Electronics (FEE) for a TOF system comprising different types of timing MRPCs has to cope with all these parameters.

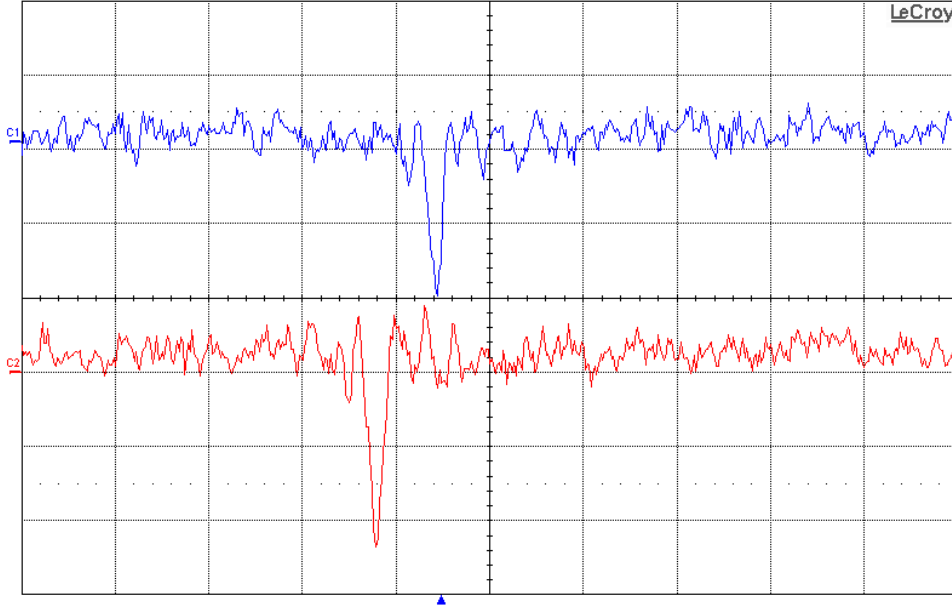


Figure 3.9: Example of signals from a differential strip MRPC. The signals are acquired with a differential probe through 100 Ohm resistors. Channel C1 (blue curve) is connected to one side of the strip and Channel C2 (red curve) to the other side. The scale on the abscissa is 5 ns/div and the scale on the ordinates is 10 mV/div in both channels.

Timing MRPC front-end systems usually have three stages: pre-amplification, discrimination and digitization. The pre-amplification and the discrimination stages are often placed on the same element of the readout chain (PCB or chip). In most cases leading edge discriminators are used because they are faster and cheaper in comparison to constant fraction discriminators. However, their timing signal is dependent on the signal size, the so-called “time walk” effect. In order to correct this effect, it is necessary to measure a parameter related to the signal size, such as the charge or the signal width. A more detailed description of the walk effect and its correction can be found in Section 3.4.4. For the signal width, the discriminator encodes the size of the input signal into the width of its output signal. A compatible Time to Digital Converter (TDC) is used to provide a timing for both edges of this signal. This is called the Time-Over-Threshold method (TOT). An example of a pre-amplified signal and the corresponding discriminated signal with TOT is shown in Fig. 3.10.

Discrete electronic components can be used for the pre-amplification and discrimination part of TOF systems based on MRPC as long as the channels counts is in the order of a few thousands. Example of this are the FEE5 used in FOPI (2400 channels) [54] and the DBO-STEP5 used in HADES (2232 channels) [55].

However, such implementations usually have some limits in terms of cost per channel, area used per channel and power consumption per channel. For systems involving in the order of 100k channels, as is the case for the existing ALICE TOF barrel ($\sim 160k$ channels) or for the CBM TOF wall ($\sim 100k$ channels), it becomes necessary to use Application-Specific

Integrated Circuit (ASIC) designs. One of such designs is the NINO ASIC developed for ALICE [56] and another is the PADI chip used in this work (see Subsection 4.2.1).

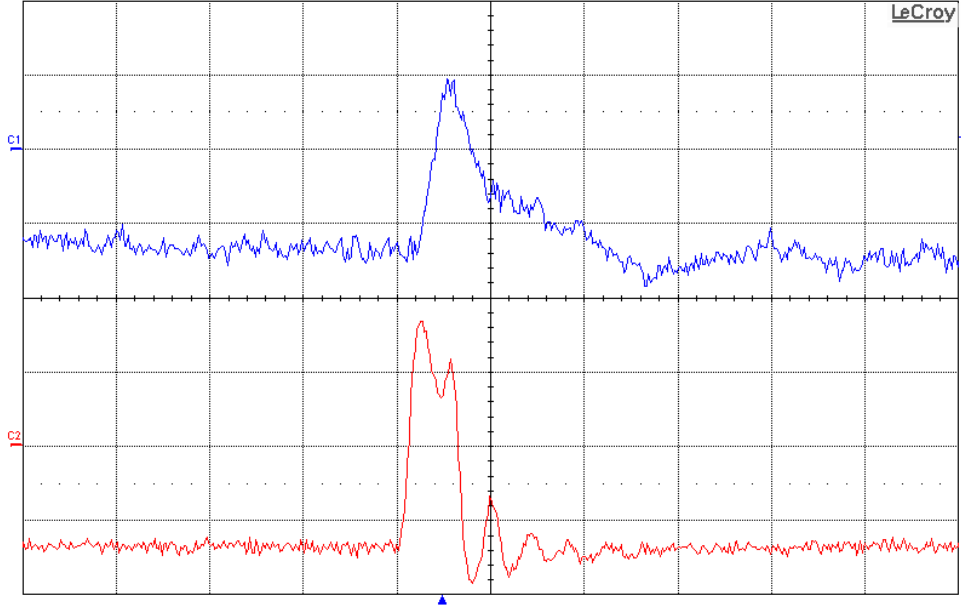


Figure 3.10: Example of processed signals from a differential strip MRPC. The signals are acquired using the PADI-3 ASIC and a differential probe. Channel C1 (blue curve) is connected to the analog output of the Pre-amplifier and Channel C2 (red curve) shows the discriminated signal. The TOT is encoded in the width of the discriminated signal. The scale on the abscissa is 5 ns/div and the scale on the ordinates is for C1 20 mV/div and for C2 100 mV/div.

The Time to Digital Converter (TDC) is usually realized by combining a clock cycle counter (coarse time) and a measurement with a finer time step within the clock cycle, called fine-time binning. In a system using this type of combination, the time resolution depends on the clock jitter, on the fine-time bins size and on how well the size of each bin is known (non-linearities, see Section 3.4.3). The fine-time measurement can be realized through many methods.

One of these methods is the direct encoding of the time of a signal edge relative to a common clock. The clock pulse is first sent through successive delay elements, the sum of the delays corresponding to the clock cycle. Each delayed clock and the input signal are used as input to a D type flip-flop (definition in Appendix C.5). By comparing the output value of adjacent flip-flops and looking for a polarity inversion, one can identify the delayed clock corresponding to an edge. The index of the delay element gives the position of the edge inside the clock cycle. If this position inside the clock cycle is combined to a clock cycle counter, one obtains a time position since the counter initialization. This is the method used for the CERN HPTDC [57] and the GET4 used in this thesis.

The TDC followed the same evolution in term of integration as the pre-amplification and discrimination stage. Solutions with multiple components were used for system with limited number of channels, as for example in the TACQUILA system used for the FOPI TOF barrel [54]. In more recent system developed for large systems, the full TDC is

implemented in an ASIC, e.g. the CERN HPTDC or the GET4 used in this thesis, or in a Field-Programmable Gate Array (FPGA), such as the VFTX used as reference system in this thesis and presented in Appendix B.4.

3.4.2 Requirements for the readout chain

The requirement for the MRPCs developed for CBM is to reach a time resolution better than 60 ps. Assuming that the event reference time can be determined with a resolution better than 30 ps, the full electronic chain including the clock system should not have a resolution worse than 40 ps in order to meet CBM goal of an 80 ps global time resolution. The TDC itself should have a time resolution of 25 ps or better. Any improvement on the TDC time resolution would relax the constraints on the detector design

Another requirement for the Pre-amplifier and discriminator is to be fully differential. Combined with a fully differential MRPC, this reduces the influence of common mode noise, and therefore decreases the amount of signals not linked to a crossing particle. This is important because such fake hits are not filtered in a free-streaming system. The TDC has to be self-triggered and to have a free-streaming readout mode to match the CBM DAQ concept. Both of the discriminator and the TDC will use the TOT method, allowing to focus on a single digitizer and to simplify the operation of the readout chain.

In Section 3.2, estimations on the particle flux and limits on the channel size in the part of the wall closest to the beam were obtained. A mean particle flux of 50 kHz/cm² and a channel area of 5 cm² mean that an electronic channel in this part of the wall will have to acquire signals at up to 250 kHz. In order to accommodate spikes in particle flux and eventual noise with a sufficient margin, the requirement for the electronics is a maximal readout rate of 400 kHz/ch.

3.4.3 TDC calibration: Non-linearities

An ideal Time to Digital Converter would have a fixed bin size for all fine-time bins, corresponding to the main clock cycle duration divided by the number of available bins. Non-linearities correspond to the situation where one or more bins have a width differing from the nominal one. This can be caused by production variations in some of the elements used to obtain a finer time slicing from the clock period or be inherent to the TDC functioning principle itself (FPGA TDCs have variable bin width, see Appendix 4.2.5). The comparison of real bin size (blue) and ideal bin size (red) for all bins on a selected channel on a GET4 v1.0 board is presented as an example in Fig. 3.11 left plot. A comparison of the real bin position (blue) and the ideal bin position (red) is shown in the right plot. This chip has 128 bins and is nominally run with a 6.4 ns clock period, so the ideal bin size would be 50 ps.

Two quantities can be used to quantify the error induced if one use a fixed bin width in the data analysis: the Differential Non-Linearity (DNL) and the Integral Non-Linearity (INL). DNL are the deviation between the real width of a bin and its nominal width. It can be expressed either in time units (ps) or in nominal width units, which correspond

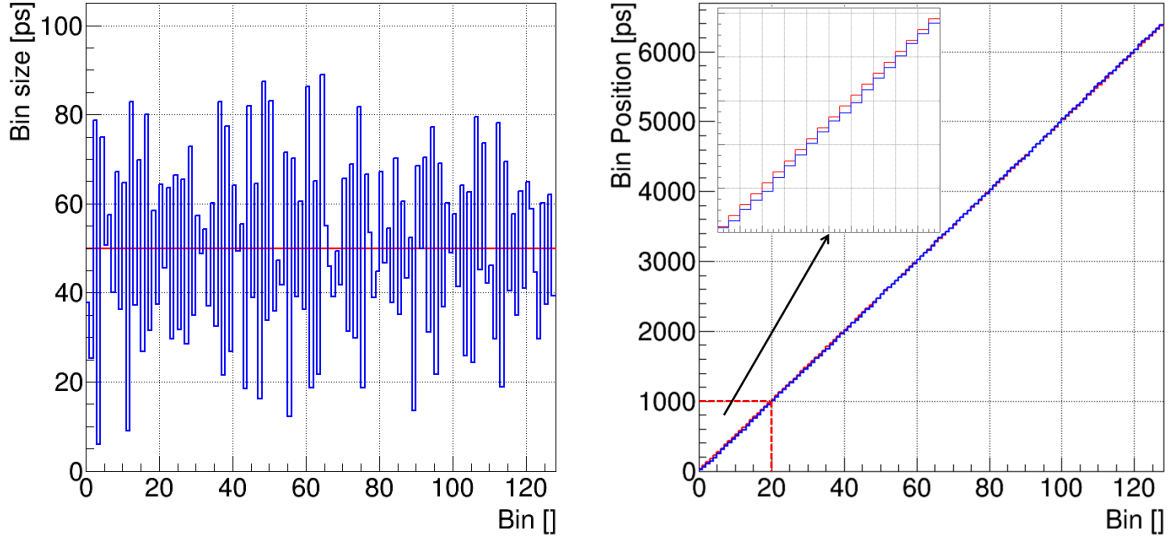


Figure 3.11: Bin size (left) and bin position (right) for a selected channel on a GET4 v1.0 board during cosmics tests. In each plot the blue line represent the real bin characteristic while the red one represent the ideal characteristic obtained when all bins have an equal size. The inset shows a zoom on the bin interval $[0,20]$.

itself to the width of the Least Significant Bit (LSB) in the fine-time counter. The DNL can be used to obtain an effective width for each bin and compensate this error. INL is the total deviation at a given bin from the nominal bin position in the fine-time range. It can be seen as the signed integration of the DNL from first bin up to a given bin. DNL and INL are usually different for each TDC timing unit, with some correlations when part of the fine-time mechanism is common (e.g. the common delay lines in the HPTDC). The DNL and INL values extracted from Fig. 3.11 for each bin are shown in Fig. 3.12.

A way to estimate the DNL and INL properties of a TDC and obtain correction values for each bin of each channel is to supply a random input signal as de-correlated as possible from the main clock to the TDC. The time distribution of such a signal would be flat inside a clock cycle. If enough entries are collected (typically 10000 Entries per bin), the resulting distribution among the fine-time bins would also be flat in the case of equal bin width and proportional to the effective width in presence of DNLs.

One can define the real width, $Size[bin]$, and position, $Pos[bin]$, of each bin to be used for the conversion from raw data to calibrated data, as:

$$Size[bin] = \frac{Entries[bin]}{\sum_{i=0}^N Entries[i]} \cdot T \quad (3.3)$$

$$Pos[bin] = \frac{Size[bin]}{2} + \sum_{i=0}^{bin-1} Size[i] \quad (3.4)$$

Here $Entries[bin]$ is the number of counts in the chosen bin. N is the total number of bins, T is the clock cycle size in ps, meaning that both $Size[bin]$ and $Pos[bin]$ are also expressed in ps.

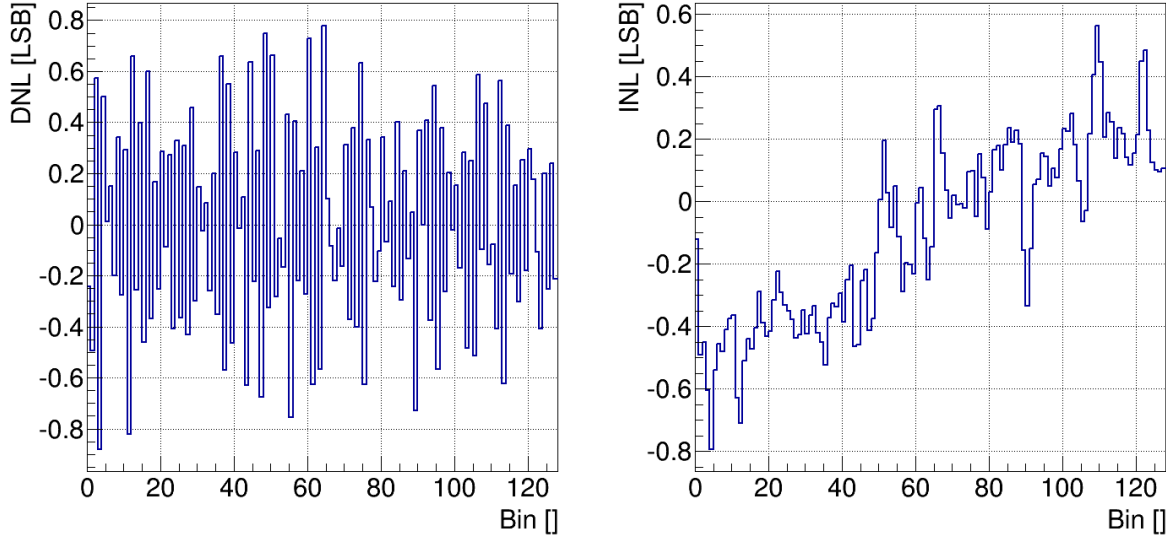


Figure 3.12: DNL (left) and INL (right) for a selected channel on a GET4 v1.0 board during cosmics tests. The value are extracted from Fig. 3.11.

In a TDC measuring time as a combination of the clock cycle counts $ClkCycle$ and the fine-time $FineTimeBin$, the raw time of a data message is the pair $\{ClkCycle, FineTimeBin\}$. The calibrated time of the data message relative to the last overflow of the clock cycle counter is given by:

$$t_{mess,calib} = ClkCycle \cdot T + Pos[FineTimeBin] \quad (3.5)$$

The unit of $t_{mess,calib}$ is ps.

3.4.4 Data calibration for discriminator effects: Walk

The PADI discrimination stage used for this thesis is a leading edge discriminator. As such, its discrimination time is dependent on the signal size as described in Fig. 3.13: a big input signal will have a steeper slope and cross the threshold earlier than a small input signal, leading to an offset in the timing edge of the PADI output. As the effect is the same for all signals of same amplitude, it can be corrected if one measure a variable depending on the signal size. In our system this is done by measuring the Time-Over-Threshold (TOT).

In order to calculate the values of the correction to compensate the walk effect for a signal, it is necessary to compare the time difference of this signal to a reference signal for different TOT values. In all the tests with detectors signals presented in this thesis, this is done using the difference between the time of a single MRPC strip and the time given by the reference system based on plastic scintillators and Photo-Multipliers Tubes (PMT). Assuming a setup with N PMTs, the time difference of the system $\Delta t_{MRPC,ref,mes}$ is given by Eq. 3.6. The time measured on the left side of the MRPC strip is $t_{MRPC,left}$

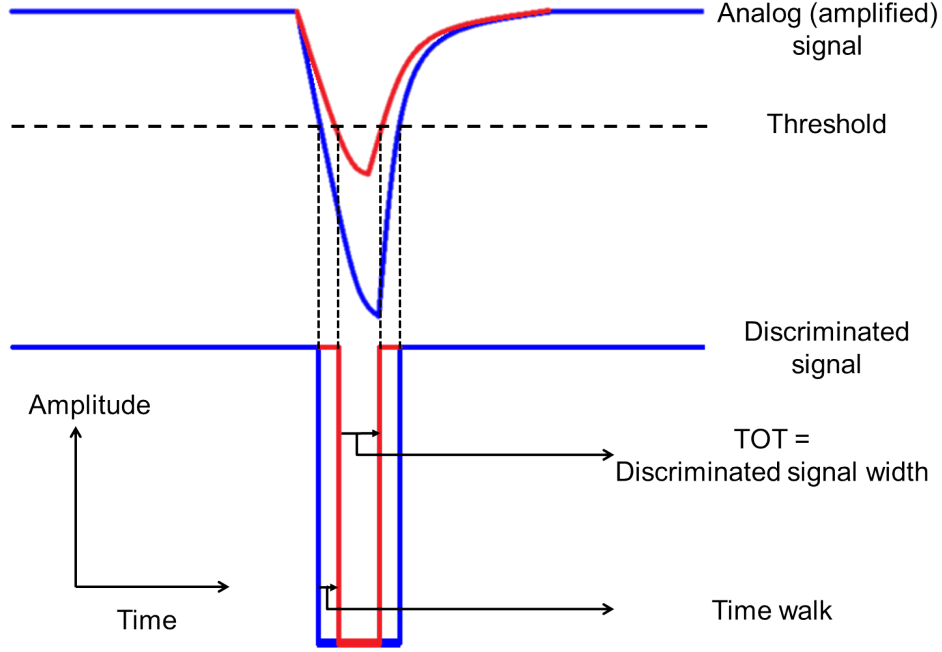


Figure 3.13: Sketch of the origin of the time-walk effect in a leading edge discriminator. The crossing time of a small signal (red) is delayed in comparison to a bigger time signal (blue). The signal width and the delay in time are correlated.

and the one measured on the right side is $t_{MRPC, right}$. The times measured with the PMTs are $t_{PMT,1}$ to $t_{PMT,N}$.

$$\Delta t_{MRPC, ref, mes} = \frac{t_{MRPC, left} + t_{MRPC, right}}{2} - \frac{1}{N} \cdot \sum_{i=1}^N t_{PMT, i} \quad (3.6)$$

In our tests only two scintillators readout on both ends were used to obtain the reference time ($N = 4$). The time difference $\Delta t_{ref, mes}$ between the two scintillators is given by Eq. 3.7. The times measured for the PMTs on the left and right side of the first scintillator are $t_{PMT,1}$ and $t_{PMT,2}$ respectively. The times measured for the PMTs on the left and right side of the second scintillator are $t_{PMT,3}$ and $t_{PMT,4}$ respectively.

$$\Delta t_{ref, mes} = \frac{t_{PMT,1} + t_{PMT,2}}{2} - \frac{t_{PMT,3} + t_{PMT,4}}{2} \quad (3.7)$$

Each of the MRPC and PMT signals has its own walk dependence. This leads to the expressions of $\Delta t_{ref, mes}$ and $\Delta t_{MRPC, ref, mes}$ in Eq. 3.8 and 3.9 respectively. In these equations, the walk offset of a signal on PMT i as function of its TOT is $walk_{PMT, i}(tot_{PMT, i})$. The walk offset of the signal on the left side of the MRPC strip as function of its TOT is $walk_{MRPC, left}(tot_{MRPC, left})$ and the walk offset of the signal on the right side of the MRPC strip as function of its TOT is $walk_{MRPC, right}(tot_{MRPC, right})$. The variables of interest are Δt_{ref} and $\Delta t_{MRPC, ref}$, which are the time differences independent of the size

of the signals.

$$\begin{aligned}\Delta t_{ref,mes} = & \Delta t_{ref} \\ & + \frac{walk_{PMT,1}(tot_{PMT,1}) + walk_{PMT,2}(tot_{PMT,2})}{2} \\ & - \frac{walk_{PMT,3}(tot_{PMT,3}) + walk_{PMT,3}(tot_{PMT,3})}{2}\end{aligned}\quad (3.8)$$

$$\begin{aligned}\Delta t_{MRPC,ref,mes} = & \Delta t_{MRPC,ref} \\ & + \frac{walk_{MRPC,left}(tot_{MRPC,left}) + walk_{MRPC,right}(tot_{MRPC,left})}{2} \\ & - \frac{1}{N} \cdot \sum_{i=0}^N walk_{PMT,i}(tot_{PMT,i})\end{aligned}\quad (3.9)$$

Ideally each of the corrections needed to compensate the walk offsets could be extracted directly by building the distribution of either $\Delta t_{ref,mes}$ (for the PMTs walk) or $\Delta t_{MRPC,ref,mes}$ (for the MRPC walk) as function of the corresponding TOT. However, some of the TOT are correlated, e.g. the ones of signals from the same scintillator or from the same MRPC strip. For this reason, it is necessary to iterate the extraction of the correction values a few times, updating the factors of each signal after another until they converge. The full procedure to obtain the correction values is schematized in Fig. 3.14 and will be described in details in the next paragraphs.

When the determination of the correction values is started, all these values are set to 0 (step (1) in Fig. 3.14).

The first part of the procedure is to obtain the corrections values for the PMTs: $corr_{PMT,i}(tot_{PMT,i})$ with $i = 1$ to 4. For this, the values for each PMT are updated one after the other, starting with the ones for PMT 1 (step (2) in Fig. 3.14). The algorithm used to perform the update of a PMT is the following:

- a. A loop is done over all events in the calibration input file.
- b. For each event where all signals (time and TOT) needed for Eq. 3.10 were measured, the following operations are done:
 - i. The value of $\Delta t_{ref,corr}$ is calculated as in Eq. 3.10.
 - ii. This value is plotted in a histogram against the TOT of the PMT for which the corrections should be updated.
- c. Once the event loop is finished, the mean value of $\Delta t_{ref,corr}$ is extracted for each TOT bin in the histogram. This value represents the correction update. It is added to the previous correction value for this TOT bin of this PMT. The operation can be done in a single operation for all bins when using the Histogram Profile and Histogram Addition features of the ROOT framework.

$$\Delta t_{ref,corr} = \Delta t_{ref,mes} - \sum_{i=1}^N corr_{PMT,i}(tot_{PMT,i}) \quad (3.10)$$

These updates are done either until the correction values converged for all PMTs or until a number of loops defined by the user is reached. An example of the histograms used for

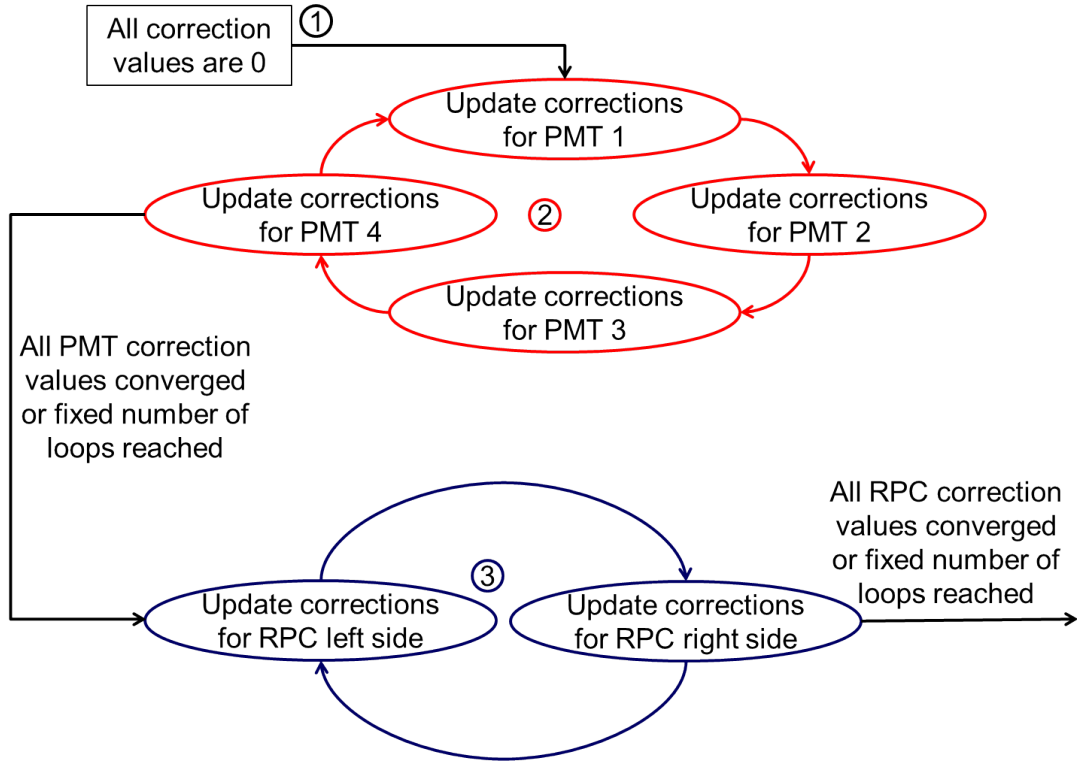


Figure 3.14: Sketch of the procedure used to obtain the correction values for the walk effect in our setups. In our case, the setup comprises four PMTs (for two plastic scintillators) and one MRPC strip readout on both sides. The loop in red (2) is performed on distributions obtained with the time difference of the reference system. The loop in blue (3) is performed on distributions obtained with the time difference between the MRPC strip and the reference system.

the update is shown in Fig. 3.15, obtained with experimental data. The left plot shows the histogram used for the first update (all correction values set at 0), with a range for the dependence on the TOT of the first PMT of 600 ps. The right plots shows the histogram obtained after the convergence of the correction values: the remaining dependence on the TOT is only a few ps, under the statistical uncertainty of the bins. As a result, the width of the $\Delta t_{ref,corr}$ distribution is strongly decreased, as can be seen in the comparison of the left and right histograms in Fig. 3.16.

The second part of the procedure is to obtain the corrections values for both sides of the MRPC strip, $corr_{MRPC,left}(tot_{MRPC,left})$ and $corr_{MRPC,right}(tot_{MRPC,right})$. For this, the values for each side are updated one after the other (step (3) in Fig. 3.14). The correction values for the PMTs determined in the previous step are left unchanged. The algorithm used to perform the update of an MRPC strip side is similar to the one for the PMTs:

- a. A loop is done over all events in the calibration input file.
- b. For each event where all signals (time and TOT) needed for Eq. 3.11 were measured, the following operations are done:
 - i. The value of $\Delta t_{MRPC,ref,corr}$ is calculated as in Eq. 3.11.
 - ii. This value is plotted in a histogram against the TOT of the side of the MRPC

strip for which the corrections should be updated.

- c. Once the event loop is finished, the mean value of $\Delta t_{MRPC,ref,corr}$ is extracted for each TOT bin in the histogram. This value represents the correction update. It is added to the previous correction value for this TOT bin of this side of the MRPC strip. The operation can be done in a single operation for all bins when using the Histogram Profile and Histogram Addition features of the ROOT framework.

$$\begin{aligned} \Delta t_{MRPC,ref,corr} = & \Delta t_{MRPC,ref,mes} - corr_{MRPC,left}(tot_{MRPC,left}) - corr_{MRPC,right}(tot_{MRPC,right}) \\ & + corr_{PMT,1}(tot_{PMT,1}) + corr_{PMT,2}(tot_{PMT,2}) \\ & - corr_{PMT,3}(tot_{PMT,3}) - corr_{PMT,4}(tot_{PMT,4}) \end{aligned} \quad (3.11)$$

These updates are done until either the correction values converged for both sides of the MRPC strip or until a number of loops defined by the user is reached.

In order to have correction values which are significant, a minimal statistics of around 100 $\Delta t_{ref,corr}$ or $\Delta t_{MRPC,ref,corr}$ values per TOT bin is needed in each histogram. This can be achieved in two ways:

1. by using a fixed TOT bin size and requesting a sufficient number of events where all needed signals are present
2. by adapting the TOT bin size to have a mean of 100 values per bin. This leads, however, to a reduced number of correction values and therefore to a smaller effect of the walk correction.

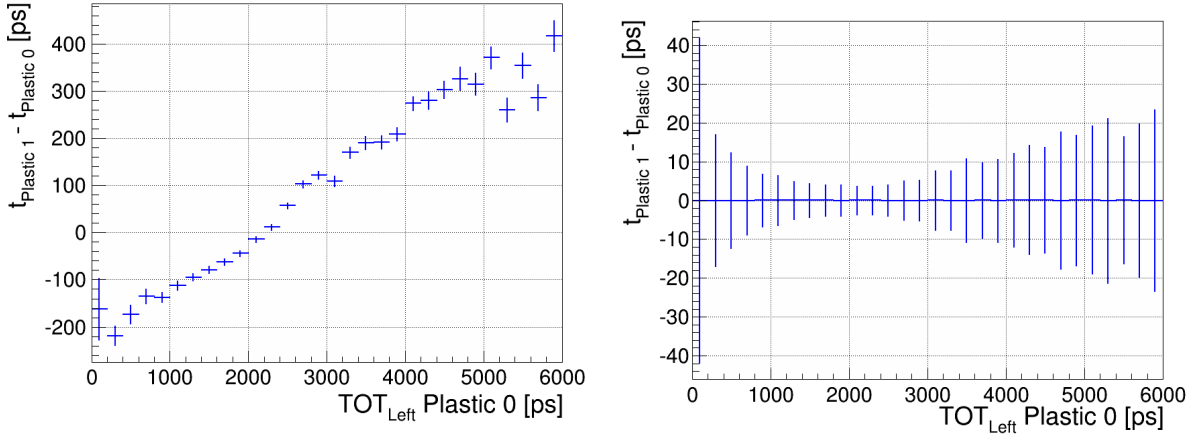


Figure 3.15: Difference between the mean time of Plastic scintillator 0 (PMT 1 and PMT 2) and the mean time of Plastic scintillator 1 (PMT 3 and PMT 4) as function of the Plastic scintillator 0 left side TOT (PMT 1) before (left) and after (right) the walk correction. The deviations from 0 in each TOT bin in the left plot are used as correction values for the first walk correction iteration. Example data from one of the cosmic tests in Autumn 2013, acquired with PADI-6/7 and GET4 v1.0 (see Subsection 4.4.5 for details).

Note that the correction values obtained in the first iteration of each loop also includes the mean value of the corresponding time difference, leading to distributions aligned on zero.

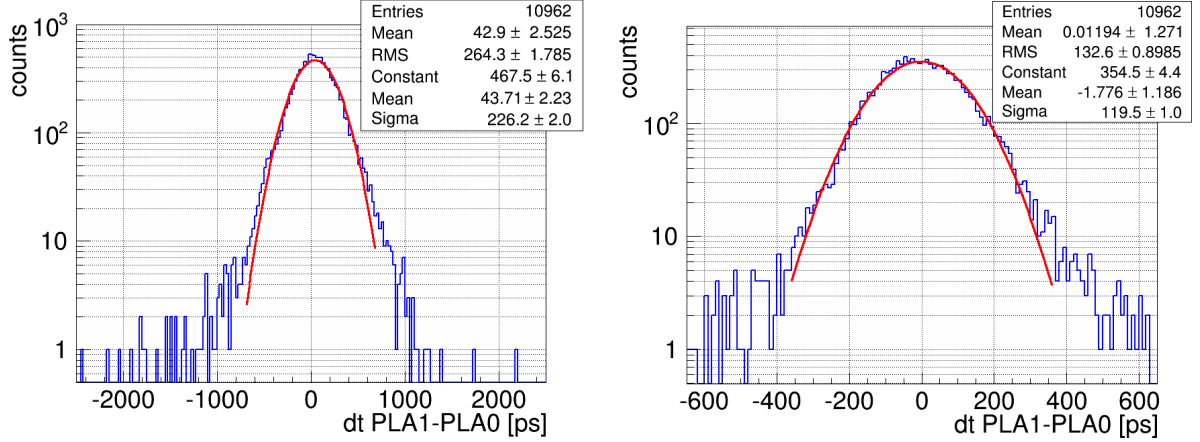


Figure 3.16: Reference system time difference ($\Delta t_{ref,corr}$ in text) before (left) and after (right) the determination of the walk correction values. Each distribution is fitted with a Gaussian restricted to $\pm 3\sigma$. The width of the fitted Gaussian is decreased by almost 2 by the walk correction. Example data from one of the cosmic tests in Autumn 2013, acquired with PADI-6/7 and GET4 v1.0 (see Subsection 4.4.5 for details).

3.5 CBM TOF Wall design

A modular design is currently planned for the CBM TOF wall. The wall would be subdivided in Super Module boxes (SM), each housing a few MRPC counters in the same gas volume. The SM are staggered to insure a proper overlap between the sensitive areas. The same is done for the MRPCs inside each SM. By keeping a reduced number of SM model types, the construction and maintenance can be made easier. The starting point for a realistic wall design is to define 5 areas corresponding to different particle fluxes, as shown in Fig. 3.17. Region A, B, C and D are used for the TOF measurement itself. Region E is an optional proposal allowing to measure the event reference time and the event plane. Different types of MRPC are designed for each area using materials giving the best compromise between cost and rate capability, as explained in Section 3.3, and using channel designs (area, strips/pads, ...) giving the best compromise between channel number and hit properties (occupancy, readout rate, ...). Table 3.1 presents some of the design parameters and characteristics for each of these area.

Based on this conceptual design, several layouts were proposed for the so-called outer part of the wall (region A, B, C) and for the so-called inner part of the wall (region D) in the CBM TOF Technical Design Report [20]. These designs start at the single MRPC level and extend up to the support infrastructure.

The proposal for the outer wall is shown in Fig. 3.18. The MRPC detectors used for the electronics test presented in Chapter 4 are implemented for this design. This design is prepared with the modularity of the wall in mind: it can be moved along the beam line and the outer SMs layer can be equipped later when SIS300 becomes available. One of the proposals for the inner wall is shown in Fig. 3.19, based on MRPCs with strip readout electrode.

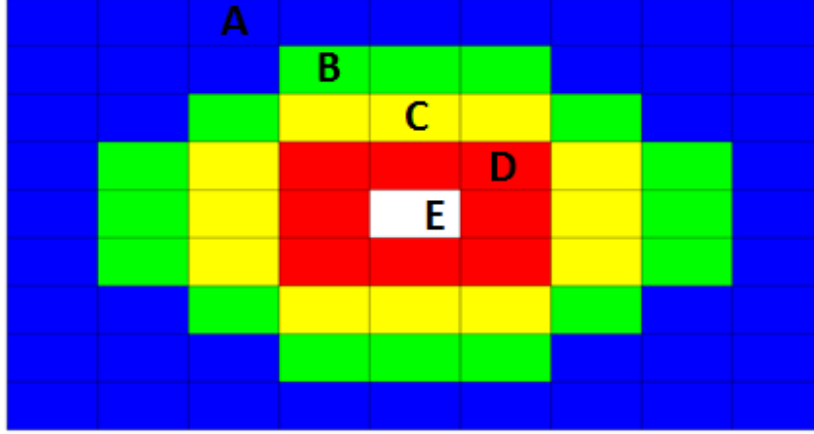


Figure 3.17: Modular design of the TOF Detector. The whole wall is divided into 5 regions (A,B,C,D,E), in which counters of different types will be mounted; they are subdivided in boxes which contain the individual detector cells. Relevant parameters of these regions are listed in Table 3.1. Figure taken from [20].

Table 3.1: Characteristics of the the TOF Wall regions (CE denotes central events). It has to be stated that these quantities are for orientation only (conceptual design), the final numbers will depend on more detailed designs, as for example the one in Fig. 3.18. Table taken from [20].

	Area/Cell cm ²	Flux kHz/cm ²	Hit/Cell/CE ·10 ⁻²	2-Hit prob. %	No. of Cells per Box	No. of Boxes	total No. of Cells
A	50	<1.9	<4.9	<2.5	330	44	14520
B	50	<3.2	<7.7	<3.9	330	16	5280
C	25	<6.0	<7.6	<3.9	840	12	7920
D	6.25	<27	<7.2	<3.7	3360	8	21120
E	4	<82	<8.3	<4.3	5250	1	4125

Using the two design shown here as illustration, one can make more realistic estimations of the SM number, channel number and wall dimensions:

- Outer wall: 70752 channels, 826 MRPCs in 218 SMs
- Inner wall: 40320 channels, 252 MRPCs in 8 SMs

For the outer wall design, the pre-amplifier and discriminator boards are placed inside the SM boxes. The TDCs are placed directly on the far side of the SM box relative to the beam pipe. By combining this TDC position with a staggering between the SMs, this outer wall design avoids both the presence of inactive areas and the presence of servicing

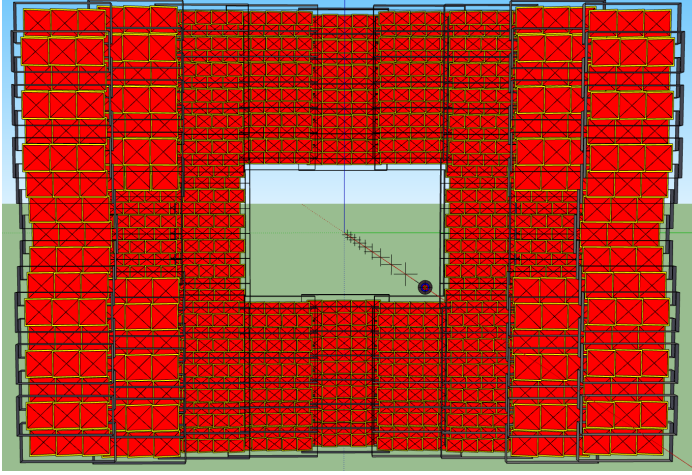


Figure 3.18: Proposed design for the CBM TOF wall outer area. This design is based on strip MRPCs. Only the edges of the SM boxes and the MRPC counters are shown. A supporting mechanical structure is also present but not shown. Figure taken from [40].

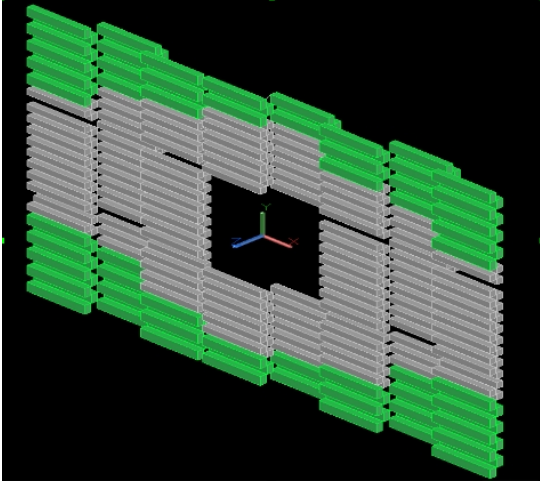


Figure 3.19: Proposed design for the CBM TOF wall inner area. This design is based on strip MRPCs. Only the MRPCs are shown. The inner block is planned to stand behind the outer wall structure and fits to the central hole of the outer wall. Figure taken from [20].

equipment in front of the active area. For the inner wall used here as illustration, the pre-amplifier and discriminator boards are placed behind (downstream) the SM boxes due to the high channel density. As the particle flux in this area could generate errors in the TDCs, the TDC board are placed 1-2 m away, behind the first or second layer of outer wall SMs, and connected to the discriminators using cables.

Chapter 4

The TOF wall Readout chain

The Readout chain of the CBM TOF Wall will be free-streaming, as will be the full experiment. This concept was described in Section 2.4. The application of this concept to the CBM TOF readout chain which was used to design the readout chain prototype is presented in Section 4.1.

The baseline option for this readout chain is based on the PADI - GET4 - ROC chain. The components of this chain are described in Section 4.2. The VME triggered system used as reference to evaluate the new chain performance will also be briefly described in the same section, with more information in Appendix B.

Two version of the chain were put under test for this work. Section 4.3 presents the results of the first one, which was based on proof of concept components. Section 4.4 describes the changes in design induced by the results of this first version and show the performance obtained with the first user dedicated prototype. In each case the acquisition and analysis software used will be detailed.

4.1 Chain Concept

The tasks the CBM TOF readout chain has to perform are:

- to digitize the input signals coming from detectors in a self-triggered way
- to timestamp them in a common time frame
- to readout the data from the Time to Digital Converters (TDC) in a free-streaming way
- to aggregate these data
- to transport them to the event builder in the First Level Event Selector (FLES)

The chain therefore needs to have sufficient bandwidth in each of these tasks in order to cope with the high rates with which all valid signals are transferred in free-streaming mode to the FLES. Fig. 4.1 shows the general concept of a free-streaming readout chain, while Fig. 4.2 shows its application in the case of the CBM TOF wall.

The FEE block is split in an analog part, the pre-amplifier and discriminator, shortened to “*Discr.*” in Fig. 4.2, and a digital part, the digitizer, shortened to TDC. The discriminator

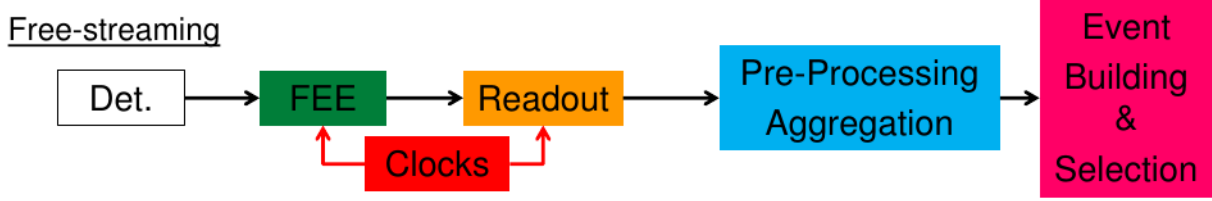


Figure 4.1: General concept of a free-streaming readout chain.

is in charge of the conversion from the RPC sharp and small signals to logical LVDS signals, as described in Section 3.4. The timing information is encoded in the leading edge and the charge in the width of the logical pulse (TOT principle). The resolution between the input signal and the output signal leading edge must be better than 20 ps. The digitizer assigns a time-stamp with a precision in the order of 10-50 ps and a resolution better than 25 ps to both edges of the logical signal (blue and red hexadecimal words in Fig. 4.2).

The connection between the Front-End Electronics (FEE) and the ReadOut Controller (ROC) will be done through copper cables or electronic boards. The ROC reads out the FEE data. It also gives the possibility to timestamp system messages against the experiment main clock and insert them in the FEE data stream. The output of the ROC is an optical fiber. As the data rate per channel, per RPC module and per SuperModule will highly depend on their position in the wall (see Section 3.5), a first aggregation at this level is needed to optimize the usage of this output link. This is done by varying the number of FEE channels per ROC.

Both the clock used for time-stamping at the ps level (timing for TOF in the FEE) and the one used for the more general time-stamping on the ns level (timing for event building in the ROC) need to derive from the main CBM clock in order to perform the time-base event building (see Section 2.4).

The optical connection between the ROC and the FLES is done through one or more layers of Data Processing Boards (DPB) for pre-processing or Data Combining Boards (DCB) for data aggregation. These boards are based on FPGA boards.

Local pre-processing can already be done on the ROC to reduce the amount of data to be transferred. After calibration, the ROC could also automatically detect noisy/ringing channels and disable them before they saturate the full data transport chain. More sophisticated data pre-processing and data formatting are performed in the DPB and DCB boards. Details about the development of the pre-processing tasks for the TOF system can be found in Ref. [58] and Ref. [59].

The “*Event Building*” pink element in Fig. 4.1 and Fig. 4.2 are implemented in software. However, due to the specificity of the free-streaming design where no hardware event definition is present, they must be considered as part of the readout chain, especially for the test setups used in this work. As such they were also an important part of the development done in this thesis and will be described in details.

The following sections will describe the first available prototypes for the CBM and present the tests performed to understand how such a system works, what are its characteristics

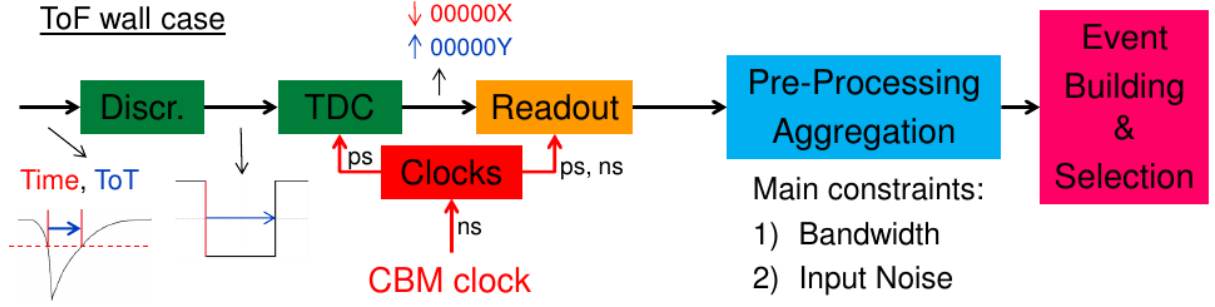


Figure 4.2: Concept of a free-streaming readout chain for TOF. The time orders (“ps”, “ns”) indicate the required time-synchronization quality.

and whether they fit our requirements.

4.2 Readout chain components

In this section the different components used to build the free-streaming readout chain prototypes will be presented. The different versions used and their improvement will be detailed for the components where it is relevant.

4.2.1 The PADI pre-amplifier and discriminator

The Pre-Amplifier and DIscriminator (PADI) is an Application-Specific Integrated Circuit (ASIC) family implemented in 0.18 μm CMOS technology. In the case of the CBM-T0F, it provides the conversion from the RPC analog signal to a logical LVDS signal encoding the threshold crossing time in its rising edge and the Time over Threshold (TOT) in its width. The requirements it has to fulfill were presented in Subsection 3.4.2. Eight versions of PADI were produced from the early prototype PADI-1 to the current 8 channel version PADI-8 [60]. Only the versions used in the tests performed for this work (PADI-2/3 and PADI-6/7) will be presented here. A description of the general functionalities of the chip can be found in the first paragraph, followed by more detailed information on each of the two versions used and a comparison of their main parameters.

General concept

A simplified block schematics of the PADI chip family is shown in Fig. 4.3. The PADI chip contains for each channel a pre-amplifier (PA) stage followed by a discrimination stage (DI) and a LVDS sender stage. The biasing block(s) are common for all channels. The threshold is applied in the feedback loop of the PA, inducing a DC baseline shift of its output. This way the discriminator stage can be set to a fixed firing point at its own 0 differential level. Signals “above threshold” then just mean they are big enough after PA amplification to compensate the offset between the PA baseline and the DI zero level. This also means that all threshold values are relative to the PA output and have

to be divided by the PA gain to obtain the input signal threshold. Thanks to its high gain, the DI itself operates between the positive and negative saturation levels: an input signal of mV range around the 0 level after PA induces a swing to the saturation level of same polarity. A buffer stage connected to the signals between PA and discriminator allows to monitor the value of the baseline (threshold cross-check) and the PA output shape (reflexions, cross-talks, ...). Following key parameters were used as design goals in

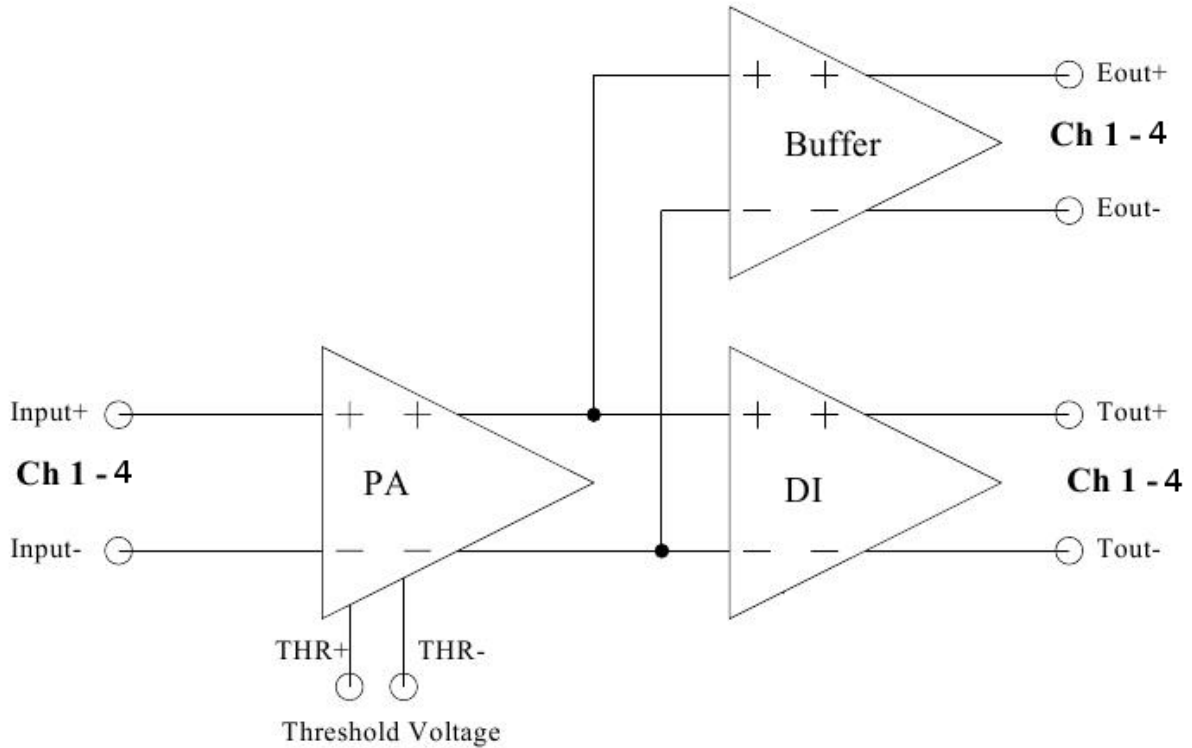


Figure 4.3: Simplified block schematics for the PADI chip family. See text for description. Figure adapted from the PADI-1 block schematics in [61].

addition to the electronics requirements:

- Fully differential design
- $\sim 50 \Omega$ input impedance (to ground, total differential impedance is 100Ω), adjustable
- Preamplifier gain ~ 100
- Preamplifier bandwidth $> 300 \text{ MHz}$
- Peaking time $< 1 \text{ ns}$
- Noise related to input $< 25 \mu\text{V}_{RMS}$
- Comparator gain > 100
- DC feedback loop for offset/threshold stabilization
- Threshold range related to input $0.5\text{-}10 \text{ mV}$
- Time resolution in the order of 20 ps for typical RPC signals

PADI-3

PADI-2 and PADI-3 are the same design with only different output signal range. This version of PADI has 4 channels. PADI-2 provides the minimum levels for the LVDS standard and was shown to maintain them on twisted pair flat cables up to 3m. PADI-3 output levels can be adjusted by using an external resistor, allowing to tailor them so that it matches the LVDS convention at the end of longer transmission cables. Mostly PADI-3 were used in this work.

The threshold voltage is externally set for each channel. A 'OR' output is present for trigger purpose with a possibility to daisy-chain PADI chips OR signals.

Fig. 4.4 shows the time resolution measured for different PA threshold values and different input signal size. The points at 10 - 15 mV single ended input and 27 mV threshold correspond to typical MMRPC signals and match CBM requirement with resolutions at 10 to 15 ps. The method used to obtain these values is described in Ref. [62].

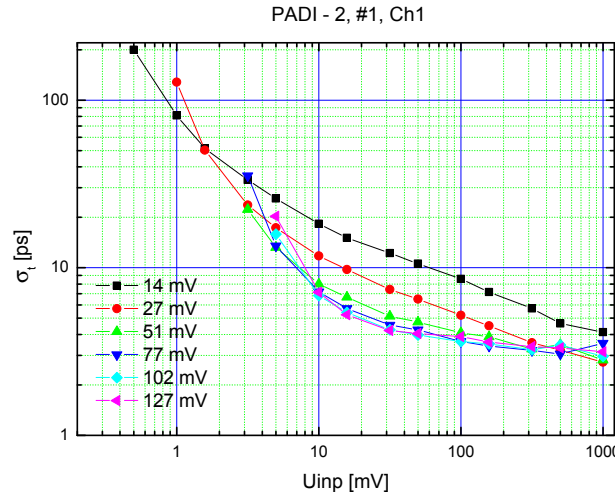


Figure 4.4: The PADI2 time resolution dependence to input signal amplitude for different threshold voltages. Figure taken from [62].

PADI-6/7

The PADI-6/7 generation was produced after detailed simulations with the CADENCE Monte-Carlo tool. These simulations led to a change in the way the output signal and the threshold are merged in the feedback loop of the PA. They are now merged before the amplifiers of the feedback loop, whereas in previous versions they shared only one of two transconductance amplifiers. This change allows a more stable gain (temperature, voltages, ...) for the loop setting the baseline level from the threshold input value.

Similarly to PADI-2/3, the PADI-6 and PADI-7 versions are almost the same chip. Their only difference is that PADI-6 additionally has two included Digital to Analog Con-

verters (DAC) with an SPI interface on each channel for threshold voltage setting (see Appendix C.2 for more information on SPI). These two DACs provide voltages of same amplitude but opposite sign, so that the common-mode voltage is not affected by the DAC value. The threshold voltage is then set through a six resistance bridge. The resistance bridge middle voltage is set either by an external potentiometer or by the internal DACs (see Fig. 4.5). The external potentiometer is common to all channels. Using this option sets a universal threshold while using the DACs gives individual channel control.

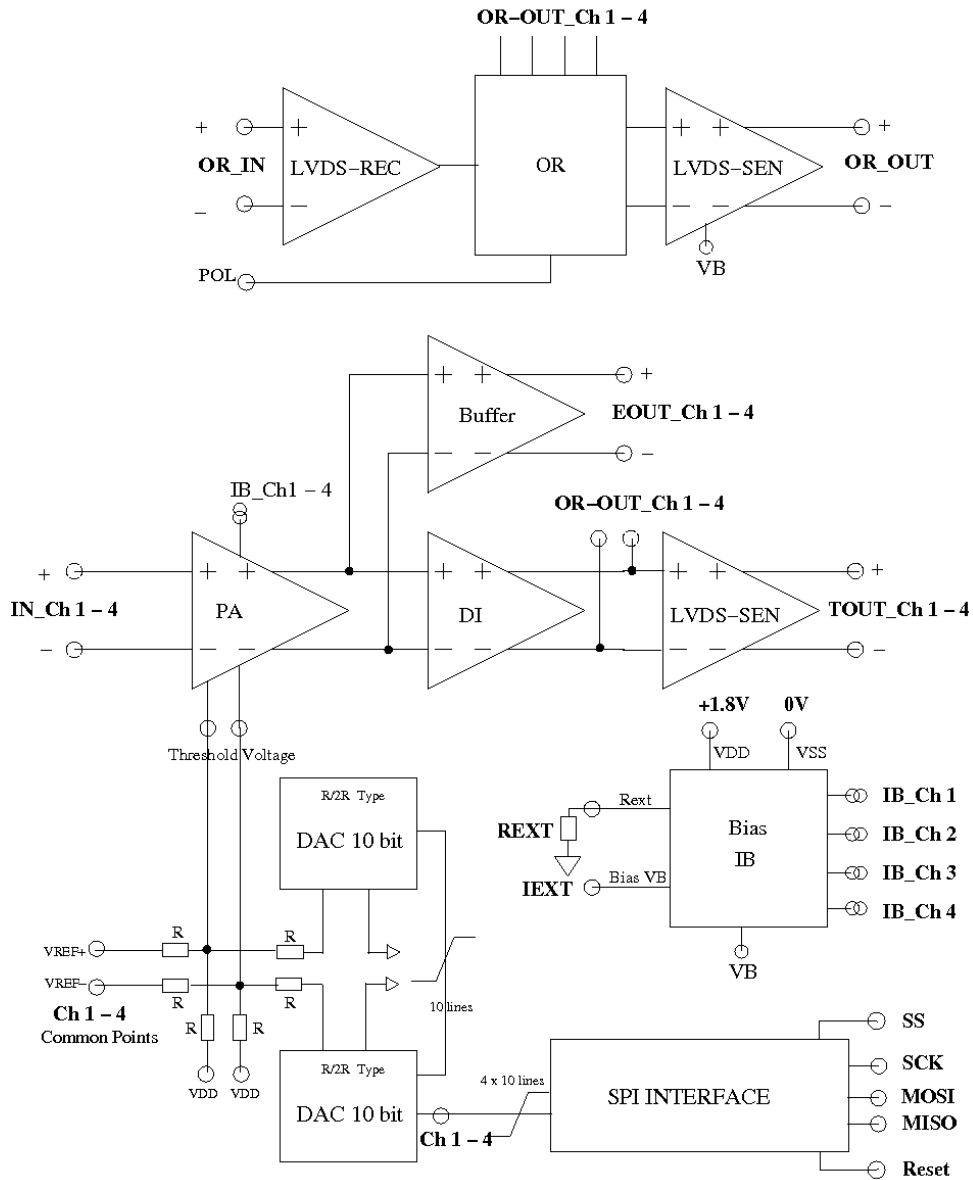


Figure 4.5: Block diagram of PADI-6. In PADI-7 the SPI interface and the 2 DACs have been left out. Figure from [60].

Fig. 4.6 shows the time resolution measured for different PA threshold values and different input signal size. The method used to obtain these values is described in Ref. [63]. The

values are in this case channel to channel time difference measurements and need to be divided by a factor $\sqrt{2}$ (equal performance assumption) to be compared to those in Fig. 4.4. They are slightly worse at ~ 14 ps for 10 mV input and ~ 16 ps for 15 mV input, but still within our specifications.

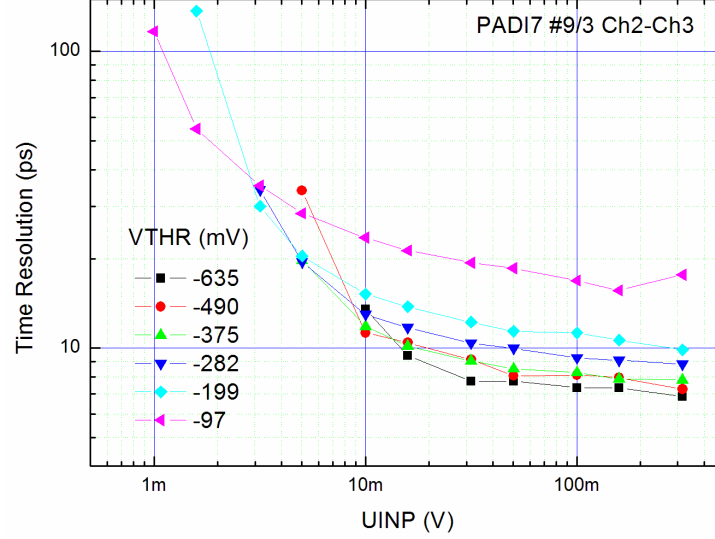


Figure 4.6: Measured PADI-7 time resolution versus input signal amplitude for the given threshold values V_{THR} . Figure taken from [60].

Comparison of the versions and of their PCBs

The main technical parameters of the PADI generations used in this work are summarized in Table 4.1.

Table 4.1: Main technical parameters of PADI-3 and PADI-6/7. Data from [60].

	Unit	PADI-2/3	PADI-6/7
Time resolution @ 10mV	[ps]	<10	<10
PA voltage gain		87.4	244
PA bandwidth	[MHz]	293	416
Linear range (ref. to input)	[mV]	± 2.9	$\pm 2.$
Noise (ref. to input)	$[\mu V_{RMS}]$	25	23.8
PA output range	[mV]	± 300	± 500
PA baseline DC offset, σ	[mV]	21.9	5.9
Input impedance range	$[\Omega]$	37 - 370	38 - 165
Power consumption	[mW/Ch]	17.4	17.7

The PADI-3 chips used for this work were bonded on Printed circuit boards (PCB) called FEET-PADI, shown in Fig. 4.7. This board is equipped with two PADI-3 chips, a pin

connector for the RPC signals input and a SAMTEC output connector for direct assembling with the FEET-GET4 (see Subsection 4.2.2). A potentiometer is present for each channel to fine tune its baseline value and adjust all channels on a FEET to the same threshold value. Another potentiometer then allows to shift the baseline of all channels in parallel in order to set the common threshold. A DAC chip with I²C command input is also present on board for an optional remote controlled setting of the common part of the threshold. The SAMTEC connector was chosen for two reason: it provides differential lines matched to 100 Ω for the eight LVDS output signals and also two separate groups of four pins (one on each side) for the power distribution and slow control communication. The FEET-GET4 board (see last paragraph of Subsection 4.2.2) is then providing both the power for the FEET-PADI and the interface between the I²C and the Readout Controller.

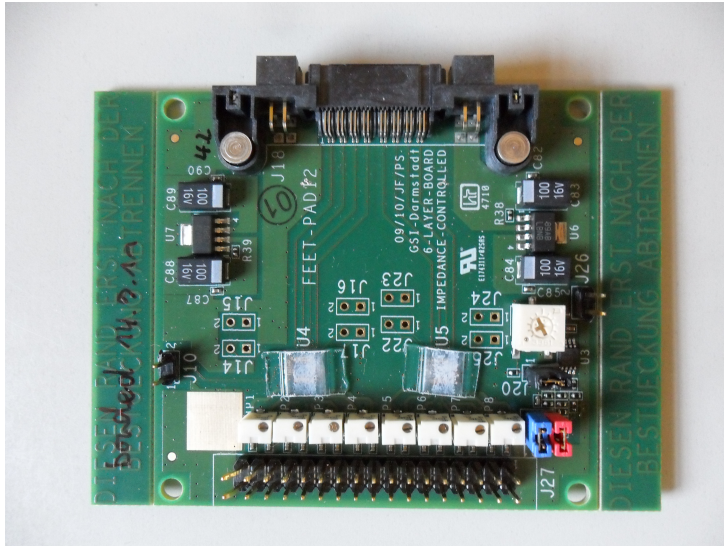


Figure 4.7: FEET-PADI PCB equipped with two PADI-3 chips. The 17 pin connector is the RPC signals input and the SAMTEC connector (top) is planned for connection to a FEET-GET4 PCB.

For the PADI-6 and PADI-7, a system with a baseboard PCB and daughter boards was developed by the GSI-EE department. This system allows to mount the discriminator boards inside the MRPC gas box, directly on the MRPC readout electrode. Each daughter PCB hosts two PADI-6 or PADI-7 chips. The baseboard provides the power distribution to each daughter board and remap their output lines to common 17 pairs connectors, separating the output signal lines from the services lines. Service lines include the OR output signals and the SPI lines used for the thresholds external configuration. A fully equipped baseboard is shown in Fig. 4.8.

4.2.2 The GSI Event-Driven TDC with 4 channels

The GSI Event-Driven TDC with 4 channels (GET4) [64], [65] is an ASIC TDC specifically designed for the CBM-TOF wall use-case and implemented in 0.18 μm CMOS technology.

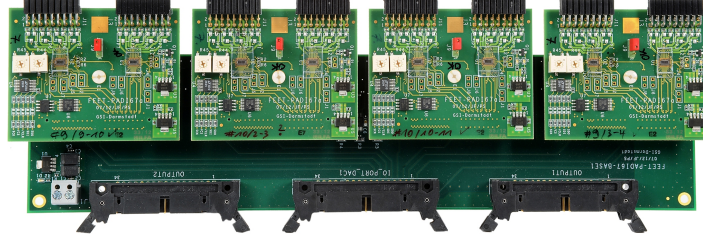


Figure 4.8: FEET-PADI6 system, with a baseboard fully equipped with 4 PADI daughter PCBs, each hosting two PADI-6 or 7 chips. The baseboard provides power distribution and separate the output signal lines on the two outer connectors from the service lines on the middle connector.

It provides a time to digital conversion with a design time resolution in the order of 20 ps for a bin size of 50 ps, along with a self-triggered readout system. Two versions were used in this work: the GET4 Proto and the GET4 v1.0. The first paragraphs will describe the functionalities of the chip common to both versions. This will be followed by a description of the GET4 Proto readout block, a description of the GET4 Proto boards and a final paragraph presenting some test results obtained by the chips developers on this version of the chip. The GET4 v1.0 version will be presented later in Subsection 4.4.1, after the results of the GET4 Proto study.

Chip organization

The chip is composed of a TDC core and a digital readout block. A simplified version of the chip block diagram can be found in Fig. 4.9. The TDC core provides the fine time-stamping. The digital part adds to it the coarse time stamp, performs the synchronization checks, builds the hit messages and controls their readout. These different functionalities will be described in following paragraphs.

Fine timing

The core of the chip is based on a Delay Locked Loop (DLL). When the DLL is locked on the input clock, the total delay chain length is exactly one clock cycle. The delayed clock from each delay element is used to control a D-type flip-flop whose data input is connected to the input channel. As there are 128 delay elements in the chain, one obtains the bin size of 50 ps from the nominal clock frequency f_{cyc} of the chip:

$$\tau = \frac{1}{f_{cyc} \cdot 128} = 50 \text{ ps with } f_{cyc} = 156.25 \text{ MHz} \quad (4.1)$$

Measuring time and TOT pairs starting from width of a few 100 ps is made possible by using two edge detection units per input channel looking for transitions in opposite directions. Inside each edge detection unit, two encoding blocks using each 64 of the flip-flops output are used, leading to a worst case double hit capability of 3.2 ns (half of a clock period). These edge detecting data encoders are used to generate the so-called

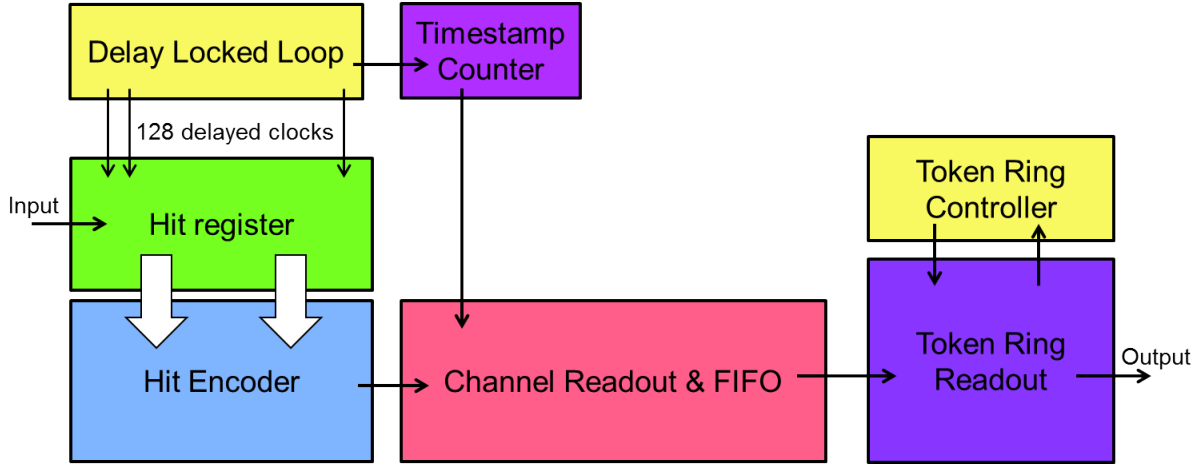


Figure 4.9: Simplified block diagram of the GET4 Proto TDC ASIC. All connections are not represented. The TDC core is composed of the Delay Locked Loop, the hit register and the hit encoder. Figure adapted from [66].

fine-time, which is the binned time position of the signal inside the current clock cycle. The encoders also generate flags used to signal that new data are ready.

Epoch mechanism and timing definition

In a free-streaming system, all measured times are relative to the last overflow of an internal clock cycle counter. In the case of GET4 it is 12 bits wide. Such an overflow is called epoch and from the counter size one can obtain the length of a GET4 epoch: $t_{epoch} = 26.2144 \mu\text{s}$. The state of the clock cycle counter when a hit happens provide the so-called time-stamp. Epoch messages are inserted in the data-stream when an overflow happens. Fig. 4.10 provides a graphical representation of the hit time definition in GET4. The hit time is built from the combination of the fine-time ($\sim\text{ps}$ timing), the time-stamp ($\sim\text{ns}$ timing) and the number of epochs since startup of the system ($\sim\mu\text{s}$ to s timing). The readout part of the chip ensures that all data message belonging to the previous epoch are sent before the epoch message so that the full context of each hit is preserved.

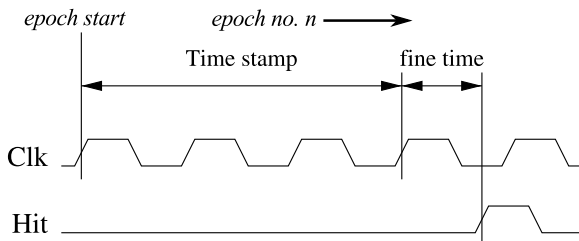


Figure 4.10: Definition of time stamp and fine time. Figure taken from [67].

Synchronization mechanism

When more than one chip is in use, one needs to ensure that the clock cycle counter of all chips start at the same time. Additionally, as described in Section 4.1, in the CBM

case the digitizers will most probably run on a different clock than the one used by the other detectors for time-stamping, even if they will be phase locked. Thus, one need also to ensure that the synchronization is checked when the rising edge of both clocks coincide at regular intervals. In the case of GET4, this is done by an external signal called *SYNC*, which uses a dedicated input. The system used to generate the clocks and the *SYNC* signal will be explained in Subsection 4.2.3.

This synchronization mechanism used in GET4 is depicted in Fig. 4.11. On the next rising edge of the system clock after a rising edge of the *SYNC* signal, the clock cycle counter will be reset. If this happens at the same time where the counter would have overflowed (transition from 4095 to 0), the epoch message will just have an additional flag set to indicate that a *SYNC* happened. If the counter was in a different state before reset, an error message will be inserted in the data stream to indicate that the synchronization was lost sometime since the last epoch message with the *SYNC* flag set.

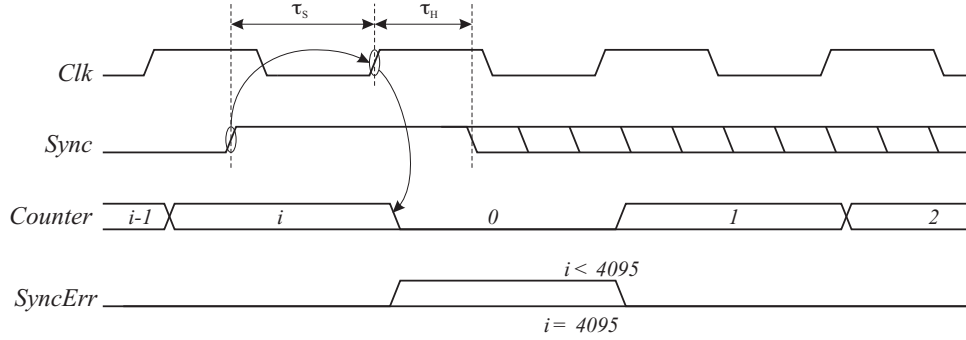


Figure 4.11: Timing diagram of the external synchronization of the time-stamp counter in GET4. Figure taken from [65].

Readout block of the GET4 Proto

The first level of data acquisition is included in the digital part of the chip, granting it its free-streaming capability. This part of the chip was modified between the two versions we used. The first chip available was the so-called “GET4 Proto”, meant mainly as a proof of concept and development tool.

If a hit is detected in any of the two encoding blocks of an “edge/channel” pair, a 30 bits internal event word is built from:

- the fine-time of both encoding block
- a flag indicating if a hit is present for each of those blocks
- some flags for epoch control
- the current time-stamp

The exact content of this word is shown in Table 4.2. The *SYNC* flag indicates that a *SYNC* pulse was received in current epoch. The *EPOCH* flag indicates that a time stamp counter overflow appeared since last sent message and that an epoch message needs to be inserted before sending the new hit(s).

In the case of the GET4 Proto, the epoch flag is stored three times to ensure by redundancy that it is properly handled: it is essential for the token ring operation if one wants to keep the right time context of the hit messages.

Table 4.2: Content of the internal event word in the GET4 Proto case [65] (see text for explanation).

Data	Data width
Fine time A	6
Hit A	1
Fine time B	6
Hit B	1
Time stamp	12
Sync	1
Epoch	3
Total	30

Each of the eight “edge/channel” pairs has an Event FIFO with seven slots. The filling state of the FIFO and the event type determine whether the event word is stored in the FIFO or thrown out. A High Water mark is activated if 6 out of the 7 slot are filled. As Epoch events have a higher priority, the hits events are not written any more when this mark is active, to ensure the last slots is reserved for epochs. If an epoch events come, it is placed in the last slot and the FIFO full flag gets active.

A token ring is used for the readout of the eight Events FIFOs (one for each “edge/channel” pair). A simplified state diagram of this token ring is available in Fig. 4.12.

Each readout unit (one per “edge/channel” pair) starts by reading an entry from its associated FIFO if available. It then wait for receiving the token. Once the token is received, if a data word was loaded from the FIFO, the unit check if the *Epoch* flag is set in it. If it is the case a signal is sent to the token ring controller and the unit will just pass through the token until the flag is reset. If the flag is not set, the unit check first if a hit is present in the first part of the data word (*Hit A*, corresponding to half the FT range). If it is the case a data message is generated and sent to output before resetting this part of the data word. It then does the same for the second part of the data word (*Hit B*). The token is then sent to the next readout unit in the ring and a data word is readout from the FIFO as soon as any is available. When the Ring Controller receives back the token from the last readout unit, it checks if the *Epoch* flags of all units are set. If it is the case an epoch message is generated and sent to the output, all *Epoch* flags are reset and the token is sent to the first readout unit. If all flags were not set the token is directly sent to the first unit.

The 24 bits output messages are written on an internal parallel bus. In the GET4 Proto, messages are then serialized and sent on a serial bus controlled by an external readout clock.

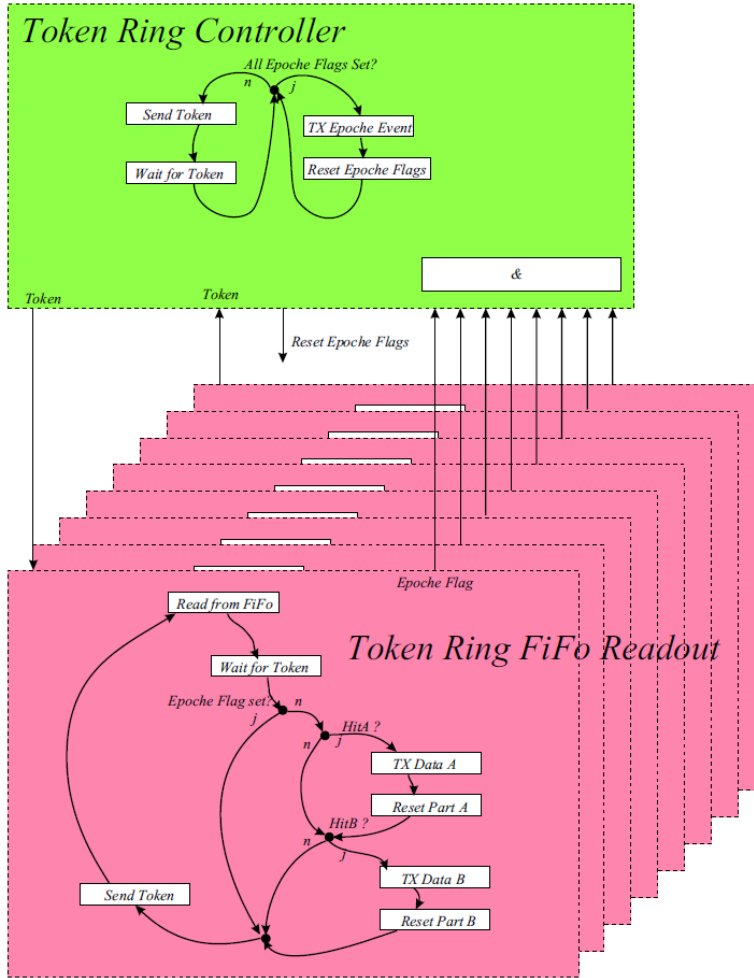


Figure 4.12: Simplified state diagrams of the token ring in the GET4 readout part for the GET4 Proto. Figures taken from [65]. For details see the text.

PCB of the GET4 Proto

This ASIC was bonded for our tests on the so-called FEET-GET4 PCB, with two chips per PCB, as depicted on Fig. 4.13. The PCB provides the following connections:

- a SAMTEC connector for the input signals from either the FEET-PADI PCB (then providing additionally power and I²C commands in the opposite direction) or an adapter board
- two connectors for shielded differential LVDS clock cables, used for the main clock and the SYNC signal
- two RJ45 connectors, one for the serial data links to the ROC and one for debug outputs

This version of the chip had a so-called “ExtSync” LVDS input, connected to the second RJ45 connector, which allowed to insert extra messages directly in the GET4 data, with a time-stamp provided from the clock counter. This was dropped in the GET4 v1.0.

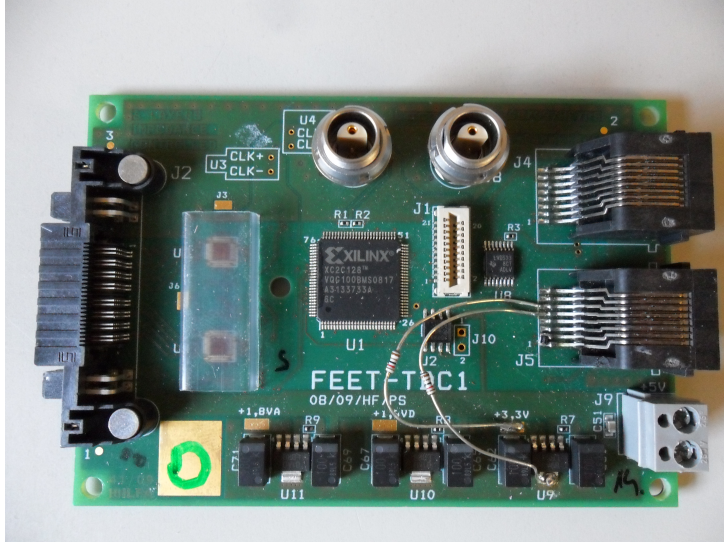


Figure 4.13: FEET-GET4 PCB equipped with two GET4 Proto chips. The SAMTEC connector (left) is for direct connection to a FEET-PADI PCB, the two LVDS connectors on top for the clocks input and the RJ45 connectors for connection to the readout controller and access to debug signals.

Characteristics

Laboratory tests were performed on this version of the chip using pulsers. In some tests the GET4 input channels were fed directly LVDS logical signals, while in other analog pulses were fed a PADI board connected to the GET4 board. To test the resolution, the pulse was split and each resulting signal fed to a channel.

The GET4 Proto channel-to-channel resolution was measured to be in the order of $\sigma_{2ch} = 34.31$ ps, corresponding to a single channel resolution of $\sigma_{1ch} = 24.26$ ps [65]. The channels were on the same board. The TOT measurement was tested in combination with the PADI-2 chip, proving that the pulse width below 1 ns can be measured with GET4 [68], [65]. The measured resolution was farther from the theoretical resolution of 14.5 ps than expected. This was understood to be due to worse non-linearities [65] (see Section 3.4.3 for explanations on non-linearities) compared to test chips called DANTE [64] with only the TDC core.

4.2.3 Clock system

As explained in Subsection 4.2.2, the GET4 TDC needs to be steered by a 156.25 MHz clock. On the other end, a 250 MHz clock is planned to be used for the coarser time-stamping of hits in the other CBM detectors and to time-stamp control signals in the ReadOut Controllers (ROC, see Subsection 4.2.4). Being able to convert the fine time-stamps of the TOF wall in the same time domain as the other data is a requirement of the time-based event building. In order to achieve this, the two clocks have to be locked one to each other and have to be a rational fraction of each other. Using frequencies of

156.25 MHz and 250 MHz gives a ratio of 5/8. This means that every 32 ns the GET4 clock rising edge and the readout clock rising edge are in coincidence. A synchronization signal is also needed to check at regular intervals that the clocks and their counters are still in coincidence in all elements of the readout chain. This is the so-called SYNC signal.

The period between two overflows of a clock cycle counter is called epoch. To establish how often the SYNC signal should be emitted, one has to consider the epoch length of both clock systems and how often they coincide. The GET4 has a clock cycle counter width of 12 bits, leading to $t_{epoch,GET4} = 26.2144 \mu s$. The time-stamps used in the ROC and in the front-end of the other CBM detectors is also based on a 12 bits counter, leading to a general CBM epoch of $t_{epoch,CBM} = 16.384 \mu s$. This means that the clock cycles counters of these elements will overflow in coincidence every five GET4 epochs, every eight CBM epochs or every $t_{coinc_epoch} = 131.072 \mu s$. One could generate a SYNC signal on every of these coincidence. However, a balance is needed between possible data losses and processing power requirement. Data losses are linked to the longest off-synchronization time, which is the interval between two SYNC signals. The processing power requirement comes from the fact that some cross-checks have to be performed in software after each SYNC signal. Therefore, it was chosen to generate the SYNC signal only every five coincidence of the counters overflow, leading to:

$$t_{SYNC} = 25 * t_{epoch_GET4} = 40 * t_{epoch_CBM} = 655.36 \mu s \quad (4.2)$$

The clock system of the CBM TOF wall is based on the Cbm-cLOCK-SYnthesizer version 2 (CLOSY2) [69] and the 1:10 clock distribution elements used successfully in the FOPI TOF barrel [54]. A diagram of the clock system is shown in Fig. 4.14. The CLOSY2 is used to generate the two clock frequencies and the SYNC signal needed for the free-streaming readout. A precision of less than 5 ps RMS for the TDC clock is the main requirement for the CLOSY2. Fig. 4.15 left and right show respectively the board naked and in its protective case for operations in experimental setups. Two to three level of splitting in a tree-like way would be necessary to provide common clocks to all TDCs.

Measurements were done on a clock system similar to Fig. 4.14. The results can be found in Table 4.3. The precision of the 156.25 MHz clock is better than 5 ps even after a 20 m clock tree and the precision of the 250.00 MHz clock is better than 6 ps. These values fully match the TOF wall requirement.

Table 4.3: RMS values of timing jitter (TIE: time interval error) for the output signal at CLOSY2 and after 2 times cascading over 20 m distance (2x10 m). Table taken from [69].

output freq.	method	@CLOSY2	20 m distance
156.25 MHz	TIE	3.2 ps	4.2 ps
	Period	2.3 ps	3.1 ps
250.00 MHz	TIE	4.0 ps	6.0 ps
	Period	4.2 ps	5.4 ps

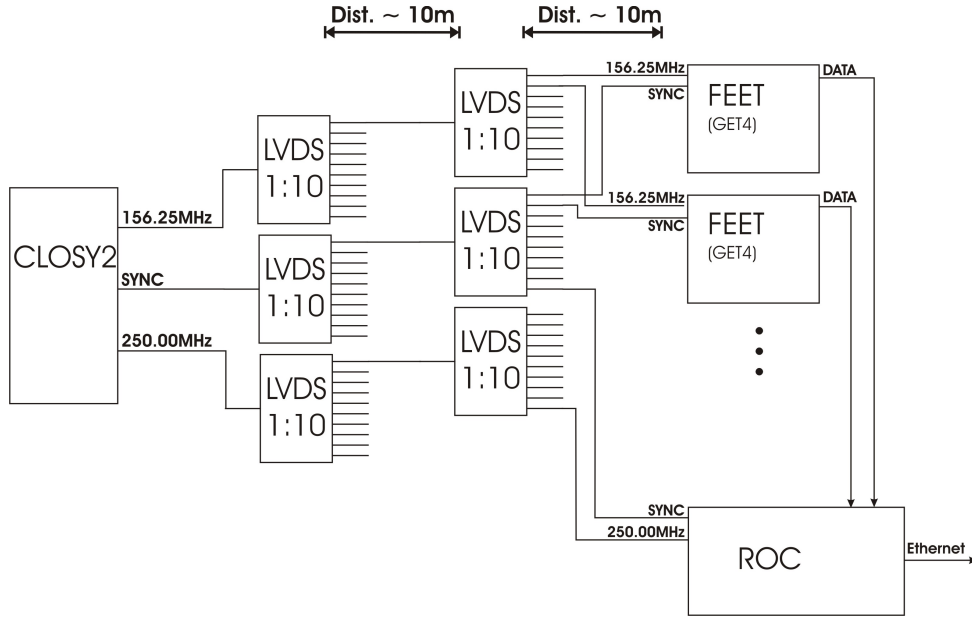


Figure 4.14: CBM TOF wall clock system diagram. Figure taken from [69].

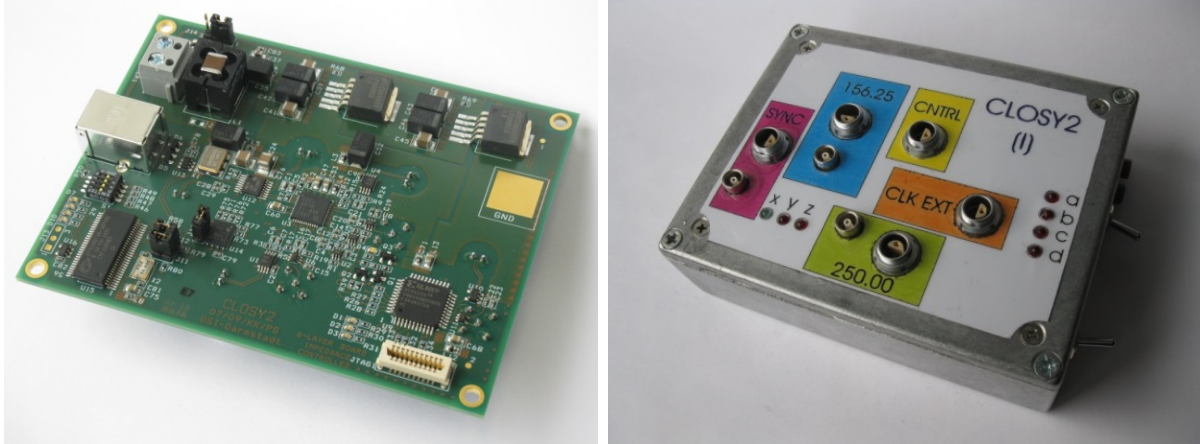


Figure 4.15: CLOSY2 board naked (left) and in its protective case (right).

4.2.4 Readout Controller

The ReadOut Controller (ROC) for the GET4 chip is a firmware loaded on the SYSCORE v2 FPGA board, pictured in Fig. 4.16. The board is based on a Xilinx Virtex-4 (XC4VFX20-10FFG672C) FPGA. This board and the communication part of the firmware are common to the prototyping of our readout chain and of the n-XYTER readout chain which is used for tests on some of the other CBM detectors [70]. It was developed at the Kirchhoff-Institut für Physik (KIP) in Heidelberg [71].

The ROC has two main tasks in our readout. The first one is to perform the continuous readout of the GET4s, configuring them on startup and checking that they are staying synchronized. The second one is to make the interface to the general CBM network (CBMTnet) [72]. As the interface to CBMnet is common to all CBM sub-systems, the

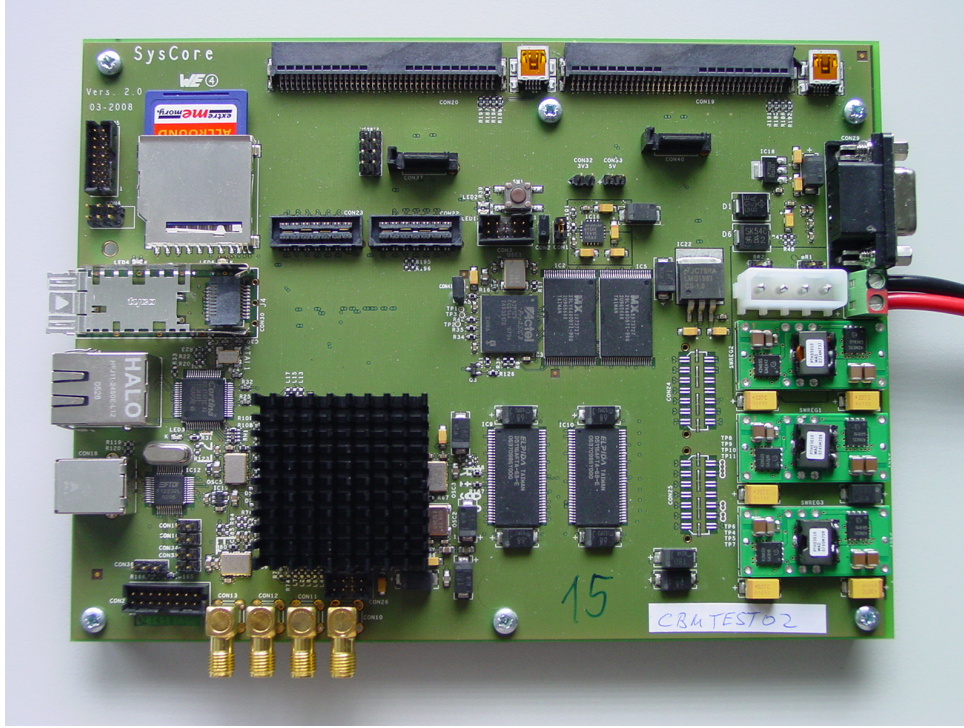


Figure 4.16: SYSCORE v2 board, used for the GET4-ROC.

firmware is organized in two modules, a transport module and a front-end module. Two versions of the transport module are available, allowing to connect the ROC either through Ethernet or via a 2.5 GBit/s optical fiber [73].

When an optical connection is used for the ROC output, the other end of the link is realized using the Active Buffer Board (ABB) [74]. This board is another CBM development based on a FPGA development board, which can be installed in a computer.

The ROC receives the 156.25 MHz clock, the 250 MHz clock, the Epoch SYNC signal and the GET4 serial data through a flat band cable and its ERNI[®] connectors (top in Fig. 4.16). The serial up-link used to send commands to the GET4 chips is also going through this connector. Due to the limited number of IO pins able to be used for differential LVDS links on the FPGA, the total number of GET4 chips which can be readout with the ROC is limited to 16 for the GET4 Proto (8 per ERNI[®] connector). The different clock domains used in the GET4 firmware can be seen in Fig. 4.17. The 156.25 MHz clock is used for the parts of the design performing the connection to the GET4. The 250 MHz clock is used for the time-stamping of the ROC system messages and to generate the 125 MHz clock used in the rest of the FPGA design. The ROC has 32 bit counters for the epochs of both the 156.25 MHz and the 250 MHz clocks. It can generate the so-called “ROC Epoch” messages on each 250 MHz clock epoch if the user enables them. This messages then contain the ROC epoch index from the corresponding epoch counter. The epoch counter for the 156.25 MHz clock is used to add an epoch index in the “GET4 Epoch” messages received from the GET4 Proto chips.

A set of General Purpose Input/Output pins allows to insert time-stamped system mes-

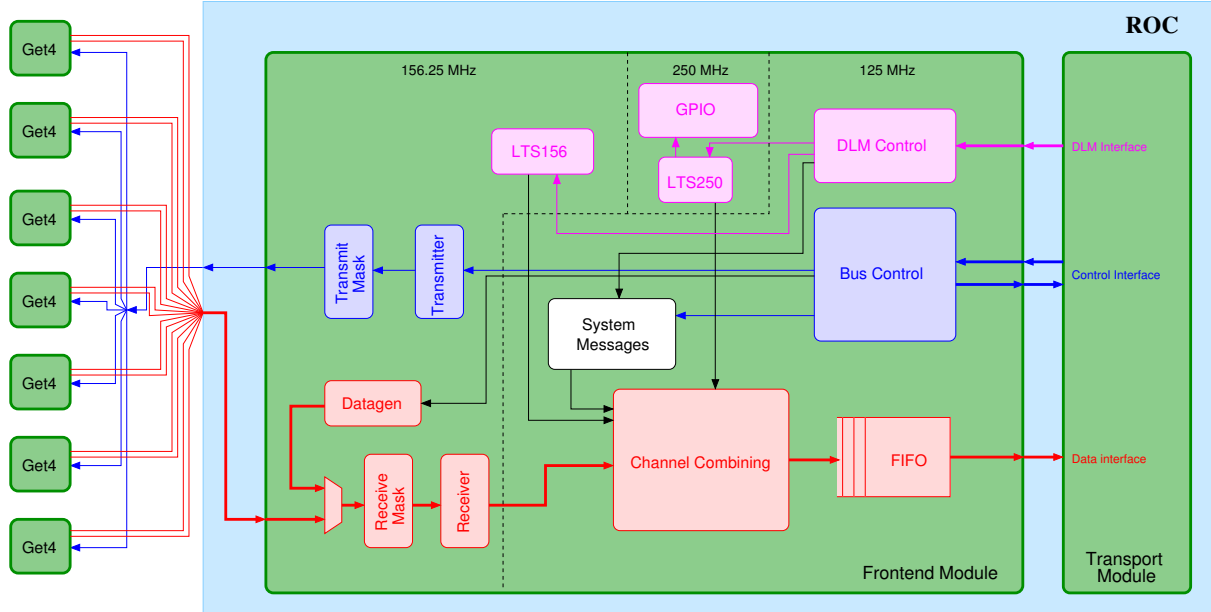


Figure 4.17: A schematic overview of the Frontend Module for the GET4 read-out. Figure taken from [20].

sages in the GET4 messages data stream. This functionality is especially useful to synchronize the free-streaming system with a triggered system. In this particular case the so-called “System SYNC” messages are used. Their use will be described in more details in Subsections 4.3.1 and 4.4.2. As the naming of GET4 signals and ROC messages can be confusing with the same shortened name for different concept, Appendix C.4 brings a summary of both with their definitions and main usages.

Different versions of the firmware were used, bringing new functionalities. The main new properties of the firmware used for the setups will be described in Sections 4.3 and 4.4 when necessary.

4.2.5 Reference triggered system

A triggered system is used as reference in most of our tests. This triggered system is implemented using 6U VME boards. The readout control is done with RIO3-RIO4 controllers from CES hosting a LYNX operating system and running the MBS DAQ framework developed at GSI. These components are described in Appendix B.1. The trigger control is done using the TRIGLOG board, also developed at GSI, which is based on the VULOM3-VULOM4 FPGA boards and described in Appendix B.2.1.

For the TDC systems, a commercial CAEN board based on the HPTDC chip, named V1290A, was used as reference for the GET4 Proto tests. It is described in Appendix B.3. An FPGA TDC board from GSI, called VFTX, was used as reference for the GET4 v1.0 tests. It is described in Appendix B.4.

4.2.6 Software

As stated in Section 4.1, the software event building is also an important part of a free-streaming readout chain. The FLES presented in Section 2.4.1 as the online event builder and event selector for the CBM experiment is still in the design phase and not adapted for the development phase (beam tests in different facilities, need for access to all data for debugging purpose). Due to this, other software were used for data acquisition, online monitoring and offline analysis in the prototyping phase.

The software chain used in the hardware tests is made of the Data Acquisition Backbone (DABC) DAQ [75], the GO4 (GSI Object Oriented On-line Off-line system) monitoring and analysis software [76], and the ROOT framework [77]. DABC and GO4 are both developed at GSI, while ROOT is developed at CERN. DABC is used for hardware readout and writing of raw-data files. It is able to write:

- data from the MBS triggered DAQ system [78],
- free-streaming data from the ROC,
- combined triggered events from the MBS DAQ with free-streaming data from ROC using a system SYNC marker written in both (see Subsection 4.2.4 and Appendix C.4)

The written data are for all cases stored in MBS event/sub-event containers inside the file.

GO4 is used for online error-monitoring and the first analysis steps such as:

- Time ordering of the messages,
- Hit building by associating rising and falling edge (if not done already by the TDC),
- Event building for the GET4 prototypes, using either trigger messages inserted in the data stream or the data themselves,
- Calibration of the bin-to-time conversion in the FPGA TDC case, where it is especially important .

This allows to go from raw-data messages to a data stream of TDC hits. The details of the tasks performed in GO4 will be described for each version of the digitizer.

ROOT is used in later analysis steps:

- RPC channel related data correction (walk correction, time alignment, ...)
- conversion of the data into detector related objects (clustering)
- extraction of the performance criteria (time comparisons, fitting, ...)

The software chain will be described in details for the different use-cases in Subsections 4.3.1 and 4.4.2.

4.2.7 Summary: Readout Chain Prototype

The prototype readout chain is depicted in Fig. 4.18. This scheme corresponds to the general TOF free-streaming readout chain concept described in Fig. 4.2.

Before the work described in this thesis was started, the time resolution of the readout chain was tested by the chips developers on a minimal version of the chain. Using a

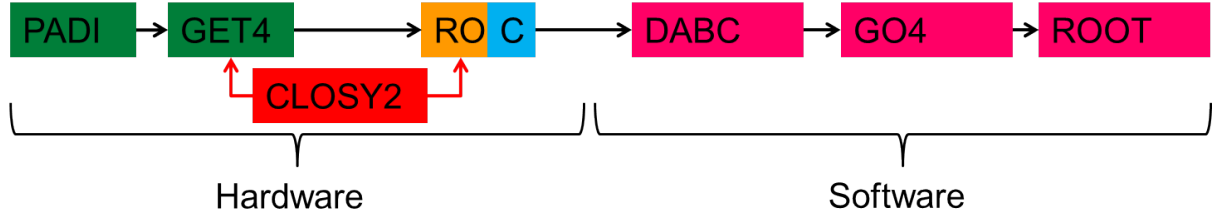


Figure 4.18: The free-streaming readout chain prototype based on the GET4 TDC, following conceptual blocks of Fig. 4.2.

pulser with analog splitting of the signals fed into two channels and the early prototypes combination (PADI-3 + GET4-Proto + ROC), the results shown in Table 4.4 were obtained [79]. This constitutes the starting point of the hardware testing done in this work with the full chain from detector to complete data analysis.

Table 4.4: Time resolution measured on the early prototype of the readout chain with PADI-3 equipped on FEET-PADI, GET4 Proto equipped on FEET-GET4 and ROC loaded on SYSCORE v2. The chip level value is for two channels in the same GET4 Proto chip. The PCB level value is for two channels in different GET4 Proto chips on the same board. The PCB-PCB level value is for two channels in GET4 Proto chips on the different boards.

	σ [ps]
chip level	36.94
PCB level	38.94
PCB-PCB level	40.22

4.3 GET4 Proto Evaluation

The first version of the free-streaming chain was built around the GET4 Proto chip. The first part of this section will describe the software chain used to unpack its data, followed by description and results of the two beamtimes performed with this version of the chain. The software chain was developed as part of this thesis.

4.3.1 Software Processing

The analysis procedure on data produced with this chip is organized in three steps:

1. hit building,
2. event building
3. calibration

Fig. 4.20 summarizes the initial software organization, where only GET4 data are processed.

The first step is realized inside a GO4 unpacker and consists itself of three operations (depicted in Fig. 4.19): data are cleaned, reordered and used to build hits. Cleaning the data is required because the ROC transfers all data to the DABC DAQ system. This means that unsynchronized data are still present, which are useless in a multi-chip environment. Those data messages are also not time ordered because there is a token ring readout system in the TDC chip. Finally the leading and trailing edges provided by the TDC have to be matched to produce full hits with time and TOT information.

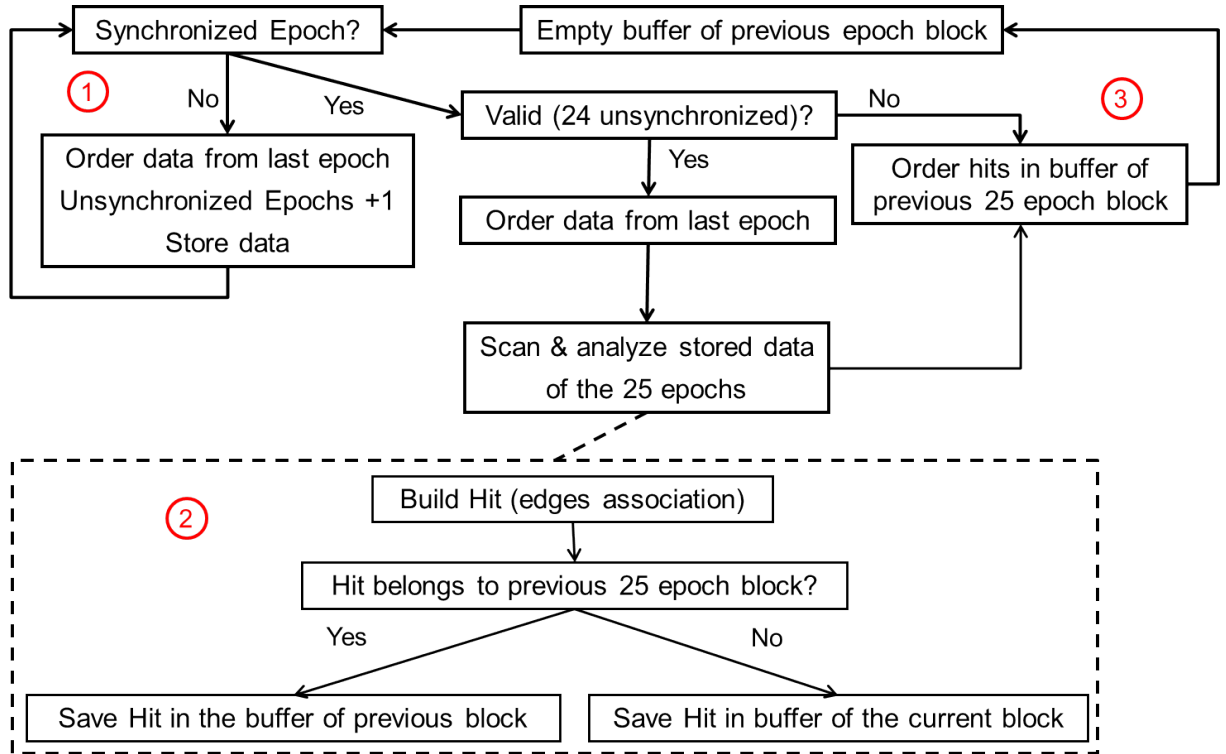


Figure 4.19: Cleaning and hit building procedure. For details, see text.

The cleaning is done by rejecting chip by chip invalid epochs blocks, i.e. groups of 25 epochs. An epoch block is invalid when the TDC loses its synchronization with the common clock system, which can be checked every 25 epochs using the SYNC flag on the GET4 epoch message. Buffers are used to store the data messages (signal edge data) between the epoch messages and to order them by their timestamps. This corresponds to stage (1) in Fig. 4.19.

If the epoch block is valid, the time sorted data messages in the 25 corresponding epoch buffers are used to build hits. The hit building is done by scanning the edge data and matching consecutive leading and trailing edges. The resulting hit is saved in the hit buffer of the epoch block to which its leading edge belong (current epoch block or previous one). This corresponds to stage (2) in Fig. 4.19. The hit buffer of the epoch blocks contains the hits from all connected chips.

The fact that an epoch with the SYNC flag is found means that all data belonging to the previous block are available, even if the current block is invalid. Therefore the content of the hit buffer for the previous block can be saved in a ROOT tree used by the next

steps. As the hits are placed in the buffer when the trailing edge is found but must be ordered by the timestamp of their leading edges for event building, a second time ordering is necessary before this data saving. This correspond to stage (3) in Fig. 4.19.

The second step, the event building, is done in a ROOT macro. Two options are available to build events:

1. The occurrence of signal coincidences is searched among the hits built during the previous step within a narrow time window. When a coincidence is found, all signals in a wider time window are associated to the event.
2. The *Ext SYNC* is used as reference. The data in a time window around this reference time are put together as event. This speeds up the data analysis as the data need to be scanned only once.

The same macro can be used for both options since the *Ext SYNC* is saved in data as an additional “fake” channel.

The third step, the calibration, is also done by a ROOT macro. The calibration consists of the walk correction on all signals as presented in Section 3.4.4.

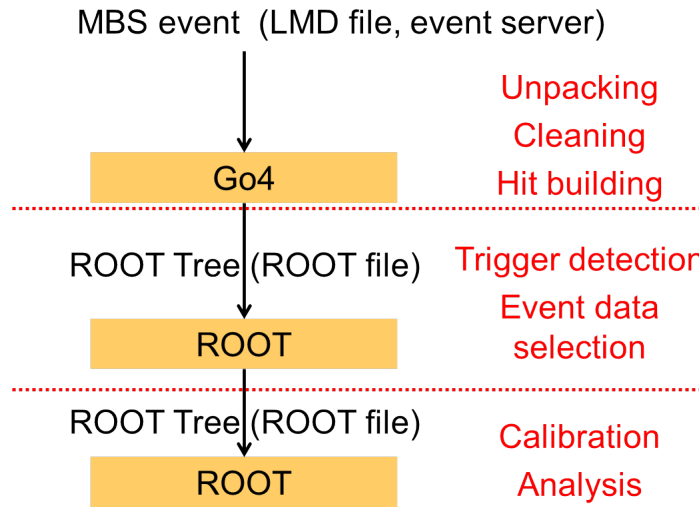


Figure 4.20: Software organization for the first COSY beamtime (in 2010), with the three steps, their software and input/output formats.

The CAEN V190A triggered TDC boards were also in use during the second beamtime at COSY (in 2011). An additional signal is then inserted at the ROC level to ensure the assignment of the proper free-streaming data block to the triggered event. This message contains an event number generated by the trigger board of the VME system (see Appendix C.4). The data from both systems are packed in the same event container, with a sub-event for the trigger board data, a sub-event for the triggered data and a sub-event for the free-streaming data. The event building step is then done inside the GET4 unpacker in GO4 instead of being a separate ROOT task. Due to this all data are unpacked in the same GO4 process, leading to the organization shown in Fig. 4.21. The *system SYNC* message replace the *Ext SYNC* of previous analysis. The main difference

is that its time stamping is done in the 250 MHz clock time domain instead of the 156.25 MHz GET4 time domain. This event building mode will be called from now on “pseudo-triggered” mode for the GET4. The term “free-streaming” mode then indicates an event building using triggers based on the offline analysis of the GET4 data themselves

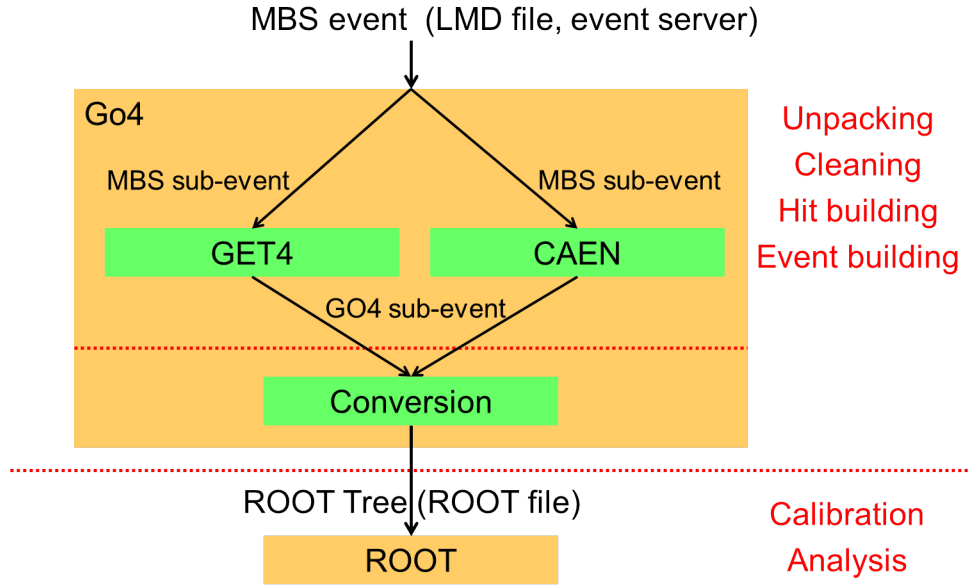


Figure 4.21: Software organization for the second beamtime at COSY (in 2011), with the three steps, their software and input/output formats.

4.3.2 First beamtime at COSY with GET4 Proto

For the first test of the GET4 system with realistic conditions (detectors signals and rates above few Hz), a proton beam of 3 GeV/c momentum and rates up to 400 Hz/cm² was used at the COoler SYnchrotron (COSY) in Jülich. Sixteen RPC strips on the Heidelberg RPC-P1 prototype (see Section A.1) were equipped with FEET-PADI and FEET-GET4 boards, while another FEET assembly was used to readout four plastics scintillators equipped on both side with Photo-Multipliers. The readout was done in pure free-streaming mode by a ROC loaded with the Ethernet firmware, the data being saved using the DABC v1 DAQ. The firmware had the following main functionalities on top of the basic GET4 readout:

- Individual GET4 masking
- GET4 Epoch counter on the ROC, the value of which being inserted in the free bits of the GET4 epoch messages
- *Datalost* flag added to epoch messages when other epoch messages or system messages were lost due to a full FIFO on the ROC since last emitted epoch

The first days of the beamtime were used for triggered data acquisition. Three runs were taken with the free-streaming system during the last night of this beamtime. During data

taking the monitoring was reduced to messages rate evolution and chip synchronization checks.

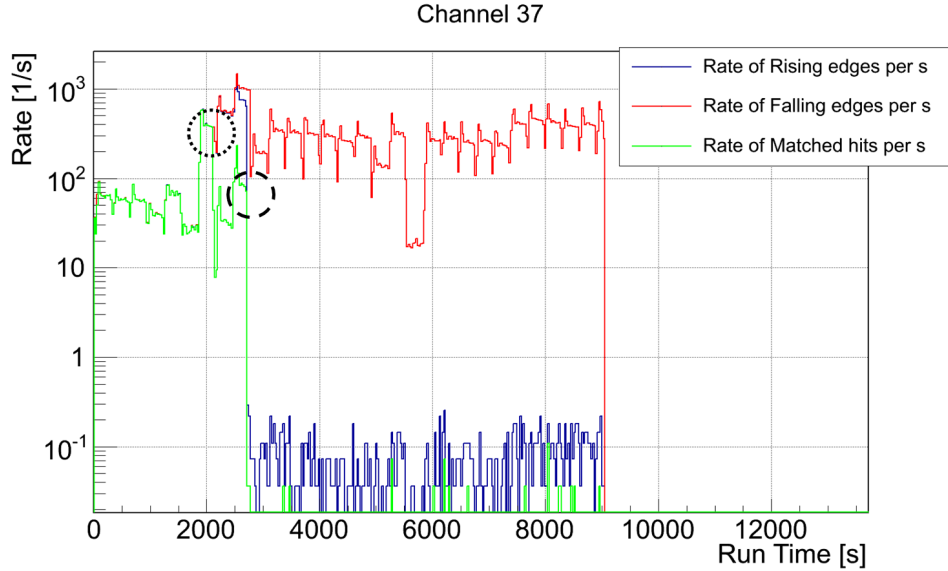


Figure 4.22: Example of the effect of a stuck buffer during COSY2010 beamtime. See text for more description.

A bug in the message management mechanism of internal FIFOs in the GET4 Proto was found during the analysis of those data. The *Epoch* flag should be inserted in parallel to the Event FIFO of each “edge/channel” pair when an epoch happen and reset also in parallel (see Section 4.2.2). On the GET4 Proto, it is in some cases either inserted twice or not properly reseted in one of the FIFOs. The conditions for this could not be precisely determined but a timing problem in the write decision logic of the FIFO was suspected by the developers and it seemed to happen more frequently in periods with higher beam rate. As the emission of the epoch message and removal of the *Epoch* flag is happening only when all eight FIFOs contains an *Epoch* flag in their first slot, the bug delays the emission of data messages for the affected FIFO by one epoch. As the data messages are time sorted by epoch, this leads to the wrong association of rising and falling edges from different epochs. The main symptoms on the analysis side are a decrease in the proportion of matched rising and falling edge relative to input edges and random spectra in the reconstructed TOT.

An additional effect is that there is then always one word with the *Epoch* flag set in the FIFO. When the bug happens more than once on the same FIFO, more and more slots become occupied by ‘extra’ *Epoch event*, until only slots reserved for *Epoch event* are left. When this happens, almost all data events are rejected.

Fig. 4.22 shows an example of this bug. The three curves describe the evolution of the hit building for TDC channel 37 as function of in-run time. The green curve of hits comes from matched rising edges (blue) and falling edges (red). After around forty minutes the rising edges are shifted by one epoch, leading to a decrease in rising/falling edges matching and around one hours after run start, the internal FIFO of the rising edge block

of channel 37 get stuck. In the figure, one can see those two glitches: the dotted circle correspond to the first glitch which shift the rising edge FIFO by one epoch, the dashed one to the last glitch which stuck the FIFO fully.

As some channels were stuck on the second beam spill and this error went unnoticed until the offline analysis was performed, most of the data were too corrupt to enable a relevant analysis on system performance such as time resolution, efficiency or their comparison to the triggered system performance. To avoid such case where the digitizers stay stuck for a few hours, modifications in the DAQ and monitoring software were introduced before the next beamtime:

- The DABC DAQ monitors the ratio of Leading and Trailing edges messages for each GET4 chip and triggers a reset of all chips if it diverges during more than two GET4 epochs, indicating a probably stuck FIFO.
- The monitoring software implemented in GO4 provides to the user an overview of the epoch value of all chips, allowing to detect GET4's offset relative to the others.
- The monitoring software implemented in GO4 provides to the user an overview of the Leading and Trailing edges time matching as well as an online coarse hit building.

Additionally, due to the limited bandwidth of the Ethernet link and the quite high variations in beam rate between spills (see Fig. 4.23), some message losses at the ROC level are suspected. To solve this, a firmware with optic readout was brought in use and additional flag inserted by the ROC to the GET4 epoch messages: the so-called *datalost* and *epochlost* flags. The *datalost* flag is used to indicate that some data were lost in the ROC buffer due to overflow during last GET4 epoch. The *epochlost* flag indicates that even the part of the buffer reserved only for epoch messages got overflowed and that at least one epoch message is missing for the chip in consideration. These two flags allow for an additional data cleaning by rejecting the 25 epoch blocks between the previous epoch with a SYNC flag and the next epoch with a SYNC flag, as in those the data synchronization cannot be ensured.

4.3.3 Second beamtime at COSY with GET4 Proto

Free-streaming data were acquired for a second time in November 2011 at COSY, Jülich, with a 3.35 GeV/c momentum proton beam, using also the GET4 Proto as TDC. Most of the setup used at this time was triggered.

System description

The setup is sketched in Fig. 4.24. It was composed of a fiber hodoscope for beam profile monitoring, three plastic scintillators equipped on both ends with photomultiplier tubes (PMT) and eight RPCs. The self-triggered hardware chain described in Subsection 4.2.7 was used to readout a fully differential RPC built in Heidelberg [80], described in more details in Appendix A.2, with 1 FEET board on each side of the detector, for a total of 8 strips. The mean time of the 4 front PMTs is used as the reference time against which

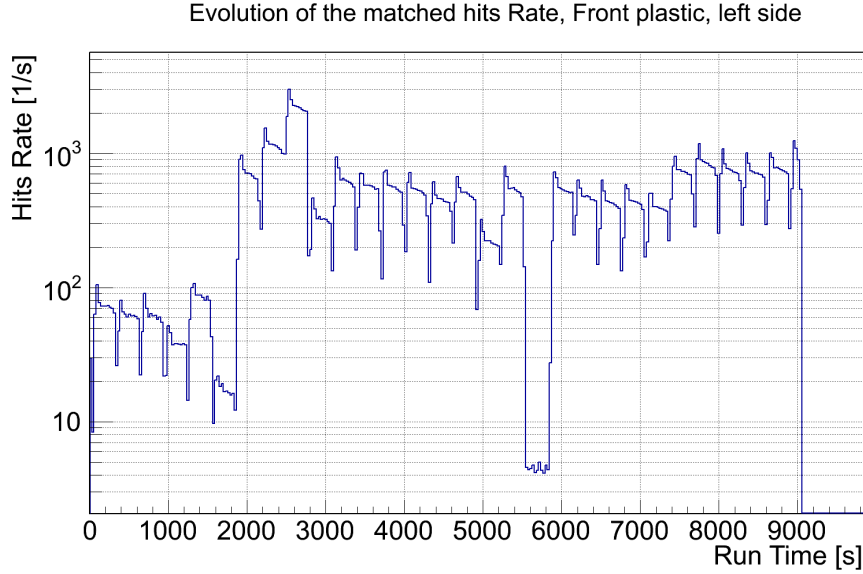


Figure 4.23: Data rate on the GET4 channel corresponding to the PMT on the front scintillator ($\sim 2 \times 4 \text{ cm}^2$) left side, as a function of time during the COSY 2010 beamtime first run with free-streaming readout.

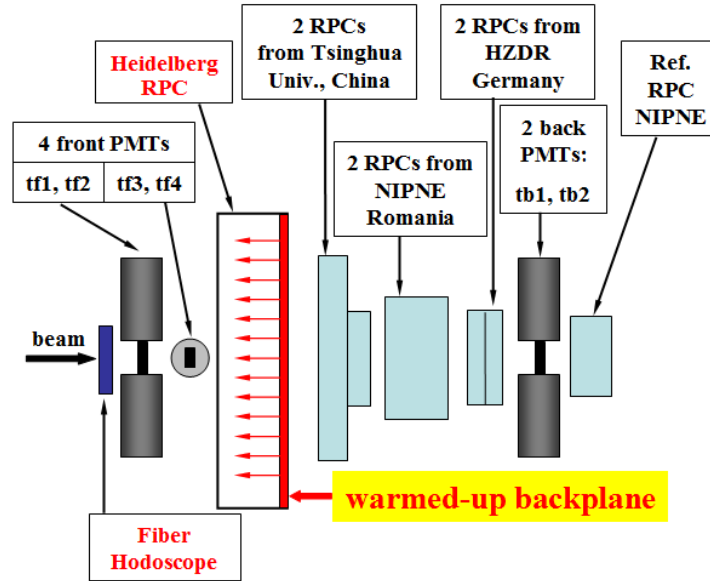


Figure 4.24: Setup used for the beamtime in COSY in November 2011. Heidelberg RPC and the fiber hodoscope (names in red) were readout by free-streaming electronics, while all other parts of the setup were readout by triggered electronics.

we evaluate the RPC timing. However since the other RPCs were readout with triggered electronics and in order to keep this reference time in a well understood readout system, the PMTs were readout in a triggered CAEN V1290A VME TDC board based on the CERN HPTDC (see Appendix B for more details). For this reason we need a hybrid system allowing to synchronize the two systems and combine the times they measured.

With the hybrid system, one can also make sure that the signal observed in the free-streaming system are fully understood using the well-tested triggered system.

The hardware trigger was built from coincidences of 4 PMT signals: two coming from both ends of one of the front scintillators, and the two coming from the back scintillator. In the analysis, we used only events with a software coincidence of all 6 PMTs, as the 4 front ones performed better and were used for time reference. The trigger rate was kept to a few hundred Hz because of the instabilities on the TDC FIFO level in the free-streaming part found in the previous beamtime (see previous section).

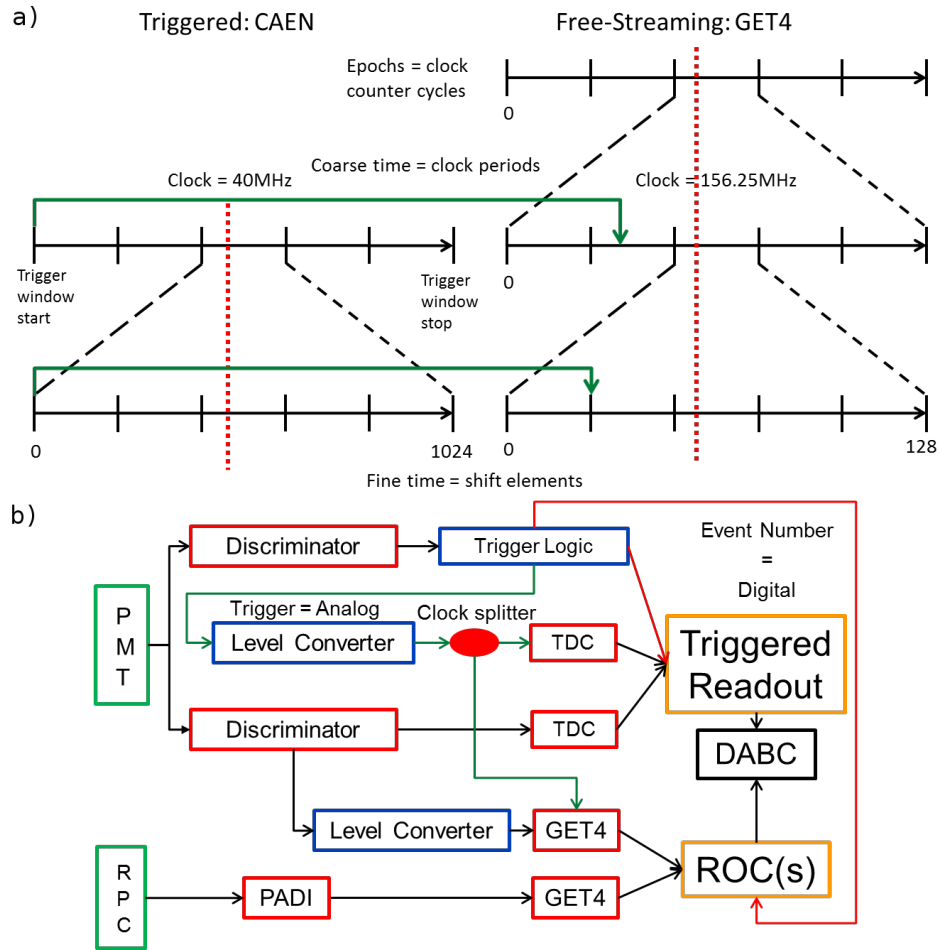


Figure 4.25: The synchronization in the hybrid system: a) Concept and b) Implementation. Green lines are time synchronization signals and red ones are event synchronization. Red dotted lines in the concept diagram indicate an interesting hit in each system. For details, see text.

The synchronization between the two systems proceeds with two levels of accuracy, as shown in Fig. 4.25 a): first at the event level, by using already existing possibilities of the DABC DAQ and our trigger board, then at the timing resolution level, by measuring the same signals with both systems. The first one is needed because the triggered time frame is event relative, giving times measured from the beginning of the trigger window, while the free-streaming time frame is absolute, giving times measured from the start of

the acquisition. This synchronization allows to match free-streaming hits with a defined triggered event. It is done by injecting in both the MBS event and all ROC data streams an event number generated by the trigger board. This number is timestamped by the 250 MHz clock by each ROC on reception and saved as a *System SYNC* message. The second level is achieved by generating a common point for each event in both the free-streaming time frame and the triggered TDC time frame at their full resolution. This is needed to compare the reference time to the detector time and evaluate the system performance, as they run on different clocks. This synchronization is realized by converting the NIM trigger signal from the triggered system to a LVDS signal accepted by both systems, splitting it with a low jitter clock splitter and re-injecting it in the inputs of an additional GET4 TDC board and an additional CAEN TDC, see Fig. 4.25 b). One PMT signal (PMT 6, labeled tb2 in Fig. 4.24) is also measured in both systems, allowing for an independent cross check of the fine time synchronization offset.

The trigger signal used for synchronization and the PMT signals were digitized in two different CAEN boards. These boards were synchronized by using a common clock and a common reset after each event (see Appendix B.3).

The firmware used for the ROC brought the following new functionalities compared to the one used for the COSY 2010 beamtime:

- Optical transport compatible with GET4 readout
- Size if the GET4 epoch counter increased
- Size if the 250 MHz epoch counter increased
- Possibility to switch off the 250 MHz epoch messages emission by the ROC
- Modified flag *datalost* and new flags *epochlost* to indicate more precisely data losses at ROC FIFOs level (see Subsection 4.3.2 for their descriptions and justifications)
- Optional flag allowing to sample the GET4 data either on the rising or on the falling edge of the serial link clock

Results

Unfortunately, we found out during analysis and confirmed with laboratory tests after the beamtime that one of the two boards used to acquire the RPC data in the free-streaming system was malfunctioning during data taking. The fine time (50 ps bin counter from the delay chain inside the TDC) uses in those data only half of the available range. Because of this, both time and TOT information are corrupted for all channels on one side of the RPC. Additionally, a second fake hit using the other part of the fine-time range is present in the affected channels. Fig. 4.26 shows this effect for one of the RPC strips covered by the trigger. This prevents us from extracting meaningful results for the full system resolution and efficiency or the electronic chain resolution. As this error involves the fine-time in the recorded data, no further recovery or improvement is possible on these COSY 2011 beamtime data. It was suspected this failure could have been caused by mechanical stress on the clock connectors of the FEET-GET4 board. To reduce this, the clock distribution is simplified and stabilized for the GET4 v1.0 by the motherboard PCB.

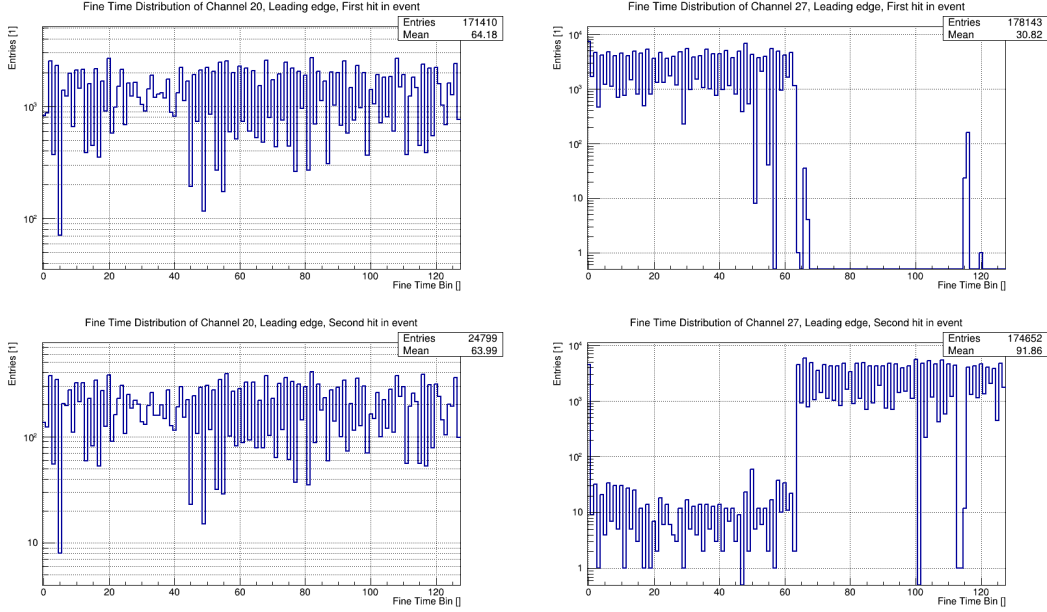


Figure 4.26: Fine Time distribution of the Leading edges for the first (top) and eventual second (bottom) hits per event, for each end of the RPC strip 4 (left on left, right on right). The GET4 reading out the right side was broken, using only 1/2 of the fine-time range and generating fake second hits.

However, the GET4 board used for the synchronization between the free-streaming and triggered system was not affected by this malfunction so we can still have a hint of the system performance by looking at the synchronization precision.

The resolution of the time synchronization part of the setup can be estimated by calculating the time difference between the PMT6 signal in the triggered system and its signal in the free-streaming system, re-aligned using the offset obtained with the trigger signal:

$$\Delta t_{PM6} = t_{PM6,CAEN} - t_{PM6,GET4} - Offset \quad (4.3)$$

$$\text{with } Offset = t_{trigger,CAEN} - t_{trigger,GET4} \quad (4.4)$$

The value is then given by the width of the difference between those two quantities (Fig. 4.27):

$$\sigma_{\Delta t_{PM6}} = 83 \text{ ps} \quad (4.5)$$

This value is worse than what could be expected by the simple combination of the typical time resolution for each part of the system: 25 to 30 ps depending on channels for the CAEN board, 25 ps for the GET4. The channel to channel jitter of the Constant Fraction Discriminator and the input to output jitter or the leading edge discriminator are both estimations.

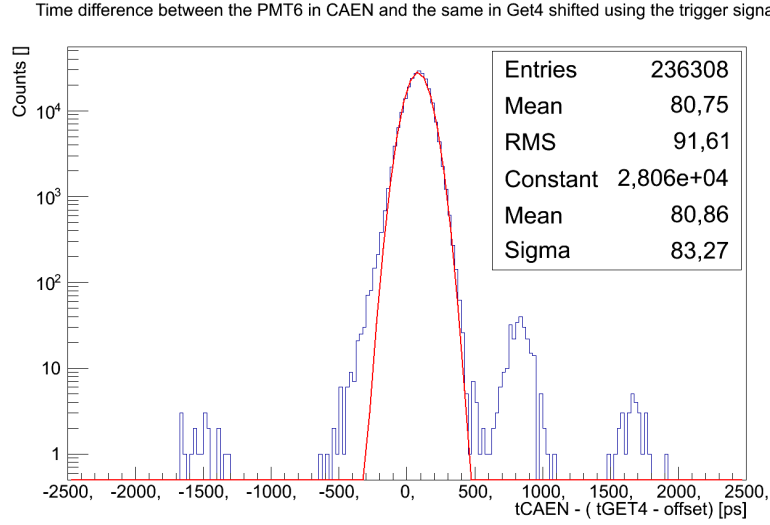


Figure 4.27: Difference between the time of PMT6 measured in the triggered system and the same recorded in the free-streaming system corrected using the trigger signal. Satellite peaks account for 0.25% of all events.

From Eq. 4.3 and 4.4 and the signal chains in Fig. 4.28, one could expect a synchronization resolution in the order of:

$$\sigma_{\Delta t_{sync}} = \sqrt{2\sigma_{CAEN \ 1 \ chan}^2 + 2\sigma_{GET4 \ 1 \ chan}^2 + \sigma_{splitter}^2 + \sigma_{LE \ discr.}^2 + \sigma_{Level \ conv.}^2} \quad (4.6)$$

$$\leq \sqrt{2 * 30^2 + 2 * 25^2 + 5^2 + 20^2 + 10^2} \text{ ps} \quad (4.7)$$

$$\leq 60 \text{ ps} \quad (4.8)$$

Two additional sources of jitter can also be suspected: the synchronization inside the triggered system between the CAEN board with the synchronization signals and the one with the PMT signals on one side, and the splitting of the synchronization signal to feed both the triggered and the free-streaming parts of the setup.

To avoid this kind of difficulties, a splitting of all signals is used in the latter tests, making all signals available in both systems and removing the need for a timing wise synchronization between them. An additional reason for this is that with RPC counters getting close to the 50 ps resolution, the synchronization contribution would become one of the biggest timing error in the system, possibly hiding other effects. In such a setup where all signals are splitted, one can compare the measurement accuracy of time differences in each system, as each difference is time frame independent.

4.4 GET4 v1.0 Evaluation

The second version of the free-streaming chain to be tested was built around the GET4 v1.0 chip. This new chip was designed taking into consideration the problems encountered

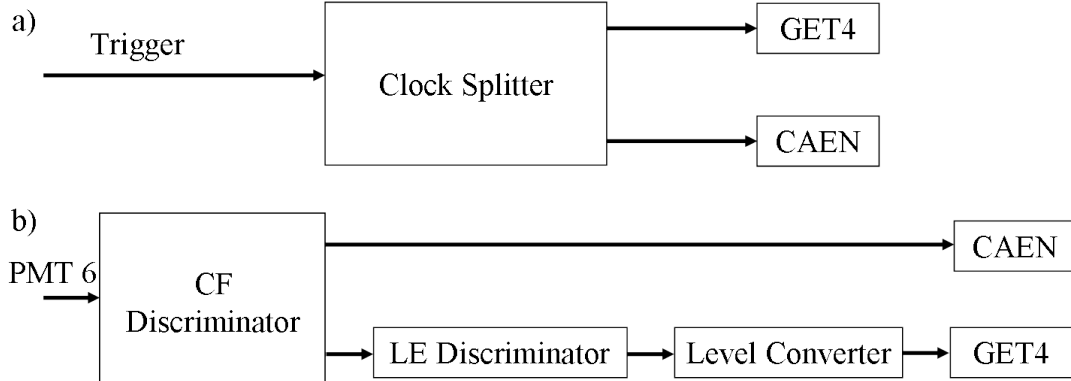


Figure 4.28: Detailed path of the PMT6 and the trigger signals in the COSY 2011 setup: a) Trigger signal b) PMT6 signal. The paths are shown from the last splitting between the signals going to the CAEN TDC on one side and the GET4 TDC on the other. CF stands for Constant Fraction and LE for Leading Edge. The same signal is on both outputs of the CF discriminator.

with the GET4 Proto. New VME boards based on the VULOM family were added to the triggered part of the setup, the so-called SCALORMU boards. These boards provide an RPC OR signal, an RPC channel multiplicity signal and scalers to monitor the signal rate of the RPC channels. The SCALORMU board is described in more details in Appendix B.2.2.

The first part of this section will describe the parts of the GET4 v1.0 which are different from the GET4 Proto. It is followed by a description the software chain used to unpack the data of the new readout chain. Finally are presented one beamtime, one pulser test and one cosmic test performed with this version of the chain and their results.

4.4.1 The GET4 v1.0 chip

Changes relative to GET4 Proto

The GET4 v1.0, which is the first version meant for normal users, brings the following improvements compared to the GET4 Proto:

- Correction of the Epoch bug, see Subsection 4.3.2 for description and Subsection 4.4.3 for more details on the modifications
- Improvement of the Differential Non Linearities (DNL)
- Channel masking \Rightarrow allow to disable noisy channel before they saturate the readout
- DLL lock bit added to each data message, allowing to know if the DLL is locked
- Slow Control command allowing to relock the DLL
- Add an on-chip 24 bit epoch counter to improve chip to chip synchronization
- 32 bit readout mode associated with an on-chip TOT calculation \Rightarrow simplifies unpacking and gives $\sim 30\%$ bandwidth gain
- Hamming encoding of important flags for each message stored in the internal FIFOs and Hamming errors counting

- Slow control messages with count of clock cycles during which internal FIFO High Water mark is active
- Generally improved error detection and more detailed error messages

The 24 bit epoch counter defines a time period of $t_{dyn} = 439.805$ s (7 min. 19.805 s) during which all times are uniquely defined. This on-chip counter can be initialized with a value sent using the serial interface. This value is loaded on the next externally synchronized epoch, thus allowing a common starting point for all chips if they all received the message in the same interval between two SYNC pulses.

Readout block

The digital readout part of the chip is the one part with the most modifications relative to the GET4 Proto. Therefore, the functioning of the GET4 v1.0 readout block will be described in details, while the TDC core functionalities are the same as the GET4 Proto ones and can be found in Subsection 4.2.2.

If a hit is detected in any of the two encoding blocks of an “edge/channel” pair, a 36 bits long internal event word is built. It consists of:

- the fine-time of both encoding block
- a flag indicating if a hit is present for each of those blocks
- some flags for epoch control
- the current time-stamp

The exact content of this word is shown in Table 4.5. The *SYNC* flag indicates that a SYNC pulse was received in current epoch. The *EPOCH* flag indicates that a time stamp counter overflow appeared since last sent message and that an epoch message needs to be inserted before sending the new hit(s).

An additional flag indicates if the DLL was in the lock state and two Hamming codes protect the *SYNC*, *EPOCH* and *DLL* flags as well as the time-stamp against data corruption. As this version is counting the epochs with an internal 24 bits counter, the same message word is used to store the 12 least significant bits of this counter for each new epoch, forming an epoch event word. This allows a cross check between the epoch values stored in the FIFO of the eight “edge/channel” pairs.

Each of these pairs has an Event FIFO with seven slots. The filling state of the FIFO and the event word type determine whether the event word is stored in the FIFO or thrown out. A High Water mark is activated if 6 out of the 7 slot are filled. As epoch events have a higher priority, the data events are not written any more when this mark is active, to ensure the last slots is reserved for epochs. If this happens a *lost event* error message is generated. If an epoch events come, it is placed in the last slot and the FIFO full flag gets active. In case an additional epoch comes before at least one entry is readout, it cannot be written in the FIFO. As the epoch synchronization is then lost, a *FIFO write error* message is generated and the FIFO is reseted.

A token ring is used for the readout of the eight Events FIFOs (one for each edge of each channel). A simplified state diagram of this token ring is presented in Fig. 4.29 for the GET4 v1.0 and higher version.

In the GET4 v1.0 case, the token ring master goes first in the Reset state on startup and then wait for the readout system to be properly initialized before sending the token to the first readout unit. On startup the readout subsystems enter the Wait state and readout data from the FIFO as soon as available. After reading a data word from the FIFO, the unit goes in the *DataAvailable* state. At this point it checks if the data word is an epoch. If it is the case the state machine goes in the *WaitEpochClear* state and signals it to the ring master. If it is not the case, it waits to receive the token and sends a data message out if data are present for *Hit A* or *Hit B* before sending out the token. Here, as a difference to the Proto case, if data are present in both *Hit A* and *Hit B*, the token is sent to the next unit after emitting the message corresponding to *Hit A* and the one corresponding to *Hit B* is sent on the next token reception. When the ring master receives back the token, it checks if all readout units are waiting for an epoch event (a.k.a. pending epoch). If it is the case, the master checks that the epoch counter in all units is the same. A discrepancy induces the emission of an *Epoch error* message and a reset of the readout system. Otherwise an epoch message is generated using the counter and sent to the output, the epoch clear signal is sent to all units and the token is sent to the first readout unit in the chain.

The output messages are written on an internal parallel bus. In the GET4 v1.0 more possibilities are open at this point compared to the GET4 Proto case with either:

- the so-called “24 bit readout mode”, which is similar to the GET4 Proto readout and where a 24 bits data message is sent for each edge of the signal
- the so-called “32 bit readout mode”, where data from the timing channels of both edge of the signal are combined to obtain directly the TOT, which is then combined with the time of the leading edge in a single 32 bits data message.

In the 32 bit readout mode, the allowed range for the TOT can be set by the user through a serial interface to the ROC. As the number of bits for the TOT field in the data message is fixed, this effectively sets the TOT binning. Combinations of data giving negative TOT are rejected.

PCB

This ASIC was bonded on the so-called “GET4 daughter board” PCB, with four chips per PCB. Fig. 4.31 shows the backside of a daughter board, where the bonded GET4 chips are visible. This PCB can be plugged on a motherboard able to host up to four daughter boards, where the power and clock distribution are performed. This new scheme was especially developed to simplify the cabling of the setup. Additionally, it improves the readout chain stability (see Subsections 4.3.2 and 4.3.3). The connection toward the ROC is done trough another daughter board, allowing easy changes in the interconnection link format. Fig. 4.30 shows a fully equipped baseboard.

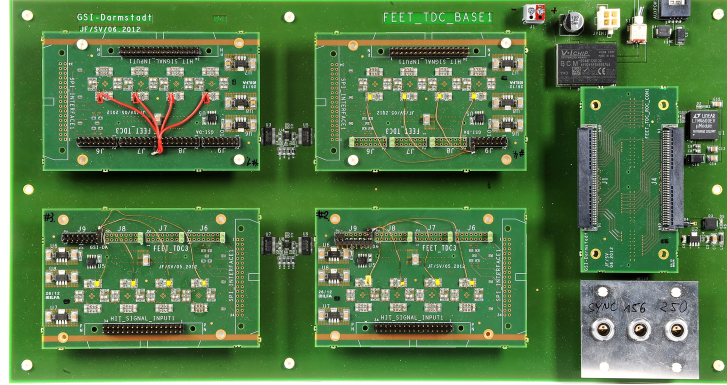


Figure 4.30: Baseboard for the GET4 v1.x chips, fully equipped with four daughter boards and a SYSCORE v2 ROC adapter board. The GET4 chips are on the backside of the daughter PCBs (More description in text).

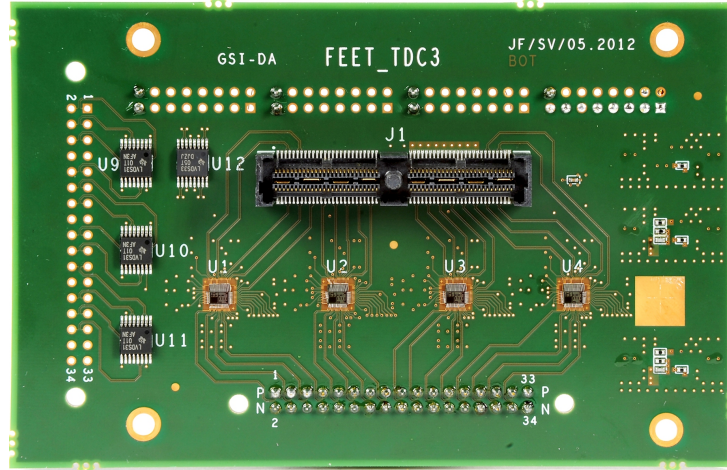


Figure 4.31: Backside of a GET4 v1.x daughter board, with four bonded GET4 v1.0 chips (More description in text).

Characteristics

The GET4 v1.0 non-linearity and resolution were measured by its developers using an internal test pattern generator present in this version of the chip. These measurements showed that the DNL were improved and are better than ± 1 LSB (or 50 ps) for all channels. With this improvement, the measured single channel resolution reaches $\sigma_{1ch} = 19.71$ ps for channels in the same chip and $\sigma_{1ch} = 27$ ps for channels on different daughter boards.

As the new 32 bit readout mode with on-ship TOT calculation should decrease the output link usage per input hit, the developers also simulated the rate capability of the chip for both readout modes using a random hit stimulus [67]. The simulation was done for different serial link readout speed. For each simulated point, the data stream rate is compared to the rate at the input of the chip, summed up for all channels. The results for the 24 bit readout mode are shown in Fig. 4.32 and the results for the 32 bit readout

mode are shown in Fig. 4.33. Table 4.6 summarizes the results for both readout modes. The table presents the rate at which the readout link saturates (too many data and error messages), while first effects start slightly before when some events are lost due to dead-time. Results are presented for different speed of the output serial link (Data Rate in the table). A 400 kHz/ch rate capability is required for the electronic chain, which corresponds to an Event rate of ~ 1.6 MHz at the chip input.

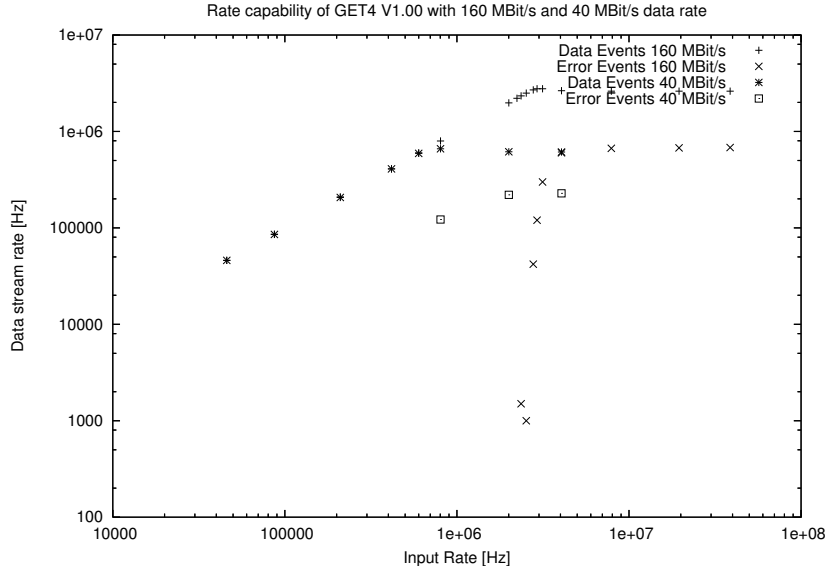


Figure 4.32: Simulation of the data rate capability of the GET4 v1.0 ASIC in 24-bit readout mode. Figure taken from [67].

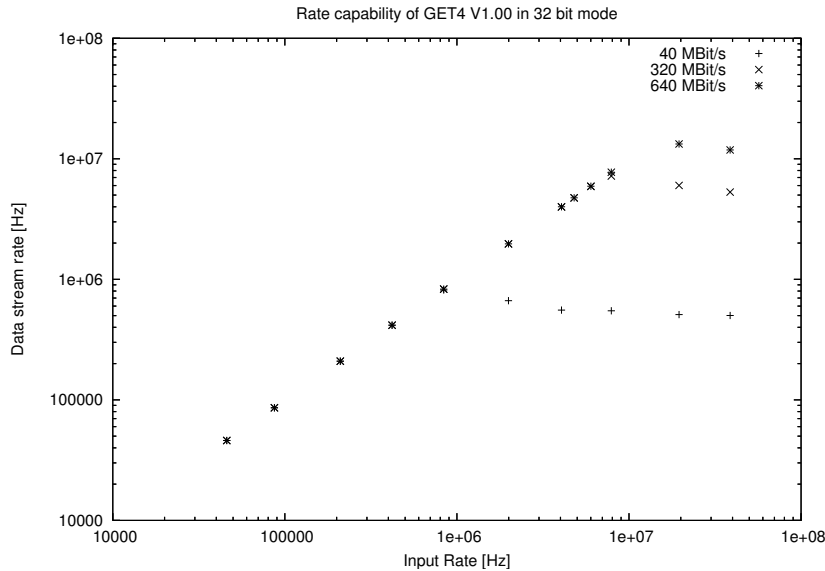


Figure 4.33: Simulation of the data rate capability of the GET4 v1.0 ASIC in 32-bit readout mode. Figure taken from [67].

These measurements are cross-checked and pushed further in Subsection 4.4.4.

ROC firmware for GET4 v1.0

The ROC firmware for the GET4 v1.0 bring the following changes:

Table 4.6: Simulated maximum event rates for GET4 v1.0. The event rates are summed up for all 4 channels (event rate/ASIC). Table taken from [67].

Data Rate MBit/s	Event Rate / MHz	
	24 Bit mode	32 bit mode
40	0.660	0.815
160	2.77	
320		7.19
640		13.28

- a cross-check is done on the counter in the GET4 Epoch messages, as the GET4 now has its own internal Epoch counters:
- the transmitted Epoch messages still contains the value of the ROC Epoch counter, but a flag indicates if the epoch value of the incoming messages was disagreeing with the ROC value
- the user can switch between both GET4 readout modes

Due to the limited number of IO pins able to be used for differential LVDS links on the FPGA of the ROC board, the total number of GET4 chips which can be readout with the ROC is limited to 8 in the GET4 v1.0 24 bit mode and 16 in the 32 bit mode.

4.4.2 Software Processing

General description

The software processing for the GET4 v1.0 evaluation is adapted to the prototype situation with either triggered data from the reference TDCs, pseudo-triggered data (a reference signal is fed to one of the GET4 chips or inserted in data by the ROC) or free-streaming data (only GET4 data are available). Unpacking, TDC calibration and a coarse hit building are realized in GO4. ROOT is used for later stages of analysis such as time corrections, cluster building and system performance extraction.

The unpacking software is organized in five stages with switchable sub-tasks, with the general goal to make as much as possible of these tasks common to the different event building schemes. The stages are unpacking, calibration, detector related tasks, matched detectors monitoring and a conversion of the data from the previous stages to a ROOT TTree file.

Triggered data processing

The VFTX TDC board is used as reference system to separate detector effects from electronic chain effects. As such, the analysis of its data is also of importance even if the system is triggered. This system represents the MRPC-prototype (detectors) evaluation system used by the CBM-TOF group. The software chain developed for it as part of this

thesis is currently used by many sub-groups as the first stage of detector data analysis. The software chain in the case of VFTX is shown in Fig. 4.34.

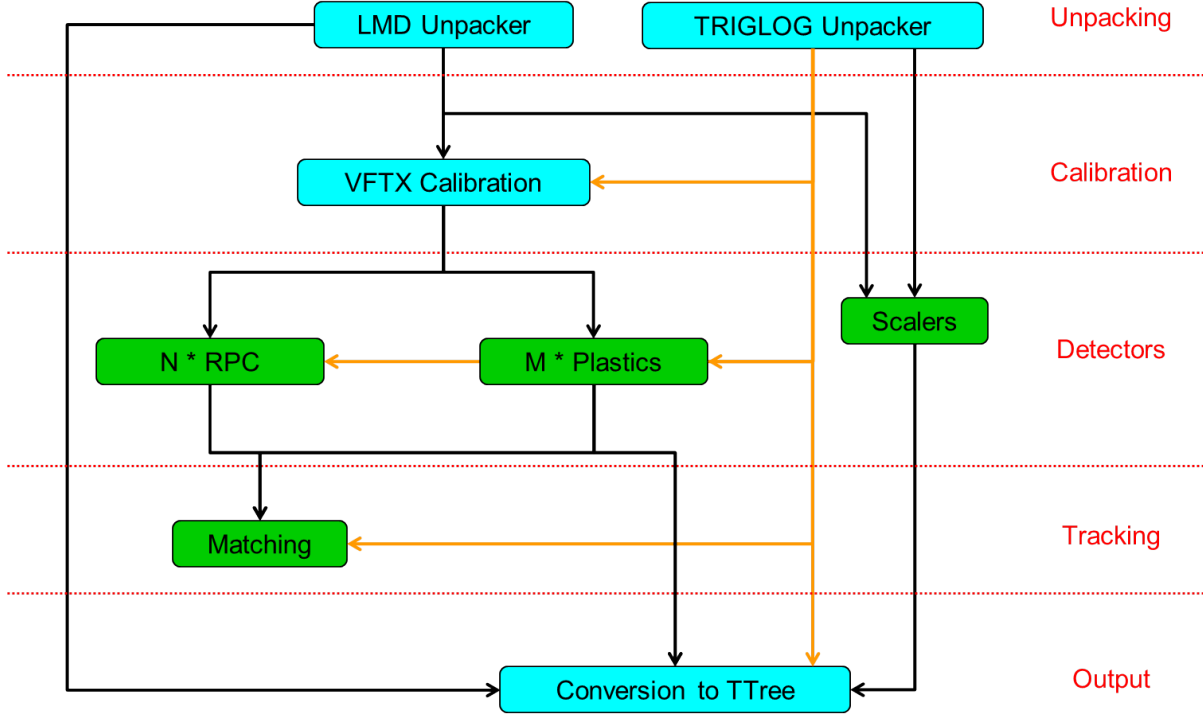


Figure 4.34: Software organization for the unpacking of VFTX (triggered FPGA TDC) data. The orange arrows originating in the TRIGLOG unpacker represent the rejection of events based on the trigger type of the event. LMD is a file format used to store MBS events.

Our event containers contain two sub-event for the triggered part of the setup, one for the data of the acquisition boards themselves (TDCs, QDCs, scalers, ...) and one for the data from our trigger board. The trigger data are unpacked in a separate tasks so that they can also be easily used for online monitoring. This organization also allows to reject events in other tasks by using the trigger type of the event.

The raw data are first extracted from the MBS sub-event and sent to sub-tasks dedicated to the unpacking of the data from the different VME boards used in the setups. The TDC data from the VFTX TDC boards are then converted from bin to time using calibration files previously generated using the method presented in Section 3.4.3. Some optional offsets can also be applied at this stage to both the time and TOT information. This can be necessary due to the different path length leading from the FPGA input to the timing units for the different channels and different edges. Without offsetting the position built from the left and right time of a RPC strip has a different mean for each strip and the TOT of some channels is shifted to negative values. Data from the other TDC systems (CAEN v1290A, GET4) are directly converted to time in the unpacker assuming a fixed bin size.

In the detectors stage, three tasks are performed. A first tasks use the TDC data now

converted to time to first build hits by matching data on both ends of RPC strips, and then RPC clusters by checking the time and space matching of neighboring fired strips. The timing at the ends of the strips (t_{left} , t_{right}) is used as described in Eq. 4.9 to calculate the position of the hit along a fired strip. In this equation one assumes a constant propagation velocity of the signal along the electrode of $v_{prop} = 18$ cm/ns, that the strip is horizontal and that it is centered on the 0 of the X axis. The mean cluster time ($t_{cluster}$) and the mean position of the cluster ($Pos_{X,cluster}$, $Pos_{Y,cluster}$) are obtained through a TOT weighted mean as shown in Eq. 4.10 to 4.12. The strips pitch is represented in these by $Pitch$ and the strip index by i_{strip} .

$$Pos_{X,strip} = (t_{left} - t_{right}) \cdot \frac{1}{2} \cdot v_{prop} \quad (4.9)$$

$$Pos_{X,cluster} = \frac{\sum_{strips} (tot_{left} + tot_{right}) \cdot Pos_{X,strip}}{\sum_{strips} (tot_{left} + tot_{right})} \quad (4.10)$$

$$Pos_{Y,cluster} = \frac{\sum_{strips} (tot_{left} + tot_{right}) \cdot i_{strip} \cdot Pitch}{\sum_{strips} (tot_{left} + tot_{right})} \quad (4.11)$$

$$t_{cluster} = \frac{\sum_{strips} (tot_{left} + tot_{right}) \cdot (t_{left} + t_{right})}{2 \cdot \sum_{strips} (tot_{left} + tot_{right})} \quad (4.12)$$

A second tasks builds on the same model Plastic scintillators hits. Here, as they can be considered simply as single strip RPCs, one just have to check the time coincidence of data on both ends of the scintillator.

A third tasks builds from the counters of the scaler boards and of the trigger board the rate per input channel and builds from it the rate per cm² of the detectors. Each VULOM board hosts its own oscillator which has a known frequency, and the counts of this reference clock are also saved in the event. By using this frequency and the ratio of the counts per input channel since last event divided by the reference counts since last event, one obtains the mean rate on this input channel since the last event. In our case the input channels were fed with the OR signal of the PADI boards of each end of the RPC. By summing up the rate of the proper input channels, one obtains the full counter rate. Averaging the left and right sides values allows to be closer to the count rate of real hits. As the total active area of the counter is known, one has then access to the mean rate per cm² of the full counter.

GET4 data processing

In the GET4 case, two configurations of the software chain are used depending on the event building scheme used.

Fig. 4.35 shows the configuration used in the pseudo-triggered case. In this configuration, the event is built by detecting the SYNC messages inserted from the triggered system in the free-streaming data, converting their time-stamp in a time domain common to the GET4 data and applying a selection time window on those data. The data from the

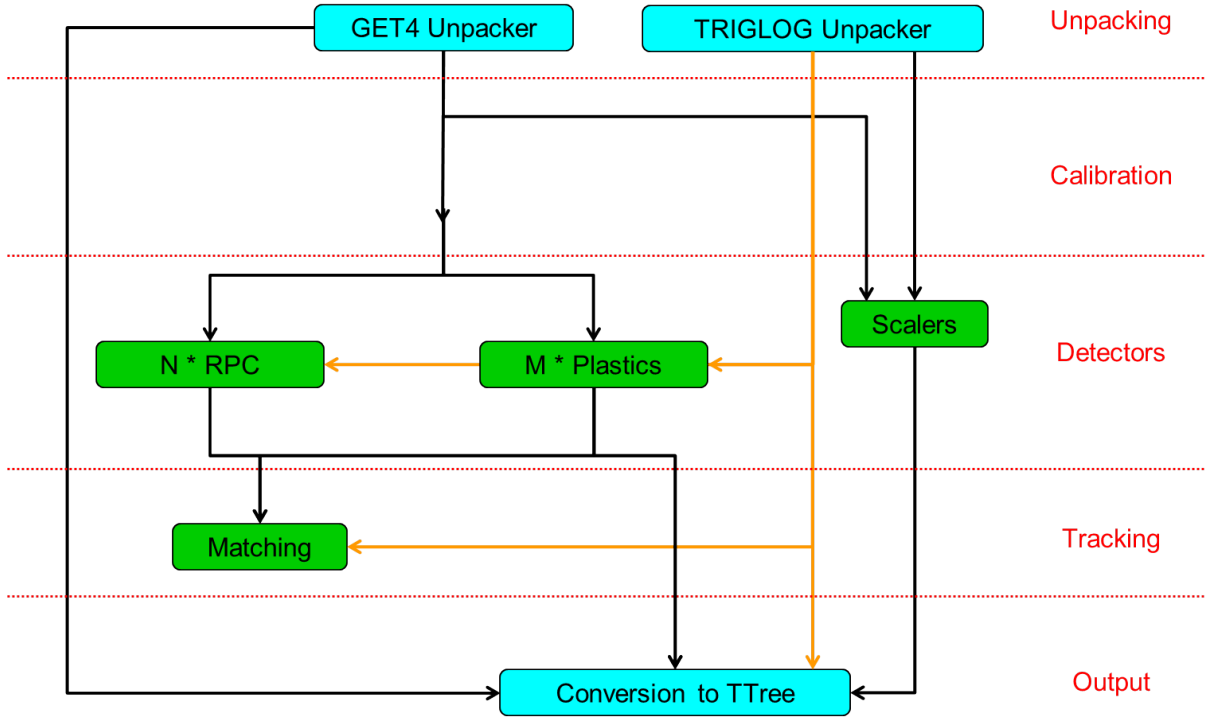


Figure 4.35: Software organization for the “pseudo-triggered” unpacking of GET4 data. The orange arrows originating in the TRIGLOG unpacker represent the rejection of events based on the trigger type of the event.

trigger board in the triggered system are also unpacked, allowing to reject events at the detectors stage.

The tasks for the detector stage of the analysis are the same as in the purely triggered case.

The algorithm for event building in GO4 in case of free-streaming data is as simple as possible to allow for online monitoring. Two alternating buffers are used to store all data from the previous epoch and the current epoch. When a coincidence of a selection of channels is found in a specified time window, the buffers are scanned and all data fitting a wider time window around the main trigger channel are saved. When the next epoch is found, all data since trigger detection are also checked. Up to 16 software triggers of up to 16 channels each can be defined. This event building mode is available only for tests with a single ROC and it is not planned to develop this line further. In future systems, event building will be based on the CBM micro-slice concept (time based analysis, see Subsection 2.4.1). For that purpose, the triggered and pseudo-triggered parts of the GO4 unpacker were ported to CbmROOT [81], which will be the base of CBM analysis and provide the tools for time-based analysis. This later development will be described in Section 5.3.

In both triggered and pseudo-triggered cases, it is assumed that there is no fixed time offset due to signal path between the edges when the TDC hits are built from pairs of leading and trailing edges like in the GET4 24 bit readout mode. All edges pairs for which

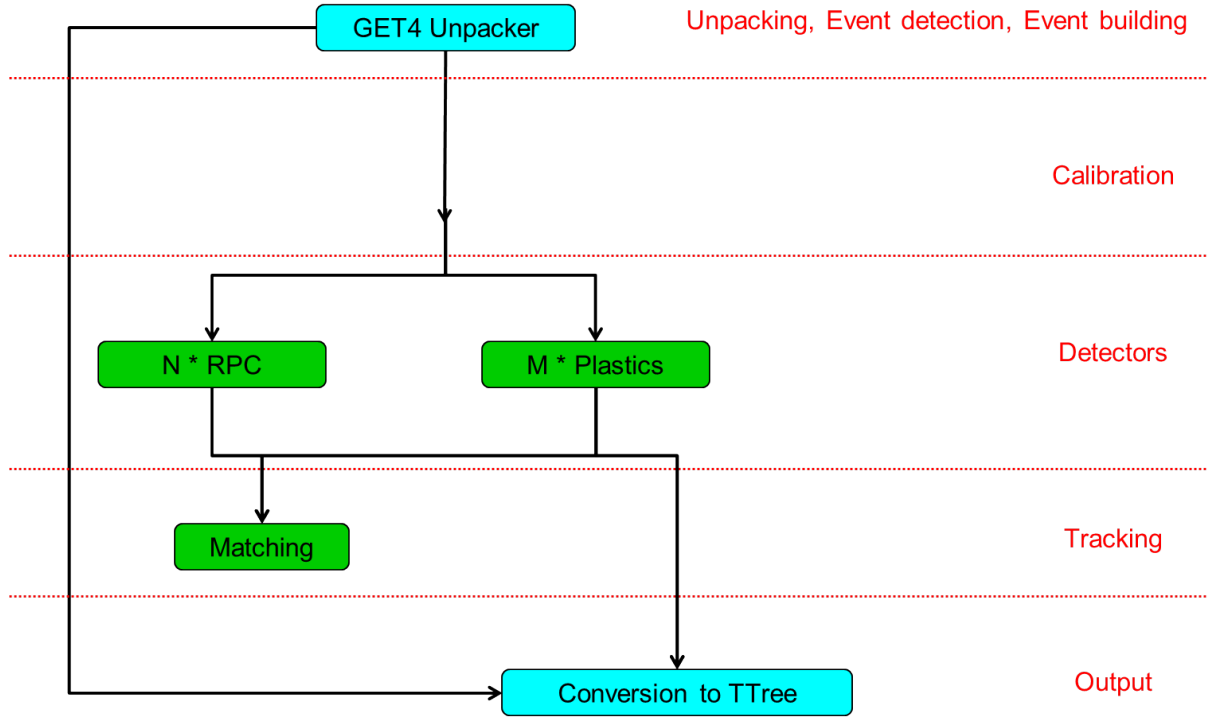


Figure 4.36: Software organization for the free-streaming unpacking of GET4 data.

the calculated TOT would be negative are rejected. This is necessary as without it one would often have ambiguous cases where two leading edges could match the same trailing edge. An example of this would be the case where a short signal comes immediately after another and due to the double edge limitation of the GET4 chip the second edge is missing:

1. Leading edge of first hit: t
2. Trailing edge of the first hit: $t + \text{TOT}(1)$
3. Leading edge of second hit: $t + \text{TOT}(1) + \Delta t$
4. Trailing edge of second hit: $t + \text{TOT}(1) + \Delta t + \text{TOT}(2)$ with $\Delta t + \text{TOT}(2) < 3.2 \text{ ns}$
 \Rightarrow not digitized

4.4.3 Beamtime at GSI with GET4 v1.0

The CBM-TOF group performed a high rate heavy-ion beamtest campaign at GSI in the FOPI cave in end of summer and autumn 2013. This test campaign was divided in four blocks:

1. 29/08/2012 to 31/08/2012: Cross-check of achievable particles fluxes in FOPI cave and new triggered electronics tests (VFTX FPGA TDC vs CAEN V1290A), Kr beam
2. 16/10/2012 to 21/10/2012: All detectors readout by VFTX, test of prototypes from Heidelberg (RPC-P2, see Appendix A.2) and Bucharest, Ni beam
3. 29/10/2012 to 05/11/2012: Same with additionally Heidelberg big prototype RPC-

P3 (Appendix A.3) and a pad counter from Tsinghua

4. 07/11/2012 to 11/11/2012: FOPI beamtime with a D beam, operation as parasite

The GET4 v1.0 became available for users a few days before the second part of this beam campaign and was integrated in the setup for the two last days of beamtest (block 4), as soon as the system could be stabilized in the laboratory. Due to the limited time with beam available for testing it, only data in the 32 bit readout mode could be acquired.

The detector setup was made of a diamond beam detector, two crossed plastic scintillators readout on both ends by PMTs and two to three successive RPC prototypes. Some of the RPC prototypes could be slid laterally to exchange them.

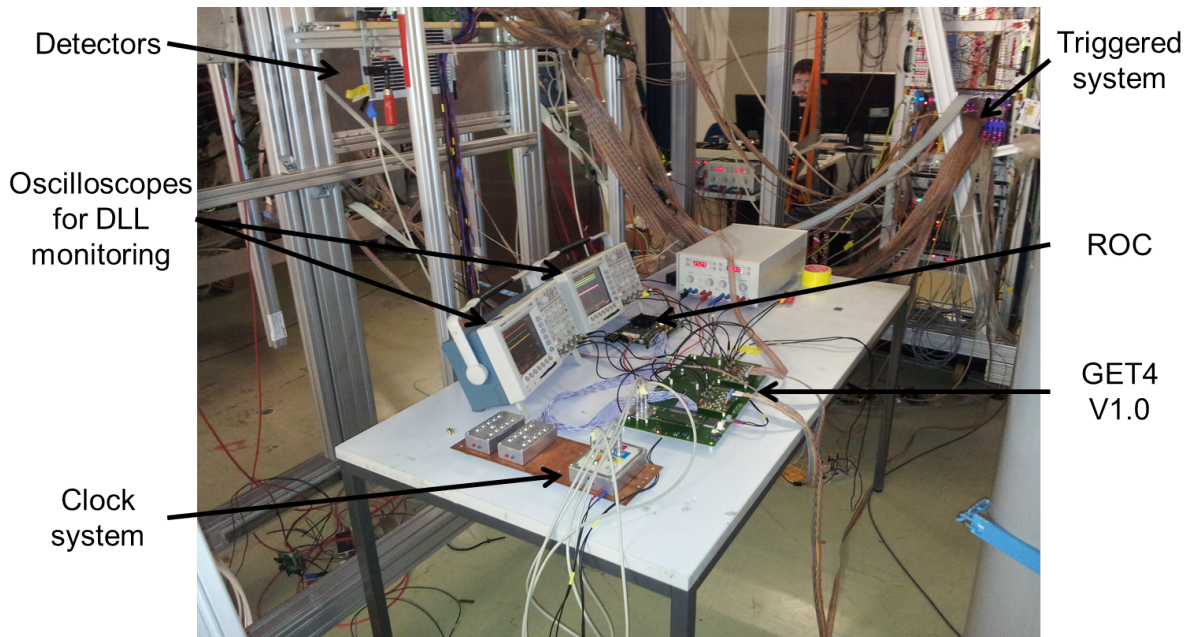


Figure 4.37: Photograph of the GET4 v1.0 setup with part of the triggered setup during the beamtime at GSI in November 2012.

Fig. 4.37 shows a photograph of the setup in the cave with indications of the different components. Fig. 4.38 is the corresponding connection scheme. 2:1 splitter boards were already in use in the triggered setup to ensure that the signals from the PADI-6/7 boards were proper LVDS signals when reaching the VFTX inputs. These splitter boards provide an image of the inputs signal on one of the output connectors and an inverted image on the other output connectors, with a jitter in the order of 10 ps between the two output signals. When the GET4 system got ready, it was plugged to the inverting output of the splitter boards, operating thus in parallel to the triggered system without disturbing it. The early ROC firmware supporting the GET4 v1.0 32 bit readout mode could only support eight GET4s (32 channels), so only the upper eight strips of the RPC-P3 and the four PMT signals were connected. The new functionalities of this firmware are:

- the support of this new readout mode
- Epoch count cross-check using the new GET4 on chip epoch counter: the ROC check on reception of each epoch message that the counter matches its own internal

counter, use the value of this internal counter in the output message and generate an error in case of mismatch.

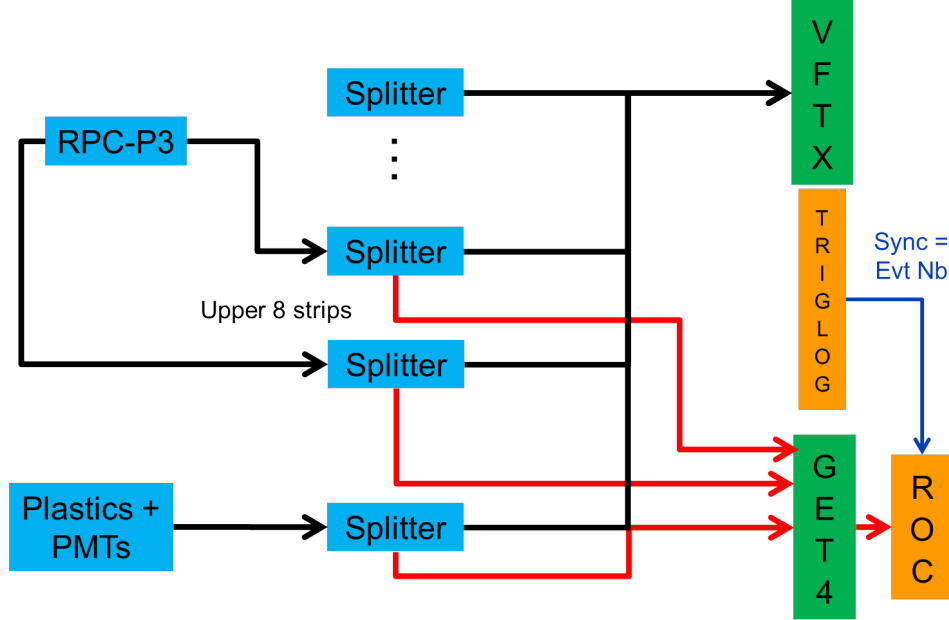


Figure 4.38: Connection scheme of parallel operation of the GET4 v1.0 setup and triggered setup during the beamtime at GSI in November 2012.

The v1.0 chip corrects the epoch bug observed with the GET4 Proto in our first beamtime (see Subsection 4.3.2). Two main changes achieve this. First all logic path of the internal FIFOs were cross-checked for proper timing with a special tool, as a bad timing problem was the prime suspect. Second, the epoch message generation logic makes use of the new on-chip epoch counter to check that the *Epoch event* in all FIFOs stem from the same epoch. When it is not the case, as would happen if one is duplicated like in the GET4 Proto bug, an error message is generated and the readout system of the chip reinitialized.

Two bugs in the v1.0 design were observed already during laboratory tests between reception of the boards and the beam test, and their workaround found in the same period. The first was the absence of the SYNC flag in the epoch messages, observed in both readout modes. This was due to a missing connection in the design. However, as the epoch bug of the Proto version was solved and the PCBs improved to have better clock lines stability, the laboratory tests showed that the clock counter and epoch counters were stable. As such, the workaround for this problem was simply a modification to the unpacking software so that all epochs are considered as synchronized. The chip is also quite sensitive to spikes on the power and clock lines, leading sometime to DLL lock losses in case of noisy environments. The v1.0 should have provided as new feature a slow control command allowing to relock the DLL, but the release of the internal reset line then have to be in phase with the clock signal. If working this would have allowed an automatic relocking by monitoring the DLL status in software and sending relock commands when necessary. This is where the second bug was found: the phase being wrong, the relocking does not happen in a reliable way. The workaround is for the operator to constantly monitor the

DLL lock state, either by the *DLL lock* flag in data messages in the 32 bit readout mode, or using oscilloscopes and the DLL control voltage (available on a debug pin of the GET4 daughter board). In case of lock loss, a manual DLL reset by an external 3.3V CMOS low active pulse is needed.

Observations

During data taking, the setup in FOPI cave had a stable power. The DLL lock was controlled on the oscilloscope during each beam breaks and online with the DLL flag in the messages. No persisting DLL lock loss were observed. The flag changed value only once, during the first data run, for one message of a single channel and the system recovered immediately. This can be seen in Fig. 4.39, which present the DLL flag value of all GET4 data message as function of the channel number for the first data run. The one occurrence is on channel 4, and the difference in counts between channels for the *lock* state of the flag are just an image of the different channel rates.

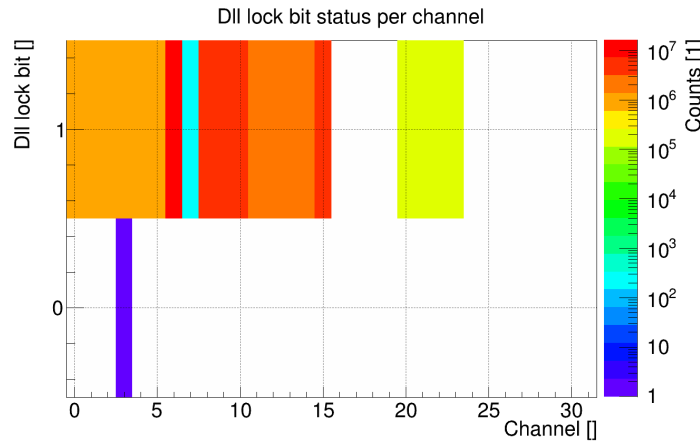


Figure 4.39: DLL flag per TDC hit message for each GET4 channel in the first GET4 v1.0 run in beamtime at GSI in November 2012.

Quite a lot of errors from the TOT building part of the 32 bit readout block were found in the data, as can be seen in Fig. 4.40 and 4.41. Error codes 0x11 to 0x13 are related to the TOT calculator. In mean one error message was for every ten data messages, meaning that around 10 % of the hits were not properly handled. This is due to the way the TOT calculator handles single edges. To operate in a simple and fast way, the calculator can handle only edges pairs in the same epoch or adjacent epochs. As an epoch represent a time interval far bigger than the typical RPC signals, it is enough. However it was designed such that a combination of rising and falling edge exceeding the one epoch distance is considered as an invalid signal and both edges are thrown out. So in case of a single edge, a valid edge could be thrown out together with it, leading again to a state with a single edge. A message is sent on any wrong combination, so any new opposite edge on the same channel generating one, a lot of *Overwrite error*(negative TOT), *TOT out of range* (TOT too big) and *Event discarded*(TOT bigger than two epochs) error messages are generated. A missing edge can happen for example in case of short pulses closer than the double hit capability (the readouts for each signal edge having each an independent

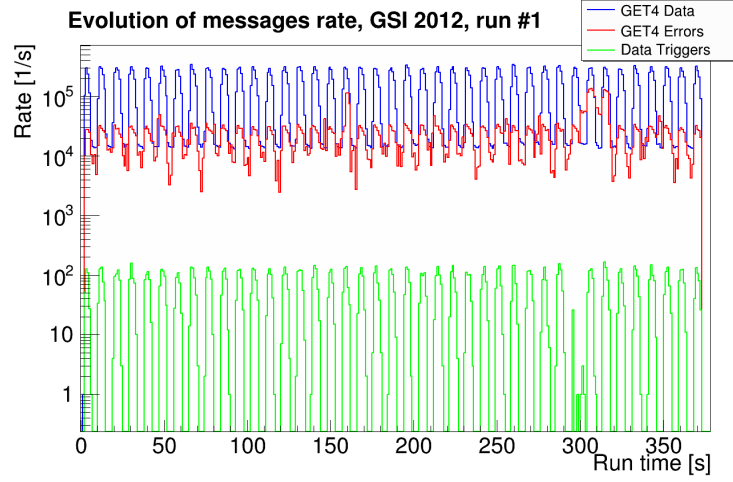


Figure 4.40: Evolution of the data and error messages rate as well as Scintillators data trigger rate in the first GET4 v1.0 run in beamtime at GSI in November 2012.

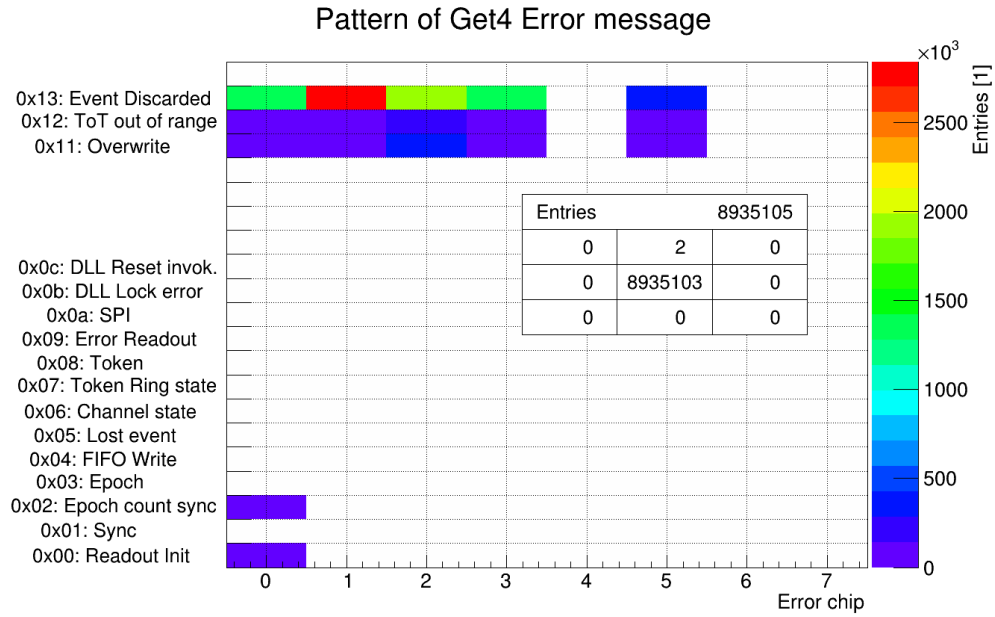


Figure 4.41: Error pattern from error messages for each GET4 channel in the first GET4 v1.0 run in beamtime at GSI in November 2012.

3.2 ns double edge capability) or of dips in the logical LVDS input signal.

From this observation, the developers designed the next iteration of the chip (GET4 v1.23) so that the TOT calculator will be configurable. A first mode of operation will match the one implemented in the GET4 v1.0: wait for the hit completion and reject the full hit. The other operation mode will be to reject the stored edge as soon as two new epochs are counted.

Due to the high errors rate, not enough complete events are available for an analysis of the system performance.

4.4.4 Pulser test of GET4 v1.0

To evaluate the performance of the new chip in a controlled environment, a pulser test was performed: only the GET4 system was used, connected to a variable frequency pulser, to evaluate its rate capability. In this test the chip was operated in 24 bit readout mode to avoid affecting the test due to the extra error messages from the TOT building in 32 bit mode that were observed in the GSI 2012 beamtime (see Subsection 4.4.3). The setup is shown in Fig. 4.42.

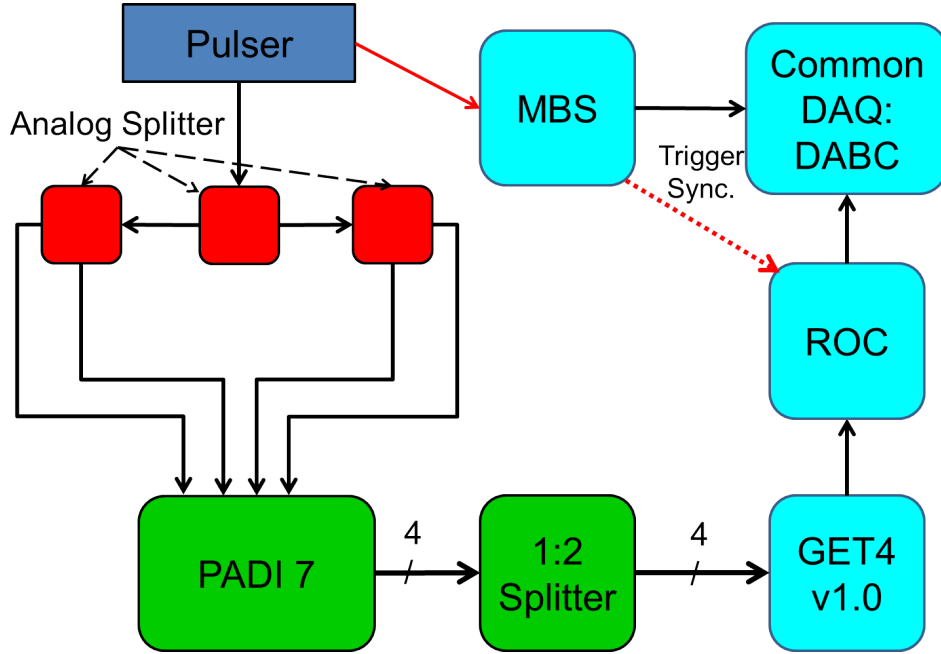


Figure 4.42: Setup for pulser tests of GET4 v1.0 in the laboratory.

Fig. 4.43 show the results of this test. The rate of events reconstructed from coincidence of all 4 channels in the data in free-streaming mode is corresponding to the input rate of the pulse up to 600 kHz, which is matching the simulations shown in Fig. 4.32. The simulation shows an input rate for the full chip while the results of this tests are presented as the input rate per channel, all four channels being fed by the same pulser. With this performance, the requirements in term of hit rate per readout channel for the CBM TOF wall (400 kHz per readout channel, see Subsection 3.4.2) are validated with a 50% margin.

4.4.5 Cosmic tests with GET4 v1.0

As no valid RPC data could be acquired during the 2012 beam campaign with GET4 v1.0 (cf Subsection 4.4.3), a setup was built in the laboratory to take data using cosmic rays.

The setup used is shown in Fig. 4.44. A plastic scintillator of 2 cm x 8 cm x 1 cm readout on both short ends by PMTs was put on top of the Heidelberg RPC-P3, which is described in Appendix A.3. A second plastic scintillator of dimensions 4 cm x 11 cm x 1 cm also readout on both short edges was placed under. Assuming straight trajectories

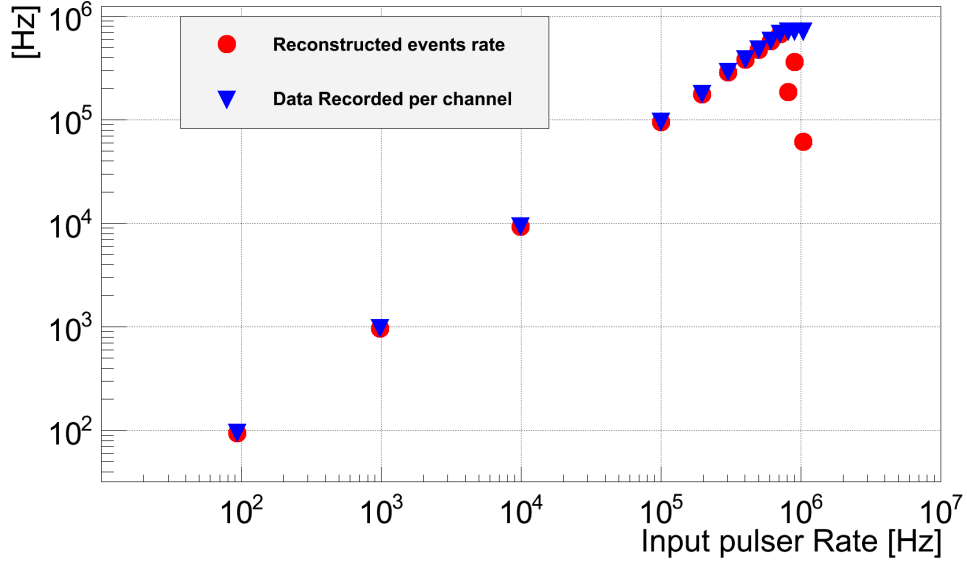


Figure 4.43: Rate capability test of GET4 v1.0 operated in 24 bit mode with a pulser. Blue markers show the recorded data rate at red ones the rate of event which could be reconstructed from data, both as function of the pulser rate.

of the cosmic particles, coincidences of their signals define a trigger area of ~ 9.5 cm x 3 cm, covering the full width of three of the prototype strips.

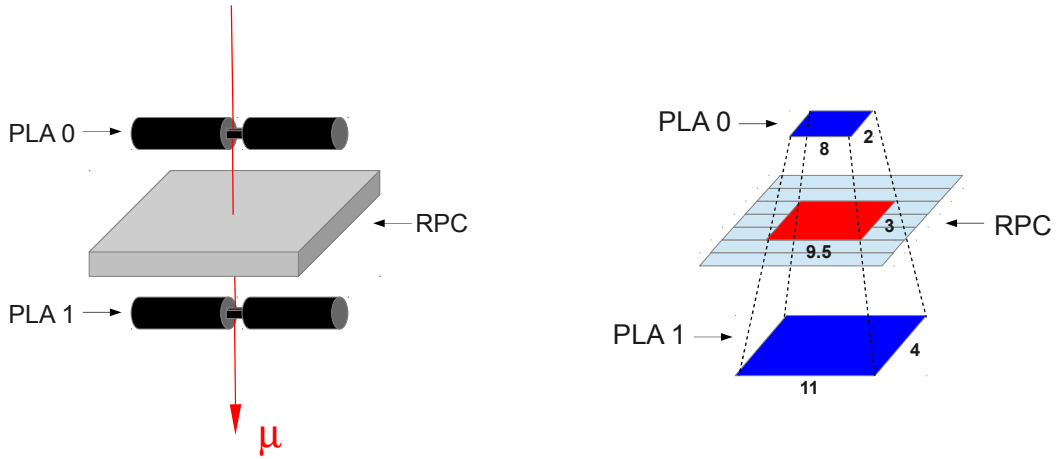


Figure 4.44: Setup scheme (left) and trigger geometry (right) of the Setup used for the cosmic rays test of GET4 v1.0.

The same setup was already used before successfully for a cosmics run using the VFTX triggered TDC. To ensure good quality of the LVDS signals between the PADI-6 boards and the TDC boards, 1:2 splitter boards were used. These boards have a 17 pairs input and provide on one output connector the original signal and on the other one the inverse of the original signal. The non-inverted signals were used for the VFTX tests. It was chosen to keep the VFTX system plugged and use the inverted output for the GET4 v1.0

testing, as described in Fig. 4.45. This open the way for three independent method to estimate the GET4 v1.0 performance, especially in terms of resolution:

- Using the system performance of the RPC+PADI+GET4 system and comparing against the RPC+PADI+VFTX system, over the full data sample and after all corrections
- Directly comparing PMT time difference between GET4 and VFTX in each event
- Directly comparing RPC time difference between GET4 and VFTX in each event

For the direct comparison, one advantage of this parallel running is that the influence of all components before the splitters can be neglected (except the signals size, as shown later). As the splitter board and VFTX were already well characterized by their developers and their performance was cross-checked in our group, one can extract the GET4 properties.

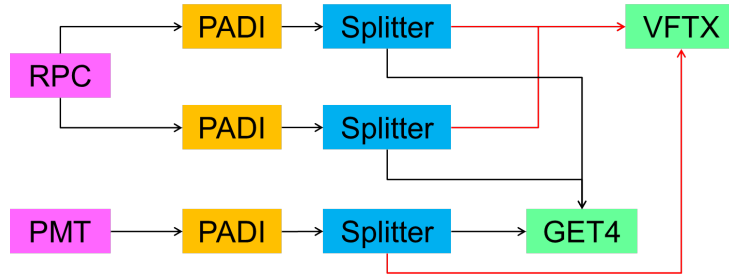


Figure 4.45: Connection scheme of the setup used for the cosmic rays test of GET4 v1.0.

As explained before, the main trigger used for the triggered part of the setup is a coincidence of the four PMT signals, corresponding to events where one can expect a full reference system time to be available. This trigger has a rate of ~ 1 count per minute. However, a buffer problem was found on the VFTX side during the analysis of the purely triggered data from the GSI 2012 beamtime (see Appendix B.4 for more details). To solve this a second more frequent trigger is defined by using one of the summed OR output of the scaler board to flush the buffers (order of 700 Hz). This trigger correspond to an OR between the full OR of all PADI boards on the left side of the counter and the full OR of the ones on the right side (at least one channel fired on at least one side).

The only difference in the ROC firmware compared to the one used in the GSI 2012 beamtime is the introduction of a suppression of the GET4 epochs: only epochs with data are transmitted by the ROC. The 250 MHz epochs are still always transmitted as they are needed for the synchronization with the triggered system.

On top of the usual walk corrections, two additional data calibration methods are used. They will be presented in following paragraphs.

Velocity spread and correction

The cosmic muons used in the test have varying velocities. To correct for this, the full system time difference with walk correction (see Eq. Eq:WalkTimeDiffSyst and 3.11 in Subsection 3.4.4) is plotted as function of the time difference in the reference system with walk correction (see Eq. Eq:WalkTimeDiffPmt and 3.10 in Subsection 3.4.4). The mean

of the system time difference in each reference time bin is then taken as value for the correction. These corrections are updated after each iteration of the walk corrections.

An example of the resulting corrections factors as function of the velocity estimator value is shown in Fig. 4.46. In this case it was the third equipped strip in the GET4 system (23rd RPC strip), in the free-streaming data based event definition case.

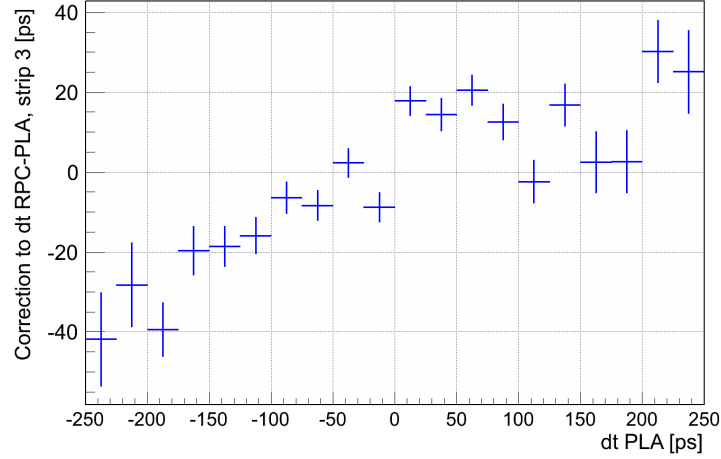


Figure 4.46: Example of the velocity correction on the data acquired during the 2013 cosmics test. The correction to be applied to the time difference between RPC strip 3 and reference system is shown as function of the difference in mean time between the two plastic scintillators.

If one use the distance of 27 cm between the scintillators and assume that the maximum at a correction of +20 ps correspond to speed of light and that the tracks are vertical, the correction of -20 ps would correspond to a velocity of 0.96 c. This is still coherent with the fact that most muons reaching Earth surface need to be relativistic (production in higher atmosphere from cosmic rays and short life time).

Track angle and correction

Similarly to the velocity spread, the cosmic muons can go trough the setup at different angles. The left-right time difference of each plastic scintillator gives an approximation of the longitudinal position where the muons passed trough it. Using the difference of this value in each scintillator, one gets an approximation of the track angle along the scintillators axis. The value Δx_{PLA} is obtained for each event using Eq. 4.13, where following the convention established in Subsection 3.4.4 $t_{PMT,i}$ represents the measured time for PMT i , $tot_{PMT,i}$ the measured TOT for the same PMT and $corr_{PMT,i}(tot_{PMT,i})$ the corresponding walk correction value. The correction is done in a similar way to the velocity one, by plotting the system time difference $\Delta t_{MRPC,ref,corr}$ against Δx_{PLA} and extracting the mean value of the system time difference in each bin. As this correction and the velocity correction are partially correlated, this process is also updated on each

iteration of the walk corrections, until both converge.

$$\begin{aligned} \Delta x_{PLA} = & (t_{PMT,1} - t_{PMT,2}) - (t_{PMT,3} - t_{PMT,4}) \\ & - corr_{PMT,1}(tot_{PMT,1}) + corr_{PMT,2}(tot_{PMT,2}) \\ & + corr_{PMT,3}(tot_{PMT,3}) - corr_{PMT,4}(tot_{PMT,4}) \end{aligned} \quad (4.13)$$

An example of the resulting corrections factors as function of the angle estimator value is shown in Fig. 4.47. In this case it was the third equipped strip in the GET4 system (23rd RPC strip), in the free-streaming data based event definition case.

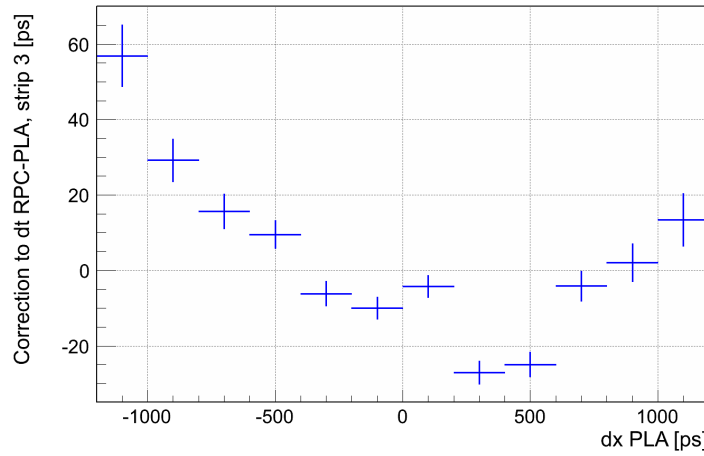


Figure 4.47: Example of the track angle correction on the data acquired during the 2013 cosmics test. The correction to be applied to the time difference between RPC strip 3 and reference system is shown as function of the difference in hit position in each plastic scintillators. This position is approximated by the left-end right-end time difference. “dx PLA” corresponds to Δx_{PLA} in the text.

The distance between the plastic scintillators of ~ 27 cm translates to a maximal angle of $\sim 19^\circ$ when one neglect their width and thickness and use only their length of 8 cm (top) and 11 cm (bottom). This corresponds to an increase in path of ~ 1.6 cm compared to the vertical track case. Assuming a speed of light velocity, one obtains an additional time of ~ 53 ps ($\pm 1^\circ$ in angle would lead to approximately ± 7 ps). Thus the range of the correction of -30 to +30 ps for most tracks matches well physics expectations.

System performance

The most important quantities to estimate the performance of the full system in terms of TOF capability are the efficiency and the time resolution of the RPC and electronics.

Table 4.7 show as an example the comparison of the system performance at an high voltage of 11.5 kV of the PADI-6 + VFTX system and of the PADI-6 + GET4 v1.0.

The “Efficiency” is defined as the proportion of events for which an RPC cluster was found among the events for which a good signal was found in the reference system (scintillators).

The timing performance of the reference system can be estimated by fitting a Gaussian on the difference of the mean time of each scintillator. Eq. 4.14 to 4.16 explicit the correspondence of this quantity to the properties of the individual scintillators. In the present analysis, a cut on this reference time difference at $3 \sigma_{\Delta t_{PMT}}$ around the mean value is used. This cut explain most of the difference between the “Total Events number” and the “Events with good reference”.

$$\Delta t_{PMT} = \frac{1}{2}(t_{1L} + t_{1R}) - \frac{1}{2}(t_{2L} + t_{2R}) \quad (4.14)$$

$$= t_{Scint.1} - t_{Scint.2} \quad (4.15)$$

$$\sigma_{\Delta t_{PMT}} = \sqrt{\sigma_{t_{Scint.1}}^2 + \sigma_{t_{Scint.2}}^2} \quad (4.16)$$

From the width of the fit one can also extract the resolution of the mean reference time, as shown in Eq. 4.17 to 4.20.

$$t_{ref} = \frac{1}{4}(t_{1L} + t_{1R} + t_{2L} + t_{2R}) \quad (4.17)$$

$$= \frac{1}{2}t_{Scint.1} + \frac{1}{2}t_{Scint.2} \quad (4.18)$$

$$\sigma_{t_{ref}} = \frac{1}{2}\sqrt{\sigma_{t_{Scint.1}}^2 + \sigma_{t_{Scint.2}}^2} \quad (4.19)$$

$$= \frac{1}{2}\sigma_{\Delta t_{PMT}} \quad (4.20)$$

The “System Time Resolution” is the standard deviation of a Gaussian fit on the distribution of the system time difference. The system time difference is built from the mean time of the RPC cluster and the reference time. The RPC cluster mean time is obtained by weighting the mean time of each strip in the cluster by its the total TOT, as in Eq. 4.21.

$$t_{RPC \text{ cluster,mean}} = \frac{\sum_{strips} \frac{1}{2}(tot_{strip,right} + tot_{strip,left})(t_{strip,right} + t_{strip,left})}{\sum_{strips} tot_{strip,right} + tot_{strip,left}} \quad (4.21)$$

This gives a first comparison point between the TDC systems. From this quantity and $\sigma_{\Delta t_{PMT}}$, one can also extract the RPC time resolution. This is described in Eq. 4.22 to 4.25. Note that $\sigma_{t_{RPC}}$ is not the resolution of the RPC detector itself as it still includes the electronics contribution.

$$\Delta t_{system} = t_{RPC \text{ cluster,mean}} - t_{ref} \quad (4.22)$$

$$= t_{RPC} - t_{ref} \quad (4.23)$$

$$\sigma_{\Delta t_{system}} = \sqrt{\sigma_{t_{RPC}}^2 + \sigma_{t_{ref}}^2} \quad (4.24)$$

$$\sigma_{t_{RPC}} = \sqrt{\sigma_{\Delta t_{system}}^2 - \frac{1}{4}\sigma_{\Delta t_{PMT}}^2} \quad (4.25)$$

The GET4 data can be analyzed with events built using either the trigger signal or the data themselves. The gain in total number of events and events with good reference

signals between the two event building option corresponds roughly to the expected dead-time of the triggered system. The RPC OR trigger has a mean rate of 1 kHz, which with a $\sim 250 \mu\text{s}$ readout time gives a dead-time ratio of 25 %. The events number win obtained by building events from the data instead of the trigger signal is ~ 25 %. The same evaluation was performed for a run with similar statistics ($\sim 10\text{k}$ events) at a high voltage of 10.5 kV. A full scan of the high voltage response was done with only the VFTX system powered. A 10k events run correspond to approximately 10 days of acquisition.

Table 4.7: Summary of the system performance for the different digitizer systems in the 2013 cosmic test at 11.5kV high voltage.

System: PADI-6 +	VFTX	GET4 v1.0 (Trigg.)	GET4 v1.0 (F.S.)
Total Events number	10593	10593	14465
Events with good reference	8461	8264	10719
Events with RPC	8314	8049	10462
RPC Efficiency [%]	98.3 ± 0.1	97.4 ± 0.2	97.6 ± 0.1
$\sigma_{\Delta t_{PMT}}$ [ps]	116.0 ± 1.0	119.4 ± 1.1	119.5 ± 1.0
System Time Resolution [ps]	72.4 ± 0.8	82.0 ± 0.9	82.2 ± 0.8
RPC Time Resolution (+el.) [ps]	43.3 ± 1.4	56.2 ± 1.4	56.5 ± 1.2
Mean cluster size [strips]	1.86	1.66	1.66
Mean cluster multiplicity []	1.14	1.13	1.13

Fig. 4.48 show the performance of the VFTX system for the different high voltage values. In this plot, the points are separated in two series, one for the runs where only the VFTX system was brought into operation and one for the two runs where both systems were run in parallel. A degradation of the performance in terms of resolution can be observed when the GET4 system is powered, for which no clear explanation is known. A possible cause could be some interference between the two clock systems. The efficiency is slightly lower both in Table 4.7 and Fig. 4.49 for the comparison to the GET4 system as one need to restrict the VFTX analysis to the eight common strips for a meaningful comparison.

Fig. 4.49 compares the performance of the GET4 systems in both event building modes to those of the VFTX, restricted to the eight common RPC strips. The system time resolution at 11.5 kV in the GET4 TDC is worse than could be expected from the trend in the VFTX data. This could be tracked down to a difference between the events where at least one of the TDC channels used in the RPC cluster have multiple data and the ones where all TDC channel have at most one full hit. In the first case the fit by a Gaussian gives a resolution of 90 ps, while the same fit in the second case gives a resolution of 76 ps closer to the expectation, as shown in Fig. 4.50. Each event type represents around 50 % of the events with RPC data in GET4, while only 5 % of events have multiple TDC hits in the VFTX system. One possible explanation is that the VFTX has an input channel deadtime of 35 ns which would hide eventual reflexions in the setup. This stresses the fact that in a free-streaming system all components have to be properly matched and designed for best performance as part of the chain: noise or reflexions immediately generate additional data

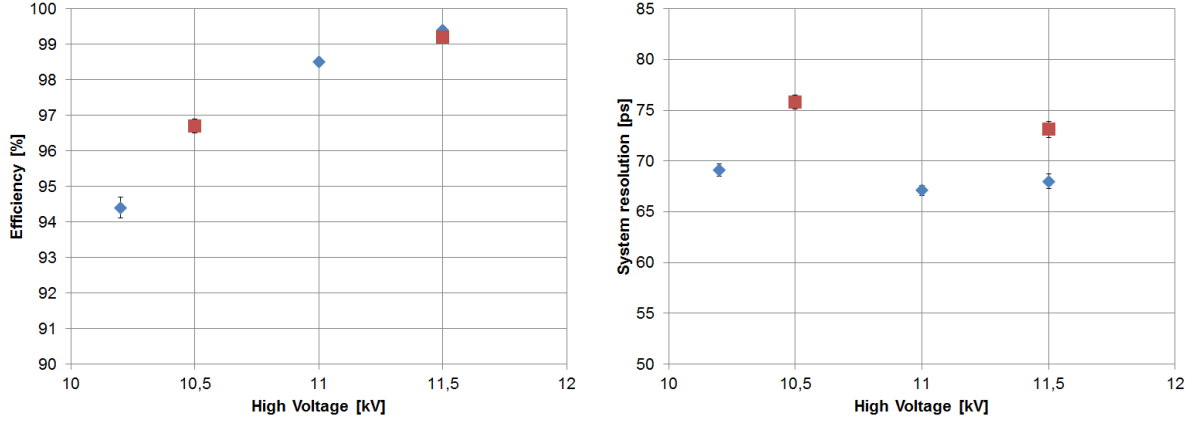


Figure 4.48: Performance of the VFTX system in terms of efficiency (left) and resolution (right) as function of high voltage. Two situations are present: only VFTX in use (blue diamonds) and VFTX running in parallel with GET4 v1.0 (red squares).

which need to be transported and can be difficult to separate from real data in analysis. If one uses the best case resolution and quadratically subtract the contribution of the reference system, the resulting RPC + electronics resolution is 43 ps at 10.5 kV and 49 ps at 11.5 kV. This is well within the CBM specification of less than 70 ps for MRPC and electronics (60 ps for the MRPC, 40 ps for the electronics).

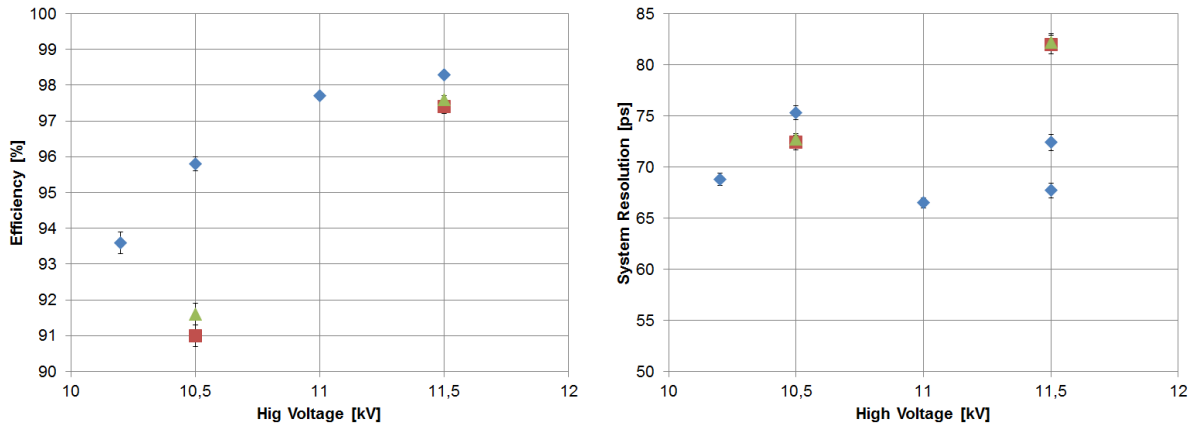


Figure 4.49: Comparison of the system performance of the GET4 v1.0 and VFTX system in terms of efficiency (left) and resolution (right) as function of high voltage. The blue diamonds represent the VFTX data, the red squares the GET4 triggered data and the green triangles the GET4 data-triggered data.

The efficiency of the system is lower in the GET4 system, with around 5% event losses at 10.5 kV and 1% at 11.5 kV. It can be observed that most of these missing hits have low TOT, as shown in Fig. 4.51 with the TOT of all hits in VFTX without a corresponding one in GET4 using the RPC OR trigger, plotted for the first of the eight common strips. This could be the result of an offset between the leading and trailing edges due to different path length inside the GET4 chip. It would induce negative TOTs at the TDC hit building

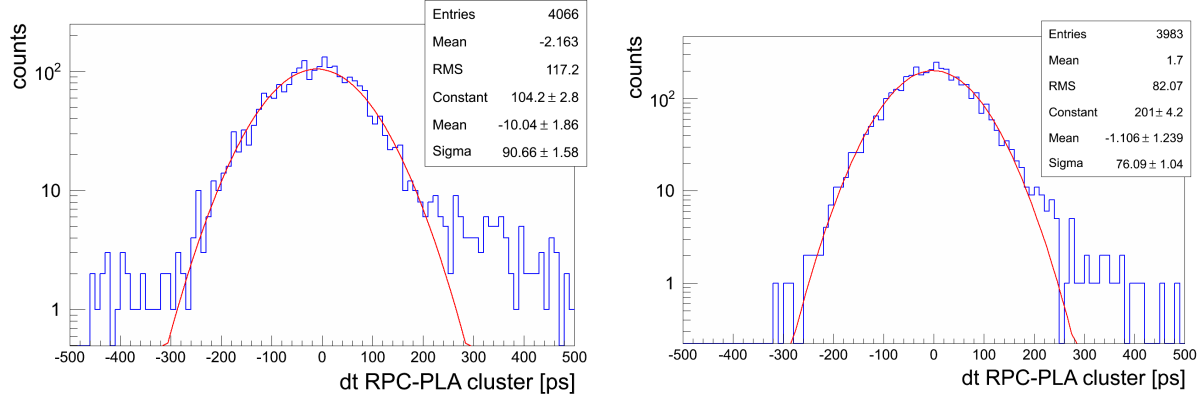


Figure 4.50: Comparison of the system resolution obtained in the GET4 v1.0 TDC at 11.5kV HV for the events with multiple data on at least one TDC channel (left) and events where all TDC channels had at most one full hit (right).

stage, which are then rejected by the software. These offset can be cross-checked and eventually measured for each channel by using pulses with two or three known width. This could not be realized due to time constraint but is planned to be made for all our TDC systems (GET4, VFTX) in the near future.

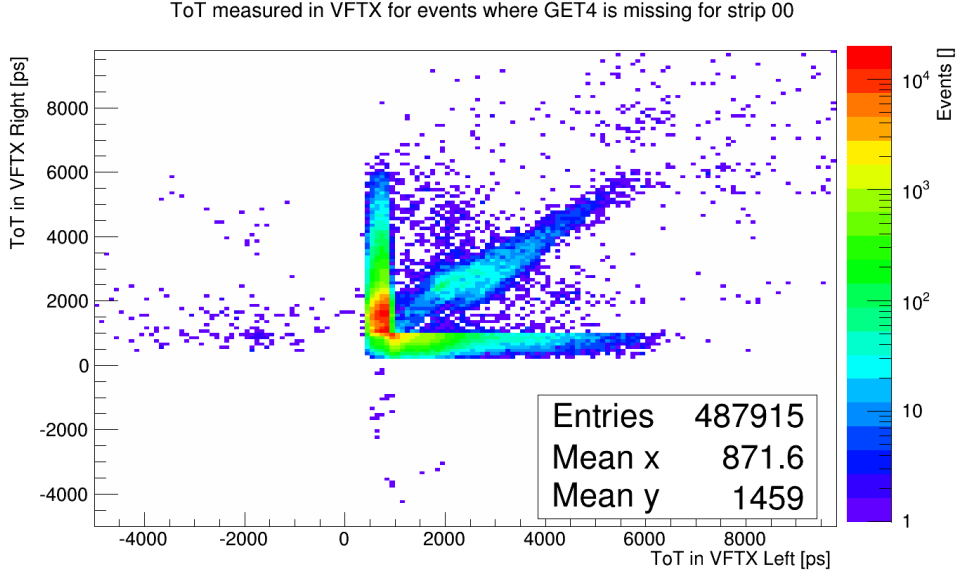


Figure 4.51: Left and right TOT in the VFTX systems for hits where the corresponding data was not found in the GET4 system, RPC OR triggering, first common strip.

GET4 v1.0 performance

The setup measure the same signals in both TDC systems for each event. By using only time differences, one can always compare the times measured in each system without

having to care about the different time frames. The VFTX FPGA TDC was already extensively tested both by its developers and our own group and the following characteristics were measured: 10 ps time resolution between channels on the same board and 12 ps time resolution between channels on different boards. The 1:2 splitter boards used in the setup were also measured and a jitter of ~ 10 ps was found between the two output signals. Knowing those two value allow to extract the time resolution of the GET4 from the width of the time difference between the two systems.

Eq. 4.26 to 4.30 describe how the value is obtained from a time difference between signals A and B, assuming the full splitter jitter is assigned to the GET4 branch. First all offsets between system time frames as well as the signal true time value cancel in Eq. 4.26, leaving only the jitter contributions left:

$$\Delta t = (t_A - t_B)_{GET4} - (t_A - t_B)_{VFTX} \quad (4.26)$$

$$\Delta t = t_{A,true} + Offset_{GET4} + Jitter_{A,GET4} + Jitter_{A,Split} \quad (4.27)$$

$$\begin{aligned} & - (t_{B,true} + Offset_{GET4} + Jitter_{B,GET4} + Jitter_{B,Split}) \\ & - (t_{A,true} + Offset_{VFTX} + Jitter_{A,VFTX}) \\ & + (t_{B,true} + Offset_{VFTX} + Jitter_{B,VFTX}) \end{aligned}$$

$$\Delta t = Jitter_{A,GET4} + Jitter_{A,Split} - Jitter_{B,GET4} - Jitter_{B,Split} \quad (4.28)$$

$$- Jitter_{A,VFTX} + Jitter_{B,VFTX}$$

All jitters contributions are assumed to be following independent Gaussian distributions. By plotting the Δt distribution for many events, fitting it with a Gaussian and extracting the resulting $\sigma_{\Delta t}$ value, one can access the GET4 single channel resolution, as in Eq. 4.30:

$$\sigma_{\Delta t}^2 = \sigma_{GET4 \text{ channel}}^2 + \sigma_{Splitter}^2 + \sigma_{GET4 \text{ channel}}^2 + \sigma_{Splitter}^2 \quad (4.29)$$

$$+ \sigma_{VFTX \text{ channel}}^2 + \sigma_{VFTX \text{ channel}}^2$$

$$\sigma_{GET4 \text{ channel}} = \sqrt{\frac{1}{2}\sigma_{\Delta t}^2 - \sigma_{VFTX \text{ channel}}^2 - \sigma_{Splitter}^2} \quad (4.30)$$

This procedure is done using either the time difference between the ends of each plastic scintillator or the difference between the ends of the RPC strips. As the RPC OR trigger was also used in all our runs (see first paragraph of this section), these time differences can be build with quite high statistics for all eight RPC strips common to both systems. To reduce eventual ambiguities in the matching between the two TDC systems, only events where a single strip fired in both systems and with a single full TDC hit (Time + TOT) on each end of this strip are used.

To extract the values presented in Table 4.8, the $\sigma_{VFTX \text{ channel}}$ value was taken at $12 \text{ ps} \pm 1$, corresponding to the resolution measured with channels on different boards. The $\sigma_{Splitter}$ value was taken at $10 \text{ ps} \pm 1$, as measured by the board developers.

Table 4.8: Summary of the GET4 v1.0 to VFTX comparison in the 2013 cosmic test. The RPC strip 8 was not used for the mean calculation (see text for explanation).

	Events	GET4 - VFTX	GET4 Resolution
Scint. 1 Time difference [ps]	45268	42.3 ± 0.1	25.5 ± 0.08
Scint. 2 Time difference [ps]	125091	45.5 ± 0.1	28.1 ± 0.06
Rpc strip 1 Time difference [ps]	10879080	38.6 ± 0.1	22.4 ± 0.07
Rpc strip 2 Time difference [ps]	2793196	36.9 ± 0.1	20.9 ± 0.08
Rpc strip 3 Time difference [ps]	1580559	35.9 ± 0.1	20.0 ± 0.08
Rpc strip 4 Time difference [ps]	3051547	44.2 ± 0.1	27.1 ± 0.06
Rpc strip 5 Time difference [ps]	2965331	45.4 ± 0.1	28.1 ± 0.06
Rpc strip 5 Time difference [ps]	1590555	42.0 ± 0.1	25.3 ± 0.06
Rpc strip 7 Time difference [ps]	979708	51.2 ± 0.1	32.7 ± 0.05
Rpc strip 8 Time difference [ps]	8073155	82.4 ± 0.1	56.1 ± 0.03
Mean of PMT and RPC times [ps]		40.6 ± 0.05	24.0 ± 0.4

To obtain the mean resolution of the GET4 system, the value extracted for each time difference is weighted with the number of events in its histogram. A problem was found in RPC strip 8 TOT distribution in both systems: the time difference between the two system show unusual dependence on the hit position along the strip. Due to this it is excluded from the mean resolution calculation. The mean value of 24.0 ps single channel resolution matches well the value measured by the developers with pulser for channels on different boards (here each strip combine GET4 chips on different boards).

It must be remarked that this cosmic test was the first stable long term operation of a complete free-streaming timing chain with such high time resolution.

Chapter 5

Data flow and simulation

To ensure a successful preparation and implementation of the free-streaming readout concept at interaction rates up to 10 MHz, it is necessary for CBM to handle simulated data and data acquired in test beams in a unified way within the CBMROOT framework. In addition, the readout chain of the sub-detectors needs to be carefully dimensioned to avoid data losses. This chapter is devoted to the development of the methods and tools needed to follow this policy for the TOF sub-detector.

Section 5.1 gives a more detailed description of the goals of the software development presented in this chapter. The CBMROOT framework is presented in Section 5.2.

To fulfill the goals presented in Section 5.1, an unpacking and calibration chain existing in the GO4 software was adapted to the CBMROOT environment. An event based digitizer using measured properties of prototype RPCs was also implemented. Detailed information on this can be found in Sections 5.3 and 5.5, respectively. Following the strategy of a unified analysis software, a common output format, the so-called “TOF Digis”, was defined and used for both the unpacker and the digitizer. A simple reconstruction step was also written and tested with the digitizer output as shown in Subsection 5.5.3. For each development branch a comparison to previously existing software results is presented. Section 5.4 presents a simplified TOF wall geometry used in CBMROOT for the simulations with the digitizer.

A method used to determine the number of readout chain components by simulations with the digitizer is shown in Section 5.6, along with the most recent estimations.

Finally, considerations on what is still necessary to achieve the transition from event-based to time-based simulations can be found in Section 5.7.

5.1 Goals

5.1.1 Unified analysis software

Fig. 5.1 shows the software situation of the TOF project when starting this part of the thesis. TOF related simulations are done in CBMROOT since the year 2000 with a direct

hit generation from Monte-Carlo data. The direct hit producer ignores for example the effects of charge sharing between channels, improved timing through clusterization or efficiency loss due to cluster overlaps. On the experimental data side, the GET4 analysis was first implemented within the GO4 framework and all the more involved analysis on the beamtime data were made through ROOT macros, as described in Subsections 4.3.1 and 4.4.2. It was done so in order to have an analysis and monitoring software ready as fast as possible.

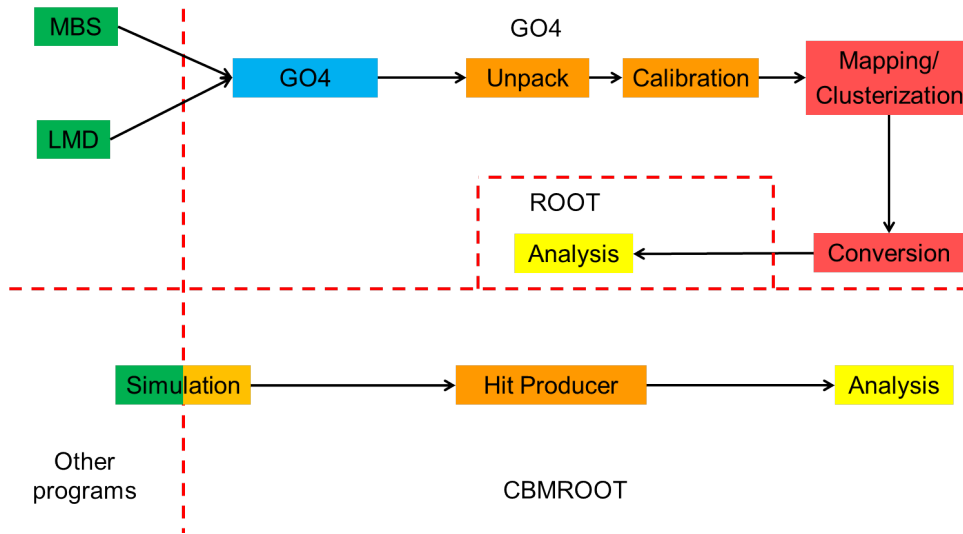


Figure 5.1: Status of the TOF wall analysis software prior to the integration of the unpackers in CBMROOT. MBS and LMD are the online and offline data sources for experimental data.

However, in order to speed up the development of reconstruction tasks such as the position alignment of channels or the cluster building, it is necessary to have compatible unpacking and simulation chains implemented in the same framework, feeding the same reconstruction tasks. Additionally, in the concept of free-streaming readout, the difference between the offline software used for the physics analysis and the online software used for event selection should be minimal in order to guarantee the selection of only the most interesting events. This leads to a software organization as sketched in Fig. 5.2: all tasks for both branches of the TOF software are implemented within CBMROOT, both branches share a common output data format and the reconstruction and analysis steps are common.

5.1.2 Common data format for unpacked TDC data

An additional requirement at this stage of the CBM TOF Wall project is to apply the same calibration scheme to the different readout systems (ASIC TDCs, FPGA TDCs, ...) in order to select the optimal solution on equal grounds. This in turn means that a common storage format has to be defined also for the unpacked TDC data, so that the

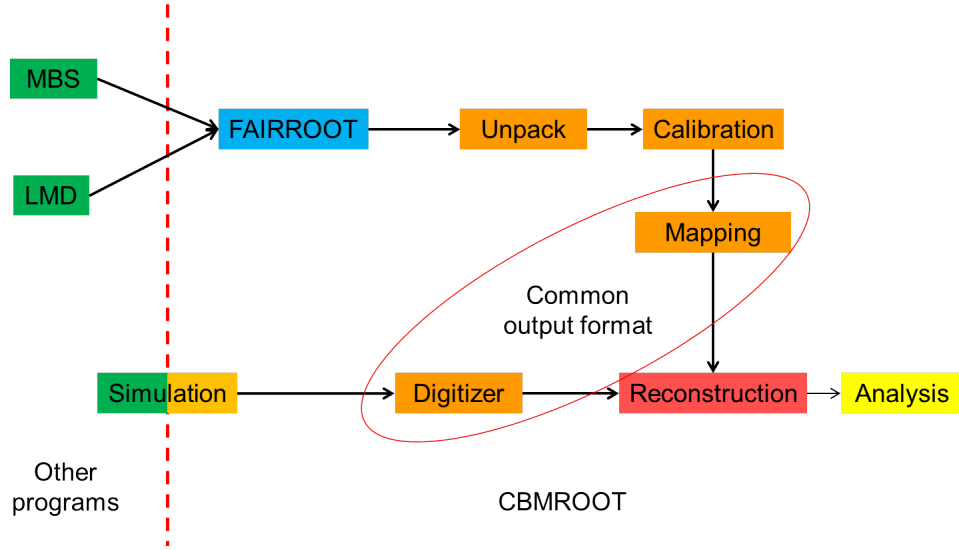


Figure 5.2: TOF wall software organization with all analysis and simulation steps in CBMROOT. MBS and LMD are the online and offline data sources for experimental data.

same calibration and hit building algorithm can be applied irrespective of the data origin. Thus, the time needed to test eventual new TDC systems is reduced as only the unpacker and the control parameters for the calibration task would have to be re-implemented.

5.1.3 Readout chain dimensioning

The readout chain can be seen as a unidirectional data transport tree, with at least 3 levels, as presented in Section 4.1: the front-end readout (ROC), the aggregation (DCB) and the data transport (optical links). An additional level can eventually perform some pre-processing tasks on dedicated hardware (DPB) to reduce the data volume that should be transported. It could be placed either between the readout and aggregation levels or between the aggregation and data transport level.

To dimension properly the number of components at each level of readout in a free-streaming system such as CBM, detailed simulations have to be performed. The first step is to find the channel geometry giving the best trade-off between physics performance, construction complexity and cost. This provides the components count for the first layer of components in the readout chain. From there, the second step is to evaluate the amount of data generated per time interval in such a design. This provides the minimal number of components for the next readout level and, with some estimation on the possible data reduction, the minimal number of components for the intermediate data combining and transport levels as well. To obtain stable operation of such a system even in the case of spikes in data rate (beam quality, noisy channels, ...), some safety margins must be applied to all dimensioning variables. The event data size estimation is realized with the event-based digitizer implemented for this thesis.

5.2 The CBMROOT framework

CBMROOT is a sub-project of the FAIRROOT framework. FAIRROOT is a C++ framework based on the CERN ROOT framework and aims to provide the simulation, detector description and analysis functionalities common to all FAIR experiments. It also provides an interface with different MonteCarlo (MC) generators (UrQMD, SHIELD, HSD, ...) and propagators (GEANT3, GEANT4, ...). Each experiment then develops on top of it the digitization and reconstruction tools adapted to its detectors geometry as well as its own physics analysis. CBMROOT is the CBM part of this effort.

5.2.1 FAIRROOT

FAIRROOT provides to the FAIR experimental groups:

- a common input scheme for MC data and real data
- tools to load and access the parameters of the analysis with version control
- a central run-manager and the base classes for successive analysis steps

The run-manager takes care of initializing the analysis steps, calling them in the right order and controlling the output data (availability, saving, ...). These steps all inherit from the FairTask class, and will be called “tasks” from here on. No executable is used as all tasks are compiled in libraries and called through macros from within the ROOT interpreter. This allows on one side for running the same macros on different platforms with minimal changes and on the other side for splitting easily the full analysis chain into different steps with intermediate storage files. The first task in an analysis can be either a physics event generator (in a generic version provided by FAIRROOT or in a specialized version by CBMROOT) or a “real data” source providing access to online/offline data in the MBS format. A more detailed description can be found on the FAIRROOT website [81].

Although this feature is beyond the scope of this work, FAIRROOT now includes the possibility of converting event-based data into a time-based data format. This can be seen as a first step towards a fully time-based simulation and analysis, which is needed in the free-streaming readout concept [82].

5.2.2 CBM specifics

CBMROOT adds the following functionalities to FAIRROOT:

- a geometric description (materials, sensitive area, ...) of the sub-detectors
- tasks performing the hit production from Monte-Carlo data in the sub-detectors
- tasks performing the hit reconstruction in the sub-detectors
- data classes describing the measured quantities in each sub-detector at various stages of reconstruction
- tasks performing track building and PID from hits in the various sub-detectors
- physics oriented analysis classes and macros

5.3 A CBM-TOF data unpacker in CBMROOT

As described earlier in this chapter, one of our goals is to obtain a unified analysis software chain for both real data and simulated data. The first step in this direction is the porting of the existing GO4 unpacking chain to the CBMROOT framework. The unpacker in CBMROOT makes use of the unpacking functionalities of the FAIRROOT framework for MBS event sources, which are providing an interface to either the MBS remote event servers or the List Mode Data files (LMD, a file format storing MBS events). The unpacker is subdivided into five logical main tasks. Some of these tasks are themselves subdivided in sub-tasks to support the different data sources (hardware) and data types (e.g. scalers, TDC, ...). The first subsection describes the C++ classes used to implement the tasks, sub-tasks and intermediate data objects. The second subsection presents results obtained with data files from our cosmic test series when using the CBMROOT unpacker and how they compare to those obtained with the original GO4 unpacker.

5.3.1 Classes organization

Fig. 5.3 shows the class organization with the names of the logical tasks and the intermediate data formats. To a great extent, the unpacking and calibration algorithms were taken over from the GO4 ones, with the major changes stemming from the move towards a TDC-independent generic approach. The five logical steps are the Data Source, also doing the unpacking, the Unpacker Monitoring, the Calibration, the Mapping and the Conversion to the output format of the former GO4 unpacker. The first three tasks each include sub-tasks to consider the different possible hardware components.

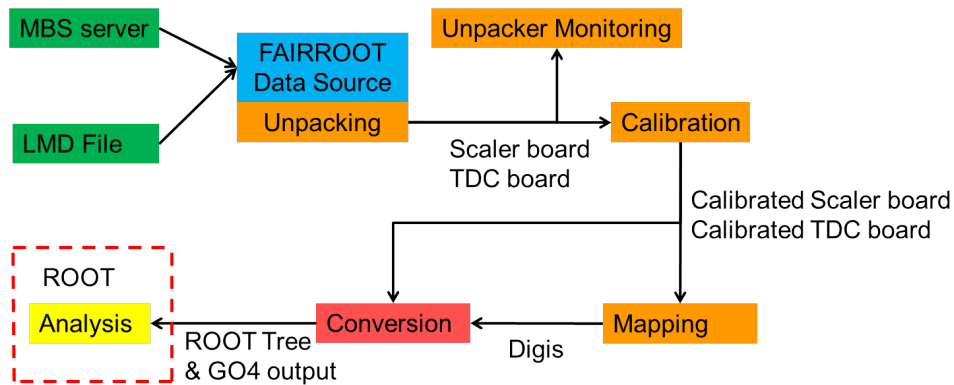


Figure 5.3: CBMROOT Unpacker organization in logical steps with main output formats. The pure FAIRROOT tasks are depicted in blue, the one using newly made CBMROOT classes in orange and the one using some classes developed for the GO4 unpacker in red. These tasks are described in more details in following paragraphs.

Unpacking

The support for reading an MBS event source in FAIRROOT allows for obtaining data either from a running event server or from a previously written file. This is done by the `FairRemoteSource` and by the `FairLmdSource` classes. As both inherit from the `FairSource` class, they can be substituted easily and are used in similar ways.

An MBS event can contain several sub-events. In the MBS events created by the DABC DAQ that we used, each sub-event corresponds to a data source (MBS DAQ, ROC, ...). The sub-event headers contains flags which are used to provide information about the sub-event, for instance the component in the setup which sent the block of data. These flags are named:

- Type
- Sub-Type
- Sub-crate
- Processor Id
- Control

These flags are used by the DABC DAQ to encode information about the data origin (VME crate, ROC, ...), the data format (Optics, Ethernet, ...) or the hardware used (Trigger board, acquisition boards, ...).

An object of the data source class mentioned above needs to be provided with objects of classes that inherit from the `FairUnpack` class. Each of these objects is then assigned a specific sub-event using the sub-event header flags. In our test setups, three types of sub-event were present: one for the ROC data, one for the TRIGLOG board data and one for all other boards in the VME crate. We correspondingly implemented three daughter classes of `FairUnpack`: `TGet4UnpackTof` (for ROC data), `TTriglogUnpackTof` (for TRIGLOG data) and `TMbsUnpackTof` (for the other triggered boards data).

These daughter classes, however, are not performing the unpacking directly. The reason for this is that an MBS sub-event, while coming from a single readout system, can contain data from different hardware, e.g. data from the VFTX TDC boards and from the SCALORMU scaler boards are present in the VME sub-event. In addition, the number of elements for each hardware type can vary between setups, especially in the case of TDC boards (GET4 or VFTX). To obtain the required flexibility, the daughter classes of `FairUnpack` that we implemented create one or more specialized unpacker objects and at the same time the corresponding containers for the unpacked data. The number of specialized unpackers depends on the number of different boards present in the data and on the parameters provided by the user: boards can be deactivated in software (ignored at the unpacker step). Each specialized unpacker then receives from the FAIRROOT run-manager an access to the data containers that it is supposed to fill.

The unpacker for the TRIGLOG boards unpacks the trigger specific information such as the trigger pattern, the event time in UNIX format (ms precision) and the input pattern. In the same time, it unpacks the content of the internal scalers of the board, as well as the counter value of an internal clock, which can be used for a more precise determination of the scalers rate. Hence, TRIGLOG data can be considered as stemming from a more

generic Scaler Board. To optimize the use of such information, the `TTofTriglogBoard` data container class is implemented as a daughter class of the `TTofScalerBoard` class used to store the data of the other scalers.

The unpacker for the VME acquisition boards can be configured to unpack the data from combinations of arbitrary numbers of the following VME boards (see Subsection 4.2.5 and Appendix B for more details on the boards):

- VFTX TDC
- SCALORMU

A single object of class `TTofVftxUnpacker` is instantiated for all VFTX boards and one `TTofScomUnpacker` for all SCALORMU boards. The `TTofVftxUnpacker` uses as output a ROOT `TClonesArray` collection of `TTofVftxBoard` objects where the number of entries matches the number of VFTX TDCs. The `TTofScomUnpacker` uses as output a ROOT `TClonesArray` collection of `TTofScalerBoard` objects where the number of entries matches the number of scaler boards (SCALORMU and TRIGLOG).

The unpacker for the GET4 is similar to the GO4 one. It performs the unpacking, the time sorting and the event building from the GET4 data. The main difference is that in CBMROOT only the pseudo-triggered event building around SYNC system messages is available. The unpacker fills an object of the class `TTofGet4Board` for each GET4.

Both `TTofVftxBoard` and `TTofGet4Board` are daughter classes of a more generic `TTofTdcBoard` class. The `TofTdcBoard` stores the single hit data in a `TClonesArray`, giving the possibility to apply the same principle to the single hit data containers: the `TTofVftxData` and `TTofGet4Data` classes both inherit from the `TTofTdcData`. As objects of this class contain all fields defining a TDC hit (Channel, Fine Time in bins, Coarse Time in clock cycles, optional TOT in bins), one can use common algorithms in the calibration step. The respective daughter class contain the board specific fields used for the unpacking side tasks as for example time sorting or event building. These fields can also be used for monitoring.

A summary of the unpacking step is shown in Fig. 5.4:

Unpacker monitoring

The `FairUnpack` and `FairSource` classes are not meant to be used for monitoring purposes, and especially not for histogramming. In the general scheme of FAIRROOT, this is done by objects of classes inheriting from `FairTask`, which are called later in the analysis. In the GO4 analysis, however, the monitoring was done directly in the unpacker. To keep the modifications to a minimum, all histogramming and monitoring tasks were just moved to dedicated methods during the conversion to CBMROOT. The `TMbsUnpTofMonitor` class, which is a child of `FairTask`, then just instantiates again an object for each active unpacker in the previous stage and calls their methods for histogram creation, histogram filling and histogram saving to file. In the unpacker for GET4 data, an event building based on time-coincidences is done inside the unpacker. This event building and the corresponding monitoring could not be separated from the unpacking functionalities as for the other unpackers. For this reason, the GET4 unpacker in CBMROOT does not comply with

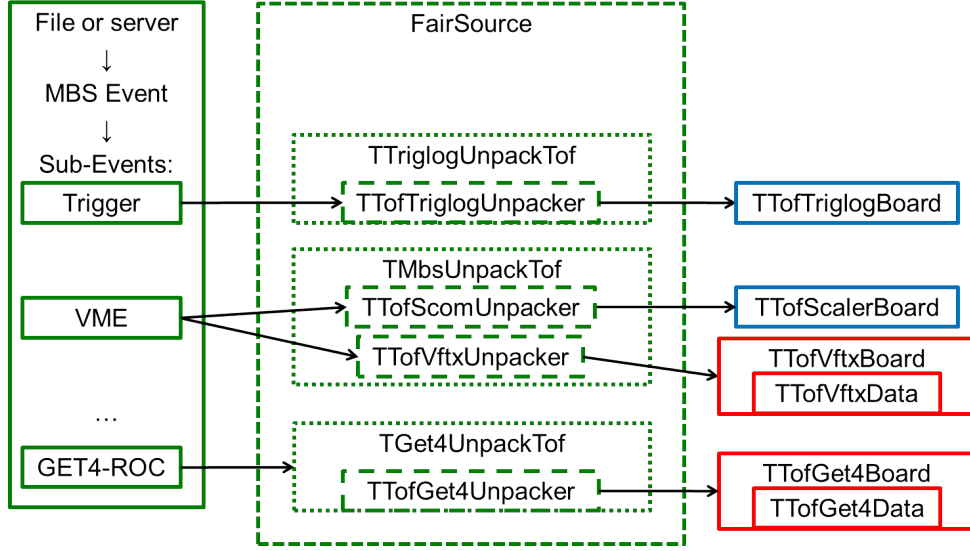


Figure 5.4: Detailed unpack step in CBMROOT with the supported MBS sub-events, the corresponding unpacking classes and output data formats. The dotted boxes indicate processing classes inheriting from FairUnpack. The blue boxes indicate output objects inheriting from TTofScalerBoard and the red ones those inheriting from TTofTdcBoard.

the desired separation between the FairUnpack functionalities (only unpacking) and the FairTask functionalities (analysis and monitoring) and it is not used in the monitoring step.

A summary of the unpacker monitoring logical step is shown in Fig. 5.5:

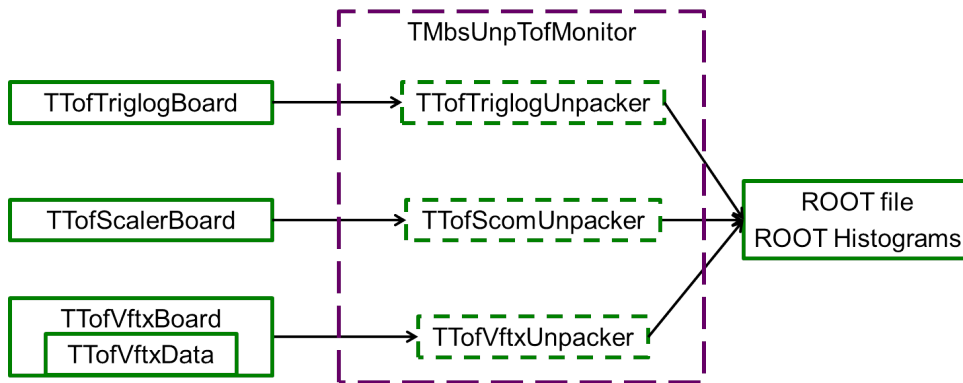


Figure 5.5: Details of the unpacker monitoring with the corresponding unpacking classes and input data formats. The long-dashed purple box indicates a class inheriting from FairTask.

Calibration

The calibration step is based on one class inheriting from FairTask, TMbsCalibTof, which itself creates and calls the calibrator classes. There are two calibrator classes, one for the scaler boards, called TMbsCalibScalTof, and one for the TDC boards, called TMbsCalibTdcTof.

TMbsCalibScalTof is common to all scaler boards compatible with the TTofScalerBoard data container. It performs two main tasks for each board in order to obtain the rate per scaler channel. First, if the TRIGLOG data with the UNIX event time are available, it generates a distribution of the board reference clock counts per unit of time and fits it with a constant at periodic intervals. The fit value is the real frequency of the reference clock. All our scaler boards use a 781.25 kHz internal clock as reference, but the real clock frequency is in most case different from the nominal one. As the real frequency is also not the same in all boards, we need to know it in order to compare data measured in different boards. This fit value can be used to compute an event-to-event time distance with a precision of around 10 times the clock period. The nominal reference clock frequency gives a precision around 13 μ s, to be compared to the ms precision of UNIX time. The second task is the calculation of the event-by-event rate per scaler channel from the counts difference of two consecutive events and the event-to-event time obtained from the reference clock. This rate per channel can also be combined for a set of channels, giving the possibility to obtain the rate per cm² of the corresponding detector channels if their surface is known. The rate per units of surface is important for our detector tests. When beam is available, it gives a way to estimate the operating conditions the counter manages to survive. When only cosmic particles are available, it provides a way to estimate the noise properties of the counters. The calibrated data of a full scaler board are stored in an object of the class TTofCalibScaler. This class can be adapted to store data from boards having more than one level of scalers for each input channel, as is the case for the TRIGLOG (Trigger input, valid trigger, accepted trigger, ...).

TMbsCalibTdcTof is common to all TDC boards compatible with the TTofTdcBoard data container. It performs two main tasks for each board. The first one is the calibration itself, through bin occupation distributions for each TDC channel. This task includes both the generation of such histograms from the fine-time data of each board, the extraction of the effective bin sizes from these histograms and the use of these bin sizes to convert the raw data from bin units to time units. This calibration corrects for both the INL and DNL of the TDC (see Subsection 3.4.3). The only parameters needed to accommodate different TDC types in this task are the fine-time size in bits and the timing clock period. The second task is the hit building by associating a leading and a trailing edge to obtain a time and TOT pair. While this can be done either on-chip or in the unpacker in the GET4 case, it can be done only after the calibration in the case of FPGA TDCs (VFTX, ...). This is due to their huge non-linearities and the fact that they digitize the opposite edges in different TDC channels. One input channel corresponds then to two TDC channels, which makes a simple bin subtraction without proper calibration pointless. Another case is for the unpacking of CAEN V1290A data, where the 6 ns minimal width for digitizing enforces the use of splitted signals and two TDC boards configured to digitize opposite

edges (see Appendix B.3). Four TOT building modes are implemented:

- Time and TOT are measured in the same TDC channel but readout in different data message, e.g. CAEN V1290A for signals longer than 8 ns
- 2 TDC channels per input channel or 2 input channels per front end channel, each digitizing one edge, e.g. data from VFTX, GET4 Proto or GET4 v1.0 in 24 bit mode
- Same input channels in 2 consecutive boards, configured to digitize opposite edges, e.g. CAEN V1290A for signals shorter than 8 ns
- Time and TOT in the same data message from the same TDC channel (just a copy of content is needed), e.g. GET4 v1.0 in 32 bit mode

The calibrated data are all stored in objects of the class `TTofCalibData`, which themselves are stored in a `TClonesArray` common to all TDC types and boards.

A summary of the calibration step is shown in Fig. 5.6:

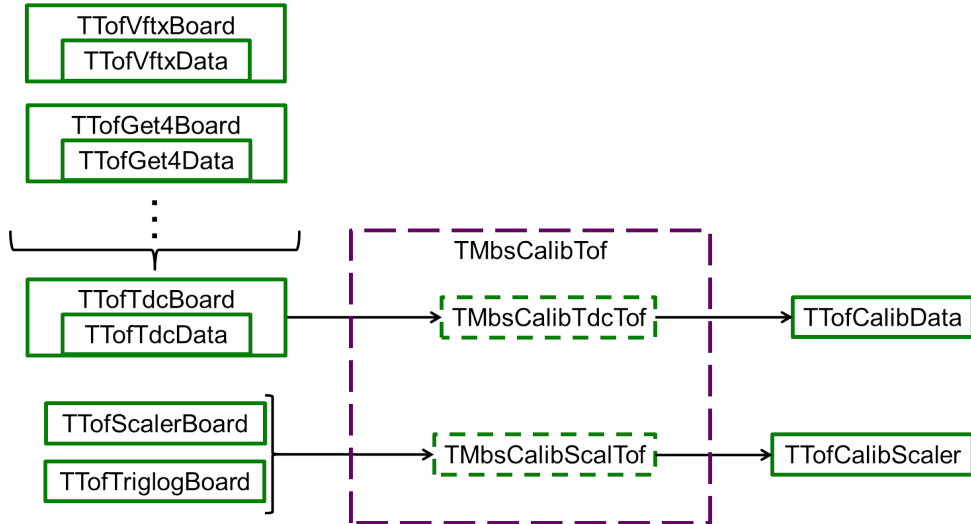


Figure 5.6: Details of the calibration step with the corresponding processing classes and input data/output formats. The long-dashed purple box indicates a class inheriting from `FairTask`. The `TMbsCalibTdcTof` class takes as input objects inheriting from the `TTofTdcData` and `TTofTdcBoard` classes, such as `TTofVftxDData` objects packed into `TTofVftxBoard` objects or `TTofGet4Data` objects packed into `TTofGet4Board` objects.

Mapping

The mapping step converts objects with electronics related address fields, the `TTofCalibData` objects, to objects with detector related address fields, the `CbmTofDigi` objects. These `CbmTofDigi` objects are the junction point between unpacked real data and simulated data. All timing detectors (plastic scintillators, RPC, diamond, ...) are saved as “RPC”, with single ended ones described as pad RPC and double ended ones described as strip RPC.

Two versions of the CbmTofDigi are implemented: the CbmTofDigi, with data rebinned in a 32-bit integer and the CbmTofDigiExp, where the data are saved as double floats. The CbmTofDigi objects correspond to a data format that could eventually be used within the CBM data transport network, while the CbmTofDigiExp objects are needed for the sake of analysis simplicity and speed.

In both cases, the Digi also contains the detector channel address, encoded in a 32-bit integer following a scheme common to all detectors in CBMROOT. The CbmTofAddress class, which inherit from the CbmAddress class, was implemented to perform the encoding and decoding of this address. This class does not hold any data member, but provides all methods to convert from separate channel identifiers (Detector, SM, RPC, ...) to a Unique Identifier (UID) and vice-versa. The fields used in the UID are defined in Table 5.1.

Table 5.1: Fields definitions of the Unique Identifier for the detector channels.

		3	2	1	0			
Field	on bits	0	0	0	0	Shift	Bits	Values
System ID	0- 3	00000000000000000000000001111				0	4	15
SM ID	4-11	000000000000000000000111111110000				4	8	256
SM Type	12-15	000000000000000001111000000000000				12	4	15
RPC ID	16-22	000000000111111100000000000000000				16	7	128
Channel Side	23	000000001000000000000000000000000				23	1	2
Channel ID	24-31	111111110000000000000000000000000				24	8	256

A summary of the mapping step is shown in Fig. 5.7:



Figure 5.7: Details of the mapping step in the CBMROOT unpacker with the corresponding processing class and input/output data formats. The long-dashed purple box indicates a class inheriting from FairTask.

Conversion to the output format of the G04 unpacker

To validate the CBMROOT unpacker, it is necessary to cross check that its output is of the same quality as the one obtained with the GO4 algorithm in Subsection 4.4.5. The main goal of the unpacker development was to reach the common storage format for simulation and real data, without starting to develop the reconstruction algorithms in CBMROOT. The easiest way to validate the unpacker performance is to re-use the already existing reconstruction, calibration and analysis algorithms presented in Subsection 4.4.5.

The resulting system performance can also be directly compared to the GO4 unpacker one. Therefore, an additional step is added to the CBMROOT unpacker to convert its output back to the GO4 unpacker output format.

The conversion task takes as input the arrays of `TTofTriglogBoard`, `TTofVftxBBoard`, `TTofCalibData`, `TTofCalibScaler` and `CbmTofDigi/CbmTofDigiExp` objects.

The trigger board information is directly saved as single unsigned integer leaves in the ROOT tree.

The VFTX calibrated data as well as the calibrated scaler data are saved in fixed-size arrays inside `TVftxBBoardData` and `Scalers_Event` objects respectively, which are both daughter classes of `TObject`.

For strip RPCs, the Digi objects of the left and the right side of a strips are merged in *Rpc_Hits* using a simple algorithm: only the first Digi on each channel is considered, generating either 0 or 1 hit per detector channel per event. For plastic scintillators with double side readout, the Digi objects of the left and right side of the same strips are matched into *Plastics_Hits* using another algorithm: Digs on each channel are associated as long as pairs can be formed (1st Digi left + 1st Digi right, 2nd Digi left + 2nd Digi right, ...). This way of building detector hits is not the optimal one as possibly the best pair is, for example, the first Digi on one side and the second Digi on the other one, but it is the most simple algorithm and the closest one to the GO4 algorithm. The resulting *Rpc_Hit* and *Plastics_Hit* objects are then stored in one vector per detector in the output ROOT tree.

A summary of the conversion step is shown in Fig. 5.8:

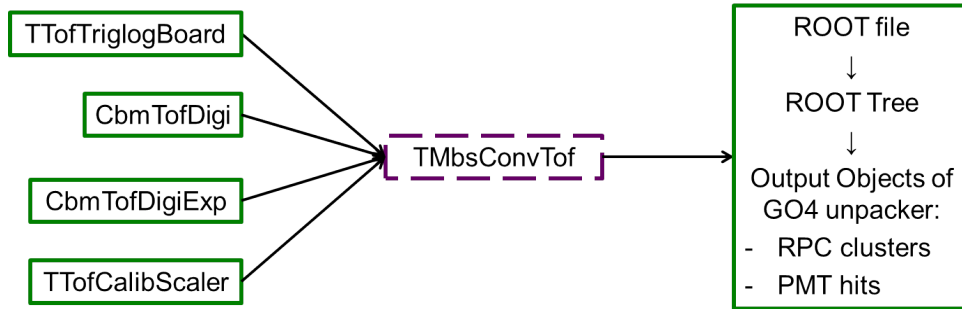


Figure 5.8: Details of the conversion step in the CBMROOT unpacker with the corresponding processing class and input/output data formats.

5.3.2 Results: Comparison with the GO4 unpacker

Table 5.2 presents a comparison of the results obtained with the GO4 unpacker and the CBMROOT unpacker for both our TDC systems in the last run of cosmic tests (see Subsection 4.4.5). The two main differences between the unpackers are that in the CBMROOT version, the VFTX edges association rejects negative TOT and that the GET4 data are calibrated for non-linearities.

An offset between edges exists in the VFTX due to signal path length differences. This can lead to negative TOT values on some channels as the full TOT spectrum is then shifted. The offset is roughly compensated for by aligning the peak value of the TOT spectrum to a fixed TOT value for all channels with RPC data. However, it is still possible that the TOT spectrum contains negative values for some channels. Along with the rejection of negative TOT values in the CBMROOT unpacker, this explains the decrease in event number for similar performance in the VFTX case.

The way of calibrating GET4 data in CBMROOT explains the loss of a few events (timing cuts) and the small improvement in time resolution. The fact that the effects are negligible within errors also confirms that the non-linearities of the GET4 v1.0 have a rather small influence on its timing performance.

Generally, the efficiency and time resolution in both systems match well between the two unpackers, demonstrating that the new unpacker in CBMROOT can be used as a replacement for the GO4 one and as a base for moving towards a purely time-based unpacking.

Table 5.2: Comparison of the system performance obtained with the GO4 unpacker and the CBMROOT unpacker for both digitizer systems in the 2013 cosmic test at a high voltage of 11.5 kV.

System: PADI-6 +	GO4		CBMROOT	
	VFTX	GET4 v1.0	VFTX	GET4 v1.0
Reference Time Resolution [ps]	116.0 ± 1.0	119.4 ± 1.1	119.4 ± 1.1	119.4 ± 1.1
Total Events number	10593	10593	10593	10593
Events with good reference	8461	8264	8419	8204
Events with RPC	8314	8049	8274	7992
RPC Efficiency [%]	98.3 ± 0.1	97.4 ± 0.2	98.3 ± 0.1	97.4 ± 0.2
System Time Resolution [ps]	72.4 ± 0.8	82.0 ± 0.9	72.2 ± 0.7	80.3 ± 0.9
Mean cluster size [strips]	1.86	1.66	1.86	1.66
Mean cluster multiplicity	1.14	1.13	1.13	1.13

5.4 Wall geometry implementation

The geometry description used for the TOF wall detector in CBMROOT is organized in RPC cells which are in turn contained in Super Modules (SM). The RPCs are subdivided into channels which represent the sensitive area.

In the current version only strips RPC are used. It describes quite well the currently planned design planned for the outer regions of the TOF wall. However, for the inner area of the wall, the decision on whether CBM will use pads readout on one side or strips readout on both sides is not yet done. For this reason, the CBMROOT geometry uses there channels having a similar area but not matching the geometry of any of the two

designs proposed in the Technical Design Report [20]. Fig. 5.9 shows a 3D view of the geometry as implemented in CBMROOT. Only the support structure of the wall and the SM boxes are made visible.

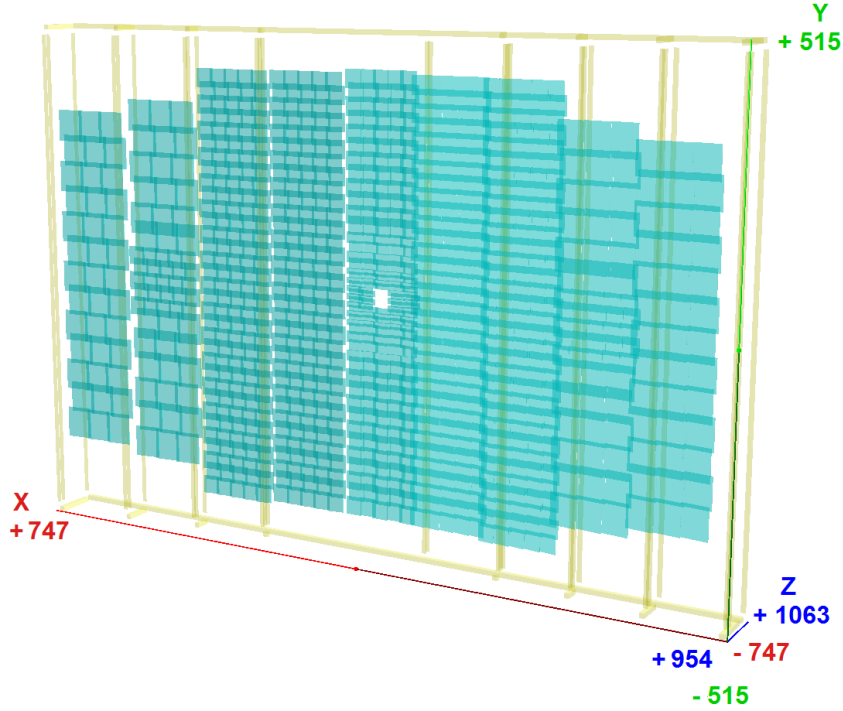


Figure 5.9: 3D view of the standard wall geometry in CBMROOT.

Table 5.3 summarizes the characteristics of the six RPC and SM types used in this geometry. The channels are the detector channels (strips, pads) and not the electronics channels. As only strips are used in the current implementation, the total number of channels needs to be multiplied by two to obtain the number of electronics channels in this design. The column entitled “region” corresponds to the areas defined in Section 3.5 (cf. Fig. 3.17 and Table 3.1).

The current standard versions of the TOF wall geometry in CBMROOT are called *v13a* and *v13b*. *v13a* corresponds to the SIS100 geometry with a wall placed at 6 m from the target and *v13b* corresponds to the SIS300 geometry with a wall placed at 10 m from the target.

5.5 A CBM-TOF digitizer in CBMROOT

5.5.1 Classes organization

The input data from the Monte Carlo (MC) generator and propagator are stored in objects of class `CbmTofPoint`. A MC track can generate a `CbmTofPoint` in any of the sensitive areas defined in the geometry file, which are in our case the gas gaps of the RPC counter.

Table 5.3: Characteristics of the RPC and SM types used for the wall geometry in the simulations.

Type	Region	Chan./RPC	RPC/SM	Chan./SM	SM	Total chan.	Total RPC
0	A,B,C	32	5	160	24	3840	120
1	A,B,C,D	32	5	160	142	22720	710
2	A	52	3	156	50	7800	150
3	D,E	96	5	480	8	3840	40
4	D,E	96	5	480	8	3840	40
5	D,E	96	2	192	10	1920	20
In total for the wall					242	43960	1080

The goal of a hit production chain is to generate the corresponding CbmTofHit objects, which describe detector channel hits.

The existing software chain until now consisted of a single task, the CbmTofHitProducerNew. It produces directly CbmTofHit objects from the CbmTofPoint on each detector channel, taking into account a global detector efficiency, a global detector resolution, the electronics resolution and the propagation time along the electrode. It assumes vertically oriented strips as detector channels. The hits are built from the time of the first CbmTofPoint signal to reach each side of the strip after propagating along it. This results in clusters always having a size of one strip. As clusters are not built later on between adjacent strips, the only multiple hits loss occurs when multiple trajectories cross the same strip. The information about the 3D geometry of the detectors and sensitive areas is stored in the CbmTofDigiPar class.

The newly developed digitization chain replaces the direct hit production by a two step conversion. The CbmTofPoints are first used to generate CbmTofDigi/CbmTofDigiExp objects. These readout channel data are then used to build CbmTofHit objects. The first step is the digitization and is performed by the CbmTofDigitizerBDF task, for “*Cbm ToF Digitizer using Beam Data Feedback*”. The CbmTofDigiBdfPar class is used to provide information about the beamtime performance of the components: counter resolution and efficiency, counter cluster size, electronics resolution, start counter resolution. This information needs to be provided for each SM type, allowing for example to simulate the influence of the measured properties of different RPC designs on the physics performance. The CbmTofDigiPar is used to access the detector geometry, as in the CbmTofHitProducerNew. Subsection 5.5.2 presents how the digitization is performed. The second step is the clusterization, performed by the CbmTofSimpClusterizer task. This is presented in Subsection 5.5.3.

Another task is added as a side branch to this new hit production chain, the CbmTofTests task, which provides additional histograms to monitor the proper operation of the digitization and clusterization as well as to cross-check the Cartesian and angular coverage of the used wall geometry. It will also be used for the components dimensioning presented in Section 5.6.

Fig. 5.10 shows a summary of both the previously existing hit production chain and the newly developed one.

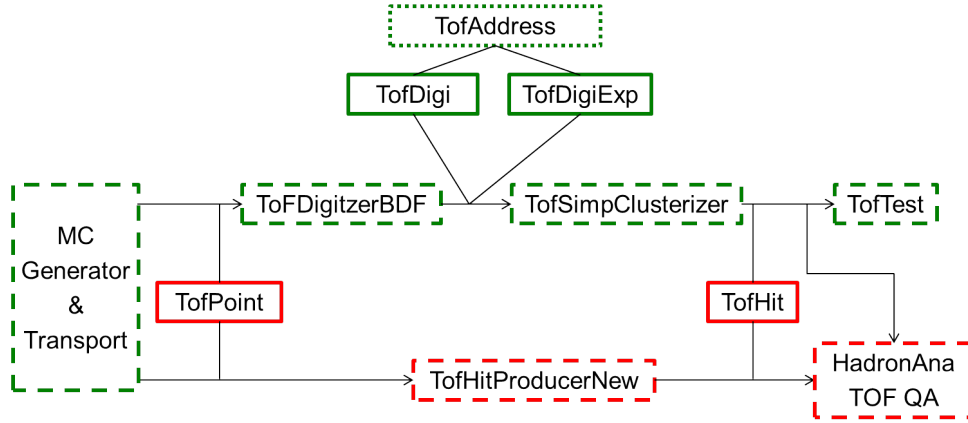


Figure 5.10: Comparison of the digitization chains for TOF in CBMROOT. Dashed boxes indicate tasks, solid-line boxes data containers and dotted boxes address converter. The red colors show parts which already existed in the direct hit conversion chain, while green ones show the parts developed and implemented for the digitizer in this thesis.

After digitization and hit building or direct hit production, the TofHits are used for the Hadron Analysis and TOF Quality Assessment (QA) tasks provided in CBMROOT by other CBM members. The output of these analysis steps is used to compare the newly developed digitizer to the previous hit producer in Subsection 5.5.4.

5.5.2 Digitization

The digitization task can be divided into different sub-tasks. One of them, the generation of the reference time jitter, is done once per event. The following sub-tasks are performed for each CbmTofPoint:

1. Determining if a MC point from the same track already fired the same readout channel in the same RPC module (previous gaps)
2. Determining if the MC point is detected by the detector (efficiency)
3. Generating the detector hit jitter (counter resolution), which is common to all detector channels where this MC point generates a signal (cluster)
4. Determining in which detector channels this MC point generates a signal
5. Generating a total TOT (charge) for the cluster and spreading it between the firing strips
6. Applying the propagation time from the hit position to the channel readout position
7. Generating and applying the FEE effects to the hit properties on each readout position (electronics jitter, gain, ...)
8. Building from this information Digi objects

Finally, the eventual overlap of Digis from different tracks (multiple hits on the same channel, close hits with overlapping cluster areas, ...) has to be resolved for each readout

channel.

Reference time

The jitter of the reference time (e.g. start detector) is generated once at the beginning of each event. One of the parameters that the user has to provide as input to the `CbmTofDigiBdfPar` class is the resolution of the start counter. The jitter is obtained from a `TRandom3` random generator of ROOT with a Gaussian distribution centered at zero and with a width equal to the start resolution provided by the user (sigma parameter). As this digitizer is designed for an event based analysis and the MC propagation define all times from the interaction, this jitter can be directly considered as the *measured start time* which will be used as origin for the event time frame. The jitter of the start counter is noted $Jitter_{Start,Event}$ from now on.

Firing detector channels and charge spread

The first test performed to determine which readout channels are firing is to check if the MC point is detected or not. As the MC points can be generated in each gap, this will be done gap-wise. In the same time, as was described in Section 3.3, the signal generated on an MRPC readout channel is a combination of the signals induced by the avalanches in all gaps. To properly emulate this, a boolean vector keeps track for each (MC track/RPC module) pair whether a cluster was already generated in a previous gap. This allows for creating a single cluster per (MC track/RPC module) pair.

The quantity measured in beamtime which the user is asked to provide to the `CbmTofDigiBdfPar` class is the efficiency of the full MRPC detector. To obtain the efficiency per gap, one assumes that all gaps have an equivalent efficiency, which is a good approximation for MRPCs with the same size for all gaps as described in Section 3.3. One assumes also that a single fired gap is sufficient to have an output signal. If E_{RPC} is the counter efficiency, e_{gap} the gap efficiency and N the number of gaps, the probability that a track does not fire the counter at all is then:

$$\overline{E_{RPC}} = 1 - E_{RPC} \quad (5.1)$$

$$= (1 - e_{gap})^N \quad (5.2)$$

The gap efficiency can then be expressed as:

$$e_{gap} = 1 - (1 - E_{RPC})^{\frac{1}{N}} \quad (5.3)$$

To determine if a MC point generates a cluster, a uniform distribution is sampled on the $[0,1]$ interval using a `TRandom3` generator and the resulting value is compared to the gap efficiency. If it is smaller, the cluster generation process continues, otherwise the next MC point is tested.

Once the hit is considered as detected, one can generate from the beamtime data the cluster properties: detector jitter (noted $Jitter_{RPC,cluster}$ from now on), total TOT (charge)

and cluster radius. The jitter is generated using the experimental counter resolution provided by the user. It is common to all readout channels of the same cluster. Like for the start counter jitter, it is generated with a Gaussian distribution centered at zero and with the counter resolution as sigma parameter. The cluster time is then the sum of the MC point time, the detector jitter and the start jitter:

$$t_{cluster} = t_{MC \text{ Point}} + Jitter_{RPC,cluster} + Jitter_{Start,Event} \quad (5.4)$$

The user provides an experimental distribution of the cluster total TOT. When the simulation starts, the normalized integral of this distribution is calculated and stored in a histogram with 10000 bins on the $[0,1]$ axis. This allows for generating TOT values following the initial distribution using a random generator and a uniform distribution. The number of bins in histogram of the normalized integral was chosen as a compromise between the simulation speed and its realism. The method is illustrated in Fig. 5.11. The

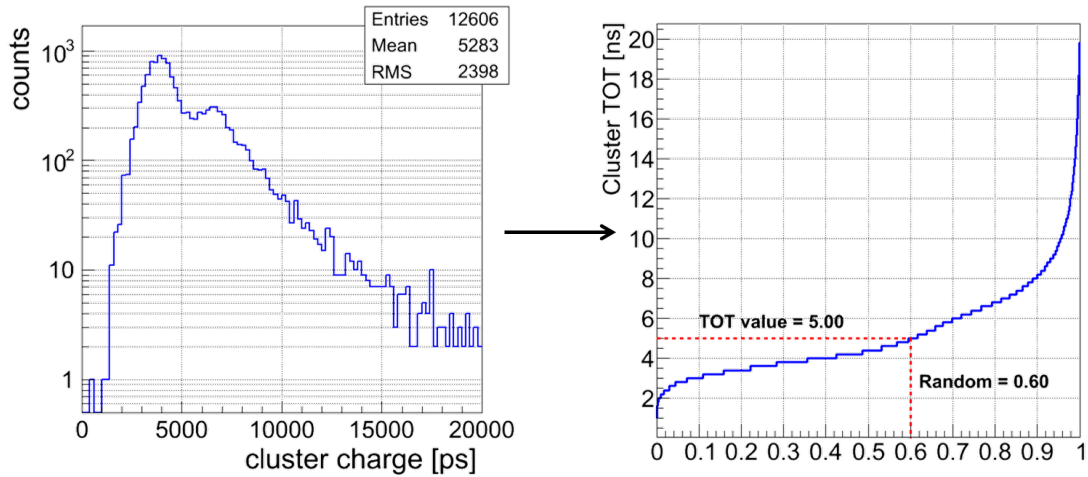


Figure 5.11: Illustration of the method used to generate total TOT values for the clusters following the experimental distribution. The normalized integral of the distribution is first built. Then a call of a random generator using a uniform distribution selects a TOT value (red dashed lines).

cluster radius is needed to determine both how many detector channels are firing and how the cluster charge is spread among them. The corresponding experimental parameter is the cluster size in strips/pads. However, there is no unique correspondence between a cluster size distribution and a cluster radius distribution as it depends on the readout channel geometry. Four approximation methods are implemented in the digitizer to obtain a cluster radius distribution from the experimentally measured cluster size distribution. For the first one, a fixed radius of 0.0002 cm is used, allowing to have a behavior similar to the direct hit producer in terms of cluster size: 99.99% of clusters then fire a single detector channel.

In the second method, a fixed cluster radius is obtained from the mean of the cluster size

distribution. The used relation is the following:

$$r_{cluster} = \frac{1}{2}(\bar{S}_{MC\ Point} - 1) \cdot w_{strip} \quad (5.5)$$

This relation is valid for the following assumptions:

- Only strips are used
- All strips have the same width w_{strip} , expressed in cm
- The RPC/strips edges are neglected
- $\bar{S}_{MC\ Point}$ is the mean cluster size expressed in strips
- All clusters are circular and have the same radius $r_{cluster}$, expressed in cm

A similar relation was not found for pads. The place for the pads relation is reserved in the code but left empty, in case of later developments by groups designing pad MRPCs.

The third and fourth methods both use a Landau distribution to obtain the radius value. In the third method, the distribution parameters are set by the user in the parameter file and the experimental cluster size distribution is ignored. The recommended values are a Most Probable Value (MPV) of 0.06 and a Sigma of 0.02 (all parameters correspond to the ROOT implementation of the Landau distribution). These empirical values were obtained by fitting the cluster size distribution obtained with cosmics and the RPC-P3 prototype (see Appendix A.3) with Landau distributions of variable parameters.

In the fourth method, a fit of the cluster size distribution in strips by a Landau function is used. If the fit fails the recommended values of the third method are used. If the fit was successful, the obtained MPV and Sigma value are used to obtain the corresponding MPV and Sigma values for a cluster radius Landau distribution from pre-loaded histograms. These histograms were generated by scanning the MPV and Sigma parameters for a radius distribution and for each pair fitting the obtained cluster size distribution with a Landau function. The main restrictions of this method are:

- Different (MPV, Sigma) for the radius values can generate the same (MPV, Sigma) for the cluster size
- Many (MPV, Sigma) for the cluster size are not covered by the limited (MPV, Sigma) scan for the radius values

In cases where no or more than one solution can be found, the user is warned and the recommended values of the third method are used.

Once the cluster radius is obtained, the firing channels are determined using the cluster charge distribution. The integration of the cluster charge distribution over the channel area gives the charge induced in the readout channel. If this value is above a user given value, the channel is considered as firing. Three charge distributions are implemented in the current version of the digitizer:

- For strips only, using directly the experimental cluster size distribution in strips (no cluster radius) and a one-dimensional Gaussian charge distribution across the strips
- A “flat disc” charge distribution of radius $r_{cluster}$
- A two-dimensional Gaussian charge distribution

For the 1D Gaussian, the cluster size is used to determine the number of strips on each side around the central one for which the induced charge will be calculated and checked.

The Gaussian is parametrized such that 99.7% of the charge fits in the firing strips ($\sigma = \text{cluster size}/3$), so in this case the cluster radius is not determined (not used). The charge in each strip is then obtained by integrating the function between the strip edges. In the 2D Gaussian option, the charge distribution is parametrized as a 2D Gaussian function with equal width along the X and Y axis. The width is calculated so that 99.7% of the charge is within the cluster radius by:

$$\sigma_x = \sigma_y = \frac{r_{cluster}}{3} \quad (5.6)$$

The two Gaussian charge distributions were implemented, but not extensively tested due to their high time/resources consumption compared to the “Flat disc” one. For the “Flat disc” option, one considers that the charge is homogeneously distributed on a surface corresponding to the cluster radius. The fraction of the charge assigned to each channel is then equal to the total charge times the fraction of the disc area contained in the channel surface. As both pads and strips can be described as rectangles and the area of intersection between a rectangle and a disc can be easily calculated, this method is the fastest available. In the case of strips, the charge assigned to a detector channel is then split equally between the two readout channels.

In case the user provides a threshold value in ns and a FEE channel gain spread value to reflect the limitations of the electronics, a gain value is generated in the first event for each readout channel. A last check will be done once a charge has been assigned to the readout channels and only channels passing the threshold after the application of the gain are considered as firing.

Digis properties

Once the firing channels are determined and the TOT has been spread between channels, the timing at each readout point has to be calculated.

The first step for this is to calculate the time offset at the readout point due to the signal propagation from the position where it is generated (x_{Hit}, y_{Hit}). This offset is noted from now on $Offset_{Prop}$. The signal propagation speed is provided by the user and assumed to be the same for all RPC types. In the digitizer tests the speed used is that of copper readout electrodes. In the case of pads, the readout point is assumed to be the center of the pad base: (x_{Base}, y_{Base}). In the case of strips, the readout point is assumed to be the center of the strip end. The width of the strip is neglected, so that only the hit position along the strip is used to obtain the offset. The offset for the top (left) and bottom (right) ends of a vertical (horizontal) strip are of course different. Both can be obtained through the following equations, where l_{strip} is the strip length and (x_{Center}, y_{Center}) is the position of the strip center.

$$\text{Pads: } Offset_{Prop} = \frac{1}{v} \sqrt{(x_{Hit} - x_{Base})^2 + (y_{Hit} - y_{Base})^2} \quad (5.7)$$

$$\text{Vert. Strips: } Offset_{Prop} = \frac{1}{v} |x_{Hit} - x_{Center} \pm \frac{l_{strip}}{2}| \quad (5.8)$$

$$\text{Hor. Strips: } Offset_{Prop} = \frac{1}{v} |y_{Hit} - y_{Center} \pm \frac{l_{strip}}{2}| \quad (5.9)$$

Finally the jitter due to the electronics ($Jitter_{Elec.}$) can be added. It is obtained by a random generator using a Gaussian with the electronics resolution provided by the user as sigma parameter.

The final time is then:

$$t_{Digi} = t_{Readout} = t_{cluster} + Jitter_{Elec.} + Offset_{Prop} \quad (5.10)$$

The Digi object is built from the readout channel indices, the readout time and the TOT.

Multiple digis merging

Due to the multiple channel cluster size, one more task remains in order to have a realistic simulated electronics output for a full event: merging the Digis occurring on the same readout channel. For simplicity sake, it was chosen to select the first digi in time per event for each readout channel. To achieve this, the Digis are first stored in a buffer for each readout channel and then ordered according to their readout time. Only the first Digi in each buffer is copied to the output of the Digitizer.

Limitations, ease of development design and outlook

The current implementation of the digitizer has some known limitations. The first one is the absence of walk effect. This would be needed to develop and cross-check the walk correction methods directly in CBMROOT. The second one is the method chosen for the merging of Digis on the same readout channel. For now no real merging is done as only the first in time is selected. A more realistic treatment would take into account both the signals overlap and the electronics double hit/edge capability. This would lead to larger TOT when a second hit starts before the the first one is over and multiple Digis per channel when they are far enough. This will be especially required when developing the time-based (free-streaming) digitizer.

The Digitizer itself is designed to allow an easy inclusion of alternative Digi generation (TOT spread, timing effects, ...) and Digi merging methods through options in the user parameter file. This was tested with the three implemented charge spreading methods.

For the near future, it is planned to add the walk effect alongside more extensive tests of the digitizer.

5.5.3 Clusterization (Hit building)

A simple Hit Builder is implemented to compare the effects of the digitizer method against the direct hit producer method. It supports for now only strips RPCs. It generates one hit per reconstructed cluster. The reconstructed cluster is defined as a set of firing

neighboring strip matching a time window and a spatial window. Both window sizes are provided by the user. A firing strip is a strips for which at least one Digi can be found on each end. The “Strip time” $t_{Strip\ signal}$ is then defined as the mean of the first Digi time of both ends. The “Strip TOT” $tot_{Strip\ signal}$ is the sum of the digis TOT. The “Strip hit position” ($X_{Strip\ signal}$, $Y_{Strip\ signal}$, $Z_{Strip\ signal}$) is obtained from the Digi time difference and the same signal velocity already used in the digitizer. This is summarized in the following equations, where it is assumed the strip is aligned with the y axis and (A,B) represent the two strip ends:

$$t_{Strip\ signal} = \frac{1}{2}(t_{Digi,A} + t_{Digi,B}) \quad (5.11)$$

$$tot_{Strip\ signal} = (tot_{Digi,A} + tot_{Digi,B}) \quad (5.12)$$

$$X_{Strip\ signal} = X_{Strip\ center} \quad (5.13)$$

$$Y_{Strip\ signal} = \frac{1}{2 \cdot v_{signal}}(t_{Digi,B} - t_{Digi,A}) \quad (5.14)$$

$$Z_{Strip\ signal} = Z_{Strip\ center} \quad (5.15)$$

To keep the algorithm as simple as possible, the inclusion of firing strips in an existing cluster is unidirectional: the strips are scanned in each RPC module from the low strip indices to the high strip indices. Due to this the spatial window is applied to the distance of the newly found strip signal to the previous one. A better method would be to apply this window to the distance to the TOT weighted center of the existing cluster. The combination of the second method with the unidirectional scan would, however, introduce a bias as scanning from low to high indices or from high to low indices would then possibly result in different clusters.

Once a not matching firing strip is found or all strips are scanned (no more firing strips), the current cluster is closed and the corresponding hit properties are calculated. The hit position (X_{Hit} , Y_{Hit} , Z_{Hit}) is the TOT weighted mean of the strip signal positions. The hit time t_{Hit} is the TOT weighted mean of the strip signal times. The hit TOT tot_{Hit} is the sum of the TOT for all included strips.

$$X_{Hit} = \frac{\sum X_{Strip\ signal} \cdot tot_{Strip\ signal}}{\sum tot_{Strip\ signal}} \quad (5.16)$$

$$Y_{Hit} = \frac{\sum Y_{Strip\ signal} \cdot tot_{Strip\ signal}}{\sum tot_{Strip\ signal}} \quad (5.17)$$

$$Z_{Hit} = \frac{\sum Z_{Strip\ signal} \cdot tot_{Strip\ signal}}{\sum tot_{Strip\ signal}} \quad (5.18)$$

$$t_{Hit} = \frac{\sum t_{Strip\ signal} \cdot tot_{Strip\ signal}}{\sum tot_{Strip\ signal}} \quad (5.19)$$

$$tot_{Hit} = \sum tot_{Strip\ signal} \quad (5.20)$$

Limitations

The first limitation of the current hit builder is as mentioned before that only strips are supported. It was deemed more reasonable to leave the implementation of the cluster building on pads to members of the groups developing pad RPCs.

The second known limitation is the position and timing errors calculation. They are at present fixed and depend only on the geometrical parameters of the strips and on the system resolution. So all strips with the same geometry would have the same values. A better way would take into account for clusters with multiple strips the timing and position spread as well as the TOT distribution.

5.5.4 Results

To validate the performance of the digitizer, its output was compared to the output of the direct Hit Producer used before. The comparison is done on the hit detection efficiency, on the hit to track association efficiency and on the purity of the PID obtained after track association. The geometry used is the “standard” one presented in Section 5.4, placed at 6 m from target for the SIS100 case and 10 m from target for the SIS300 case. The input data sample is 10 k Au+Au events, obtained with the URQMD generator for minimum bias and central events, 10 A GeV (SIS100) and 25 A GeV (SIS100). A known feature of the URQMD version used here is that it does not describe the formation of spectator fragments and instead split the remains of the nuclei in free protons and neutron. This leads to an artificial excess at low angles in the minimum bias case. In order to still have a meaningful comparison for the protons at this centrality, the SHIELD generator is also used to obtain 10 k minimum bias events at 10 A GeV.

The parameters given to the digitizer are the same for all RPC types:

- RPC efficiency of 99% (to match HitProducer parameters)
- RPC time resolution of 60 ps (to match HitProducer parameters)
- Start time resolution of 40 ps (nominal, same as HitProducer)
- Electronics time resolution of 40 ps (nominal, same as HitProducer)
- Cluster total TOT (charge) distribution from Heidelberg RPC-P3 cosmics test
- Landau distribution for the Cluster radius with parameters best fitting RPC-P3 cosmics test cluster size distribution
- Flat disc as Cluster charge distribution

Table 5.4 presents one example of the values extracted from the simulated data, in the case of SIS300 central events. The four other cases are treated in the same way.

The TOF Points detection efficiency is obtained by building for each particle species the ratio of particles reaching the position of the TOF wall after MC propagation (CbmTof-Point objects) and of particles produced by the event generator (MC tracks). This gives the maximal efficiency possibly achievable with this particular wall geometry and position, which is independent of the hit production method.

The TOF Hits efficiency is the ratio of the TOF Hits produced out of the TOF Points and of MC tracks. Comparing it to the TOF Points detection efficiency gives an idea of the

losses due to multiple hits on the same readout channel, adjacent clusters and overlapping clusters.

The Global Tracks efficiency is the ratio of the TOF Hits which could be associated to a CBM track from the other detectors (STS and TRD mainly) and of MC tracks. This is a necessary step as for PID the particle momentum from the fitted track is needed. Comparing it to the TOF Hits efficiency can give hints in case of insufficient position precision in the TOF wall (bad matching).

The Global PID efficiency is the ratio of the number of Global Tracks assigned to a particle type and of the MC tracks of this type. As such, it can be above the MC point efficiency (contamination by misidentified tracks).

The quality assessment variable is the purity of the PID. The PID is obtained by assigning a species to particles depending on their m^2 (obtained from TOF) and momentum (from track fit) values. The limits between species in the (p, m^2) plane are obtained by fitting the distribution of single species at a 2σ level. The purity is then the proportion of Global Tracks (track + TOF hit pairs) for which the original MC particle ID match the PID assigned by the TOF methods within all particles assigned by TOF to a species.

Table 5.4: Example of efficiencies and purity obtained for the five main hadrons identified by TOF. In this the simulation parameters were the following: SIS300 configuration (wall at 10m from target, 25 AGeV beam energy), URQMD generator, central events, 10k events.

Particle	MC Tracks	TOF Points	TOF Hits	Global Tracks	Global PID	
		Eff. [%]	Eff. [%]	Eff. [%]	Eff. [%]	PID purity [%]
p	1620067	59.2	53.1	31.6	22	93.4
			54.9	32.1	22.6	95.2
π^-	3247190	42.6	38.4	23.3	22	81.2
			39.9	23.8	22.1	84.3
π^+	2952556	43.4	39.2	23.9	22.9	80.2
			40.6	24.3	22.9	83.1
K^-	127910	39.6	35.5	23	20.6	69.7
			36.9	23.5	23.3	71.5
K^+	400844	41.8	37.6	22.9	18.3	78.2
			39	23.4	20	80.4

From the efficiency values, one can establish two criteria to compare the digitizer to the direct Hit Producer: the absolute loss and the loss relative to the Hit Producer value. For the purity only the absolute loss is used. Table 5.5 show an example of these values as obtained from the content of Table 5.4.

Table 5.6 presents the range of values for each of the comparison criteria when considering all the centrality-energy-generator cases. For the efficiency, some losses were expected

Table 5.5: Example of efficiencies and purity losses as well as Relative efficiency losses (rel. to the original Hit Producer case) obtained for the five main hadrons identified by TOF. Negative values indicate cases where using the more realistic digitizer leads to less particles being detected/identified. In this the simulation parameters were the following: SIS300 (10m, 25 AGeV), URQMD, central, 10k events.

Particle	TOF Hits		Global Tracks		Global PID		
	Digi Loss [%]	Rel. Loss [%]	Digi Loss [%]	Rel. Loss [%]	Digi Loss [%]	Rel. Loss [%]	Purity loss [%]
p	-1.77	-3.2	-0.5	-1.6	-0.6	-2.7	-1.84
π^-	-1.47	-3.7	-0.5	-2.2	-0.1	-0.3	-3.11
π^+	-1.39	-3.4	-0.4	-1.6	0	0.1	-2.89
K^-	-1.33	-3.6	-0.4	-1.9	-2.7	-11.5	-1.86
K^+	-1.36	-3.5	-0.4	-1.8	-1.7	-8.5	-2.14

as the digitizer merge adjacent firing channels and introduce the possibility of clusters overlap. The observed values for both the absolute losses (~ 1 to 2 % at hit level, 0.5 to 1 % at global track level) and the scale of losses relative to the direct Hit Producer (2.5 to 4 % at hit level, 1.5 to 2.5 % at global track level) are all within expectations.

The PID efficiency depends a lot on the fitted limits of the particle species in the (p, m^2) plane. Some losses were also expected due to the fact that clusters stemming from particles of different species are merged with the new digitizer chain. Therefore, the mean time assigned to the hit will not match the momentum of the assigned track, leading to the wrong PID assignment. The effect is stronger for the kaons because they have the lowest initial statistics, leading to the high maximum loss value of 11.5 %. The losses in PID efficiency for protons and pions are staying within $0-3$ % as expected.

For the purity, a worsening is also to be expected for the same reason as for the PID efficiency. The particle species limits for the PID assignment can not be trusted for the minimum bias case due to the too low statistics for kaons in the limited simulation presented here, so only values from central event simulation are used to obtain the purity loss in Table 5.6. The loss of purity is limited to 2 to 3 % for all five species, which is pretty good and indicates that most of the PID efficiency loss leads to non-identified tracks (out of all fit limits) instead of a wrong PID assignment. Thus the digitizer is validated for large scale simulations. These simulations with statistics in the order of $100k$ to $1M$ events will be performed on computing farms to obtain more detailed comparisons and validate the digitizer for physics simulations.

5.6 Components dimensioning results

The number of readout chain components needed to equip the full wall can be evaluated on the basis of the proposed TOF wall layout (cf. Section 3.5), by using the wall geometry implemented in the simulation framework (cf. Section 5.4). Table 5.7 gather these

Table 5.6: Range of values when considering all the centrality-energy-generator cases for each of the comparison criteria.

Hits		Tracks		PID		
Eff. Loss. [%]	Rel. Loss. [%]	Eff. Loss. [%]	Rel. Loss. [%]	Eff. Loss. [%]	Rel. Loss. [%]	Purity Loss [%]
1-2 %	2.5-4 %	0.5-1 %	1.5-2.5 %	0-3 %	0-11.5%	2-3 %

numbers for the SIS300 configuration. Two options are considered for the digitizer: the GET4 ASIC tested in this work and an FPGA TDC under development at GSI. However in order to estimate the number of components in the transport part of the readout chain, simulations of the data rates are still necessary.

Table 5.7: Number of channels, needed FEE chips and ROCs for the full SIS300 TOF wall for both GET4 and the FPGA TDC option. Table taken from [20].

TDC system	GET4	FPGA
Channels per PADI-8 chip	8	8
Channels per TDC chip	4	32
FEE chips per ROC	40-48	6-24
Maximal number of channels per SM	960	960
Maximal number of PADI-8 chips per SM	120	120
Maximal number of TDC chips per SM	240	30
Maximal number of ROCs per SM	5	2
Total number of Channels (without spares)	87920	87920
Total number of FEE-PADI8 (without spares)	11140	11140
Total number of FEE-TDC (without spares)	22280	2860
Total number of ROCs(without spares)	532	175

Fig. 5.12 shows the mean hit rate for each electronic channel obtained with the CBM-ROOT digitizer, 10 k Au+Au events simulated using URQMD and the “standard” wall layout given in Section 5.4. The rates are scaled up for an interaction rate of 10 MHz. These estimations are done for both the SIS100 (10 A GeV, 6 m from target) and SIS300 (25 A GeV, 10 m from target) configurations. A few hundred channels in the region close to the beam pipe exhibit really high rates in the order of 1 MHz. This is thought to be due to the fact that the URQMD version used does not describe the formation of spectators in the fragmentation area, but instead disintegrate the beam nuclei, leading to a high number of free protons and neutrons. Fig. 5.13 represents the same data after resorting the channels in rate bins. The interesting observation that can be drawn from this figure is that all channels (with the exception of channels in the above mentioned fragmentation area) are staying under a mean rate of 400 kHz. This value is only 66 % of the maximum rate capability demonstrated in Subsection 4.4.4 for the GET4 v1.0 in 24 bit readout

mode. As the 32 bit readout mode should bring an increased rate capability, one can say that the GET4 chip matches well the expected data rate.

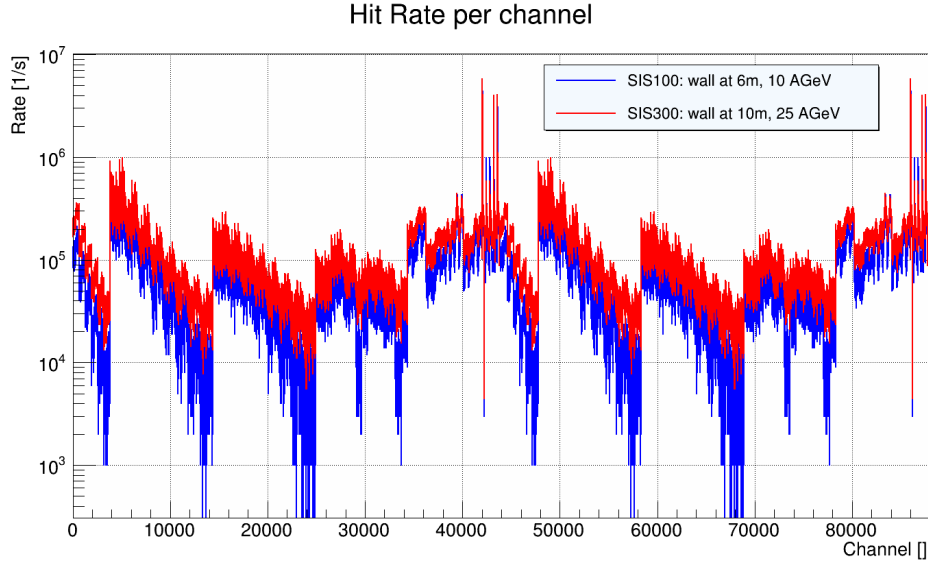


Figure 5.12: Simulated hit rate per electronic channel in 10 MHz Au+Au collisions at SIS100 (10A GeV) and SIS300 (25A GeV). The high rate values above 1 MHz (313 ch. @SIS100, 184 ch. @SIS300) are believed to be artefacts due to beam fragmentation in the URQMD model.

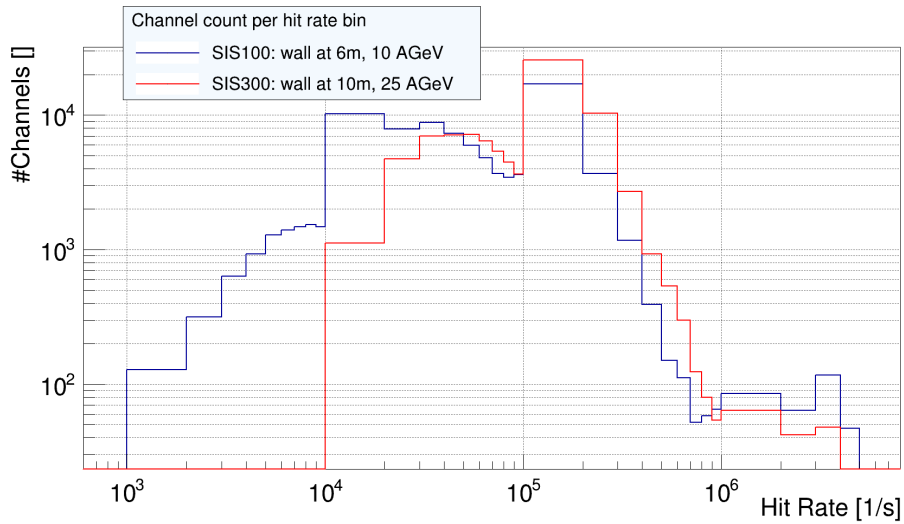


Figure 5.13: Same data as in Fig. 5.12, after resorting the channels in rate bins.

By summing the data rate for all channel connected to a same ROC, it is also possible to estimate the number of optical links (2.5Gb/s each) which are needed for the first level of data transport (ROC output) and the number needed after one level of data

combination (DCB output). In the FPGA TDC case, the hardware used as reference is the TRB3 board from the HADES experiment, which hosts a big central FPGA and four smaller peripheral ones. The components numbers obtained for the GET4 and FPGA TDC options are presented in more details respectively in Tables 5.8 and 5.9. To obtain these values, the following assumptions about their parameters were made:

- Left and right channels of an RPC are always connected to the same ROC (in groups of 32 channels).
- In case of GET4: There are at most 48 GET4 per ROC. 40, 42 or 48 chips could be connected by means of 3 types of motherboards (same FPGA firmware).
- In case of GET4: the Syscore v3 can be used as a ROC with 2 output optical links (SFPs), each 2.5 Gb/s [83].
- In case of FPGA TDC: The TRB3 board can be used with up to 4 HUB add-on boards. Each HUB add-on board has 6 SFPs, and the corresponding peripheral FPGA would act as ROC. The central FPGA would act as a DCB.
- In case of FPGA TDC: One TRB3 board is counted as one “ROC” \Rightarrow up to 24 input SFPs and 2 output SFPs per board [84] [85].
- Different SMs do not share ROCs (or HUB for FPGA TDC option).
- In case of high data rates, a TRB3 HUB can also be used for output.
- A hit on an electronic channel is encoded in 2x32 bits, similar to the size of a CbmTofDigi introduced in Section 5.3.
- Optical links have 80% of their nominal bandwidth available for data transport (due to messages such as control, epochs, errors, ...).
- Nominal Bandwidth of optical links is 2.5 Gb/s.
- The minimal number of 1st links is determined either by simulated data size or number of ROCs.
- The minimal number of 2nd links is determined only by simulated data size.

It can be seen from these tables that the increase of the channel number per digitizer in the FPGA TDC case brings a real diminution in the number of digitizer but more importantly also in both the number of ROCs and of initial optical links. This is partially compensated by the increase of price per unit, which leads to an equivalent total cost for both options. It must be remarked that at present the GET4 v1.0 is the one and only free-streaming TDC system successfully operated up to the extraction of detector parameters. The CBM TOF group will of course investigate both option further and tests aiming at a free-streaming FPGA TDC are already ongoing. The unified analysis software developed within this thesis will take here all its importance both to speed up the analysis software development and to compare systems performance

5.7 Towards a time based analysis

Fig. 5.14 summarize the analysis organization currently available. Solid lines indicate tested steps, while the dashed line shows the untested one. The goal of unifying the unpacking and simulation chains was achieved in the sense that the unpackers tasks and the common data containers are now available in CBMROOT. However, the data

Table 5.8: Numbers of Electronic channels, FEE chips (Discriminators), TDCs, ROCs (SYSCORE v3) and optical links needed for the full TOF wall (SIS300 configuration) for the option with GET4 as TDC. Table adapted from [20].

SM Type	Electronic Ch.	FEE	TDC	ROC	1st Links	2nd links
0	7680	960	1920	48	48	20
1	45440	5680	11360	284	284	115
2	15600	2100	4200	100	100	25
3	7680	960	1920	40	40	31
4	7680	960	1920	40	40	34
5	3840	480	960	20	20	20
Total	87920	11140	22280	532	532	245

Table 5.9: Numbers of Electronic channels, FEE chips (Discriminators), TDCs, ROCs (TRB3 of HADES) and optical links needed for the full TOF wall (SIS300 configuration) for for the option with FPGA TDCs. Table adapted from [20].

SM Type	Electronic Ch.	FEE	TDC	ROC/DPB	1st Links	2nd links
0	7680	960	240	12	20	20
1	45440	5680	1420	71	115	115
2	15600	2100	600	50	50	25
3	7680	960	240	16	31	31
4	7680	960	240	16	34	34
5	3840	480	120	10	20	20
Total	87920	11140	2860	175	270	245

reconstruction was not tested using the tasks originally developed for the simulation. The reason for this is that the current reconstruction tasks rely heavily on a geometry file which was developed for the wall simulation (see Section 5.4). As the tools used to generate it are not easily adaptable for now, it was not yet possible to generate a geometry file corresponding to any of the test setups described in Section 4.4.

A common feature of the analysis chain and the simulation chain developed within CBM-ROOT in the scope of this thesis is that they are both event based. Even in the case of the free-streaming GET4 data, a time window around a special signal inserted in each event in the data files was used to obtain a “pseudo-triggered” behavior. To have a fully free-streaming system, the analysis chain will have to be made asynchronous relative to the input data, with an intermediate stage building event out of selected data from time-based data containers.

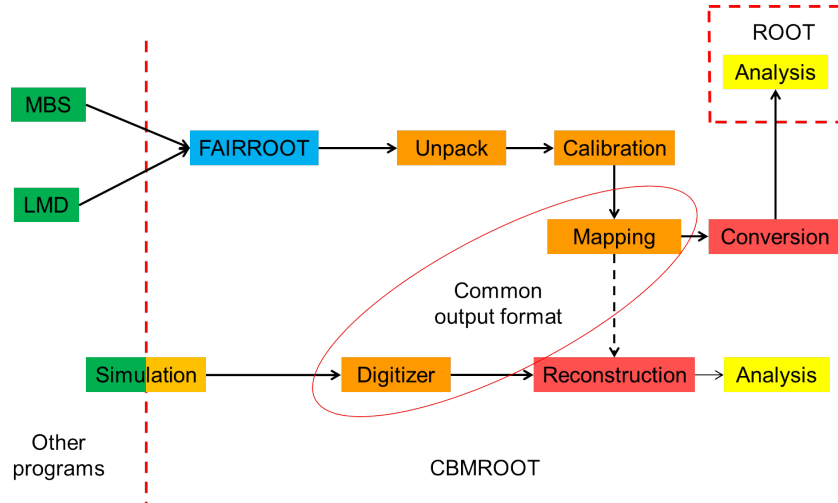


Figure 5.14: Currently available TOF wall analysis softwares organization using CBM-ROOT and pure ROOT macros. The dashed arrow indicates the untested combination.

Chapter 6

Conclusion and Outlook

This thesis presents the development of a free-streaming readout chain for the Time-Of-Flight (TOF) system of the Compressed Baryonic Matter experiment (CBM) in both its hardware and software aspects.

CBM is a fixed target spectrometer that will be built at the Facility for Anti-proton and Ion Research (FAIR) in Darmstadt, Germany, where it should receive its first beam in 2018. CBM's main objective is to study the properties of strongly interacting matter at the high baryonic densities reached in heavy ion collisions in the FAIR energy range: 2 to 35 A GeV for Au+Au. Eventual phase transitions are especially looked after. The observables for this program include both the bulk particles, which can also be measured by other experiments, and very rare observables that are only accessible to CBM. To enable the measurement of e.g. charmed particles, CBM is specifically designed to be able to acquire data for interaction rates up to 10 MHz even in the most heavy systems, such as Au+Au. In order to operate at such high rate, detectors with a high particle flux capability are needed together with a new approach for the Data Acquisition (DAQ) system. Contrary to most up to date High Energy physics experiments, CBM will run without a central trigger system built on hardware components. Instead, a combination of self triggered digitization electronics, high bandwidth transport and pre-processing systems, online event building and online event selection will be used. This is the so-called “*free-streaming*” paradigm.

While the online event selection is only required for observables like the J/Ψ decay to dileptons, it will be also available for all other running cases, which would normally just use the ~ 25 kHz archiving capability planned for minimum bias events in CBM. For some of these less demanding probes, an online event selection using the charged hadrons Particle Identification (PID) capabilities of CBM could nevertheless provide an enhancement of the statistics contained in the archived event sample. Such is the case for the multi-strange anti-hyperons when event containing particles identified as \bar{p} are selected. A study of the acquisition days needed to obtain a specified number of events containing \bar{p} or a specified \bar{p} signal significance was done in this thesis for different interaction rate scenarios. It demonstrated that sufficient statistics can be obtained in a reasonable runtime duration thanks to CBM high rate capability.

The charged hadron PID in CBM will be mainly provided by a Time-Of-Flight system

with a global time resolution below 80 ps, based on Multi-gaps Resistive Plate Chambers (MRPC). MRPCs are gas detectors delivering the crossing time of charged particles with a high time resolution and a high efficiency. This technology is nowadays proven to be suited to build TOF systems with a large number of channels at reasonable cost. The current design for the CBM TOF system is a wall equipped with MRPCs of 4 to 5 types, each type being adapted to the particle flux conditions of a part of the wall. The main goal of this thesis was to test and improve a readout chain compatible with all those counter types and obeying the “*free-streaming*” paradigm. This readout chain is composed of a Pre-Amplifier and DIscriminator chip (PADI), a Time to Digital Converter (TDC) and a ReadOut Controller (ROC). The main requirement for the readout chain is for the TDC to have a time resolution better than 25 ps. The other requirements are the measurement of the signal size through the Time-Over-Threshold (TOT) method, a hit rate capability of at least 400 kHz per electronic channel and a double-hit capability below 5 ns.

Two versions of the readout chain were assembled in the scope of this work, using elements developed at GSI in Darmstadt (PADI and TDC) and at KIP in Heidelberg (ROC). The first one was a “proof of concept”, built around the *PADI 3* discriminator and the *GET4 Proto* TDC. Using the results of the tests, the developers of both ASICs designed new versions and a first “user dedicated” version of the chain was assembled, based on the *PADI 6/7* and on the *GET4 v1.0*. Dedicated acquisition and analysis software was developed for each version within the GO4 framework, including the software needed for a triggered system used as reference.

The first version of the readout chain was tested twice with proton beam at the COoler SYnchrotron (COSY) in Jülich. During the first beamtime, the GET4 and the ReadOut Controller (ROC) were operated in purely free-streaming mode and the data-transport was done over a 100 Mbits/s Ethernet link. The RPC used was the Heidelberg RPC-P1 prototype. A bug in the readout part of the *GET4 Proto* was discovered during the analysis of the data from this beamtime, that leads to a synchronization loss between timing channels. This bug got corrected in the *GET4 v1.0*. It was also observed that the output link of the ROC needed more bandwidth to accommodate beam rate variations, along with more detailed status messages from the ROC data buffers. In all further beamtimes, the ROC was connected to the DAQ computer with an optical fiber link.

A hybrid readout system was developed for the second beamtime at COSY, which combines data from a well understood triggered system and data from the free-streaming system. One goal of this type of system is to verify the performance of the detectors and discriminators used to feed the free-streaming system independently of the latter one. The other justification for the hybrid system is to decouple the tests of counter prototypes connected to the triggered system from the tests of the new free-streaming readout chain. For this second reason, the signals from the time reference system were acquired only in the triggered system during this beamtime. To realize the hybrid system, two levels of synchronization are needed: one at the event level and one at the timing level. For the event level synchronization, each triggered event is matched to the corresponding messages in the triggerless system thanks to an event number generated by the triggered system and inserted with a timestamp as a *System SYNC* message in the free-running data-stream. The building of an event with the free-streaming data around this *System SYNC* message is called from now on “pseudo-triggered” mode. In order to synchronize

the time-frames of the triggered and free-streaming TDC systems, a certain set of signals was split and measured in both readout systems. During the analysis of the data, a problem was found in the data of the RPC channels covered by the time reference system. This problem was tracked down to mechanical stress on the clock connectors of the GET4 boards (PCB). To avoid this, the PCB was redesigned by its developers for the next *GET4 v1.0* version: it now hosts up to 32 chips instead of 2 and uses an on-board clock distribution instead of cables. The quality of the time synchronization obtained with the signals measured in both systems could, however, be evaluated. The measured value of 83 ps is worse than the expected 60 ps. Therefore, in further tests all signals needed for the analysis are measured in the free-streaming system.

The second version of the readout chain is centered on the *GET4 v1.0* chip. The bugs found in the *GET4 Proto* are corrected in this version. The timing performance of the TDC core are also improved and new functionalities provided, such as on board Time-Over-Threshold calculation. This last improvement allows to send a single 32 bit data message per input signal instead of one 24 bit message for each edge of the signal. This version of the readout chain was tested three times: once during a beamtime, once with a pulser and once with cosmic particles.

The in-beam test was performed with the Heidelberg RPC-P3 prototype. Its main goal was to evaluate the performance of the new on-chip TOT calculation. The online monitoring and the analysis of archived data resulted in two observations. The first one is that all chips operated in a stable way relative to clock synchronization, with a single synchronization loss being automatically recovered. The second observation is that a large number of error messages from the TOT calculator are present in the data. The origin of the error messages was investigated and this problem is solved in the next GET4 version, *GET4 v1.23*. For the two later tests of the *GET4 v1.0*, only the 24 bits readout mode is used, where the TOT building is done in software.

The channel rate capability of the *GET4 v1.0* was evaluated in the second test, in order to validate the simulations done by the chip developers. The analog output of a variable frequency pulser was split to feed all four channels of a *PADI 7* and *GET4 v1.0* system. The simulations of the TDC were confirmed, with a successful event reconstruction up to 600 kHz per channel. This is well above the 400 kHz per channel required for CBM.

In the third and final test of the readout chain, its performance in terms of time resolution and efficiency was measured and compared to those of a triggered system based on a FPGA TDC board called VFTX. The test was realized with cosmic muons. The analysis shows that for an RPC High Voltage of ± 11.5 kV, the free-streaming system achieves a system time resolution of 82 ps for an efficiency of 97% in both pseudo-triggered and free-streaming (data based) event reconstruction modes. This is within CBM requirements. The time resolution of the system is 10 ps worse than that of the triggered FPGA TDC system, which matches well the expected characteristics of both systems. In order to evaluate the timing performance of the *GET4 v1.0* itself, a second analysis was realized on the same data. A mean value of 24 ps for the time resolution of single channels was obtained over 16 TDC channels (4 chips). This validates the developers tests with pulser signals and matches the CBM requirements of 25 ps for the time resolution of the TDC. The test with cosmic particles presented in this thesis is the first time a complete free-streaming readout chain was operated in a stable way over a long period with real detector

signals and a good resolution.

A second goal of this thesis was to prepare software for the transition to a fully time-based analysis performed within the CBMROOT framework. In order to validate all elements of the online selection software, the data from the unpacking software and the simulated data should be processed by the same reconstruction software. As a first step towards this, the unpacking and calibration software used for the hardware tests was adapted to the CBMROOT environment. The output of this newly developed unpacker was compared to that of the GO4 one and no significant differences were found. A new data container, the so-called *TofDigi*, was designed and implemented with the aim of being the common output of the unpacking and simulation branches of the TOF software in CBMROOT. A realistic digitizer was then written for the simulation of the CBM TOF wall, which allows to take into account the real properties measured for RPC prototypes, e.g. the channel multiplicity per hit. The output of this digitizer is the previously mentioned *TofDigi*. A simple cluster reconstruction step was also implemented, which performs the conversion from the *TofDigi* to the *TofHit* data container used by the physics analysis software. The output of a CBM physics simulation performed with the new simulation chain was then compared to that of the existing direct production of *TofHit* from Monte Carlo data. The observed differences in terms of PID efficiency and purity are within what is expected for the more realistic approach. Therefore, the newly developed digitizer is now used by the CBM TOF group to simulate the performance of the TOF wall. The digitizer output is also used to evaluate the number of elements needed for each layer of the readout chain in order to avoid data losses. Two options were investigated for the TDC: the GET4 chip previously used in this work and a new FPGA TDC based on the TRB3 system. This dimensioning of the readout chain is part of the CBM TOF Technical Design Report, to be published soon.

The adequacy of the GET4 performance with CBM requirements was only proven in a low rate situation. The next version of the GET4 chip, *GET4 v1.23*, just became available for integration on PCBs and laboratory testing. In the near future, it will be tested under high rate conditions, hopefully proving the validity of the on-chip TOT building concept. On this hardware side, another promising recent development is the FPGA TDCs, which now provide time resolutions in the order of 10 ps with all the flexibility of FPGAs. However, their readout is for now only triggered. If they are successfully modified to operate in free-streaming mode, they would also be good candidates for the CBM TOF readout chain, provided they are sufficiently radiation tolerant. Another point to stress is that until now the data analysis software is free-streaming only in the sense that it enables the definition of triggers from data at the unpacking stage. The simulation package is also fully event based. The development of an analysis software adapted to time-based data containers will be a major effort of the CBM-TOF group in coming months. The time-based simulation will be needed to evaluate the physics performance to be expected from the CBM TOF wall.

Publications

- P.-A. Loizeau and N. Herrmann, A Free-Streaming Readout for the CBM Time of Flight wall, in Proceedings of the XI Workshop on Resistive Plate Chambers and Related Detectors, [PoS\(RPC2012\)082](#)
- Y. Wang, J. Wang, X. Zhu, Y. Li, J. Cheng, N. Herrmann, I. Deppner, Y. Zhang, P. Loizeau, P. Senger et al., Beam test results of two kinds of high-rate multi-gap resistive plate chambers, IEEE NSS, Conf. Rec., N13-44, 684 (2009) , [DOI:10.1109/NSSMIC.2009.5402035](#)
- J. Wang, Y. Wang, X. Zhu, W. Ding, Y. Li, J. Cheng, N. Herrmann, I. Deppner, Y. Zhang, P. Loizeau, P. Senger, D. Gonzalez-Diaz, Development of multi-gap resistive plate chambers with low-resistive silicate glass electrodes for operation at high particle fluxes and large transported charges, Nuclear Instruments and Methods in Physics Research A, 621, 2010, 151-156, [DOI:10.1016/j.nima.2010.04.056](#) [52]
- I. Deppner et al., The CBM time-of-flight wall, Nuclear Instruments and Methods in Physics Research A, 661, 2012, 121-124, [doi:10.1016/j.nima.2010.09.165](#) [46]
- I. Deppner, N. Herrmann, M. Ciobanu, J. Fr ijhauf, M. Kis, P.-A. Loizeau, K. Wisniewski and C. Xiang, A glass type Multistrip-MRPC prototype for the low rate region of the CBM Time-of-Flight wall, JINST, 7, 2012 P10008, [DOI:10.1088/1748-0221/7/10/P10008](#)
- M. Petris, M. Petrovici, V. Simion, D. Bartos, G. Caragheorgheopol, I. Deppner, K. Doroud, N. Herrmann, M. Kiss, P. Loizeau, Y. Zhang, M.C.S. Williams, Toward a high granularity and high counting rate, differential readout timing MRPC, Nuclear Instruments and Methods in Physics Research A, 661, 2012, 129-133 [doi:10.1016/j.nima.2010.09.162](#) [43]
- M. Petrovici, M. Petris, V. Simion, D. Bartos, G. Caragheorgheopol, F. Constantin, L. Radulescu, J. Adamczewski-Musch, I. Deppner, K. Doroud, N. Herrmann, S. Linev, P. Loizeau, M.C.S. Williams, High counting rate, two-dimensional position sensitive timing RPC, JINST, 7, 2012, P11003, [DOI:10.1088/1748-0221/7/11/P11003](#)
- C. Z. Xiang, N. Herrmann, I. Deppner, P.-A. Loizeau, K. Wisniewski, Y. P. Zhang, D. C. Zhou, J. Fr ijhauf, S. Linev, S. Manz, W. F. J. M ijller, The online data pre-processing for CBM-TOF, JINST, 8, 2013, P02002, [DOI:10.1088/1748-0221/8/02/P02002](#)

Appendix A

CBM MMRPC prototypes

All the MRPC prototype used for this thesis were designed and built by I. Deppner. They are presented in full details together with their test results in Ref. [40].

A.1 RPC-P1

The RPC-P1 is a fully symmetric differential MRPC with strips as readout channels. A pictorial view of its cross section is shown in Fig. A.1. A top view of the counter in its gas tight box is shown in Fig. A.2. The counter has 8 gaps created by 220 μm thick fishing lines placed between 0.55 mm thick float glass plates. The High Voltage (HV) electrodes are realized by Licron[®] conductive layers sprayed on the top and bottom glass plates. The HV is brought by a copper strip glued on each of these conductive layers. The pickup electrodes are realized with PCB plates which also provide a support for the MRPC. Each electrode contain 16 copper readout strips with a pitch of 1 cm and a strip width of 0.7 mm, for a total active area of 28 x 16.5 cm². Kapton[®] foils of 75 μm thickness are used to insulate the readout strips from the HV electrodes. The MRPC signals are brought to connectors on the side of the gas tight aluminum box by 110 Ω twisted pair cables soldered directly on the readout electrodes. The counter is designed to obtain an impedance of 100 Ω in order to minimize the signal reflections.

A.2 RPC-P2

The inner layout of RPC-P2 is identical to that of RPC-P1 (number of gaps, gap size, strip pitch and width). The number of strips is increased to 32. Two versions of this prototype were built, one with float glass, shown in Fig. A.3, and another with a low-resistive glass, the so-called “Chinese glass”, shown in Fig. A.4. Modifications are made on the strips length, on the strips connection to the front-end electronics and on the HV electrode design.

The strips in this prototype are 27 cm long, defining an active area of 32 x 27 cm². These dimensions are close to those planned for the counters in the intermediate rate region of

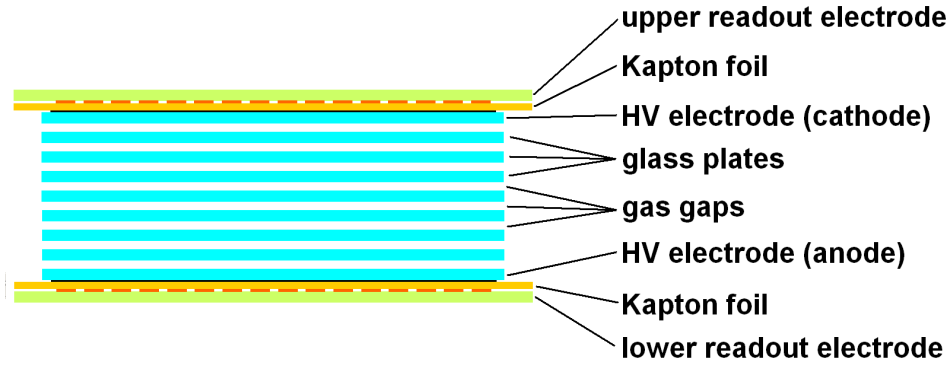


Figure A.1: A pictorial view of the cross section of this fully symmetric differential RPC-P1. The elements are described in text. Figure taken from [40].

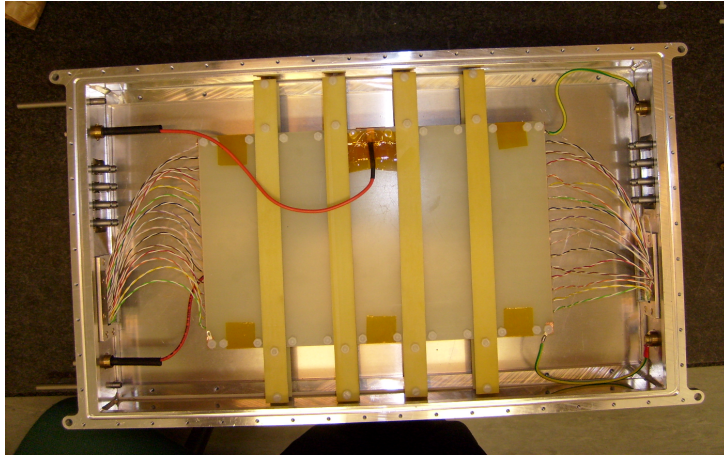


Figure A.2: Photograph of the prototype RPC-P1 embedded in a gas tight aluminum box. Figure taken from [40].

the CBM TOF wall. Since the version with “Chinese glass” has a higher rate capability, RPC-P2 can be considered as a full-size prototype for the intermediate rate region (see Section 3.5).

The end of the strips on the readout electrode was redesigned: $50\ \Omega$ transmission lines are used to bring the signals to 17 pins connectors with a standard pitch. The odd pins are connected to ground and the even pins to the strips. The connector used allow to plug either twisted pair cables with $100\ \Omega$ impedance and 17 pairs or directly a PADI-3 board. As results of tests on this version showed the benefits of placing the discriminator boards inside the gas box [40], all discriminators are placed in the gas box for the “Chinese glass” version of RPC-P2.

In both versions, the HV electrode is realized by Licron[®] sprayed on the Kapton[®] foils instead of the glass. A short strip is drawn with the Licron[®] on one side of the electrode to bring the HV without needing the copper strip of RPC-P1.

Only the float glass version was used with GET4, during the beamtest at COSY in

2011. The “Chinese glass” was tested with beam at GSI in 2012, but only with triggered electronics.

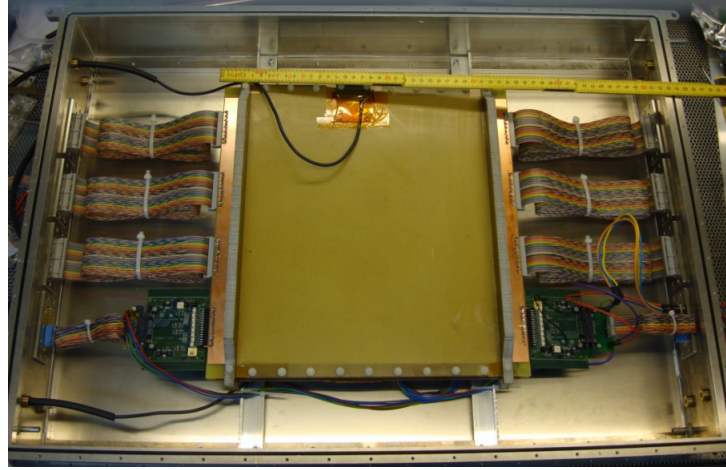


Figure A.3: Photograph of the RPC-P2 embedded in its gas tight aluminum box. The MRPC has connectors on the pickup electrode which allow to connect either a twisted pair cable or the preamplifier card. On each side one of the PADI3 boards was placed inside the box and the 3 others outside. Figure taken from [40].

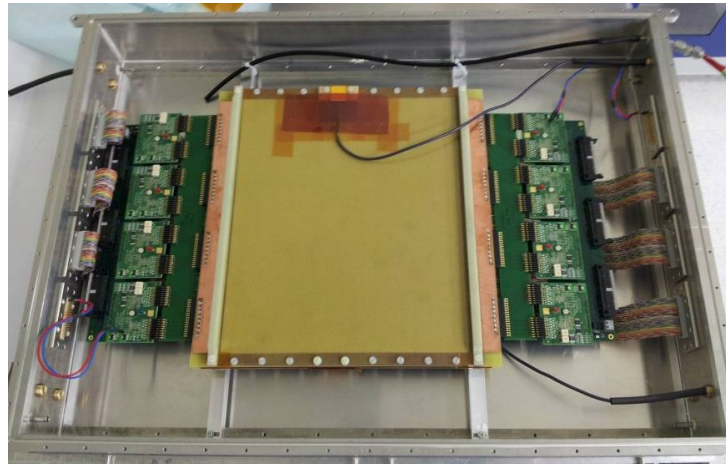


Figure A.4: Photograph of the RPC-P2 prototype embedded in the gas tight aluminum box. A motherboard equipped with four PADI-7 daughter boards is used to place all discriminators inside the gas box. Each daughter board hosts 2 chips for a total of 8 channels. Figure taken from [40].

A.3 RPC-P3

The RPC-P3 is a full size demonstrator for the low rate region of the CBM TOF wall (see Section 3.5). This part of the wall will be subject to particle fluxes below 1 kHz/cm^2 . Therefore the prototype is built with normal float glass, which is far cheaper than the previously mentioned “Chinese glass”.

The internal structure is the same as for RPC-P2. The counter has an active area of $53 \times 52 \text{ cm}$. In order to obtain a strip number fitting the 8 channels of the PADI-6/7 discriminator boards, the strip width is changed to 7.6 mm and the strip pitch to 9.4 mm. This results in 56 readout strips, readout by 7 discriminator boards. The counter is shown in Fig. A.5 in a gas box designed to host two of these prototypes.

This prototype was used for the GET4 v1.0 tests at GSI in 2012 and with cosmic rays in Heidelberg in 2013.

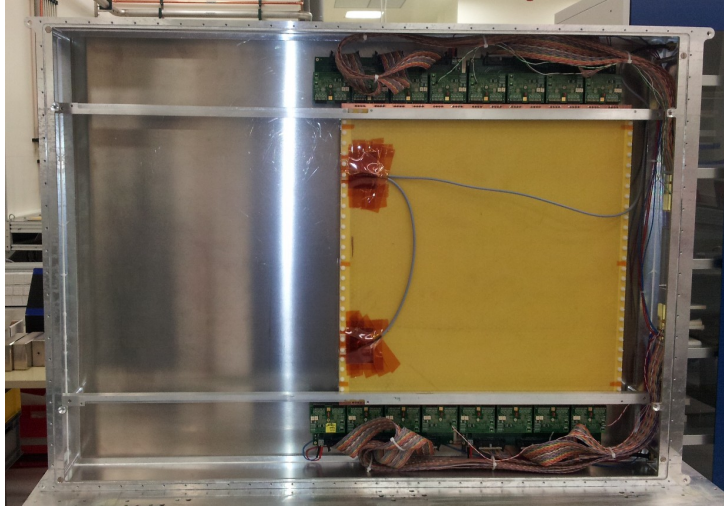


Figure A.5: Photograph of the RPC-P3 prototype for the low rate region. Figure taken from [40].

Appendix B

Triggered components

B.1 VME, RIO and MBS

The Versa Module Europa bus (VME) is a computer bus specification developed in 1981 over the Eurocard standard, which defined only mechanical parameters [86]. It was standardized in 1987 and is now used in many applications. The original 16-bit bus standard was updated several times. The current version, called VME64, defines two bus types: a 64 bit bus 6U-sized boards and a 32-bit bus in 3U boards. The triggered electronics systems used for this thesis are built on 6U VME crates and boards.

The RIO boards are a family of VME processor boards produced by the CES company [87]. These boards are developed with the backward compatibility in mind, in order to accommodate applications such as accelerators, particle physics experiments or aeronautics, where the equipment lifetime spans over several decades. The versions used for this thesis are the RIO3, which is based on a PowerPC 750 CPU, and the RIO4, which is based on a PowerPC 7448 CPU. The RIO boards are sold as a package with a LynxOS license. LynxOS is a closed source Unix-like Real-Time Operating System (RTOS) developed by LynuxWorks [88]. It is used in applications such as avionics, aerospace, the military, industrial process control, telecommunications and particle physics data acquisition.

The Data Acquisition System (DAQ) used for our triggered setup is the so-called Multi Branch System (MBS). MBS is the standard DAQ at GSI for SIS18 experiments [78]. It is entirely written in C and based on LynxOS. It can readout data from the CAMAC, Fastbus and VME systems if a trigger module developed at GSI is installed. It writes data as MBS events, which are themselves divided in MBS sub-events, into List Mode Data (LMD) files. An easy interface is provided to connect online analysis software like GO4.

B.2 VULOM based boards

The VME Universal LOGic Module (VULOM) is a family of boards developed at GSI [89]. The VULOM 3 boards used in this thesis are based on a Virtex 4 FPGA. Fig. B.1 show

a photograph of the board. The board provides differential inputs and differential ECL outputs. The FPGA can be easily programmed from a FLASH memory, directly via the VME interface or over a JTAG interface. The following inputs and outputs are available:

- 16 dedicated multi-standard inputs (LVDS, ECL)
- 16 configurable I/Os (four groups of 4): multi-standard inputs (LVDS, ECL) or ECL output
- 16 dedicated ECL outputs
- Two LEMO inputs (TTL and NIM level)
- Two LEMO outputs (TTL or NIM level)
- Two character alphanumeric display
- Additional 2x8 LVDS input/output through a daughter board

The board also has an on-board 781.25 kHz clock.

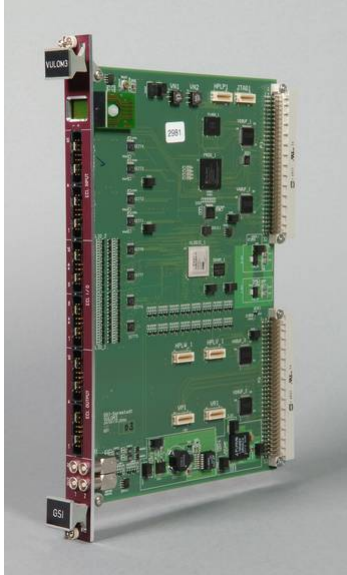


Figure B.1: Photograph of a VULOM 3 board. Figure taken from [89].

B.2.1 TRIGLOG

The TRIGger LOGic (TRIGLOG) board is a trigger board implemented with the VULOM 3 hardware. It provides a trigger matrix allowing to define up to 16 triggers from combinations of the 16 input signals. For the combinations, each input signal can be either requested or rejected. The triggers can be downscaled by a programmable multiple of 2. The trigger signal is provided both as trigger pattern on the 16 ECL outputs and as a single pulse on one of the NIM outputs.

It is also possible to define up to 3 on-board pulsers which can be used as input for the trigger matrix. The pulser frequency is programmable and derive from the on-board clock. The board provides scalers for the 16 input signals and the 16 triggers. For the triggers, scalers are present at the output of the trigger matrix, after downscaling and after taking into account deadtime and trigger priority. Starting from the GSI 2012 beamtime, an additional scaler is implemented for the on-board clock, providing a time reference to

estimate the rates of the input signals and triggers.

Registers allow the MBS to access the following values through the VME bus on each event:

- Input pattern: active input signals when the trigger was found
- Trigger pattern: all triggers fired in this event
- Input signal scalers
- Trigger scalers (matrix output, downscaled and accepted triggers)
- On-board clock scaler

When equipped with a daughter board, the version of TRIGLOG used in the tests presented here provides the *System SYNC signal* presented in Appendix C.4 for up to 16 other systems. The event number from the MBS acquisition is encoded in this signal to allow a data source synchronization, for example by the DABC DAQ software.

B.2.2 SCALORMU

The SCALer-OR-Multiplicity board is based on the VULOM 3 hardware. It provides three functionalities: scalers for input signals, OR outputs based on the input signals and a multiplicity output from selected input channels.

Scalers are provided for all 32 front panel inputs and for the 16 channels of the daughter board, which are all configured as input. In a similar way to the TRIGLOG board, all these scalers and an additional on-board clock scaler can be readout by MBS through the VME bus on each event. When the inputs are connected to the OR output of the PADI boards, this allows to monitor the RPC signal rate.

From the input signals, an OR signal is generated and sent to the NIM output of the board. This allows to build a trigger where one is sure at least one RPC channel fired.

Finally, the 16 channels ECL output is used to provide a multiplicity signal. The first channel is ON as soon as any of the input channels get a signal. The second channel switches ON when two input channels receive signals in coincidence. This is done up to the 16th output channel, which switches ON only when at least 16 input channels received a signal in coincidence. The multiplicity signal can also be used as trigger when connected to the input channels of a TRIGLOG board.

B.3 CAEN V1290

The V1290A is a 32 channels multi-hit TDC produced by CAEN [90]. The board accepts both LVDS and ECL input signals. It is based on the CERN High Performance Time to Digital Converter (HPTDC) ASIC [57].

The HPTDC is a 32 channels TDC ASIC with a nominal bin width of 98 ps and a time resolution in the same order. It can be set in a so-called Very High Resolution Mode mode, where four TDC channel are cascaded on a single input channel to obtain a bin width of 25 ps for and RMS time resolution better than 35 ps. The chip then has 8 high resolution input channels. Therefore, the V1290A houses 4 HPTDC chips in a 1-unit wide VME 6U module, pictured in Fig. B.2.

The HPTDC can be configured to measure both the leading and trailing edges of the input signals. It has however a double edge capability of only 6 ns. As the PADI output for MRPC signals is typically between 1 and 6 ns wide, our setups were always made of pairs of TDC boards, configured to measure opposite edges. The PADI output single was split to feed both TDC boards.

The V1290A has an on-board 40 MHz clock, which can be used when operating a single board. For our multiple boards systems, we used the external clock connector and the clock system used for the TACQUILA in the FOPI experiment [54]. A reset signal generated by the TRIGLOG board after the readout of each event was also used to insure the internal counters of all boards were synchronized.

Another noteworthy feature of the board is the presence of a look-up table for each channel, which is used to compensate the INL. These look-up tables are loaded by the manufacturer in a FLASH memory on the board, automatically applied by default and necessary to achieve the 35 ps RMS resolution. An example of the loop-up table readout from the FLASH memory for one channel is shown in Fig. B.3. More detailed information on the V1290A board can be found in its manual [90].



Figure B.2: Photograph of a CAEN V1290A board. Figure taken from [90].

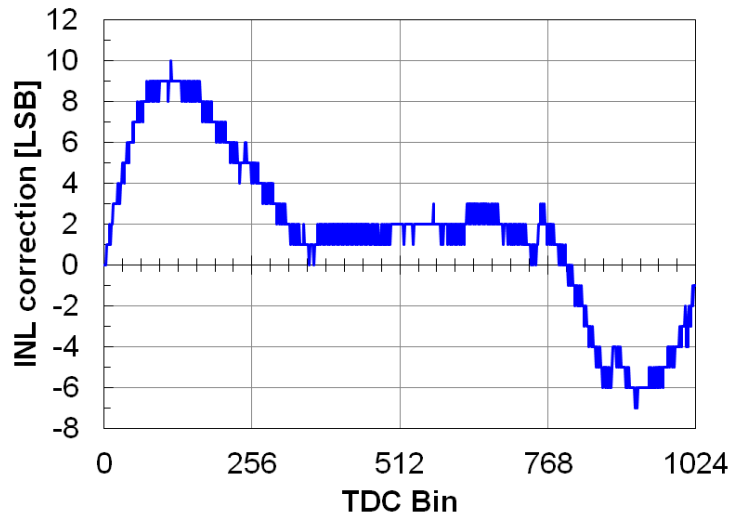


Figure B.3: INL compensation table (look-up table) readout from the FLASH memory for a channel on a V1290A board. The correction is expressed in Least Significant Bit (LSB).

B.4 VFTX

The VME FPGA TDC X (VFTX) is an triggered FPGA based TDC board with a mean time resolution of 10 ps between two channels on the same board. The VFTX 1 is the first version of the board, which was used in this thesis, and is based on the Xilinx Virtex 4

FPGA. It was developed at GSI as a dedicated FPGA TDC board after early tests with modified VULOM 4 boards [91] (VULOM 4B). The board can be equipped either with a daughter board providing 16 NIM SMA input channels or with a daughter board providing 32 differential LVDS channels.

The fine-time generation is done using the Tapped-Delay-Line (TDL) method, with two TDL per timing channel to reach the better than 10 ps time resolution (for more details see Ref. [92] and [93]). The time resolution achieved depends on the number of TDL used per channel. One advantage of the FPGA design is that the best compromise between the number of channels and the desired time resolution per channel can be chosen without changing the hardware. As an example, firmwares for a 16 channel (single edge) version of the board with 7 ps time resolution or for a 32 channels (single edge) version of the board with 10 ps time resolution are available. Due to space constraints on the FPGA used in the VFTX 1, only 58 timing channels can be implemented per board in the 2 TDL per channel case.

Each timing channel can measure one edge of a signal. Therefore, in order to measure TOT, it is necessary to split the signal in the FPGA and to use two timing channels per input channel. Due to this, the version of the firmware used in this thesis has only 28 channels with TOT measurement.

The non-linearities of this kind of TDC are important, as can be seen for example in the bin-width distribution in Fig. B.5. The timing channels for the leading and trailing edges also do not have the same bin sizes. These non-linearities need to be corrected in order to obtain the best time resolution and to have the possibility of calculating the TOT. The 10 ps resolution between two channels on the same board is obtained after this correction. When only one VFTX 1 is in use, its on-board 200 MHz can be used. However, when more than one board is in use, a common 200 MHz clock is needed, which can be fed to an external clock input on the front of the board. In all setups with VFTX presented in this thesis, this common clock is created by a modified CLOSY 2 board. The same clock distribution as for the GET4 is then used to provide it to all boards. With this system, a time resolution of 12 ps between two channels on different boards was obtained [20].

The internal data buffers of the VFTX 1 do not have a protection against overflow, as would be the case for example if new hits were rejected when the buffer is full. Instead, buffer overflows lead to a corruption of the data in the buffers. This would especially happen during acquisition with cosmic particles, where the coincidences of the reference system happen only on a minute scale, while the RPC counter dark noise is a few counts per seconds. To avoid this, a trigger on the RPC OR was used during the cosmic tests in 2013 aside the looked after trigger on the reference system coincidences. This way the buffers stay most of the time empty. In addition it provides enough data to generate the time calibration values from the same data file.

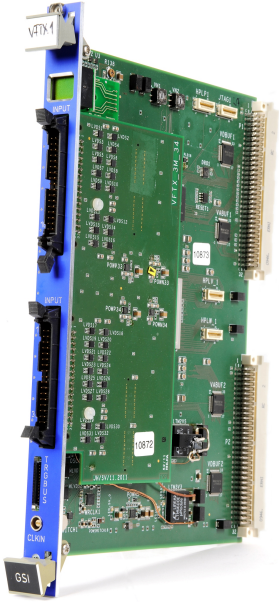


Figure B.4: Photograph of a VFTX 1 board. Figure taken from [20].

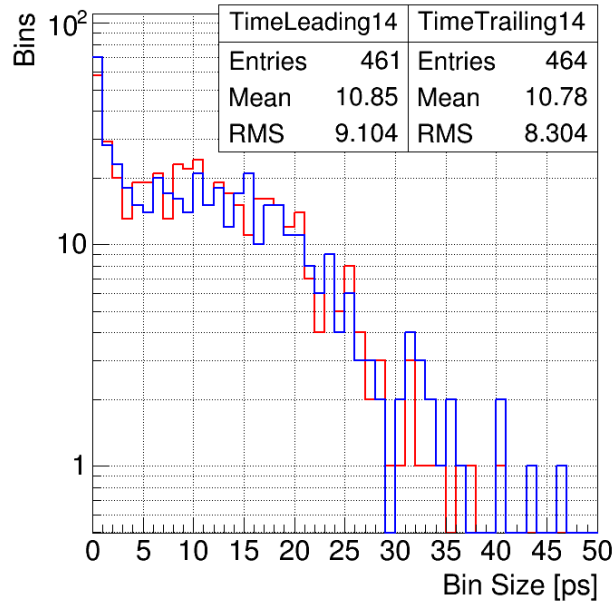


Figure B.5: Bin width plot of the timing channels for the leading (blue line) and trailing (red line) edges for input channel 14 on a VFTX 1 board. The bin size for both timing channels is around 10.9 ps.

Appendix C

Keywords and Acronyms

C.1 LVDS

Low-Voltage Differential Signaling (LVDS) is a technical standard for differential serial communications [94]. It defines only the electrical properties of the signal and leaves the communication protocol to the application designer. Information is transmitted in LVDS by comparing the voltage difference between two wires at the receiver. LVDS typical implementation uses a constant current of 3.5 mA. On the receiver side, the wires are connected to a termination resistor of 100-120 Ω impedance. The impedance is adapted to that of the transmission cable to minimize reflections. The observed voltage is then ± 350 mV depending on the current polarity. The sign of the measured voltage defines the logic levels. The main advantages of LVDS are that it allows for high speed data transmission through low cost twisted pair copper cables and requires low power to operate.

C.2 SPI

The Serial Peripheral Interface (SPI) is a de-facto standard named by Motorola [95]. It defines a synchronous serial data link that operates in full duplex mode through a 4-wires connection. The bus defines a master and one or more slaves. The master initiate the communication and can select one or more slaves as recipient through their individual Slave Select wires. Fig. C.1 presents an example of a connection with a single slave. The four logic signals defined in SPI are:

- SCLK : Serial Clock (output from master)
- MOSI : Master Output, Slave Input (output from master), also called SDO
- MISO : Master Input, Slave Output (output from slave), also called SDI
- SS : Slave Select (active low, output from master), also called Chip Select (CS)

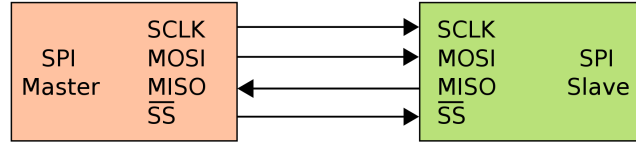


Figure C.1: Example of a single slave SPI connection. Figure taken from [95].

C.3 NIM standard

The Nuclear Instrumentation Module (NIM) standard defines mechanical and electrical specifications for electronics modules used in experimental particle and nuclear physics [96]. The modules all share a common height (221 mm) and depth (246 mm) and have a width which is a multiple of the standard width (34 mm). The modules are housed in a so-called NIM crate, which must provide on its backplane at least ± 12 and ± 24 V DC power through a standardized connector. The standard also defines pins for optional ± 6 V DC and 220 V or 110 V AC pins.

In the standard are also defined specifications for the cables, connectors, impedance and levels to be used for the logic signals. The so-called NIM signals follow a current based logic, with a nominal current of -16 mA defining the logic 1 (the logic 0 is the absence of current). This corresponds to -0.8 V when measured through a $50\ \Omega$ resistor.

As this standard does not provide any data communication between the modules through the crate backplane, it is nowadays widely replaced by the VME standard. It is still, however, commonly used for elements not requiring any communication, such as logical level converters, amplifiers or high voltage sources.

C.4 SYNC signal and SYNC messages

SYNC signal

The *SYNC signal* is a logical pulse used to synchronize the coarse time counter of the GET4 chips. In the currently planned CBM TOF readout chain, it is generated every $655.36\ \mu\text{s}$, which corresponds to 40 periods of the CBM main clock counter and 25 periods of the GET4 coarse time counter. In order to be recognized by the GET4, it needs to be active for at least one GET4 clock cycle. The next rising edge of the GET4 clock after the SYNC rising edge then defines the synchronization point of the chips, where all coarse time counter should be 0. More details on how the GET4 reacts to the SYNC signal can be found in Subsection 4.2.2.

Ext SYNC signal

The GET4 Proto has a so-called *Ext SYNC* input. When an LVDS logical pulse is received on this input, a special message is inserted in the GET4 data stream with the current value of the clock cycle counter as timestamp. This message allows to build event as in a trigger system, but do not provide any event synchronization with other systems as no event number is included. For this reason, it was used only in the first beamtime at COSY in 2010 presented in Subsection 4.3.2.

SYNC messages

The *System SYNC signal* is a digital signal generated by the TRIGLOG module on accepted trigger. It is a serial LVDS signal composed of a START pattern followed by a 32 bits event number. This signal is transferred to the one of the ROC GPIO inputs through a twisted pair cable. When the START pattern is detected by the ROC, a timestamp is generated against the 250 MHz main clock of CBM. The event number from the System SYNC signal is then associated to this time stamp in a system message, which is inserted in the GET4 data-stream. the same event number is inserted in the data readout from the TRIGLOG board by the MBS DAQ. This allows to match data from many ROCs or from heterogeneous systems such as ROC + MBS by matching the event numbers inserted in all data sources. One tool to do this data sources alignment is the DABC DAQ from GSI.

C.5 D type flip-flop

In electronics, a flip-flop or latch is a circuit that has two stable states and can be used to store state information [97]. The D type flip-flop means *Data* flip-flop or *Delay* flip-flop. The usual symbol for a D flip-flop is drawn in Fig. C.2. It captures the value of its Data (D) input on a specific point of the cycle of its Clock input (\triangleright) (e.g. the rising edge of the clock). This value is then propagated to the output Q (and eventually the opposite is propagated to \bar{Q}). Changes of the logic level on the D input at other times of the clock cycle do not have any influence on the output. This is summarized in Table C.1. D flip-flops can be considered as memory cells or a delay lines.

Table C.1: Truth table of a D type flip-flop. X denotes a *Don't care* condition, meaning the signal level is irrelevant. Table taken from [97].

Clock	D	Next Q
Rising edge	0	0
Rising edge	1	1
Non-Rising	X	Q

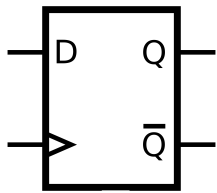


Figure C.2: Symbol of a D flip flop elements with its usual input/output names.

Bibliography

- [1] K. Fukushima and T. Hatsuda, Rept.Prog.Phys. [74](#), 014001 (2011)
- [2] Y. Aoki et al., Nature [443](#), 675 (2006)
- [3] Z. Fodor and S. Katz, JHEP [0404](#), 050 (2004)
- [4] L. McLerran and R.D. Pisarski, Nucl.Phys. [A796](#), 83 (2007)
- [5] A. Andronic et al., Nucl.Phys. [A837](#), 65 (2010)
- [6] B. Friman et al., Lect.Notes Phys. [814](#), 1 (2011)
- [7] M. Gyulassy and L. McLerran, Nucl.Phys. [A750](#), 30 (2005)
- [8] The Brahms, Phenix, Phobos, and Star Collaborations, Nucl.Phys. [A757](#), 1 (2005)
- [9] B. Muller et al., Ann.Rev.Nucl.Part.Sci. [62](#), 361 (2012)
- [10] C. Blume, J.Phys. [G31](#), S57 (2005)
- [11] A. Andronic et al., Phys.Lett. [B673](#), 142 (2009)
- [12] J. Randrup and J. Cleymans, Phys.Rev. [C74](#), 047901 (2006)
- [13] J. Cleymans et al., Phys.Rev. [C73](#), 034905 (2006)
- [14] Y. Zhang, [3 lambda H and 4 lambda H production in Ni+Ni collisions at 1.91A GeV](#). Ph.D. thesis, University of Heidelberg (2013)
- [15] H. Stoecker et al., Nucl.Phys. [A827](#), 624C (2009)
- [16] [Nica white paper](#)
- [17] C. Höhne, J.Phys.Conf.Ser. [420](#), 012016 (2013)
- [18] W. Cassing et al., Nucl.Phys. [A691](#), 753 (2001)
- [19] A. Andronic et al., Nucl.Phys. [A772](#), 167 (2006)
- [20] N. Herrmann et al., Technical Design Report for the CBM Time-of-Flight System (TOF). Tech. rep., GSI. Not published yet

BIBLIOGRAPHY

- [21] CBM collaboration. [CBM - Technical Status Report](#) (2005)
- [22] W. Mueller, J.Phys.Conf.Ser. **50**, 371 (2006)
- [23] A.A. Alves et al., JINST **3**, S08005 (2008)
- [24] J. Heuser et al., [Technical Design Report for the CBM Silicon Tracking System \(STS\)](#). Tech. rep., GSI (2013)
- [25] C. Lippmann, Nucl.Instrum.Meth. **A666**, 148 (2012)
- [26] J.W. Keuffel, Rev. Sci. Instrum. **20**(3), 202 (1949)
- [27] V. Parkhomchuck et al., Nucl. Instrum. and Methods **93**(2), 269 (1971)
- [28] R. Santonico and R. Cardarelli, Nucl.Instrum.Meth. **187**, 377 (1981)
- [29] E. Cerron Zeballos et al., Nucl.Instrum.Meth. **A374**, 132 (1996)
- [30] N. Herrmann, Particle Detectors at their limits (Time Of Flight) (2013). IRTG spring school
- [31] [FAIR Green Paper - The Modularized Start Version](#) (2009)
- [32] [FAIR Baseline Technical Report](#) (2006)
- [33] S. Bass et al., Prog.Part.Nucl.Phys. **41**, 255 (1998)
- [34] G. Agakishiev et al., Phys.Rev. **C84**, 014902 (2011)
- [35] G. Agakishiev et al., Eur.Phys.J. **C41**, 475 (2005)
- [36] CBM collaboration. [Nuclear Matter Physics at SIS-100](#) (2005)
- [37] J. de Cuveland and V. Lindenstruth, J.Phys.Conf.Ser. **331**, 022006 (2011)
- [38] W. Mueller, [DAQ Summary](#) (2013). 21st CBM collaboration meeting, GSI Darmstadt
- [39] I. Vassiliev and C. Simon, private communication (2013)
- [40] I. Deppner, [Development of a fully differential Multi-gap Resistive Plate Chamber for the CBM Experiment](#). Ph.D. thesis, University of Heidelberg (2013)
- [41] W. Llope, Nucl.Instrum.Meth. **A661**, S110 (2012)
- [42] J.B. Wang et al., Nucl.Instrum.Meth. **A661**, S125 (2012)
- [43] M. Petris et al., Nucl.Instrum.Meth. **A661**, S129 (2012)
- [44] Y. Wang et al., Nucl.Instrum.Meth. **A661**, S134 (2012)
- [45] S. An et al., Nucl.Instrum.Meth. **A594**, 39 (2008)

- [46] I. Deppner et al., Nucl.Instrum.Meth. **A661**, S121 (2012)
- [47] D. Gonzalez-Diaz, [Research and developments on timing RPCs. Application to the ESTRELA detector of the HADES experiment at GSI](#). Ph.D. thesis, Universidade de Santiago de Compostela (2006)
- [48] D. Gonzalez-Diaz et al., Nucl.Instrum.Meth. **A555**, 72 (2005)
- [49] V. Ammosov, [Beam test of pad tRPCs with ultra thin glass](#) (2009). XIII CBM meeting, Darmstadt
- [50] A. Akindinov et al., Nucl.Instrum.Meth. **A572**, 676 (2007)
- [51] L. Lopes et al., Nucl.Phys.Proc.Suppl. **158**, 66 (2006)
- [52] J.B. Wang et al., Nucl.Instrum.Meth. **A621**, 151 (2010)
- [53] L. Naumann et al., Nucl.Instrum.Meth. **A635**, S113 (2011)
- [54] M. Kiš et al., Nucl.Instrum.Meth. **A646**, 27 (2011)
- [55] D. Belver et al., IEEE Trans.Nucl.Sci. **57**, 2848 (2010)
- [56] F. Anghinolfi et al., Nucl.Instrum.Meth. **A533**, 183 (2004)
- [57] J. Christiansen, [Manual for the CERN HPTDC ASIC](#). Digital Microelec. Group, CERN
- [58] C. Xiang, The data pre-processing for CBM-TOF. Ph.D. thesis, Central China Normal University (2013)
- [59] C. Xiang et al., JINST **8**, P02002 (2013)
- [60] M. Ciobanu et al., PADI, an ultrafast Preamplifier - Discriminator ASIC for Time-of-Flight Measurements. Accepted by IEEE Trans.Nucl.Sci. (2014)
- [61] M. Ciobanu et al., IEEE Nucl.Sci.Symp.Conf.Rec. **2008**, 2018 (2008)
- [62] M. Ciobanu et al. CBM Progress Report 2008, p. 54 (2008)
- [63] M. Ciobanu et al. CBM Progress Report 2012, p. 72 (2012)
- [64] H. Flemming and H. Deppe, IEEE Nucl.Sci.Symp.Conf.Rec. **2007**, 322 (2007)
- [65] H. Deppe and H. Flemming, IEEE Nucl.Sci.Symp.Conf.Rec. **2009**, 295 (2009)
- [66] H. Flemming and H. Deppe, *Manual for the GET4 Proto*. GSI EE
- [67] H. Flemming and H. Deppe, [Manual for the GET4 v1.20](#). GSI EE
- [68] M. Ciobanu et al., IEEE Nucl.Sci.Symp.Conf.Rec. **2009**, 401 (2009)

BIBLIOGRAPHY

- [69] K. Koch, IEEE Nucl.Sci.Symp.Conf.Rec. **2009**, 324 (2009)
- [70] C. Schmidt, Proc. TWEPP-07 p. 84 (2007)
- [71] S. Manz et al., JINST **5**, C11017 (2010)
- [72] F. Lemke, [Unified Synchronized Data Acquisition Networks](#). Ph.D. thesis, University of Mannheim (2012)
- [73] S. Manz, The Read Out Controller for the GET4 v1.0 Chips Using the Optical Communication Module (2012). Internal documentation
- [74] W. Gao et al., in *Real Time Conference, 2009. RT '09. 16th IEEE-NPSS* (2009), pp. 527–531
- [75] [DABC website](#)
- [76] [GO4 website](#)
- [77] [ROOT website](#)
- [78] N. Kurz. [MBS website](#)
- [79] J. Frühauf et al. CBM Progress Report 2010, p. 54 (2010)
- [80] I. Deppner et al., JINST **7**, P10008 (2012)
- [81] [FAIRROOT website](#)
- [82] V. Friese, J.Phys.Conf.Ser. **331**, 032008 (2011)
- [83] N. Abel et al., SysCore V3 Specification (2012). Internal Report
- [84] C. Ugur et al., JINST **8**, C01035 (2013)
- [85] J. Michel et al., JINST **8**, C02034 (2013)
- [86] Wikipedia. [VMEbus](#)
- [87] [CES website](#)
- [88] Wikipedia. [LynxOS](#)
- [89] GSI EE. [VULOM page on the GSI EE website](#)
- [90] CAEN Nuclear, [Manual for the CAEN V1290A VME TDC board](#)
- [91] GSI EE. [VFTX page on the GSI EE website](#)
- [92] E. Bayer and M. Traxler, IEEE Trans.Nucl.Sci. **58**, 1547 (2011)
- [93] E. Bayer and M. Traxler, IEEE Nucl.Sci.Symp.Conf.Rec. **2011**, 876 (2011)

- [94] Wikipedia. [Low-voltage differential signaling](#)
- [95] Wikipedia. [Serial Peripheral Interface Bus](#)
- [96] Wikipedia. [NIM](#)
- [97] Wikipedia. [Flip-flop \(electronics\)](#)

BIBLIOGRAPHY

Curriculum Vitae

Personal Information

Name	Pierre-Alain Loizeau
Date of birth	02.04.1985
Place of birth	Cholet/France
Citizenship	French

School Education

1991 - 1996	Primary school, Saint Macaire en Mauges (FR)
1996 - 2000	Secondary school, Saint Germain sur Moine (FR)
09/2000 - 06/2003	Lycée Europe Robert Schuman, Cholet (FR)
07/2003	Baccalauréat général, Science French second term graduation

Academic Studies

09/2003 - 07/2004	CPGE, PCSI, Lycée Clémenceau, Nantes (FR) 1st year of preparation classes for the competitive entrance examinations to French engineering schools
09/2004 - 06/2005	CPGE, PSI, Lycée Clémenceau, Nantes (FR) 2nd year of preparation classes for the competitive entrance examinations to French engineering schools
09/2005 - 09/2008	École Nationale Supérieure de Physique de Strasbourg (ENSPS) (now Télécom Physique Strasbourg), Strasbourg (FR) specialty in “Physics and modeling”
09/2008	Diplôme d’Ingénieur de l’ENSPS, French engineer diploma
09/2007 - 07/2008	Université Louis Pasteur, Strasbourg (FR), major in physics
07/2008	Master in Science, major in physics

Graduate School

since 12/2008	PhD student at the Physikalisches Institut der Uni. Heidelberg Supervisor: Prof. Norbert Herrmann
---------------	--

March 28, 2014

BIBLIOGRAPHY

Acknowledgment

First and foremost, I have to express my thanks to Prof. Dr. Norbert Herrmann for proposing me this project and trusting me all along its course. This was an endeavor I would have never dreamt of before coming to Heidelberg and I am really grateful for all the advices and support he gave me. I cannot express how much his passion for physics and vision on future experimental research gave me motivation in moments of doubt and still push me to go as far as possible in this field.

I truly appreciate the fact that Prof. Dr. Ulrich Uwer agreed to be a second referee of this thesis. My thanks also go to Prof. Dr. Peter Fischer and Prof. Dr. Carlo Ewerz for willing to take part in my final examination committee.

My colleagues in Heidelberg and Darmstadt Dr. Ingo Deppner, Dr. Yapeng Zhang, Jochen Frühauf, Dr. Changzhou Xiang and Christian Simon became not only work partners, but also true friends I believe. This was a real help during these five years far from home. Many thanks especially to Ingo and Christian for their careful proof-reading of this thesis, which helped to bring my “Frenglish” toward true English.

These thanks of course extend to our Heidelberg colleague Victoria Zinyuk and post-docs Dr. Krzysztof Wiśniewski and Dr. Krzysztof Piasecki, from whom I learned a lot about acquisition systems and analysis frameworks during the early phases of this work. The explanations of Dr. Mircea Ciobanu, Dr. Yvonne Leifels and Dr. Mladen Kis were also essential in my understanding of readout chain and acquisition systems and I am really thankful for this.

Finally, I would like to thank all the members of the FOPI and CBM collaborations whom I met during beamtimes and meetings, especially those in the CBM-TOF group, for their advices and the feeling of being part of a community working towards a common goal.

I am sure I forget some people, but be assured that I am truly and humbly grateful for all the help and advices I received in the course of those five years, without which I would have never been able to succeed in this project.

Remerciements

Je tiens tout particulièrement à exprimer mes remerciements aux personnes suivantes :

À mes parents Agnès et Alain bien sûr, pour leur soutien, pour avoir toujours tout fait pour me permettre d'aller au bout de mes rêves, même quand ils semblaient fous, et pour m'avoir toujours assuré un nid douillet dans leur maison.

À mes frangins, Denis et Thomas, et à ma belle-sœur Céline, parce que la famille, son amour et le temps passé à faire des choses non sérieuses ensemble sont indispensables dans un tel projet. À mon neveu et filleul Noah, qui par son arrivée m'a fourni la motivation nécessaire durant la dernière phase de cette thèse, en me rappelant qu'en science on travaille bel et bien pour les générations à venir !

À mes grand-pères, qui chacun à leur façon m'ont appris qu'on pouvait avoir les pieds sur terre tout en gardant un esprit ouvert sur les chose en dehors de nos domaines de prédilection. Porter leur prénoms me fournit des racines solides bien qu'ils soient partis.

À tous mes potes de l'Ouest, François, Florian, Guillaume, Nicolas et tous les autres, pour avoir toujours été là quand je débarquais à l'improviste pour un week-end et pour m'avoir toujours pardonné mes longues absences de nouvelles. A ceux de PS, en particulier Gaëtan Hanen, avec qui j'ai survécu à la prépa et à l'école d'ingénieurs et pu partager tant de discussions sur des bouquins.

À M. Landrin, pour m'avoir fait découvrir à 13 ans les sciences physiques et la méthode expérimentale, ainsi qu'à tous les enseignants en physique et matières techniques qui ont suivi. Sans eux je n'aurais jamais pu envisager de combiner vie professionnelle et curiosité personnelle d'un telle manière.